

# **NUCLEATION AND GROWTH OF ALPHA LACTOSE MONOHYDRATE**

**A Thesis presented in partial fulfilment of the requirements for the degree of  
Doctor of Philosophy in Process Engineering at Massey University**

**Jeremy Mcleod**

**2007**



## **ABSTRACT**

Lactose represents approximately one third of the total solids in bovine milk. In the dairy industry, lactose is recovered from whey and whey permeates using a crystallisation process that involves both evaporation and a cooling stage. A good understanding of the lactose crystallisation kinetics enables both these processes to be operated at conditions that maximise the yield and minimise capital and processing costs.

This study has looked at the nucleation and growth kinetics of the lactose crystallisation process. A model has been produced that can accurately predict the changing concentration profile as lactose is removed, via growth, from an industrial solution. This model incorporated the available literature information and expanded on it where required.

The primary nucleation of alpha lactose monohydrate was investigated on the laboratory scale. The work identified the changing relationship, which occurs with increasing supersaturation, as lactose nucleation moves from being dominated by the heterogeneous mechanism to the homogenous mechanism. The absolute supersaturation at which the mechanism changes was found not to be affected by the solution temperature and agitation rate; however the presence of impurities lowered the supersaturation required for homogeneous nucleation.

The effect of mixing on the primary nucleation rate was studied in a Rushton turbine agitated vessel and through a Venturi. Increasing the agitation rate increased the frequency of activated molecular collisions but the critical nucleus size remained constant. A strong correlation was found, for both mixing systems, between the nucleation rate and the frequency of vortex shedding.



## ACKNOWLEDGEMENTS

This work has been a process of growth, both of lactose and personally. It could not have been completed without the guidance and assistance of many wonderful people. I would like to thank:

My primary supervisor Tony Paterson; thank you for your constant support throughout the project. It has been a privilege and extremely rewarding to do a PhD under your supervision. My secondary supervisors John Bronlund and Jim Jones for your valuable contributions and ideas. Getting you both in Tony's office for meetings at the same time was a challenge and when you were both there the conversations seemed to nucleate uncontrollably on to anything but lactose.

Thank you to Fonterra and FoRST for their support and funding of this project. In particular, my industry supervisor John Thomas who was there for help when needed but who really just let me get on with things. Aggy Mills, Andy Williams, Daniel Hovell, Frank Lin, Gorrey Chui, Marcel Gesterkamp, Raymond Joe, Sue Veitch and Tony Styles and who all shared their lactose knowledge with me. Many thanks also to various other people at Fonterra Kapuni (The Lactose Company), Clandeboye, Hautapu and Edendale sites for their help.

Experiments are very hard to carry out with equipment and for this I would like to thank Anne-Marie Jackson, Bruce Collins, Humphrey O'Hagan, John Edwards, Mike Sahayam and all the other the staff in the Institute of Technology and Engineering for pointing me in the right direction and for helping me convert my ideas into reality. Also, thank you Gayle Leader, Joan Brooks and Trish O'Grady for all your assistance.

Many thanks to Anna, Adi, Craig, Nick, Preyas, Rachel, Richard, Ros, Scott and Stephen who were there for part or all of my postgraduate experience. You provided support, entertainment and helped starve off the madness for a little longer.

A special thank you to Tracey who has supported me for the whole PhD journey in Hawera and in Palmerston North.

My family, Dad, Mum, Jamie, Anna and Fraggie who were providing love, support and encouragement long before this project even started.



## TABLE OF CONTENTS

<b>ABSTRACT.....</b>	<b>iii</b>
<b>ACKNOWLEDGEMENTS.....</b>	<b>iv</b>
<b>TABLE OF CONTENTS.....</b>	<b>vi</b>
<b>LIST OF FIGURES.....</b>	<b>xi</b>
<b>LIST OF TABLES.....</b>	<b>xvii</b>
<b>LIST OF EQUATIONS.....</b>	<b>xix</b>

Chapter 1    Project overview .....	1-1
-------------------------------------	-----

1.1    Problem definition .....	1-1
---------------------------------	-----

1.2    Industrial lactose production .....	1-3
--	-----

1.3    Conclusion .....	1-4
-------------------------	-----

Chapter 2    Crystal growth rates in a lactose and water system .....	2-5
---	-----

2.1    Introduction.....	2-5
--------------------------	-----

2.2    Lactose properties .....	2-5
---------------------------------	-----

2.2.1 $\alpha$ -Lactose monohydrate .....	2-6
---	-----

2.2.2    Beta lactose .....	2-7
-----------------------------	-----

2.2.3    Mutarotation.....	2-8
----------------------------	-----

2.2.4    Solubility.....	2-11
--------------------------	------

2.2.5    Dissolution .....	2-14
----------------------------	------

2.3    Crystal growth theory.....	2-15
-----------------------------------	------

2.3.1    Growth rate dispersion.....	2-16
--------------------------------------	------

2.3.2    Growth rate hysteresis.....	2-16
--------------------------------------	------

2.4    Lactose crystal growth.....	2-17
------------------------------------	------

2.4.1    Supersaturation .....	2-18
--------------------------------	------

2.4.2    Temperature .....	2-19
----------------------------	------

2.4.3    Mixing.....	2-22
----------------------	------

2.4.4    Summary of literature .....	2-23
--------------------------------------	------

<b>2.5</b>	<b>Techniques for measuring crystal growth .....</b>	<b>2-23</b>
2.5.1	Weight.....	2-24
2.5.2	Concentration .....	2-24
2.5.3	Heat of crystallisation .....	2-26
2.5.4	Measuring changing dimensions.....	2-27
2.5.5	Selection of a method for crystal growth measurements .....	2-28
<b>2.6</b>	<b>Crystal growth experiments.....</b>	<b>2-28</b>
2.6.1	Method .....	2-29
<b>2.7</b>	<b>Results and discussion .....</b>	<b>2-32</b>
2.7.1	Effect of agitation rate .....	2-32
2.7.2	Effect of supersaturation .....	2-33
2.7.3	Effect of temperature .....	2-35
2.7.4	Effect of crystal size.....	2-40
2.7.5	Growth rate dispersion.....	2-41
<b>2.8</b>	<b>Conclusion .....</b>	<b>2-45</b>
Chapter 3 Industrial crystal growth rates.....		3-47
<b>3.1</b>	<b>Introduction.....</b>	<b>3-47</b>
<b>3.2</b>	<b>Literature review .....</b>	<b>3-48</b>
<b>3.3</b>	<b>Measuring lactose crystal growth in permeates.....</b>	<b>3-54</b>
3.3.1	Lab scale investigation.....	3-54
3.3.2	Industrial scale measurements .....	3-58
<b>3.4</b>	<b>Results and discussion for laboratory measurements .....</b>	<b>3-60</b>
3.4.1	Solubility.....	3-60
3.4.2	Effect of temperature on growth rate .....	3-61
3.4.3	Effect of supersaturation on growth rate.....	3-63
3.4.4	Effect of crystal origin on growth rate .....	3-65
<b>3.5</b>	<b>Model of <math>\alpha</math>-lactose monohydrate crystal growth.....</b>	<b>3-68</b>
3.5.1	Mutarotation.....	3-68



3.5.2	Solubility.....	3-69
3.5.3	Lactose growth rate.....	3-70
<b>3.6</b>	<b>Industrial results and discussion .....</b>	<b>3-73</b>
<b>3.7</b>	<b>Conclusion .....</b>	<b>3-77</b>
Chapter 4 Nucleation .....		4-79
<b>4.1</b>	<b>Introduction.....</b>	<b>4-79</b>
<b>4.2</b>	<b>Nucleation literature .....</b>	<b>4-79</b>
4.2.1	Primary nucleation .....	4-80
4.2.2	Induction time .....	4-82
4.2.3	Secondary nucleation .....	4-84
<b>4.3</b>	<b>Studies of lactose nucleation .....</b>	<b>4-85</b>
4.3.1	The effect of supersaturation on lactose nucleation.....	4-86
4.3.2	The effect of temperature on lactose nucleation .....	4-90
4.3.3	The effect of impurities on lactose nucleation.....	4-91
<b>4.4</b>	<b>Measuring lactose nucleation.....</b>	<b>4-94</b>
4.4.1	A review of techniques for measuring nucleation .....	4-94
4.4.2	Nucleation in a lactose and water solution .....	4-97
4.4.3	Nucleation in simulated whey permeate .....	4-100
4.4.4	Nucleation in industrial permeate .....	4-101
<b>4.5</b>	<b>Results and Discussion.....</b>	<b>4-103</b>
4.5.1	Relating Absorbance to Number of Crystals .....	4-103
4.5.2	Determination of time to reach critical number of nuclei ( $t_N$ ) .....	4-104
4.5.3	Nucleation in a lactose and water Solution.....	4-107
4.5.4	Nucleation in simulated whey permeate .....	4-113
4.5.5	Nucleation in industrial permeate .....	4-114
<b>4.6</b>	<b>Comparison with literature.....</b>	<b>4-117</b>
<b>4.7</b>	<b>Conclusion .....</b>	<b>4-118</b>

Chapter 5	Nucleation: The effect of mixing.....	5-121
<b>5.1</b>	<b>Introduction.....</b>	<b>5-121</b>
<b>5.2</b>	<b>Mixing and nucleation .....</b>	<b>5-121</b>
5.2.1	Ultrasound induced nucleation .....	5-122
5.2.2	Agitation induced nucleation .....	5-124
5.2.3	The effect of shear flow on nucleation .....	5-125
<b>5.3</b>	<b>Theory of mixing and fluid flow .....</b>	<b>5-127</b>
5.3.1	Mixing levels .....	5-127
5.3.2	Cavitation.....	5-129
5.3.3	Reynolds number .....	5-131
5.3.4	Power input .....	5-132
5.3.5	Vortex formation.....	5-133
5.3.6	Shear .....	5-138
<b>5.4</b>	<b>Experimental investigation into effect of mixing .....</b>	<b>5-138</b>
5.4.1	Effect of agitation on nucleation.....	5-139
5.4.2	Effect of shear on nucleation .....	5-139
5.4.3	Flow through an orifice/Venturi.....	5-140
<b>5.5</b>	<b>Results and discussion .....</b>	<b>5-146</b>
5.5.1	Agitated vessel .....	5-146
5.5.2	Shear flow .....	5-153
5.5.3	Venturi .....	5-155
<b>5.6</b>	<b>Conclusion .....</b>	<b>5-169</b>
Chapter 6	Use of the model in industry .....	6-171
<b>6.1</b>	<b>Introduction.....</b>	<b>6-171</b>
<b>6.2</b>	<b>Optimisation with regard to growth .....</b>	<b>6-171</b>
<b>6.3</b>	<b>Heat transfer from a crystalliser .....</b>	<b>6-176</b>
6.3.1	Surface area.....	6-178

6.3.2	Overall heat transfer coefficient.....	6-179
6.3.3	Temperature driving force .....	6-181
6.3.4	Application of the heat transfer model.....	6-182
<b>6.4</b>	<b>Nucleation optimisation.....</b>	<b>6-187</b>
6.4.1	Results from industrial study .....	6-188
6.4.2	Relating industrial results to theory .....	6-190
6.4.3	The effect of surface area.....	6-194
<b>6.5</b>	<b>Conclusion .....</b>	<b>6-198</b>
Chapter 7	Project Overview .....	7-201
<b>7.1</b>	<b>Introduction.....</b>	<b>7-201</b>
<b>7.2</b>	<b>Conclusions.....</b>	<b>7-201</b>
<b>7.3</b>	<b>Suggestions for future work.....</b>	<b>7-204</b>
Chapter 8	References.....	8-205
Chapter 9	Nomenclature .....	9-217
<b>Appendix</b>		
	Preparation of simulated whey permeate	A1-1
	Particle size distributions for industrial growth rate measurements	A2-2
	Cylinder used for Venturi experiments	A3-4
	Determination of overall heat transfer coefficient for jacketed crystalliser	A4-5
	Industrial nucleation calculations	A5-7
	Compact Disk Description (Model and raw data)	A6-11



## LIST OF FIGURES

Figure 1-1 Cream is delivered to the Waipu dairy factory in January 1916 (McLauchlan, 1996).....	1-2
Figure 1-2 Overview of lactose recovery process.....	1-3
Figure 2-1 Diagram of lactose molecule (Roelfsema <i>et al.</i> , 2002).....	2-5
Figure 2-2 Crystallisation of alpha and beta lactose from solution .....	2-6
Figure 2-3 Diagram of $\alpha$ -lactose crystal grown in an aqueous solution (Roelfsema <i>et al.</i> , 2002) .....	2-7
Figure 2-4 The $\beta/\alpha$ lactose mutarotation equilibrium ratio at temperatures between 0 to 100 °C as determined by (Roetman & Buma, 1974) .....	2-9
Figure 2-5 Mutarotation coefficients .....	2-9
Figure 2-6 The effect of temperature on the lactose mutarotation rate.....	2-10
Figure 2-7- The relationship between pH and the lactose mutarotation rate in water at 25 °C (Troy & Sharp, 1930) .....	2-11
Figure 2-8 Collation of lactose solubility data from literature .....	2-12
Figure 2-9 Correction factor F used to account for $\beta$ -lactose suppression of $\alpha$ -lactose solubility from work by (Visser, 1983).....	2-13
Figure 2-10 30 °C Literature $\alpha$ -lactose growth rate data expressed using common units of $\mu\text{m}\cdot\text{min}^{-1}$ for growth rate and $(C\alpha-C\alpha_s)$ for supersaturation .....	2-19
Figure 2-11 The effect of supersaturation on the $\alpha$ -Lactose monohydrate crystal growth rate from (Jelen & Coulter, 1973) .....	2-20
Figure 2-12 The effect of supersaturation on the $\alpha$ -Lactose monohydrate crystal growth rate from (Thurlby, 1976).....	2-20
Figure 2-13 The effect of supersaturation on the $\alpha$ -Lactose monohydrate crystal growth rate from (Shi <i>et al.</i> , 1989) .....	2-21
Figure 2-14 The effect of supersaturation on the $\alpha$ -Lactose monohydrate crystal growth rate from (Shi <i>et al.</i> , 1990) .....	2-21
Figure 2-15 The effect of supersaturation on the $\alpha$ -Lactose monohydrate crystal growth rate from (Butler, 1998).....	2-22
Figure 2-16 Vessel used for laboratory scale growth rate experiments.....	2-30
Figure 2-17 The effect of the agitation rate on the growth rate of alpha lactose monohydrate crystals .....	2-32

Figure 2-18 Comparison of alpha lactose monohydrate crystal growth rates collected in this study with results reported in the literature.....	2-33
Figure 2-19 Particle size measurements of $\alpha$ -lactose crystals before growth and after growth of four hours at the supersaturations of 5.23 and 10.18 (g Ca-Ca <sub>s</sub> g/100g water) .....	2-34
Figure 2-20 $\alpha$ -lactose monohydrate crystal growth rate measurements obtained between 5°C and 60°C viewed from perspective of relative supersaturation...	2-35
Figure 2-21 $\alpha$ -lactose monohydrate crystal growth rate measurements obtained between 5 °C and 60 °C viewed from perspective of absolute supersaturation ...	2-36
Figure 2-22 Mean normalised $\alpha$ -lactose monohydrate crystal growth rates and 95 per cent confidence interval ranges.....	2-37
Figure 2-23 Comparison of data and predictions of $\alpha$ -lactose monohydrate crystal growth rate from This Work (TW) and the work of (Butler, 1998) (Bu) .....	2-38
Figure 2-24 Comparison of growth rate measured in this work with that where temperature is given as a variable (Butler using Equation 2-8, This work using Equation 2-11) .....	2-39
Figure 2-25 Growth rate of 200-225 $\mu$ m lactose crystals compared against equation developed using growth rate results for 300-600 $\mu$ m lactose crystals .....	2-40
Figure 2-26 Particle size measurements of $\alpha$ -lactose crystals before growth and after growth of four hours at the supersaturations of 5.23 and 10.18 (g Ca-Ca <sub>s</sub> g/100g water); expressed on linear scale .....	2-41
Figure 2-27 The crystal size distribution of $\alpha$ -lactose monohydrate crystals before growth viewed as a histogram.....	2-42
Figure 2-28 Weibull distribution showing shape factors 0.5, 1.5 and 3.0 (Lawless, 2003) .....	2-43
Figure 2-29 Prediction of crystal size distribution using a single common growth rate and the two growth rate dispersion models.....	2-44
Figure 3-1 Lactose removal from concentrated permeate solution in an industrial crystalliser as measured and predicted by Werner <i>et al.</i> , (2002) .....	3-51
Figure 3-2 Crystallisation profile one, from Butler, (1998) no scale provided .....	3-52
Figure 3-3 Crystallisation profile two, from Butler, (1998) no scale provided .....	3-52
Figure 3-4 Crystallisation profile three, from Butler, (1998) no scale provided .....	3-53

Figure 3-5 Solubility of lactose in permeate: measured for different batches of permeate (A represents plant A, B represents plant B).....	3-60
Figure 3-6 Growth rate of lactose crystals in whey permeate compared against the growth rate observed for a lactose water solution (A represents plant A, B represents plant B) .....	3-62
Figure 3-7 Comparison of the normalised (as function of supersaturation) growth rates for growth at 30 °C and 45 °C in whey permeate concentrate.....	3-63
Figure 3-8 Normalised (as function of supersaturation) growth rate results for $\alpha$ -lactose monohydrate crystals grown in permeate compared against the mean value obtained for crystals grown in lactose water solution .....	3-64
Figure 3-9 Comparison of impure (crystals that had formed in permeate) crystal growth rates with Equation 3-8 developed using refined (crystals formed in a lactose water solution) crystals .....	3-65
Figure 3-10 Prediction of crystal size distribution using a single common growth rate and the growth rate dispersion models.....	3-67
Figure 3-11 Comparison of the Weibull generated growth rate distributions required to predict the crystal size distribution after growth had occurred.....	3-67
Figure 3-12 Batch one – measured and predicted concentration profiles for the crystallisation. Original P uses Equation 2-8 given by Butler, (1998) Predicted uses Equation 3-8 and the modified solubility equation.....	3-74
Figure 3-13 Batch two – measured and predicted concentration profiles for the crystallisation. Original P uses Equation 2-8 given by Butler, (1998) Predicted uses Equation 3-8 and the modified solubility equation.....	3-74
Figure 3-14 Batch three – measured and predicted concentration profiles for the crystallisation. Original P uses Equation 2-8 given by Butler, (1998) Predicted uses Equation 3-8 and the modified solubility equation.....	3-75
Figure 3-15 Batch four – measured and predicted concentration profiles for the crystallisation. Original P uses Equation 2-8 given by Butler, (1998) Predicted uses Equation 3-8 and the modified solubility equation.....	3-75
Figure 4-1 The different mechanisms of nucleation (Myerson, 2002) .....	4-80
Figure 4-2 Comparison of homogenous and heterogeneous nucleation mechanisms (adapted from Lacmann, Herden, & Mayer, 1999) .....	4-80

Figure 4-3 The nucleation rate data of Shi <i>et al</i> , (1990), Griffiths <i>et al</i> , (1982), Kauter, (2003) and Butler, (1998) expressed in terms of absolute alpha supersaturation.	4-89
Figure 4-4 Temperature vs. nucleation rate data from Shi <i>et al</i> , (1990) viewed in terms of absolute alpha supersaturation.....	4-90
Figure 4-5 Effect of temperature on the lactose nucleation rate as reported by Kauter, (2003).....	4-91
Figure 4-6 Comparison of secondary nucleation rate in water, in simulated whey permeate and in industrial permeate (Cent A is industrial permeate A that had been centrifuged to remove the undissolved solids) (Results reproduced from Kauter, (2003).....	4-92
Figure 4-7 Baffled 750 ml vessel and Rushton agitator used for the nucleation experiments .....	4-97
Figure 4-8 Image of the mixing equipment used for the nucleation experiments ....	4-98
Figure 4-9 Results from investigation into the effect of pre-mixing cooling time on nucleation results (Results show mean and 95 per cent confidence limits)....	4-100
Figure 4-10 Polarised filter and Neubauer counting chamber used for counting of nuclei.....	4-102
Figure 4-11 The relationship between the absorbance at 550 nm and the number of crystals per ml solution (determined by sampling solution and counting the crystals under a light microscope) .....	4-103
Figure 4-12 Comparison of number of crystals in solution at different absorbencies..	4-104
Figure 4-13 Typical absorbance curve for induction time experiments (Relative supersaturation 4.61, mixing speed 400 r·min <sup>-1</sup> , temperature 25 °C) .....	4-104
Figure 4-14 The effect of the selected absorbance value on the calculated the nucleation rate .....	4-106
Figure 4-15 Effect of temperature on the time required to reach the critical absorbance value of 0.1; measured over a range of absolute supersaturations.....	4-107
Figure 4-16 Effect of temperature on the theoretical nucleation rate of lactose; determined at the absolute alpha lactose supersaturations of 10, 20, 30 and 40 (g/100 water).....	4-108
Figure 4-17 Nucleation results viewed using classical nucleation theory (Temperature 40 °C).....	4-110



Figure 4-18 Nucleation results viewed using classical nucleation theory (Temperature 25 °C).....	4-111
Figure 4-19 Nucleation results viewed using classical nucleation theory (Temperature 50 °C).....	4-111
Figure 4-20 Nucleation results viewed using classical nucleation theory (Temperature 60 °C).....	4-112
Figure 4-21 Comparison of lactose nucleation in simulated whey permeate (SW) and water (W) (Temperature 40 °C).....	4-113
Figure 4-22 Permeate nucleation measured using microscope (Absolute $\alpha$ -lactose supersaturation 20.12 g per 100 g water, relative supersaturation 2.71) .....	4-114
Figure 4-23 Time to reach critical absorbance value of 0.1 as measured for supersaturated lactose solutions made up of water, simulated whey permeate and industrial permeate (Temperature 40 °C) .....	4-114
Figure 4-24 Comparison of lactose nucleation in whey permeate (P), simulated whey permeate (SW) and water (W) (Temperature 40 °C).....	4-115
Figure 4-25 Comparison of nucleation results from this study with literature nucleation rates reported for a lactose water solution.....	4-118
Figure 5-1 The scheme of the growth and destruction of a cavitation bubble (Devarakonda <i>et al.</i> , 2003).....	5-122
Figure 5-2 Concentration driving forces in crystallisation from solution (Mullin, 2001) .....	5-123
Figure 5-3 Induction time as a function of supersaturation for potassium sulphate crystallisation (A) without ultrasound, (B) $P_{\text{Dissipated}} = 0.043W \cdot g^{-1}$ (C) $P_{\text{Dissipated}} = 0.114W \cdot g^{-1}$ (Lyczko <i>et al.</i> , 2002) (D) Lines by this work added to demonstrate that at higher supersaturations slope is similar, and that a second mechanism appears below a certain supersaturation .....	5-124
Figure 5-4 Flow regions at conditions of supercavitation (redrawn from Yan & Thorpe, 1990).....	5-130
Figure 5-5 Changes in the Strouhal number versus changes in the Reynolds number (reproduced from (Pankanin, 2005)).....	5-134
Figure 5-6 Flow in a Rushton agitated tank, showing radial jet, large scale ring vortices and tip vortices (Reproduced from Sharp & Adrian, 2001).....	5-135

Figure 5-7 Flow of water through a diverging channel (a) Reynolds number# 70 (b) Reynolds number 350 (Nakayama, 1988) .....	5-136
Figure 5-8 The position of the solution in a cone and plate rheometer .....	5-140
Figure 5-9 The critical dimensions of the classical Venturi tube (reproduced from Spink, 1967).....	5-141
Figure 5-10 Design of Venturi used this work with 1.0 mm orifice.....	5-141
Figure 5-11 Design of Venturi used this work with 2.0 mm orifice.....	5-142
Figure 5-12 Design of Venturi used this work with 3.0 mm orifice.....	5-142
Figure 5-13 Diagram showing equipment used for conducting the Venturi initiated nucleation experiments .....	5-143
Figure 5-14 Set-up of system used for Venturi experiments .....	5-144
Figure 5-15 The ram movement on the lactose pump during the plunging phase of the Venturi nucleation experiments (images used to determine the fluid velocity) ...	5-144
Figure 5-16 Agitated vessel used to collect supersaturated lactose solution exiting the Venturi tube .....	5-145
Figure 5-17 The relationship between the mixing rate of supersaturated lactose solutions in a Rushton agitated vessel and the time required to reach the critical number of nuclei .....	5-147
Figure 5-18 Homogeneous and heterogeneous nucleation curves for supersaturated lactose solutions at different mixing rates in a Rushton agitated vessel.....	5-147
Figure 5-19 Supersaturation vs. energy input required to reach $N_{crit}$ for Rushton agitated supersaturated lactose solutions .....	5-151
Figure 5-20 Supersaturation vs. number of impellor revolutions required to reach $N_{crit}$ for Rushton agitated supersaturated lactose solutions .....	5-152
Figure 5-21 Change in lactose solution viscosity over time at different shear stresses applied using a plate and cone rheometer .....	5-153
Figure 5-22 Change in lactose solution viscosity at different shear stresses applied using a plate and cone rheometer .....	5-154
Figure 5-23 Viscosity of lactose solution over time with a delay (Shear Stress 4.0 Pa). Measured using a plate and cone rheometer .....	5-155
Figure 5-24 Comparison of Venturi orifice diameter on the number of crystals produced per ml of at different power inputs. Experiments used 200 ml of	

solution with an absolute alpha lactose supersaturation of 26.17 g per 100 g water.....	5-157
Figure 5-25 Power per unit volume where the volume under consideration is that of the throat of the Venturi tube .....	5-158
Figure 5-26 Comparison of the Venturi orifice diameter on the number of crystals per ml at different Reynolds numbers (log scale) Experiments used 200 ml of solution with an absolute alpha lactose supersaturation of 26.17 g per 100 g water.....	5-159
Figure 5-27 Comparison of the Venturi orifice diameter on the number of crystals per ml at different Reynolds numbers (linear scale) Experiments used 200 ml of solution with an absolute alpha lactose supersaturation of 26.17 g per 100 g water.....	5-160
Figure 5-28 Comparison of the Venturi orifice diameter on the number of crystals per ml based on the relationship given for Strouhal number. Experiments used 200 ml of solution with an absolute alpha lactose supersaturation of 26.17 g per 100 g water.....	5-161
Figure 5-29 Bubbles in bulk solution after the lactose solution had been passed through the 1.0mm Venturi at a flow rate of $1.02 \times 10^{-4} (\text{m}^3 \cdot \text{s}^{-1})$ (Cav number. 0.009). Images taken using a Lasentec PVM.....	5-162
Figure 5-30 Comparison of how the Venturi orifice diameter changed on the number of lactose crystals formed per ml of solution at different cavitation numbers. Experiments used 200 ml of solution with an absolute alpha lactose supersaturation of 26.17 g per 100 g water.....	5-163
Figure 5-31 Nucleation of differently supersaturated solutions passed through a Venturi with a 1.0 mm orifice. Results compared using Strouhal relationship ....	5-165
Figure 5-32 Lactose nucleation in supersaturated lactose-water solutions agitated by a Rushton Turbine (Temperature 40 °C). Included also are the four supersaturations studies using the Venturi these are marked by the black triangles .....	5-166
Figure 5-33 Regression equation fitted to 90 g lactose monohydrate per 100 g water (2.91) and 100 g lactose monohydrate per 100 g water (3.31) results from 1mm Venturi experiments; 95 per cent confidence limits included .....	5-167

Figure 6-1 Dissolved lactose concentration profile of crystalliser cooled as per industrial conditions.....	6-173
Figure 6-2 Dissolved lactose concentration of crystalliser cooled based on achieving concentration difference of 10 g lactose/100 g water .....	6-174
Figure 6-3 Dissolved lactose concentration profile of crystalliser using supersaturation of 20g total lactose/100 g water .....	6-175
Figure 6-4 Temperature profiles for crystalliser using different cooling rates .....	6-175
Figure 6-5 Jacket cooled crystalliser.....	6-177
Figure 6-6 Lactose nucleation at walls in an industrial crystalliser where the cooling driving force lowers the solubility faster than can be absorbed by crystal growth .....	6-178
Figure 6-7 Dissolved lactose concentration profiles of crystalliser cooled using different cooling models .....	6-184
Figure 6-8 Total anhydrous lactose supersaturation for different cooling profiles (based on temperature bulk solution).....	6-185
Figure 6-9 Total anhydrous lactose supersaturation for different cooling profiles (based on temperature of cooling water) .....	6-186
Figure 6-10 Crystal particle size distributions of lactose crystallised at different supersaturations.....	6-189
Figure 6-11 Final crystals produced where initial conditions were 59 per cent solids and 72 °C.....	6-189
Figure 6-12 Final crystals produced where initial conditions were 62 per cent solids and 72 °C.....	6-190
Figure 6-13 Final crystals produced where initial conditions were 62 per cent solids and 78 °C.....	6-190
Figure 6-14 Position of industrial feed in relation to nucleation curves generated using laboratory results for industrial permeate (Points based on prediction of $t_N^{-1}$ using an equivalent relative supersaturation determined from absolute supersaturation) .....	6-191
Figure 6-15 The laboratory permeate nucleation from results Figure 4-23 viewed as single nucleation mechanism .....	6-192
Figure 6-16 Dissolved lactose concentration profile for different initial nucleation events .....	6-196

Figure 6-17 Particle size distributions for simulated nucleation events .....	6-197
Figure 6-18 Total anhydrous lactose supersaturation profiles of the bulk solution for different initial nucleation events.....	6-197



## LIST OF TABLES

Table 2-1 Physical properties of crystalline lactose <sup>a</sup> (Roelfsema <i>et al.</i> , 2002) <sup>b</sup> (Itoh, Katoh, & Adachi, 1978) <sup>c</sup> (Harper, 1992).....	2-6
Table 2-2 Concentration measurement techniques (Loffelmann & Mersmann, 2002) 2-	25
Table 2-3 Comparison of growth rates as measured using laser diffraction and weight change .....	2-35
Table 2-4 Normalised (as function of supersaturation) rates of crystal growth at 15 °C, 30 °C, 45 °C and 60 °C .....	2-37
Table 2-5 Parameters used in predicting final crystal size distribution .....	2-44
Table 3-1 Components of the remaining liquor after lactose has been removed through crystallisation (Fonterra data, 2005) .....	3-48
Table 3-2 Measured non lactose solids in different permeates at 45 °C.....	3-61
Table 3-3 Comparison of the normalised (as function of supersaturation) growth rates for growth at 30 °C and 45 °C in whey permeate concentrate.....	3-62
Table 3-4 Normalised (as function of supersaturation) crystal growth results with and calculated student's t value .....	3-64
Table 3-5 Comparison of impure (crystals that had formed in permeate) and refined crystal (crystals formed in a lactose water solution) growth rates at 45 °C and an absolute alpha supersaturation of 8.15 .....	3-65
Table 3-6 Parameters used in predicting crystal size distribution after growth had been allowed to occur .....	3-66
Table 4-1 The appearance of crystal nuclei at 30 °C, in solutions saturated at temperatures between 46 °C to 96 °C –reproduced from (Herrington, 1934a) 4-86	
Table 4-2 Induction time for $\alpha$ -lactose monohydrate crystallisation at a range of supersaturations (Raghavan <i>et al.</i> , 2001).....	4-87
Table 4-3 Effect of temperature on initial homogeneous nucleation point compared used relative and absolute alpha lactose supersaturations .....	4-112
Table 4-4 Homogenous and heterogeneous nucleation parameters for water, simulated whey permeate and industrial permeate, determined using classical nucleation theory .....	4-115

Table 4-5 Comparison of mineral components measured in simulated whey and whey permeate.....	4-117
Table 5-1 Homogenous and heterogeneous nucleation parameters for different mixing rates in a Rushton agitated vessel .....	5-148
Table 6-1 Measured and calculated results for industrial crystallisations .....	6-193
Table 6-2 Conditions used to generate concentration profiles and the mean final particle size (Brackets are experimentally determined values).....	6-195



## LIST OF EQUATIONS

Equation 2-1 Equilibrium ratio of $\beta$ lactose to $\alpha$ lactose.....	2-8
Equation 2-2 Equilibrium ratio of $\beta$ -lactose to $\alpha$ -lactose as a function of temperature .....	2-9
Equation 2-3 Mutarotation rate coefficient.....	2-9
Equation 2-4 Reaction rate for conversion of $\alpha$ -lactose to $\beta$ -lactose .....	2-10
Equation 2-5 Equation for the equilibrium solubility of lactose below 93.5 °C.....	2-13
Equation 2-6 Determination of $\alpha$ -lactose solubility .....	2-13
Equation 2-7 Correction factor for $\alpha$ -lactose solubility.....	2-14
Equation 2-8 $\alpha$ -Lactose monohydrate growth rate reported by Butler, (1998) .....	2-22
Equation 2-9 Prediction of the water activity of non-electrolyse solutions.....	2-26
Equation 2-10 Modified Zweitering Equation (Armenante & Nagamine, 1998).....	2-33
Equation 2-11 Growth rate equation developed from experimental work .....	2-36
Equation 2-12 Equation used to normalise measured growth rates.....	2-37
Equation 2-13 Weibull distribution function .....	2-43
Equation 3-1 Equilibrium ratio of lactose in solution.....	3-69
Equation 3-2 Temperature effect on the equilibrium constant of lactose solution...	3-69
Equation 3-3 Description of rate mutarotation equilibrium.....	3-69
Equation 3-4 Temperature effect on the dissolved alpha and beta lactose mutarotation rate.....	3-69
Equation 3-5 Solubility of lactose in water.....	3-69
Equation 3-6 $\alpha$ -lactose solubility .....	3-70
Equation 3-7 Correction factor to account for solubility depression of $\alpha$ -lactose caused by the presence of $\beta$ -lactose in solution.....	3-70
Equation 3-8 $\alpha$ -lactose monohydrate crystal growth rate (used to determine the mean growth rate in a crystal population) .....	3-71
Equation 3-9 Growth of individual crystals.....	3-71
Equation 3-10 Mass of all crystals in solution.....	3-71
Equation 3-11 Mass balance for lactose in crystalliser.....	3-72
Equation 3-12 Mutarotation rate .....	3-72
Equation 4-1 Driving force for nucleation.....	4-80
Equation 4-2 Driving force for nucleation expressed as a function of relative supersaturation (Kashchiev & van Rosmalen, 2003).....	4-81

Equation 4-3 Supersaturation expressed as a relative function of the equilibrium concentration.....	4-81
Equation 4-4 Classical nucleation equation for homogeneous nucleation .....	4-81
Equation 4-5 Classical nucleation equation for heterogeneous nucleation .....	4-82
Equation 4-6 Nucleation as a sum of homogenous and heterogeneous nucleation ..	4-82
Equation 4-7 Relating induction time to nucleation rate .....	4-83
Equation 4-8 Incorporation of induction time into classical nucleation equation ...	4-83
Equation 4-9 Determination of molecular volume .....	4-83
Equation 4-10 Prediction of interfacial energy .....	4-84
Equation 4-11 Prediction of critical nucleus size .....	4-84
Equation 4-12 Equation used to convert absorbance reading to number of crystals nucleated in the solution .....	4-103
Equation 4-13 Equation used to fit curve to induction times measured at different supersaturations.....	4-109
Equation 5-1 Equation for determining the effective viscosity of a particle fluid mixture .....	5-126
Equation 5-2 Kolmogorov length scale .....	5-128
Equation 5-3 Kolmogorov time scale .....	5-128
Equation 5-4 Determination of the cavitation number .....	5-130
Equation 5-5 Reynolds number for flow in a pipe.....	5-131
Equation 5-6 Reynolds number for flow in an agitated vessel .....	5-131
Equation 5-7 Power consumed by a mixer .....	5-132
Equation 5-8 Power input per unit mass of fluid .....	5-132
Equation 5-9 Velocity head of a fluid.....	5-133
Equation 5-10 Power stored in a flowing fluid.....	5-133
Equation 5-11 Frequency of vortex generation for flow obstructed by a cylinder .	5-133
Equation 5-12 Frequency of macroinstabilities in an agitated vessel.....	5-135
Equation 5-13 Vortex shedding frequency for flow through an orifice.....	5-136
Equation 5-14 Shear in an impeller agitated tank.....	5-138
Equation 5-15 Equation used to fit curve to induction times measured at different supersaturations.....	5-146
Equation 5-16 Pre exponential factor $C$ .....	5-148
Equation 5-17 Zeldovich factor .....	5-149
Equation 5-18 Number of nucleation sites in system .....	5-149

Equation 6-1 Heat flow from crystalliser.....	6-176
Equation 6-2 Surface area available for heat transfer .....	6-178
Equation 6-3 Determination of overall heat transfer coefficient using empirical relationships .....	6-179
Equation 6-4 Empirical equation for determining Nusselt number for product side....	6-180
Equation 6-5 Determination of the heat transfer coefficient on product side.....	6-180
Equation 6-6 Heat transfer coefficient for jacket side .....	6-180
Equation 6-7 LMTD for crystalliser cooling water .....	6-181
Equation 6-8 Heat flow from crystalliser to cooling water (working included).....	6-182
Equation 6-9 Simplified nucleation equation used for examining industrial results ....	6-192
Equation 6-10 Equation for the number of lactose molecules required to form a stable nuclei.....	6-195



# Chapter 1 Project overview

## 1.1 Problem definition

Art relates to something to be done or produced by skill, science to something to be known (Walker Read, 1999). Crystallisation as a purification and separation process has a long history and falls somewhere in the middle of the two. It has been argued that the first pure chemical produced artificially, alum, was manufactured by crystallisation, prior to 1500BC Singer, (1948) in Garside, (1983). Research on crystallisation has moved the understanding closer to that of a science. However, crystallisation on the industrial scale is still partly an art, with experience and “gut feeling” being important factors in the daily operation.

Lactose,  $C_{12}H_{22}O_{11}$ , or 4-0- $\beta$ -d galactopyranosyl-D-glucopyranose has been studied since at least 1633 when Fabrizio Bartoletti identified it in milk. In 1780 it was determined, by Carl Scheele, to be a sugar (Roelfsema, Kuster, Heslinga, Pluim, & Verhage, 2002). Mammalian milk is the primary source of lactose, a fact evident in the word itself, which is derived from “lac” the Latin word for milk.

In the early years of New Zealand dairy production lactose was a waste product with its perceived value clearly illustrated by the following statement. *“Since 1908 dairy farmers in Waipu, like most farmers supplying butter factories, had separated their milk on the farm and supplied the cream in cans, which were picked up at the road-side daily and taken to the factory. The ‘waste’ that was left was skim milk that is all the protein and lactose portion of the milk. This comprised about 66 per cent by solids and over 80 per cent by volume, and was sometimes dumped but usually fed to pigs”*(Haysmith, Landsford, & McKenzie, 2002). Due to advances in technology, lactose is no longer simply dumped or fed to the pigs. It is now extracted using crystallisation, and refined for use in both the food and pharmaceutical industries.



**Figure 1-1 Cream is delivered to the Waipu dairy factory in January 1916 (McLauchlan, 1996)**

This project sets out to develop a model of the lactose crystallisation process, which can be used in an industrial environment to predict the effect of changes to the process conditions. The work also intends to contribute to the body of knowledge on crystallisation.

A crystallisation process can be divided into two sub events; the first is nucleation (the formation of the crystal), the second is crystal growth. A review of the literature on lactose crystallisation finds that the majority of the knowledge exists in the area of growth. Work done by Butler, (1998) provides a model of the lactose crystallisation process that can be used, with accurate growth rate data, to predict the growth of a mass of lactose crystals in a lactose solution. In a later study done by Werner, Tretiakov, Paterson, & Mcleod, (2002) a model using the work of Butler was developed and applied to a industrial crystallisation event. They found that the model was not able to follow an industrial lactose crystallisation. It was proposed that impurities in the industrial permeate lead to growth inhibition that slowed the rate of lactose removal from the bulk solution. In order for a model to be useful industrially, an understanding of the factors that change the lactose crystals growth rate is required.

The literature on the lactose nucleation process is limited. Nucleation, as applied to all solution based crystallisations, can be divided into two categories; primary, which is the formation of new crystals not stimulated by the presence of other crystals of the same species; and secondary, which is nucleation induced by the presence of crystals

of the same species. Within these two categories Myerson, (2002) lists eight additional sub categories, two for primary and six for secondary. Understanding the occurring nucleation mechanisms is a difficult, yet important, task when wanting to manipulate the final crystal size distribution.

## 1.2 Industrial lactose production

The crystallisation of lactose in the industrial environment being investigated here occurs from whey permeate, a by-product from the processing of milk of kine. Crystallisation serves as a method for recovering a product with an economic value. In addition to this, it removes a component that when left in the whey permeate, creates an environmental problem due to its high biological oxygen demand. An overview of the process used for the recovery of lactose is provided in Figure 1-2.

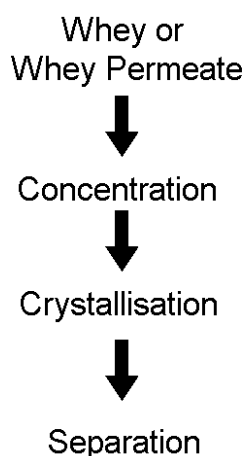


**Figure 1-2 Overview of lactose recovery process**

A brief study of four Fonterra lactose-manufacturing sites found that the foremost priority in production is to maximise the yield. The study also identified two distinctly different methods of producing lactose existed between the sites.

The main difference was in the process used to extract the lactose from the whey permeate concentrate, in particular, where the major nucleation event takes place. An evaporative crystallisation technique is used at two of the lactose manufacturing sites. In this process nucleation and a large portion of the crystal growth occurs in the crystallising evaporators. The liquor is then pumped to crystallisation vessels where it is cooled. The cooling process lowers the solubility of the lactose; the resulting increase in supersaturation is absorbed by the crystal growth. This contrasts with the

other two lactose plants, which have been designed so the crystallising tanks are used for nucleation and crystal growth. The desire to have nucleation occurring only in the crystallising tanks means that the evaporators are operated at temperatures where by supersaturation is maintained below that at which nucleation is expected to occur.

The study of the different manufacturing sites highlighted areas where an improved understanding of growth and nucleation would be beneficial. A model that could accurately predict growth would enable optimisation of crystalliser cooling. It is desirable that when cooling a crystalliser supersaturation is maintained at a level that reduces any further nucleation. Crystals formed later in the process are, due to their small size, difficult to recover and process. A greater understanding of the nucleation process will improve the ability to correctly set operating parameters when targeting a final crystal size.

### **1.3 Conclusion**

The aim of this project is to advance the understanding of lactose crystallisation. A brief study of the New Zealand lactose industry and review of the literature has identified three major areas that this project will focus on:

- Development of a method to study lactose crystal growth at different temperatures and supersaturations. The growth study will also investigate deviations in the growth rate of crystals in individual batches of whey. This will allow the information that already exists on the growth of lactose crystals to be applied to individual industrial situations.
- Improving the understanding of the lactose nucleation process. Identifying the major variables involved in controlling this process.
- Use the obtained research results to extend the current model. This will deliver a model that can be used to investigate a range of industrial crystalliser design set-ups and operating parameters.



## Chapter 2 Crystal growth rates in a lactose and water system

### 2.1 Introduction

Crystal growth determines the final specific properties of crystals, including their morphology and size distribution (Salvatori, Muhr, Plasari, & Bossoutrot, 2002). The adsorption of material from solution on to the crystal surface during growth is both, driven by supersaturation and lowers the supersaturation. For this reason the growth rate is an important parameter when endeavouring to control and model changes in the cooling rate, nucleation and yield.

The growth of alpha lactose monohydrate crystals in lactose water solutions has been is well documented in the literature. This chapter will review these studies and validate them with a program of experiments. The results obtained for a lactose-water system will be used to compare growth rates obtained from industrial liquors as documented in chapter three.

### 2.2 Lactose properties

The lactose molecule is a disaccharide made up the two monosaccharide-sugars, D-glucose and D-galactose, which are joined by a  $\beta$ -1,4-glycosidic linkage. The structure of the molecule is shown in Figure 2-1.

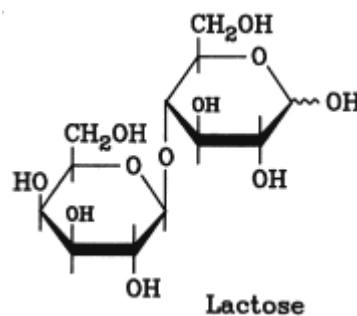


Figure 2-1 Diagram of lactose molecule (Roelfsema *et al.*, 2002)

In the solid form, lactose can exist as either amorphous lactose, crystalline lactose, as either  $\alpha$ -lactose or  $\beta$ -lactose or as a mixture (Dincer, Parkinson, Rohl, & Ogden,

1999). The physical properties of  $\alpha$ -lactose monohydrate and  $\beta$ -lactose are shown in Table 2-1. These are the two most commonly manufactured crystalline forms.

Properties	$\alpha$ -Lactose monohydrate	$\beta$ -Lactose
Melting point (MP)	<sup>a</sup> 201-202 °C	<sup>b</sup> 229.5 °C
Entropy	<sup>a</sup> 0.415 kJ K <sup>-1</sup> mol <sup>-1</sup>	<sup>a</sup> 0.386 kJ K <sup>-1</sup> mol <sup>-1</sup>
Enthalpy of Formation ( $\Delta H$ )	<sup>a</sup> -2481 kJ mol <sup>-1</sup>	<sup>a</sup> -2233 kJ mol <sup>-1</sup>
Heat of Solution ( $\Delta S$ )	<sup>c</sup> 18.091 kJ mol <sup>-1</sup>	<sup>c</sup> 3.290 kJ mol <sup>-1</sup>
Gibbs Free Energy ( $\Delta F$ )	<sup>a</sup> -1750 kJ mol <sup>-1</sup>	<sup>a</sup> -1564 kJ mol <sup>-1</sup>
Specific Heat (cp)	<sup>a</sup> 0.450 kJ K <sup>-1</sup> mol <sup>-1</sup>	<sup>a</sup> 0.408 kJ K <sup>-1</sup> mol <sup>-1</sup>
Density ( $\rho$ )	<sup>a</sup> 1540 kg m <sup>-3</sup>	<sup>a</sup> 1590 kg m <sup>-3</sup>

**Table 2-1 Physical properties of crystalline lactose** <sup>a</sup> (Roelfsema *et al.*, 2002) <sup>b</sup> (Itoh, Katoh, & Adachi, 1978) <sup>c</sup> (Harper, 1992)

The process by which these two forms are crystallised out of solution is shown as Figure 2-2. A further discussion on their properties is carried out in sections 2.2.1 and 2.2.2.

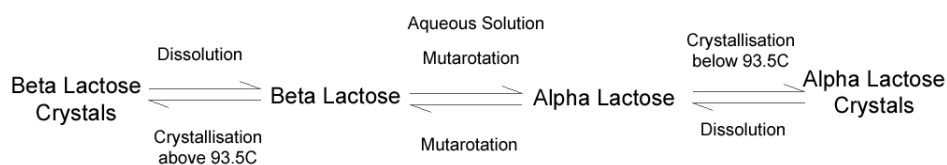


**Figure 2-2 Crystallisation of alpha and beta lactose from solution**

### 2.2.1 $\alpha$ -Lactose monohydrate

$\alpha$ -Lactose monohydrate makes up the bulk of commercially produced lactose and is the crystal form investigated in this work. The monohydrate term refers to the single water molecule incorporated into the crystal structure for every lactose molecule. It is formed by crystallisation of a supersaturated lactose solution at temperatures below 93.5 °C (Roetman, 1972). When crystallisation occurs from an aqueous solution, a tomahawk shaped crystal form is formed. The tomahawk shaped crystal is shown in Figure 2-3. Alpha lactose monohydrate crystallises in the monoclinic space group with  $a = 0.7982$  nm,  $b = 2.1562$  nm and  $c = 0.4824$  nm.

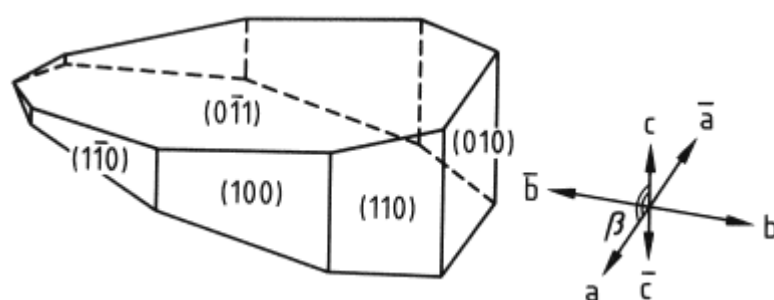


**Figure 2-3 Diagram of  $\alpha$ -lactose crystal grown in an aqueous solution (Roelfsema *et al.*, 2002)**

A crystal morphology distinctly different than the tomahawk shape was obtained by Dincer *et al.*, (1999) who grew alpha lactose monohydrate crystals in a dimethyl sulphoxide solution. This reduced the rate of mutarotation and therefore the  $\beta$ -lactose concentration. At a low  $\beta$ -lactose concentration, growth occurred predominately in the  $c$  direction, as represented by Figure 2-3. As the  $\beta$ -lactose concentration was increased the growth occurred more in the  $a$  and  $b$  directions. The study showed that  $\beta$ -lactose has an inhibitory nature on the growth of  $\alpha$ -lactose monohydrate crystals. Raghavan, Ristic, Sheen, Sherwood, Trowbridge, & York, (2000) found that the tomahawk shape of an alpha lactose crystal results from the  $\beta$ -lactose in the solution inhibiting the growth of some faces. Lactose crystals which have had been damaged through the breaking off of a particular face, show faster than normal growth rates until the face is healed. This is not observed for the 010 (top) face, which inline with no growth normally occurring on this face, does not grow back. This suggests the original nucleus is located in the apex at the 010 face (van Krevald & Michaels, 1965) and (Bhargava & Jelen, 1996).

### **2.2.2 Beta lactose**

Above temperatures of 93.5 °C  $\beta$ -lactose becomes the stable crystal form produced from an aqueous solution (Olano, Corzo, & Martinez-Castro, 1983). The high temperature required for production means that cooling in a standard agitated tank crystalliser is not an effective method for production.  $\beta$ -Lactose methods of manufacture include the drying of a lactose solution as a film above 100 °C on a heated surface, (Suplee & Flanigan, 1934), and heating a lactose slurry under pressure (Asano, Aoki, & Yamazaki, 1978).  $\beta$ -Lactose crystals were prepared by heating a supersaturated lactose solution under reflux conditions (Itoh *et al.*, 1978).  $\beta$ -Lactose

crystals are anhydrous and are an uneven sided diamond when crystallised from water and curved needle-like prisms when crystallised from ethanol (Fox, 1997). The crystals have a melting point of 229.5 °C (Itoh *et al.*, 1978).

### 2.2.3 Mutarotation

A fresh  $\alpha$ -lactose monohydrate solution has a specific optical rotation of 89.4°. This compares to a fresh solution of  $\beta$ -lactose that has a specific optical rotation of 35.0°. When a single anomer of lactose is dissolved in water, a mutarotation reaction changes one form to the other. This can be observed as a change in optical rotation of the solution until an equilibrium between the  $\alpha$ - and  $\beta$ - forms is attained (Hartel & Shastry, 1991) (Roetman & Buma, 1974). At equilibrium, the conversion from one anomer to the other continues to occur, but the rate of conversion becomes equal. This equilibrium ratio can be represented by  $K$  as shown in Equation 2-1. The conversion between  $\alpha$ -lactose and  $\beta$ -lactose molecules occurs by the rotation of a hydroxyl group on the C-1 carbon of the glucose molecule. During mutarotation the ring opens up at the number one carbon molecule and the spatial arrangement of the hydroxyl group changes to give either the  $\alpha$  or  $\beta$  form. This open ring structure is unstable and only occurs at the transition state (Roetman, 1972).

$$K = \frac{[C_{\beta}]}{[C_{\alpha}]}$$

**Equation 2-1 Equilibrium ratio of  $\beta$  lactose to  $\alpha$  lactose**

The equilibrium ratio of  $\beta$ -lactose to  $\alpha$ -lactose was shown by Roetman & Buma, (1974) to decrease with increasing temperature from 1.64 at 0 °C to 1.36 at 100 °C. Three methods were used to obtain the results. Method 1 determined the  $\beta/\alpha$  ratio from specific optical rotations at various temperatures, method two determined optical rotations at a constant temperature and method three used different mixtures of  $\alpha$ -lactose and  $\beta$ -lactose crystals to determine the equilibrium ratio. Their results have been reproduced in Figure 2-4. From this data Equation 2-2 was developed.

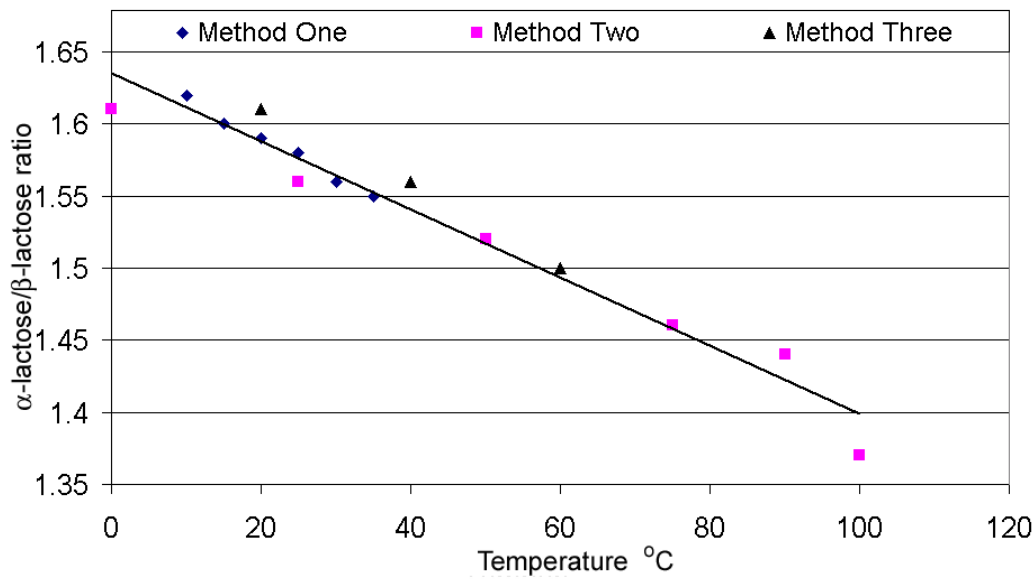


**Figure 2-4 The  $\beta/\alpha$  lactose mutarotation equilibrium ratio at temperatures between 0 to 100 °C as determined by (Roetman & Buma, 1974)**

$$K = -0.0024T + 1.6353$$

**Equation 2-2 Equilibrium ratio of  $\beta$ -lactose to  $\alpha$ -lactose as a function of temperature**

The lactose mutarotation kinetics can be defined by the mutarotation rate coefficient. At equilibrium, the rate of transformation from  $\alpha$ -lactose to  $\beta$ -lactose should equal the rate of transformation from  $\beta$ -lactose to  $\alpha$ -lactose, as shown in Equation 2-3 (Werner *et al.*, 2002).

$$K = \frac{k_1}{k_2}$$

**Equation 2-3 Mutarotation rate coefficient**

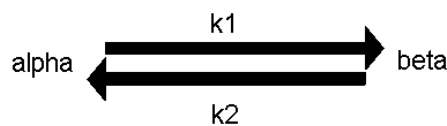


**Figure 2-5 Mutarotation coefficients**

The time taken to reach the  $\alpha$ -lactose and  $\beta$ -lactose equilibrium ratio is a function of the mutarotation rate. The mutarotation rate changes with temperature, pH and impurities in the system. Equation 2-4 establishing the relationship between temperature and mutarotation rate, for lactose in water, was determined by fitting the

Arrhenius equation to the results from (Haase & Nickerson, 1966a), (Haase & Nickerson, 1966b), (Kendrew & Moelwyn-Hughes, 1940) (van Krevald, 1969). Values of  $2.25 \times 10^8 \text{ s}^{-1}$  and  $68.46 \times 10^3 \text{ J}$  were obtained for  $k_o$  and  $E_a$  respectively. The relationship between the temperature and the mutarotation rate is shown in Figure 2-6.

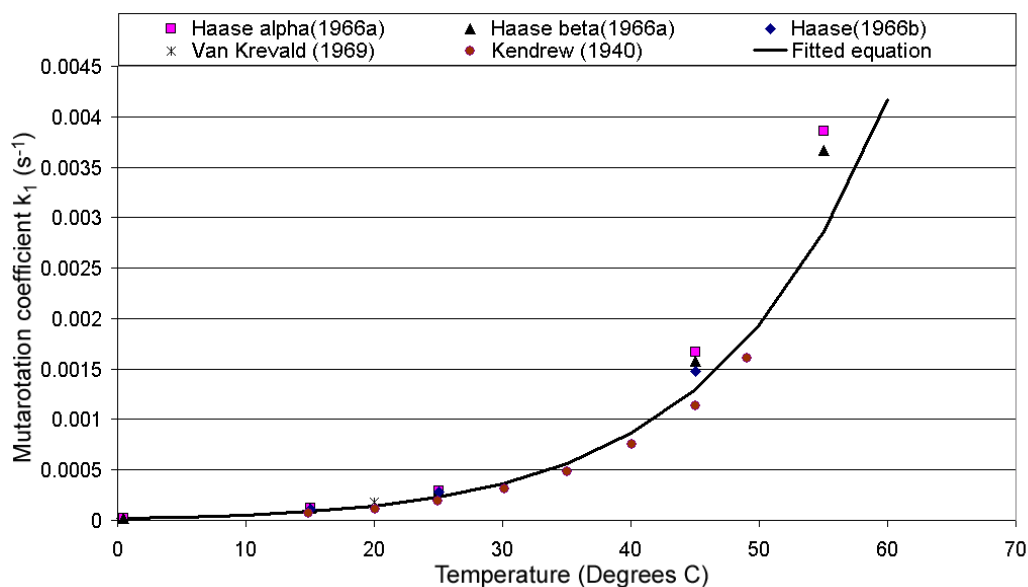


**Figure 2-6 The effect of temperature on the lactose mutarotation rate**

$$k_1 = k_o \exp \frac{-E_a}{RT_K}$$

**Equation 2-4 Reaction rate for conversion of  $\alpha$ -lactose to  $\beta$ -lactose**

Impurities in the solution can change the lactose mutarotation rate. These may alter the pH or interfere with the transition from  $\alpha$ -lactose to  $\beta$  lactose. Patel & Nickerson, (1970) found that the lactose mutarotation rate increased by 1.8 to 1.9 times in a simulated whey salt solution. The presence of sucrose was found to decrease the mutarotation rate. The mutarotation of lactose is accelerated by molecules, and by ions other than those of hydrogen and hydroxyl. The phenomenon is attributed to general acid base catalysis. The catalytic influence of weak acids is much greater than that of weak bases (Herrington, 1936). The effect of pH of the mutarotation rate of lactose remains approximately constant between pH 2.0 and pH 7.0. Outside this range, it is dramatically increased. The “U” shaped trend in Figure 2-7 shows this.

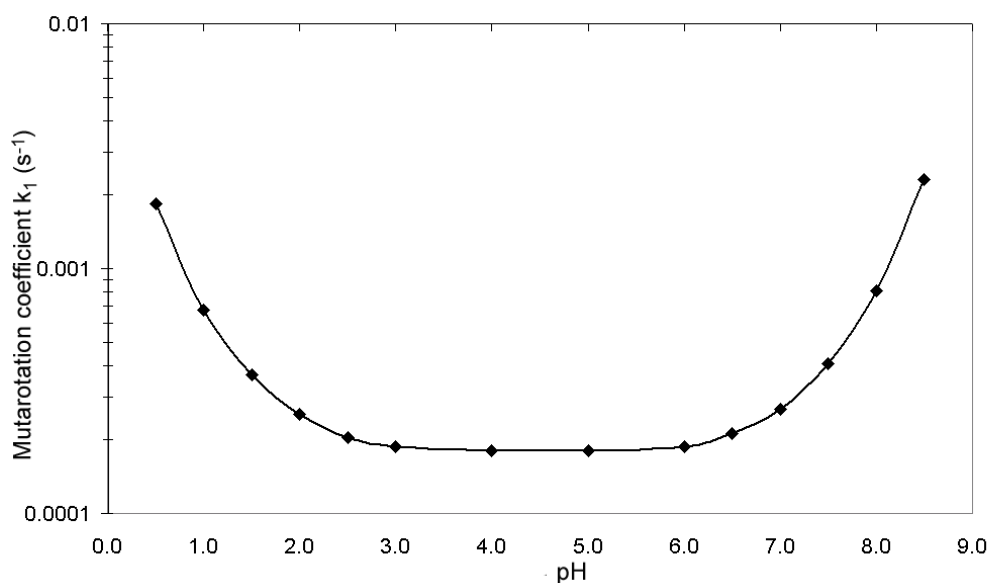


**Figure 2-7- The relationship between pH and the lactose mutarotation rate in water at 25 °C (Troy & Sharp, 1930)**

Haase & Nickerson, (1966b) concluded that compared with the crystallisation rate, mutarotation occurs rapidly providing ample  $\alpha$ -lactose for crystallisation to continue. Twieg & Nickerson, (1968) found that if the rate of crystallisation of  $\alpha$ -lactose is faster than the rate at which it is made available through mutarotation then mutarotation could control the crystallisation rate. The ratio of crystal surface area to solution volume determines the growth rate limiting process. A small growing surface will mean that the rate at which the  $\alpha$ -lactose is removed from solution is much slower than the mutarotation rate. The opposite will apply for a large surface area.

## 2.2.4 Solubility

In solution crystallisation, the solubility of a system is defined the equilibrium point. For dissolution, it represents the point of saturation where no more solute will dissolve into the solvent. For crystallisation, it is the point at which no more solute can be removed. A system with a concentration of solute greater than the solubility concentration is supersaturated. The more supersaturated a system is the stronger the driving force for it to move towards equilibrium. The solubility of lactose in water is much lower than is observed for other similar sugars. At 25 °C for instance the solubility of sucrose is 207 g per 100 g water and that of lactose is only 21.8 g anhydrous lactose per 100 g water (Visser, 1983).

The amount and rate at which lactose will dissolve is dependent on the form of the initial substance.  $\beta$ -Lactose is more soluble and dissolves faster than  $\alpha$ -lactose monohydrate. The  $\alpha$ -lactose dissolution process occurs in two stages, if an excess amount of  $\alpha$ -lactose is put into solution the initial solubility will be reached quickly. As mutarotation occurs and conversion of  $\alpha$ -lactose to  $\beta$ -lactose proceeds then more  $\alpha$ -lactose will dissolve until the equilibrium ratio is reached (Roetman, 1972). The dissolution process during this phase is governed by the mutarotation kinetics (Hodges, Lowe, & Paterson, 1993).

The final solubility of lactose can be determined by adding excess  $\alpha$ -lactose monohydrate to water and agitating it, at a constant temperature, for long enough to establish the mutarotation and solubility equilibrium. The dissolved lactose can then be determined by either weighing the mass of undissolved lactose or by measuring the concentration of the supernatant (Visser, 1982).

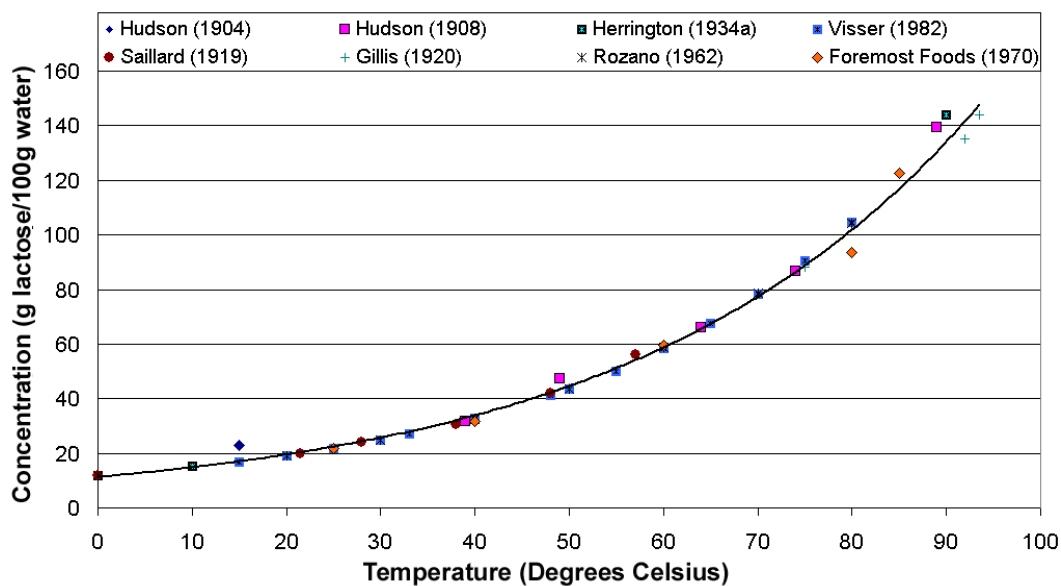


**Figure 2-8 Collation of lactose solubility data from literature**

The literature data, collated in Figure 2-8, was used to develop Equation 2-5, which describes the equilibrium solubility of lactose below 93.5 °C. The fit has an  $R^2$  value of 0.997.



$$C_{Ls} = 10.9109 \exp^{0.028047T}$$

**Equation 2-5 Equation for the equilibrium solubility of lactose below 93.5 °C**

The dissolved  $\alpha$ -lactose concentration governs the growth rate of  $\alpha$ -lactose monohydrate. Many carbohydrates depress the solubility of other carbohydrates and similarly Visser, (1983) found that the presence of  $\beta$ -lactose suppresses the solubility of  $\alpha$ -lactose. To account for this Visser developed Equation 2-6 to calculate the  $\alpha$ -lactose solubility in the presence of  $\beta$ -lactose.

$$C_{as} = \frac{C_{Ls} - FK(C_L - C_{Ls})}{1 + K}$$

**Equation 2-6 Determination of  $\alpha$ -lactose solubility**

F is a temperature dependent correction factor which was put forward by Visser, (1983) to account for the suppressing effect the presence of  $\beta$ -lactose has on the solubility of  $\alpha$ -lactose. The relationship of F with temperature can be seen in Figure 2-9. It can be calculated using Equation 2-7, which was obtained from an exponential fit to the data. The exponential fit was plotted using CurveExpert 1.3 and has an  $R^2$  value of 0.99.

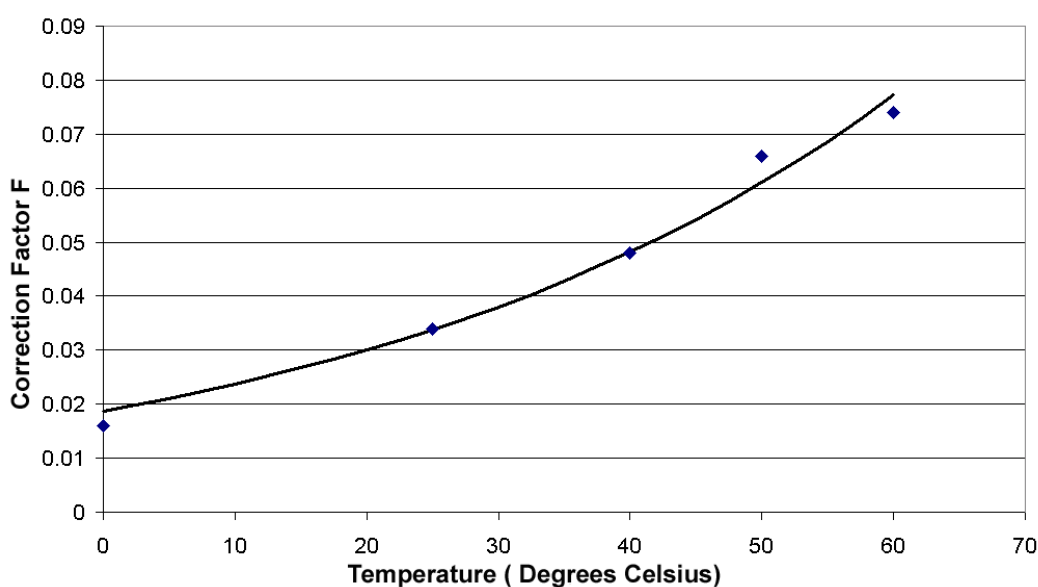


**Figure 2-9 Correction factor F used to account for  $\beta$ -lactose suppression of  $\alpha$ -lactose solubility from work by (Visser, 1983)**

$$F = 0.0187 \exp^{0.0236T}$$

**Equation 2-7 Correction factor for  $\alpha$ -lactose solubility**

Lactose solubility is altered by impurities that can either suppress or increase the solubility. Alcohols were shown to decrease lactose solubility. Increasing the alcohol-water ratio and the chain length of the alcohol both decreased solubility (Majd & Nickerson, 1976), (Olano, 1979). Bhargava, 1995) found that the addition of salts to a lactose solution changed the lactose solubility. LiCl, MgSO<sub>4</sub> and Ca-Lactate decreased the solubility and CaCl<sub>2</sub> and K<sub>2</sub>HPO<sub>4</sub> increased the solubility. Herrington, (1934b) found that the lactose solubility increased when it was dissolved in solutions containing CaCl<sub>2</sub> or CaNO<sub>3</sub>.

### **2.2.5 Dissolution**

Dissolution is the opposite of crystallisation, as crystal mass is lost rather than gained. The dissolution of  $\alpha$ -lactose crystals into solution occurs in two stages with the initial stage occurring up to the  $\alpha$ -lactose solubility limit. This stage is controlled by the disassociation of  $\alpha$ -lactose molecules from the crystal structure (Lowe & Paterson, 1998). Once the alpha lactose solubility limit is reached, further dissolution will occur as alpha lactose is converted to beta lactose. Hodges *et al.*, (1993) found that above the  $\alpha$ -lactose solubility limit, the dissolution rate is governed by the first order kinetics of the mutarotation reaction from alpha to beta lactose. The rate of dissolution was found by Butler, (1998) to be up to 100 times faster than growth with the equivalent sized driving force.

Raghavan, Ristic, Sheen, & Sherwood, (2002) investigated dissolution of  $\alpha$ -lactose monohydrate was on a single crystal scale using a flow cell. They found that the crystals showed a high degree of anisotropy in their dissolution behaviour and highlighted the importance of lattice strain in the definition of the dissolution from the separate faces.

## 2.3 Crystal growth theory

Crystal growth is thought to occur in a layer-by-layer fashion, molecules in solution must de-solvate and adsorb on to the crystal surface to form each layer. Considered energetically, molecules bond to sites where they have maximum contact with other molecules, making it more favourable to grow in existing layers rather than form new ones. Crystal growth theory aims to determine where the layers come from and what the growth rate limiting factors are (Myerson, 2002).

Growth is thought to consist of the following major steps

- Bulk diffusion of growth units through the diffusion boundary layer
- Surface diffusion of growth units through the adsorption layer
- Integration of growth units into the crystal lattice (Farhadi & Babaheidary, 2002).

The crystal growth rate limiting factor is the slowest of the three steps (Farhadi & Babaheidary, 2002). The controlling step for the growth of the crystals will also influence the relationship observed between the growth rate and the solution supersaturation. Under conditions where diffusion is the controlling mechanism for growth a linear relationship will be observed. Where the integration of the growth units on to the crystal lattice is the controlling factor a squared relationship will be observed.

The mechanism controlling growth can change with changing levels of supersaturation and a more linear growth rate is often observed at higher supersaturations, with a squared relationship being observed at lower supersaturations (Mohan & Myerson, 2002). The supersaturation is the driving force of crystal growth. On the fundamental level it is the chemical potential difference that exists between a molecule in a supersaturated solution and a molecule in a saturated solution (Mohan & Myerson, 2002). The supersaturation of a solution can be achieved in a variety of ways. These include, cooling the solution to a temperature where the solubility point is exceeded, removal of solvent, or the addition of a solubility lowering substance. In the industrial manufacture of  $\alpha$ -lactose monohydrate a combination of evaporation and cooling is used to generate supersaturation.

### **2.3.1 Growth rate dispersion**

It has been observed that crystals in suspension grow at different rates even though the system conditions remain constant. This occurrence is identified as growth rate dispersion (Zumstein & Rousseau, 1987). Growth rate dispersion was proposed by Zumstein & Rousseau, (1987) to be a result of the dislocation networks of individual crystals. Butler, (1998) proposes that it occurs due to the different densities of screw dislocations on the crystal surfaces.

The dispersion in the growth rates of individual crystals that have varying histories leads to the broadening of the crystal size distribution, even where the initial population of the crystals are of identical size (Girolami & Rousseau, 1985). White & Kishi, (1995) demonstrated that individual sucrose crystals have a growth rate that is innate to the crystal. Growth rate dispersion must be considered in any test that investigates the influence another variable has on the overall growth rate. When examining the effects of growth rate dispersion it is important to have a well-mixed system, otherwise the differences observed could be due to variations in growth conditions (Ma, Tafti, & Braatz, 2002).

#### **2.3.1.1 Common history seed**

The use of common history seed was found by Butler, (1998) to be effective for modelling the effects of growth rate dispersion for a lactose crystallisation. Common history seed is seed that has nucleated at the same instance in time, in the same solution. Each of these seed crystals has its own growth rate, which remains constant relative to the growth rates of the other common history crystals (Butler, 1998).

### **2.3.2 Growth rate hysteresis**

Different crystal growth-rates can result from growth hysteresis. A result of post nucleation conditioning growth hysteresis varies from growth rate dispersion. It describes an effect where different crystal growth rates can be observed at a given supersaturation depending on the cooling history of the crystals. A crystal growing at high cooling rate can continue to grow at appropriate reduced rates as the cooling rate is lowered. Yet a crystal that has slowed or stopped growth due to a low cooling rate

remains slow growing when the cooling rate is increased (Kubota, Yokota, Doki, Sasaki, & Mullin, 2002).

It is believed that a low cooling rate and the subsequent low supersaturation level which it creates, results in a slower rate of integration of the crystal growth units on to the crystal surface. This permits a greater number of impurities to be incorporated in the surface of the crystal. Kubota *et al.*, (2002) found that increasing the impurity concentration increased the effect of the hysteresis. In contrast, no hysteresis was seen for a pure system. For potassium sulphate crystals, increased levels of impurity and longer exposure time to the low supersaturation were found to increase the effect of the growth hysteresis (Guzman, Kubota, Yokota, & Ando, 2001).

Lactose crystallisation is a process that has potential for growth rate hysteresis. It has been identified in the literature that even in solutions that are considered pure, growth retarding impurities still exist in the form of lactose phosphates (Visser, 1983) and  $\beta$ -lactose (Dincer *et al.*, 1999), (Garnier, Petit, & Coquerel, 2002), (van Krevald, 1969). In a solution of whey or whey permeate the concentration and number of growth retarding impurities that could become adsorbed to the surface is even greater. No work could be found in the literature that examined the effect of growth hysteresis on lactose growth rates.

## **2.4 Lactose crystal growth**

There have already been many studies in the area of lactose crystal growth. While the individual research draws valid conclusions from the results seen, as a collective body of knowledge the exact effect of key variables is inadequately defined. Two explanations are proposed for this lack of clarity. The first is the inconsistency in the units used to present the results; the second is the different periods in time the results were collected. In the second case the results collected are perfectly valid but there is a need to update their presentation to account for new knowledge, in particular the work done by Visser, (1983) showing the effect of  $\beta$ -lactose in suppressing the solubility of  $\alpha$ -lactose.

Three variables emerge from the literature as being important factors in the growth of lactose crystals from water. These are supersaturation, temperature and the mixing rate. Each of these variables can be manipulated on the industrial scale and so needs consideration here.

### **2.4.1 Supersaturation**

The literature demonstrates that a higher supersaturation leads to an increased growth rate. The units used to describe supersaturation vary. The most commonly used are absolute supersaturation defined as the difference between the concentration and the solubility concentration, and relative supersaturation, which is the concentration divided by the solubility concentration. The attachment of  $\alpha$ -lactose molecules to the crystal face drives growth; because of this, the use of absolute  $\alpha$ -lactose gives the best understanding into the effect supersaturation has on growth of alpha lactose crystals. When viewing growth rate results as a function of relative supersaturation it is necessary to consider that any temperature effect observed may be a result of the exponential relationship between lactose solubility and temperature.

The units used by Shi, Hartel, & Liang, (1989), Shi, Liang, & Hartel, (1990) and Butler, (1998) for expressing the growth of lactose crystals were  $\mu\text{m}\cdot\text{min}^{-1}$ . To preserve current trends these units will be used in this work. The units are convenient as they allow the modelling of individual crystal growth and are easily related to the bulk removal of lactose where the particle size distribution and mass of crystals in solution are known.

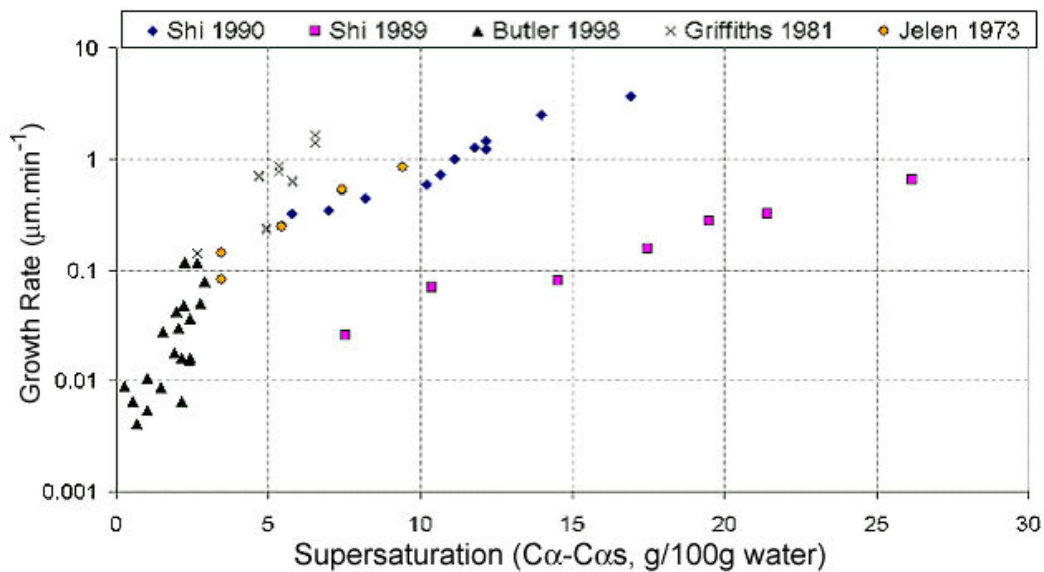


Figure 2-10 30 °C Literature  $\alpha$ -lactose growth rate data expressed using common units of  $\mu\text{m}\cdot\text{min}^{-1}$  for growth rate and  $(C\alpha-C\alpha_s)$  for supersaturation

Figure 2-10 shows the growth rate data at 30 °C of Shi *et al.*, (1989), Shi *et al.*, (1990), Butler, (1998), Griffiths, Paramo, & Merson, (1982) and Jelen & Coulter, (1973) extracted and converted to constant units. Excluding the results obtained by Shi, (1989), the results are consistent. The difference is believed to be due to the method of growth rate measurement and reporting. Shi, (1989) used a microscopic cell to measure growth rates and the number-average is given, for all other data the mass-average growth rate is reported.

## 2.4.2 Temperature

The relationship between temperature and the growth rate of lactose crystals is not clear with different results being reported in the literature. The analysis is complicated by the use of a supersaturation ratio when studying the relationship. Because the solubility of lactose increases exponentially with increasing temperature, presenting growth rate results as a function of a relative supersaturation will give a different temperature effect to that seen when the results are viewed as a function of absolute supersaturation.

The most recent study of lactose crystal growth was carried out by Butler, (1998) who demonstrated increasing temperature leads to an increased growth rate, when absolute supersaturation is used. To investigate the relationship between temperature and

growth rate the data of Butler, (1998), Shi *et al.*, (1989), Shi *et al.*, (1990), Jelen & Coulter, (1973) and Thurlby, (1976) has been extracted and converted into common units. Due to varying experimental methods, it was considered that a better representation of the temperature effect could be gained if each data set was presented separately. The results are shown in Figure 2-11 to Figure 2-15.

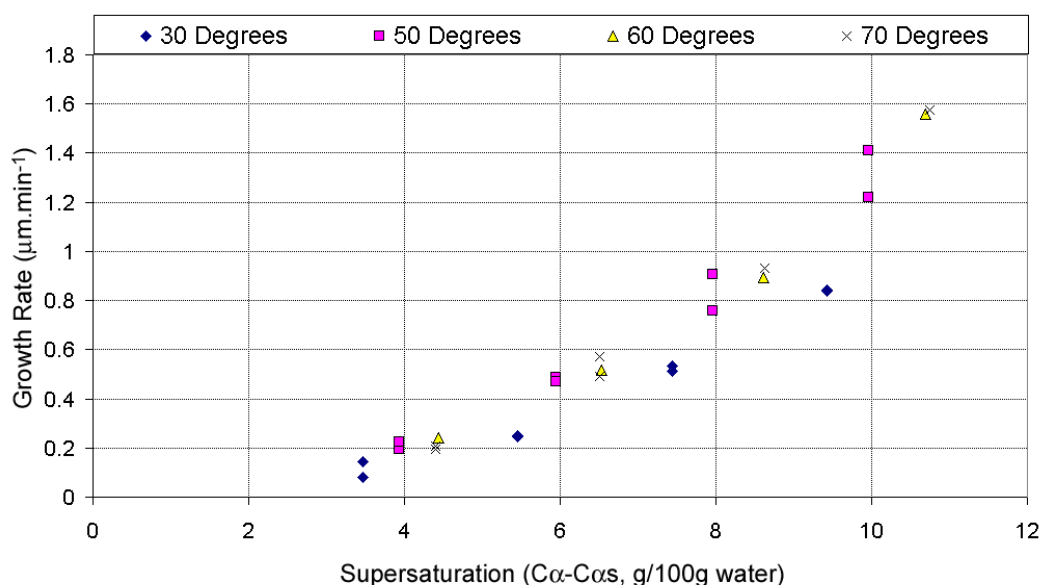


**Figure 2-11 The effect of supersaturation on the  $\alpha$ -Lactose monohydrate crystal growth rate from (Jelen & Coulter, 1973)**

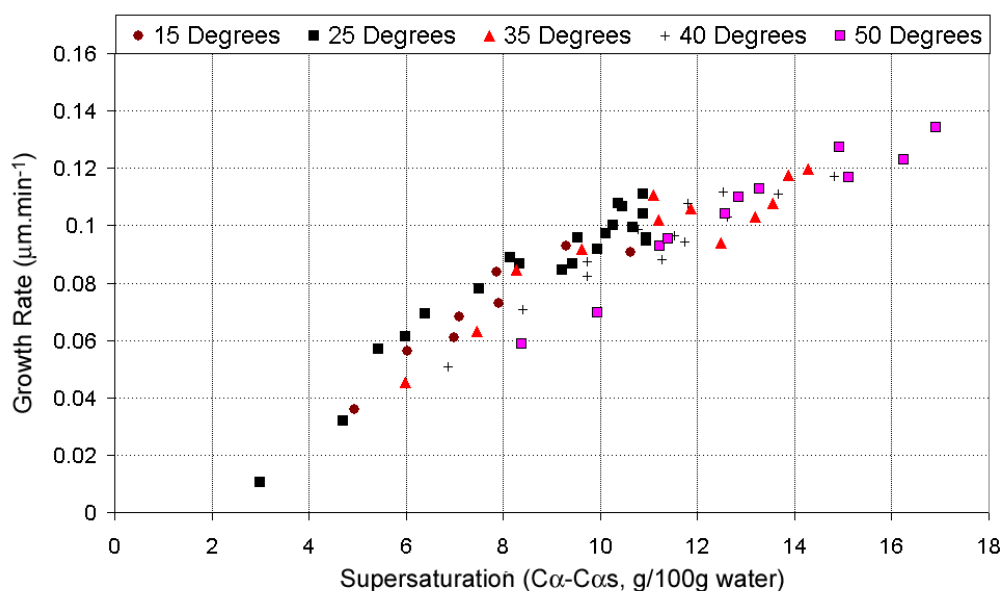


**Figure 2-12 The effect of supersaturation on the  $\alpha$ -Lactose monohydrate crystal growth rate from (Thurlby, 1976)**



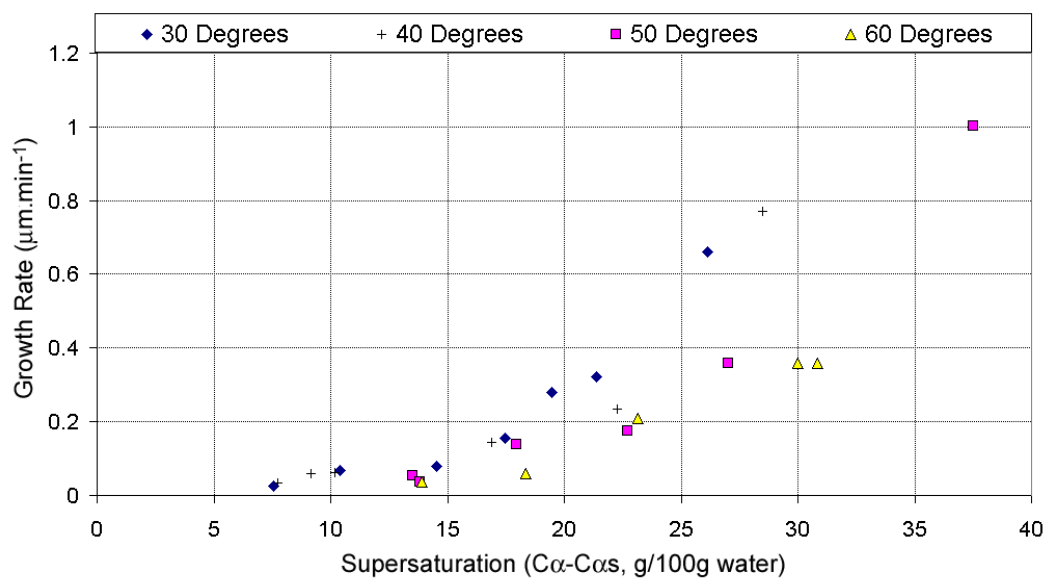


Figure 2-13 The effect of supersaturation on the  $\alpha$ -Lactose monohydrate crystal growth rate from (Shi *et al.*, 1989)

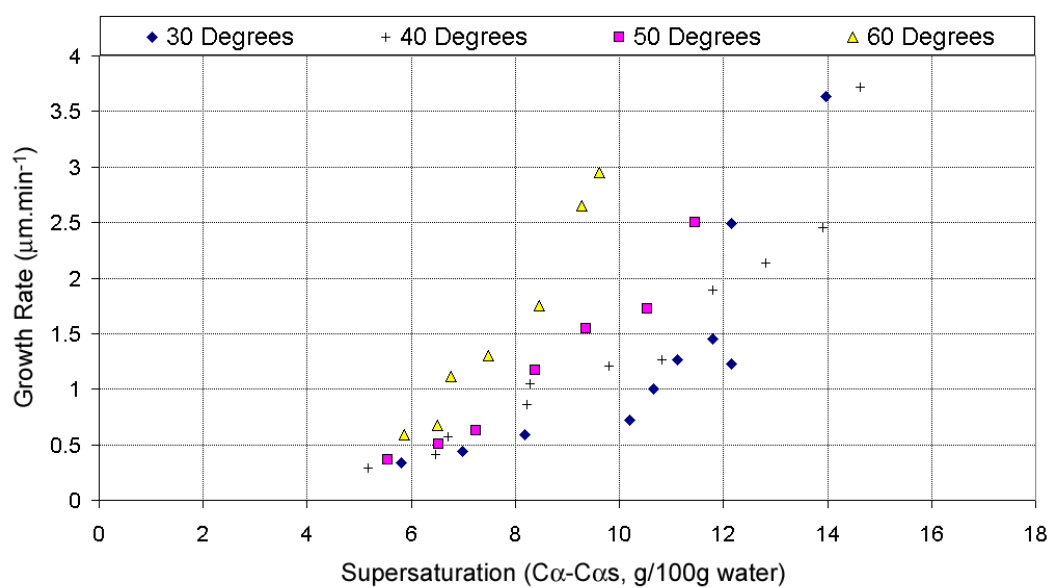
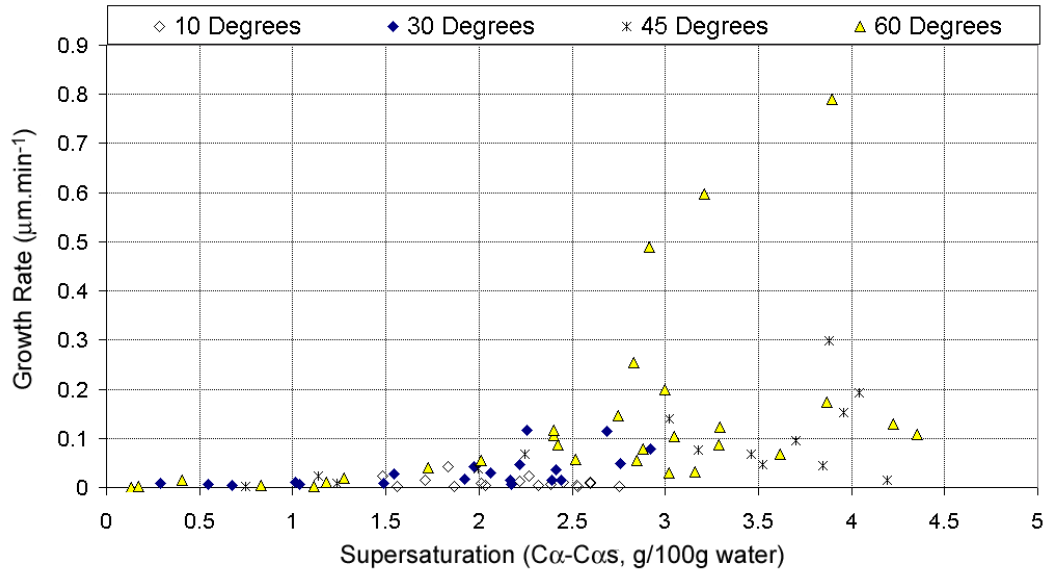


Figure 2-14 The effect of supersaturation on the  $\alpha$ -Lactose monohydrate crystal growth rate from (Shi *et al.*, 1990)



**Figure 2-15 The effect of supersaturation on the  $\alpha$ -Lactose monohydrate crystal growth rate from (Butler, 1998)**

The work of Butler, (1998) reported a growth rate equation developed from the data collected, this equation is presented as Equation 2-8.

$$G = k_g (C_\alpha - C_{\alpha s})^2$$

$$k_g = 0.00013T$$

**Equation 2-8  $\alpha$ -Lactose monohydrate growth rate reported by Butler, (1998)**

The equation presented by Butler, (1998) includes a temperature effect. In contrast with this, the results presented in Figure 2-11 to Figure 2-15 show no clear effect of temperature. All the data with the exception of Shi *et al.*, (1990) and three of the 60 °C data points from the results of Butler can be interpreted as demonstrating temperature does not significantly change the growth rate. This lack of agreement in the literature results requires more investigation. A study into the relationship between temperatures and the growth of  $\alpha$ -lactose monohydrate crystals will be carried out in this work.

### 2.4.3 Mixing

Mixing is the “third variable” in an industrial crystallisation over which some control is possible. Agitation acts to keep the crystals in suspension and maintains an even supersaturation throughout the crystalliser. Beyond preserving homogeneity and

suspending crystals, the effect of agitation on growth depends on the growth mechanism. For example if the incorporation of molecules on to the surface is the rate-limiting step then an increase in agitation will have only a limited influence the growth rate. Alternatively, if mass transfer to the crystal surface is controlling the rate of crystal growth then increased agitation will result in a faster growth rate. This is due to the increase in the relative velocity between the surface and the solution (Hartel & Shastry, 1991). The many factors such as Reynolds number, power input and mixing rate that need to be considered during scale up make mixings' effect much more difficult to model than that of supersaturation or temperature.

van Krevald & Michaels, (1965) investigated and compared the effect of no agitation with that of very gentle agitation on a rotating flask and found the growth rate of single crystals to be similar. Haase & Nickerson, (1966b) found that when crystals were agitated at a rate that kept them in suspension, the growth rate was increased due to the increased surface area available. When crystals are not suspended in solution only the surface layer is available for growth. Diffusion of  $\alpha$ -lactose was found to be rapid compared to surface integration provided that agitation was sufficient to keep the crystals in suspension (Thurlby, 1976). This suggests that if the crystals are agitated at a rate that keeps them in suspension, the mixing rate is not critical to growth. Despite this conclusion, additional investigation into mixing is needed and it will be examined as part of this study.

#### **2.4.4 Summary of literature**

The results from the literature demonstrate a need to investigate further the growth of  $\alpha$ -lactose monohydrate. The measurements in this study will help clarify how supersaturation, temperature and mixing alter the  $\alpha$ -lactose monohydrate growth rate. They will also provide a basis against which the industrial media growth measurements in chapter four can be compared.

### **2.5 Techniques for measuring crystal growth**

The literature contains numerous different techniques for measuring the growth of crystals in the laboratory. Many of the techniques have been used to measure the  $\alpha$ -lactose monohydrate growth rate. A background into the different techniques was

developed in a review of the literature. This information was then used to determine the most suitable method for measuring lactose growth in whey permeates. A summary of the methods from the literature is provided in the sections below.

### **2.5.1 Weight**

The crystal growth rate can be measured directly from the mass gained over a known time. The mass deposited is determined by weighing the crystals at time zero ( $t_i$ ) and any time after ( $t_{i+j}$ ). Thurlby, (1976) used weight to determine a growth rate for lactose in a lactose-water solution. The technique grew a small mass of crystals in a comparatively large volume of solution. The large solution to crystal mass ratio means that growth can be considered to occur at a relatively constant supersaturation. Use of the constant composition approach requires that a range of experiments at different supersaturations be carried out. This allows the effect of changing thermodynamic conditions (supersaturation) on the growth rate to be quantified (Achilles, 1997).

Determining crystal growth using weight change is dependent on being able to accurately determine the weight difference of the crystals before and after growth has occurred. A common source of potential error is that of additional mass. This can be introduced through the nucleation of new crystals, through the collection of other fine particles existing in the growth medium or through the presence of any remaining solution on the crystal surface. Removal or quantification of these errors needs to be considered if selecting this approach.

### **2.5.2 Concentration**

One alternative to measuring growth by weight change is to measure the change in solute concentration. This approach requires that the concentration can be measured accurately. It is also necessary to be able to quantify the effect any nucleation has in changing the concentration.

To overcome the nucleation problem Muhr, Leclerc, & Plasari, (1997) proposed using a crystal mass with a large surface area. The large surface area makes growth the dominant factor for the decrease in supersaturation. Additionally, the large initial surface area permits any surface area changes arising from growth or nucleation, to be assumed negligible. Validation of this assumption requires that the seed is reweighed

at the end of each experiment and that the mass change is no greater than 5 per cent; data which fall outside this criteria are discarded (Salvatori *et al.*, 2002).

The concentration of a solute in solution can be measured using a number of different techniques. Nine of these techniques are reviewed by Loffelmann & Mersmann, (2002) and reproduced in Table 2-2.

Technique	Method	Measurement
Acoustics	Ultrasonic	Sonic speed, phase shift
Chemistry	Titration	Concentration
Conductometry	Kohlrausch-cell, inductive measurements	Electrolytic conductivity
Gravimetric	Densimeter	Density
Optics	Refractometer, interferometer, polarimetry, turbidimetry	Refractive index, interference, rotation of light, turbidity
Physics	Viscometer, quartz-crystal oscillator	Viscosity
Potentiometry	Ion Specific electrodes, ion specific membranes	Ionic Conductivity
Radiometry	Nuclear Radiation	Adsorption Spectra
Spectroscopy	Spectrophotometry, infrared spectroscopy	Adsorption Spectra

**Table 2-2 Concentration measurement techniques (Loffelmann & Mersmann, 2002)**

Absent from Table 2-2 is a technique for determining the mass of dissolved solids in the solution (Mohameed, Abu-Jdayil, & Al Kateeb, 2002). A small sample of the solution is drawn through a micro screen to remove any solids in the solution. The sample is then left in an oven at 120°C until complete evaporation occurs, and then placed in a desiccator for cooling. The difference in weight before and after can then be used to evaluate the concentration. The solution composition is required to determine the concentration of the substance of interest. As crystallisation occurs the ratio of the solids in solution will change, this limits this approach to pure solutions.

#### 2.5.2.1 Water activity

Section 2.3 discussed that the fundamental driving force of crystallisation is the difference in chemical potential of the supersaturated solution and that of the crystal face (Kim & Myerson, 1996). The concentration difference between a saturated solution and the supersaturated solution are often used in place of the chemical potential, with the assumption that the activity coefficient of a supersaturated solution is equal to that of a saturated solution. This has the potential to cause errors when

evaluating the true kinetics of a crystallisation (Mohan & Myerson, 2002). Solute activity of the supersaturated solution can be computed from the water activity data using the Gibbs-Duhem relationship. Given this it becomes possible to establish a relationship between the water activity, the chemical potential and the concentration of a supersaturated solution (Kim & Myerson, 1996). Crystallisation can then be followed by monitoring changes in water activity.

Miracco, Alzamora, Chirife, & Ferro Fontan, (1981) found that the water activity ( $a_w$ ) of lactose in solution at 25 °C could be accurately predicted by Equation 2-9, when a  $Y$  value of 10.2 was used.  $X_1$  and  $X_2$  represent the molar fractions of water and solute, lactose, respectively.

$$a_w = X_1 \exp(-Y X_2^2)$$

**Equation 2-9 Prediction of the water activity of non-electrolyse solutions**

Using this prediction, the water activity of a saturated lactose solution at 25 °C is calculated at 0.987. This high value for water activity means that this technique would require a very sensitive water activity probe. Without this, the limited range over which the measurements would be taken would make the technique subject to large errors. The salts in whey permeates are likely to alter the water activity of the solution. This also makes the technique unsuitable for this study.

### **2.5.3 Heat of crystallisation**

Crystal growth is an enthalpic process that involves a change of state as material is adsorbed from the liquid into the solid form. This change of state results in an energy transformation as molecules leave the solution and new bonds are formed. Where it is possible to measure this energy and to account for any additional energy transfers, the rate of crystal growth can be determined calorimetrically. There are reports in the literature of this approach being used to measure crystal growth. For example the study by Darcy & Wiencek, (1998) where a differential scanning calorimeter (DSC) was used by to measure the enthalpies and growth kinetics of lysozyme crystallisation under isothermal conditions.

Lactose crystallisation from the amorphous form has been studied using a microcalorimeter to measure the heat released as the crystallisation occurs (Darcy &

Buckton, 1998). A microcalorimeter can measure very low heat flows. This characteristic makes it suited for measuring the energy transformation occurring during the growth of a lactose crystal. No literature could be found that used this apparatus for measuring crystal growth from solution. The absence of nucleation in this technique would be important, as any additional surface area created would exaggerate the results. This requirement limits the application of the method to supersaturations below the nucleation threshold. It would also necessitate pre-treatment of the crystals to prevent surface based nucleation events.

The microcalorimeter approach only examines the growth of a single crystal, meaning growth rate dispersion is not considered. This is a drawback to using results on the industrial scale. The technique may however prove useful for the examining how impurities change growth rates. Similar size crystals with an identical history could be grown in different media and their heat generation compared. The success of this would require understanding any additional reactions occurring in the medium.

#### **2.5.4 Measuring changing dimensions**

A microscope connected to a PC through a camera and a frame-grabbing device provides a simple way of observing the growth of single crystals over time. The growth of gypsum crystals was studied by Simeone, Palomba, & Volpicelli, (2002) using this technique. This technique allows the growth of individual faces to be observed eliminating the need for shape factors or assumptions of sphericity. The growth process can be observed in one of two ways, either through direct observation of the growth, or by removing the crystals from their growth medium, examining, and recording them at a series of time intervals. Direct observation makes a constant study of the growth possible and has the advantage that once set-up no further interference with the crystals is required. Its main limitation is the number of crystals that can be studied, making it susceptible to large variations from growth rate dispersion. Shi *et al.*, (1989) studied the formation and growth of lactose crystals, observing that mass transfer potentially limited growth of the crystal enclosed in a cell. Because lactose crystallisers in the industrial environment are agitated, results obtained from a technique where crystals have little if any agitation would have limited application on the industrial scale. Use of this technique also depends on clear

visibility in the growth medium. As whey permeate is opaque, measuring growth with this technique would be difficult.

An alternative to direct observation of crystals is to grow crystals in a crystalliser and then remove them periodically for examination under a microscope. This technique provides a better representation of the industrial environment than direct observation. The problems with this technique are alterations in the growth rate and damage to the crystals that may occur during their removal from solution. Such consequences can be minimised by only making examinations prior to and at the completion of a crystallisation. This approach removes the capacity to study the changes in the growth rate over the course of the crystallisation and may still present problems when removing crystals for the final examination.

### **2.5.5 Selection of a method for crystal growth measurements**

In determining the method to use for measurement of the growth rate of lactose crystals one of the central considerations was that the test could be used in the measurement of lactose crystal growth in concentrated permeate. A number of the methods are unable to cope with the opaque nature and existence of insoluble non-lactose fines in permeate concentrates. After considering these properties, it was concluded that the best way to measure growth was to monitor the weight change observed during crystallisation at constant supersaturation. Concentration was also considered as a method but was rejected given the possibility that lactose crystals may be subject to growth rate hysteresis. A description of growth hysteresis is provided in section 2.3.2.

## **2.6 Crystal growth experiments**

The lactose crystals used in the study were sieved out from a single sample taken from the large drier at the Fonterra Kapuni site. Lactose at this stage of the process has passed through a number of unit operations, including a continuous crystallisation, to give pharmaceutical grade purity, it is, however, unmilled. Sieves were used to separate out crystals of the size fraction 300 to 600  $\mu\text{m}$ . Crystals of this large size fraction were used as they were easily removed from any fine crystals that might have nucleated and grown during the experiments.



A large single sample was taken to allow all the crystals used in the growth experiments to be considered to have come from a “common” source. Common as defined in this work considers the container in which the crystals were stored as the point of common origin. In the work of Butler, (1998) common history describes crystals that are believed to have originated from a single nucleation event. The approach taken by Butler was not used, as it was not possible, under conditions where a single nucleation event could be guaranteed, to obtain a large enough mass of large crystals to carry out the number of experiments planned. In addition to this, because the crystals used in this study were obtained from a continuous crystallisation process, it was proposed that, despite the preselection of large crystals, a mix of fast and slow growers would be present in the crystals sample. This proposal is investigated in this chapter and in chapter three.

It is stated in section 2.5.1 that one of the problems with using weight as a technique to measure crystal growth rates is the potential for nuclei to form, giving an inflated result. To avoid this effect experiments need to be carried out at supersaturations below the nucleation threshold. This limits the range of supersaturations where growth can be measured. Higher supersaturations can be used when making growth measurements if a filter is used to collect the lactose crystals of interest and allow any nuclei to pass through. In this work, a 250  $\mu\text{m}$  sieve was used to remove any fine crystals.

### **2.6.1 Method**

In a 300 ml Schott Bottle 200 ml of lactose and water solution was prepared by dissolving a calculated mass of lactose into a calculated mass of distilled water. The lactose to water ratio was set at the concentration that gave the desired supersaturation at the temperature investigated. This solution was dissolved at 85 °C until no crystals were visible and then for an additional 15 minutes to ensure any “ghost” nuclei were dissolved. The hot solution was then filtered through a Whatman number one filter paper and then reheated to 85 °C for a further 15 minutes. The solution was then added to the preheated vessel used to grow the crystals. The vessel was then placed in a water bath where it was cooled to the temperature at which the growth experiments

were to be conducted, after which a singular mass of crystals was added. The mass of crystals added was between 0.4 and 0.5 grams. This represents approximately 5000 to 7000 crystals. The solution was continuously stirred for four hours, selected as it allowed two sets of experiments to be carried out in a day, whilst still allowing sufficient growth for a measurable mass change. The stirring rate was  $300 \text{ r}\cdot\text{min}^{-1}$ , this, as shown later in section 2.7.1, was the minimum rate required to keep the crystals suspended in the solution.

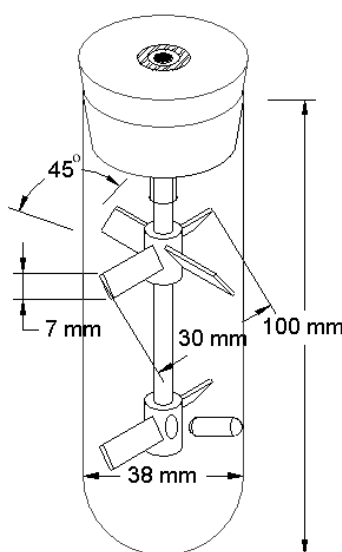


**Figure 2-16 Vessel used for laboratory scale growth rate experiments**

The growth vessel was designed so it could be used to measure growth in industrial permeate concentrates. It was found in preliminary experiments that removal of the crystals from the whey permeate concentrates was difficult if the entire volume of growth medium was passed through the  $250 \mu\text{m}$  filter. To overcome this, the solution was gently centrifuged to remove the crystals from the bulk solution. To avoid errors associated with transfer of the solution from a stirred vessel the vessel used was an 80 ml glass centrifuge tube. The agitator used was designed to fit inside a centrifuge tube. A magnetic flea inserted into the base of the stirrer provided the mechanism for driving the agitator when the vessel was placed on a magnetic stirrer plate. A diagram of the set-up used is presented in Figure 2-16.

After growth, the solution was gently centrifuged at  $2000 \text{ r}\cdot\text{min}^{-1}$  in a Heraeus Labofuge A for 60 seconds. Following centrifugation the bulk of the solution, about

90 per cent, was removed from the surface of the crystals, by syringing it off. A slightly supersaturated lactose solution, 23.75 g lactose per 100 g water, was used to wash the crystals from the centrifuge tube and on to the filter. Once on the filter, the crystals were washed further using the slightly supersaturated lactose solution to remove any fine particles. A final wash was carried out using a lactose-saturated ethanol solution. The lactose saturated ethanol solution was prepared by adding 200 g of lactose crystals to one litre of ethanol. The solution was then agitated at room temperature overnight to dissolve the lactose. Prior to use, any undissolved crystals were removed by passing the solution through a 0.45  $\mu\text{m}$  filter. Lactose has a much lower solubility in ethanol than it does in water. This property reduced the dissolved lactose remaining on the crystal surface. Without the ethanol-wash inflated weights, due to the presence of lactose in the solution remaining on the crystal surface, are obtained when the crystals are dried.

Once separated and washed, the crystals and dish were placed in an oven to dry at 80 °C for two hours. The dishes were then removed and placed in a desiccator for one hour to cool, they were then weighed and the weight compared to the initial mass of crystals added. This information was used to determine the growth of the crystals. The growth rate was converted from change in weight to  $\mu\text{m}\cdot\text{min}^{-1}$ . The conversion determined the increase in the mean initial particle diameter required to give the corresponding mass increase. The initial diameter used was that measured using the Malvern MasterSizer 2000 at the Fonterra Kapuni site. The MasterSizer used was set up for carrying out measurements on lactose crystals and the crystals were dispersed in isooctane.

At the beginning and conclusion of each test the dissolved solids concentration of the solution was measured using an Atago handheld refractometer. These values were compared and where this change was greater than 1° brix (approximately 1 g lactose per 1 g solution) the results were discarded, as it was deemed that the conditions no longer represented a constant supersaturation.

## 2.7 Results and discussion

### 2.7.1 Effect of agitation rate

The literature suggests that agitation rate is not important so long as the crystals are maintained in suspension. To verify this, a series of experiments were carried out. The measurements were made at 30 °C using a  $\alpha$ -lactose absolute supersaturation of 5.23 g per 100 g water (Relative supersaturation 1.53). The agitation rates studied ranged from 0 to 400  $\text{r}\cdot\text{min}^{-1}$ . The results are presented in Figure 2-17. Two replicates were carried out at each stirring rate, the exception being at 300  $\text{r}\cdot\text{min}^{-1}$  with eight experiments being conducted. The error bars show the standard deviation of the 300  $\text{r}\cdot\text{min}^{-1}$  data.

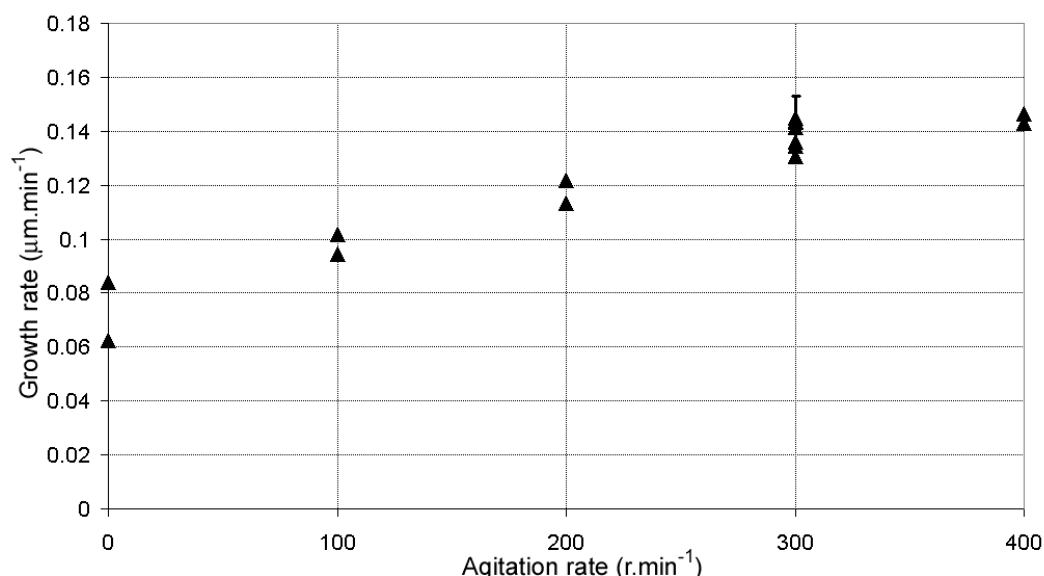


**Figure 2-17 The effect of the agitation rate on the growth rate of alpha lactose monohydrate crystals**

Figure 2-17 shows, in the absence of agitation, the measured growth rate is about a half the maximum observed at 300  $\text{r}\cdot\text{min}^{-1}$ . As agitation is progressively increased and more crystals are suspended the growth rate increases. The growth rate appears to reach its maximum at 300  $\text{r}\cdot\text{min}^{-1}$ . It was at this speed that all crystals were consistently suspended in the solution; prior to this a localised concentration of crystals appeared at the base of the vessel. This values correlates well with the calculated agitation speed of 228  $\text{r}\cdot\text{min}^{-1}$  required for suspending the crystals. This value was determined using Equation 2-10, a form of the Zweitering Equation

modified for a pitched blade turbine. The results in Figure 2-17 confirm the conclusion reached by (Haase & Nickerson, 1966b).

$$N_{js} = \left[ 2.27 \left( \frac{D_T}{D_{imp}} \right)^{0.83} \left( 0.7 \frac{I_c}{D_T} + 1 \right) \right] \frac{v^{0.1} d_p^{0.2} (g \Delta \rho_s / \rho_L)^{0.45} W_p^{0.13}}{D_{imp}^{0.85}}$$

**Equation 2-10 Modified Zweitering Equation (Armenante & Nagamine, 1998)**

The agitation rate is only one of many variables of that need consideration when transferring mixing results to different vessels. Because of this the rate reported here is specific to the system used. The requirement that to achieve maximum growth crystals need to be kept suspended should be applicable to all lactose crystallisations.

### 2.7.2 Effect of supersaturation

The relationship between the growth rate and supersaturation was investigated at 30 °C. This temperature was used so the results could be compared with the literature results in Figure 2-10. The absolute supersaturation range studied was 0 to 10.81 g  $\alpha$ -lactose per 100 g water (Relative supersaturation 1 to 2.05). Above this supersaturation significant nucleation of  $\alpha$ -lactose monohydrate occurred during the growth period. This altered the concentration beyond the point where a constant supersaturation could be assumed.

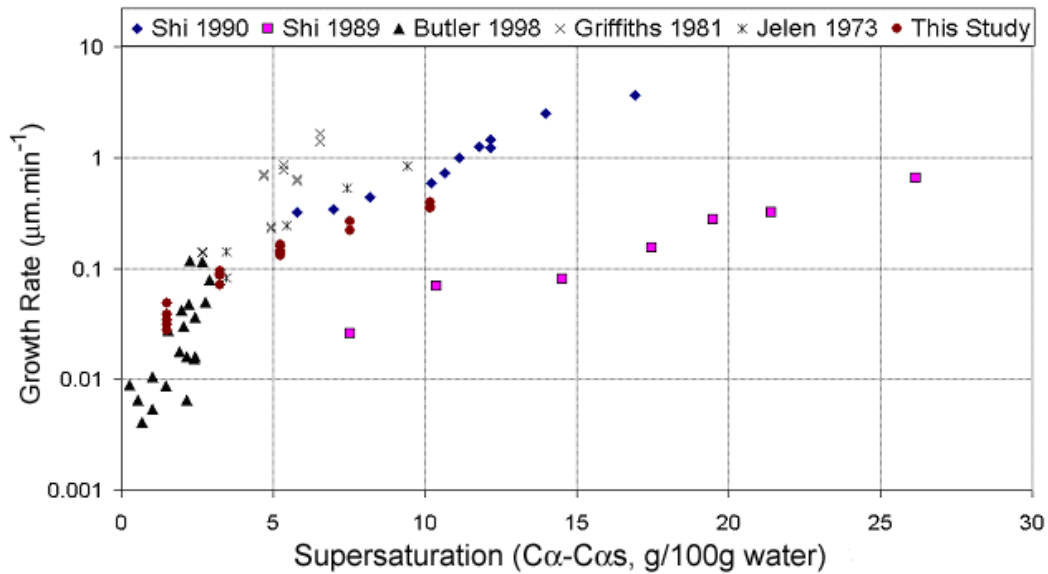


**Figure 2-18 Comparison of alpha lactose monohydrate crystal growth rates collected in this study with results reported in the literature**

The results collected from this study are plotted in Figure 2-18 against the literature results. The results in this work show a close similarity with the previously reported mass-average growth rate results. The work of Shi, (1989) is not considered because it uses a number average to report growth rate. It was therefore concluded that the experimental method used here provides an accurate representation of the lactose crystal growth rate.

To provide an alternative measure of the growth rate, two of the crystal populations from the growth rate tests were analysed using a Malvern MasterSizer 2000. The MasterSizer uses light scattering to determine the particle size and produces a size distribution where the diameter given is that of the equivalent sphere. The particle size distributions obtained from the MasterSizer are shown in Figure 2-19. The similarity of shape and lack of a secondary peak or fines tail illustrate the effectiveness of the sieving technique for eliminating any nuclei that form during the growth experiments.

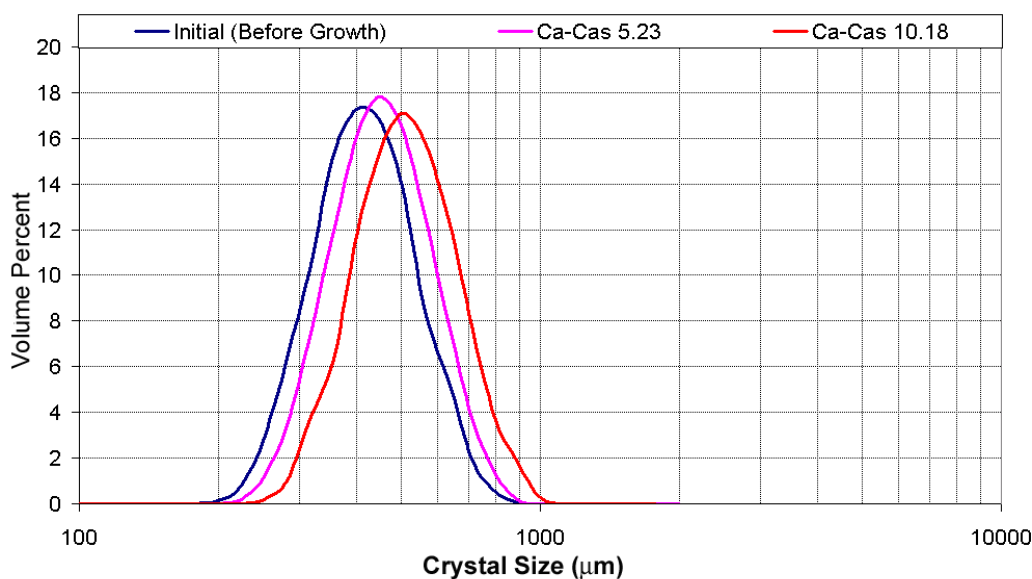


**Figure 2-19 Particle size measurements of  $\alpha$ -lactose crystals before growth and after growth of four hours at the supersaturations of 5.23 and 10.18 (g Ca-Ca<sub>s</sub> g/100g water)**

Reported in Table 2-3 are the mean [4,3] diameters, the volume weight particle size obtained from the MasterSizer. To compare the results from the two-growth rate measurement methods the crystals were assumed spherical. This assumption is incorrect but as the shape factor is constant, the calculations are unaffected. Taking the simplest approach, growth can be calculated from the difference between the final and initial volume weighted mean crystals sizes obtained from a MasterSizer and

dividing by the time over which the experiments were run (four hours). The comparison between the two sets of results is presented in Table 2-3.

Malvern					Weight Change		
Supersaturation g $\alpha$ /100g water	Initial Size ( $\mu\text{m}$ )	Final Size ( $\mu\text{m}$ )	Difference ( $\mu\text{m}$ )	Growth rate ( $\mu\text{m}\cdot\text{min}^{-1}$ )	M intl (g)	M Fin (g)	Growth rate ( $\mu\text{m}\cdot\text{min}^{-1}$ )
5.23	453	492	39	0.162	0.4285	0.5498	0.163
10.18	453	541	88	0.366	0.4234	0.7351	0.358

**Table 2-3 Comparison of growth rates as measured using laser diffraction and weight change**

The results in Table 2-3 show good agreement. This demonstrates that weight change can be used to show a change in crystal dimensions despite it not being a direct measure.

### 2.7.3 Effect of temperature

The relationship between temperature and the growth of  $\alpha$ -lactose monohydrate was studied over 5 °C to 60 °C. The range represents the typical industrial conditions under which  $\alpha$ -lactose monohydrate crystals are grown. Growth rate has been plotted as relative supersaturation in Figure 2-20 and as absolute supersaturation in Figure 2-21.

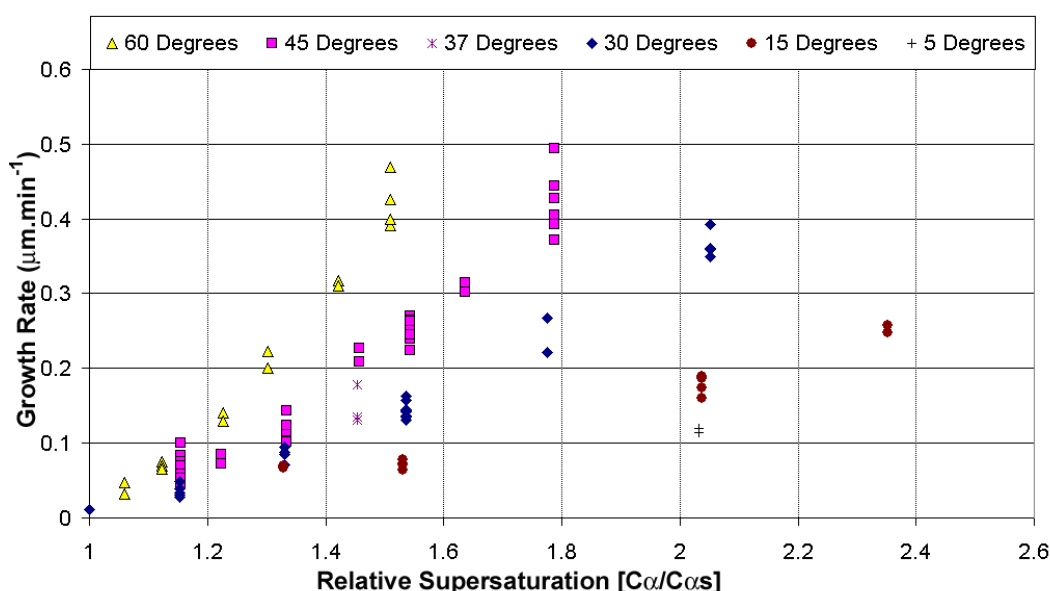


**Figure 2-20  $\alpha$ -lactose monohydrate crystal growth rate measurements obtained between 5°C and 60°C viewed from perspective of relative supersaturation**

Figure 2-20 shows that when viewed a function of relative supersaturation a significant temperature effect on the growth rate of lactose crystals appears. Some of

this is due the relationship between temperature and lactose solubility. To determine if temperature still affected growth when the solubility component was removed Figure 2-21 was plotted using absolute supersaturation.

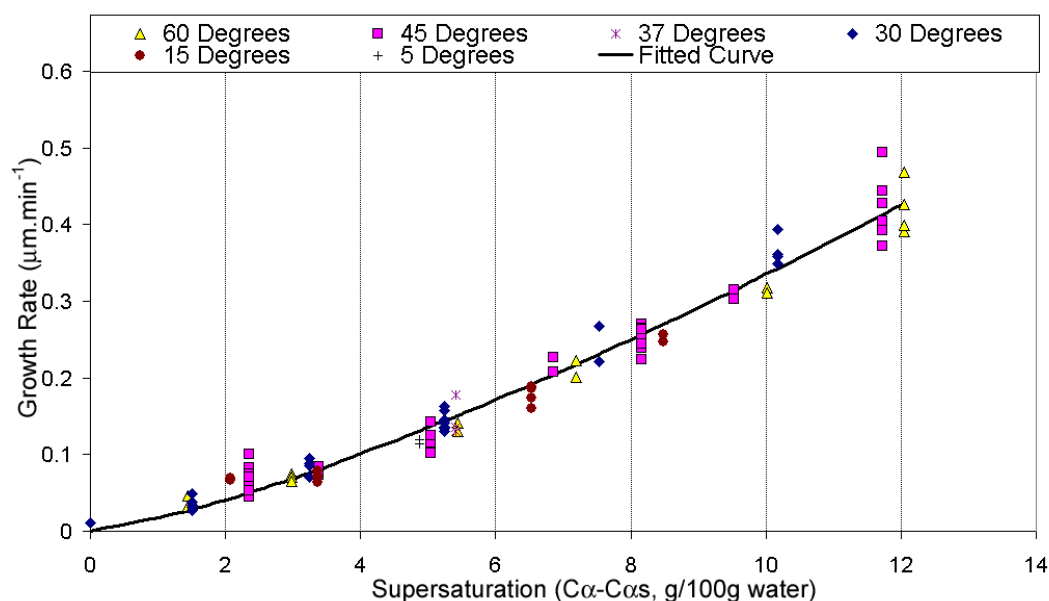


**Figure 2-21  $\alpha$ -lactose monohydrate crystal growth rate measurements obtained between 5 °C and 60 °C viewed from perspective of absolute supersaturation**

Figure 2-21 shows that excluding its effect on solubility temperature has no effect on the rate at which alpha lactose monohydrate crystals grow. A power curve was fitted to all the data using the program CurveExpert 1.3 and Equation 2-11 was obtained. This equation has a  $R^2$  value of 0.984.

$$G=0.0173(C\alpha - C\alpha_s)^{1.31}$$

**Equation 2-11 Growth rate equation developed from experimental work**

The influence of temperature can be studied by removing the effect of supersaturation. For the data collected in this study this was done, as shown in Equation 2-12, by dividing the measured growth rates by the supersaturation to the to the power of 1.31. The temperature independent growth rate values were determined from the data collected at temperatures of 15 °C, 30 °C, 45 °C and 60 °C. These conditions provided a reasonable temperature range and sample size. Table 2-4 shows the mean normalised growth rates, standard deviations and sample sizes. Using these values, the 95 per cent confidence interval range was determined for each temperature and from this the dependence of the growth rate on temperature was assessed.



$$N_{Grate} = \frac{M_{Grate}}{(C\alpha - C\alpha s)^{1.31}}$$

Equation 2-12 Equation used to normalise measured growth rates

Temperature	Growth Rate $\mu\text{m}\cdot\text{min}^{-1}/(C\alpha - C\alpha s)^{1.31}$	St.dev	n
15 °C	0.0171	0.0044	11
30 °C	0.0177	0.0028	26
45 °C	0.0180	0.0049	32
60 °C	0.0171	0.0034	16

Table 2-4 Normalised (as function of supersaturation) rates of crystal growth at 15 °C, 30 °C, 45 °C and 60 °C

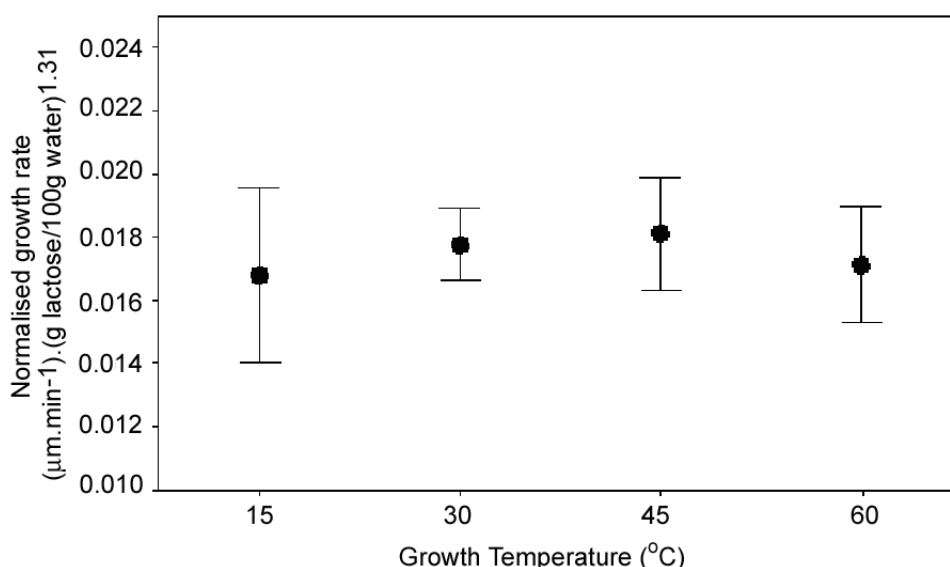
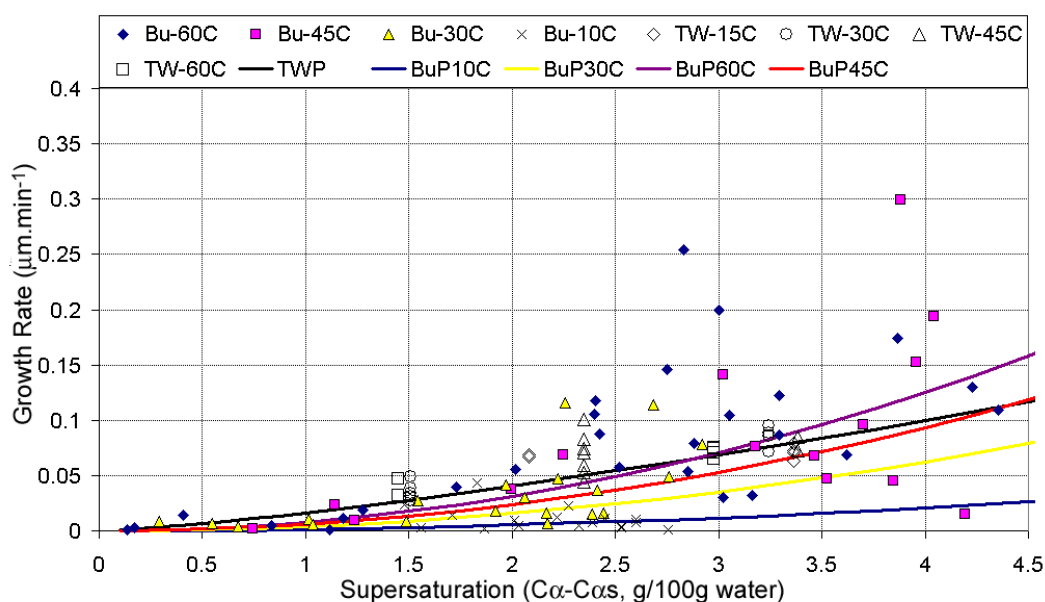


Figure 2-22 Mean normalised  $\alpha$ -lactose monohydrate crystal growth rates and 95 per cent confidence interval ranges

The results in Figure 2-22 show the effect of temperature on the  $\alpha$ -lactose monohydrate crystals growth rate to be statistically insignificant. This agrees with literature data that when viewed using absolute supersaturation, shows growth rate to be independent of temperature. As the results show growth to be unaffected by temperature provided absolute supersaturation is used, Equation 2-11 was accepted as the growth rate for the rest of this study

Butler, (1998) reported a temperature effect and incorporated this into Equation 2-8 given for growth. This equation was used by Werner *et al.*, (2002) when predicting the concentration profile of an industrial crystalliser. To establish if the exclusion of temperature from the growth equation creates an observable difference Equation 2-11

was compared against that given by Butler over a range of temperatures. Due to the method used, Butler was limited to an absolute  $\alpha$ -lactose supersaturation of about 3 to 4 g per 100 g water. The exact value depended on the temperature used. Consequently, any supersaturation outside this range represents an extrapolation of Butler's results.



**Figure 2-23 Comparison of data and predictions of  $\alpha$ -lactose monohydrate crystal growth rate from This Work (TW) and the work of (Butler, 1998) (Bu)**

Figure 2-23 shows the results collected in this study and the results collected by (Butler, 1998). Shown also are the predictions made using the growth rate equation of Butler and the prediction made using the equation developed within this work. The predictions have been limited to the range of supersaturations investigated by Butler. The equation developed in this work fits the data of Butler and the data from this work well. It predicts a faster growth rate than the equation of Butler at supersaturations 2 g  $\alpha$ -lactose per 100 g water and lower. Above this supersaturation, the difference between the two equations is dependent on temperature. Figure 2-24 compares the two equations over a supersaturation range greater than that investigated by Butler.

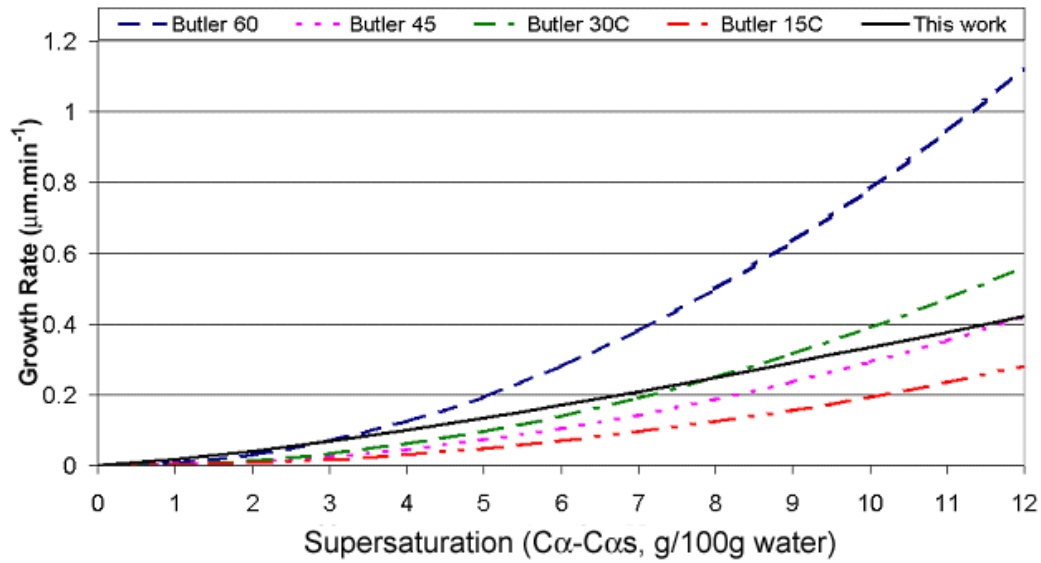


**Figure 2-24 Comparison of growth rate measured in this work with that where temperature is given as a variable (Butler using Equation 2-8, This work using Equation 2-11)**

Figure 2-24 shows that at the higher supersaturations the variation in the predicted growth rates becomes larger. At 60 °C the difference between the results predicted using Equation 2-11 and the result predicted by Butler, (1998) is more than twofold. This result shows that when extrapolated outside the supersaturation range for which it was developed the equation given by Butler becomes inaccurate. Where rapid cooling is desired this difference may be important when using growth to control supersaturation and minimise nucleation.

A second difference between Equation 2-8 and Equation 2-11 is the exponent term. In Equation 2-8 an exponent term of two was used by Butler, (1998) this compares with the value of 1.31 in Equation 2-11. It was stated in section 2.3 that under conditions where diffusion is the controlling mechanism for growth a linear relationship will be observed. Where the integration of the growth units on to the crystal lattice is the controlling factor a squared relationship will be observed. The mechanism controlling growth can change with changing levels of supersaturation a more linear growth rate is often observed at higher supersaturations, with a squared relationship being observed at lower supersaturation levels (Mohan & Myerson, 2002). This may explain why in the work of Butler, (1998) a squared term was found to give a close fit to the results obtained, yet when higher supersaturations were investigated in this work an exponent of 1.31 was obtained.

## 2.7.4 Effect of crystal size

One concern with the growth rate method used here was the use of crystals with a specific size range. Butler, (1998) asserts that where a group of crystals is removed from the bulk, the median growth rate will be a fraction of that observed in the initial distribution. Despite Shi *et al.*, (1989) demonstrating growth to be size independent, there was a concern that the selected large crystals in the growth experiment may have inflated the growth rates measured above what would have been seen had a sample representative of the total population been used. The crystals used in this work differ from the common nucleation seed used by Butler. The crystals in this study were from a continuous crystallisation process and will have nucleated at different times. This means that a larger crystal is not necessarily a fast grower, as would be the case if the crystals had originated from a single nucleation event.

To determine if using crystals from the upper end of the size distribution had biased the growth rate measurement towards fast growers a series of experiments were carried out using crystals from the same sample but from a lower size sieve fraction (212-250  $\mu\text{m}$ ). Three supersaturations and two temperatures were considered and multiple experiments were carried out at each condition.

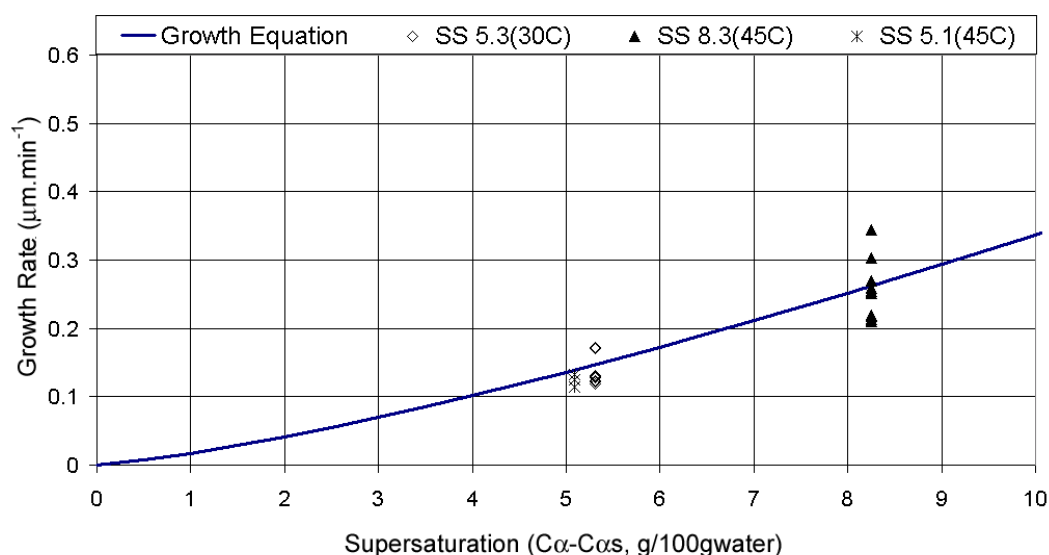


**Figure 2-25 Growth rate of 200-225  $\mu\text{m}$  lactose crystals compared against equation developed using growth rate results for 300-600  $\mu\text{m}$  lactose crystals**

The growth rate measurements carried out using the small crystals are presented, in Figure 2-25. The growth equation determined using the larger crystals is also plotted. The results show Equation 2-11 provides a good representation of the mean lactose crystal growth rate for the smaller crystals. It is therefore concluded that the equation developed from crystals selected from the continuous industrial crystalliser has not been biased towards faster growing crystals. The results also show that lactose crystal growth is size independent confirming the work by Shi *et al*, (1989).

## 2.7.5 Growth rate dispersion

Growth rate dispersion of lactose crystals growth was identified by Shi *et al*, (1989) and Butler, (1988). To investigate if this growth rate dispersion had been occurring during these studies the particle size distributions from Figure 2-19 were replotted on a linear scale in Figure 2-26.

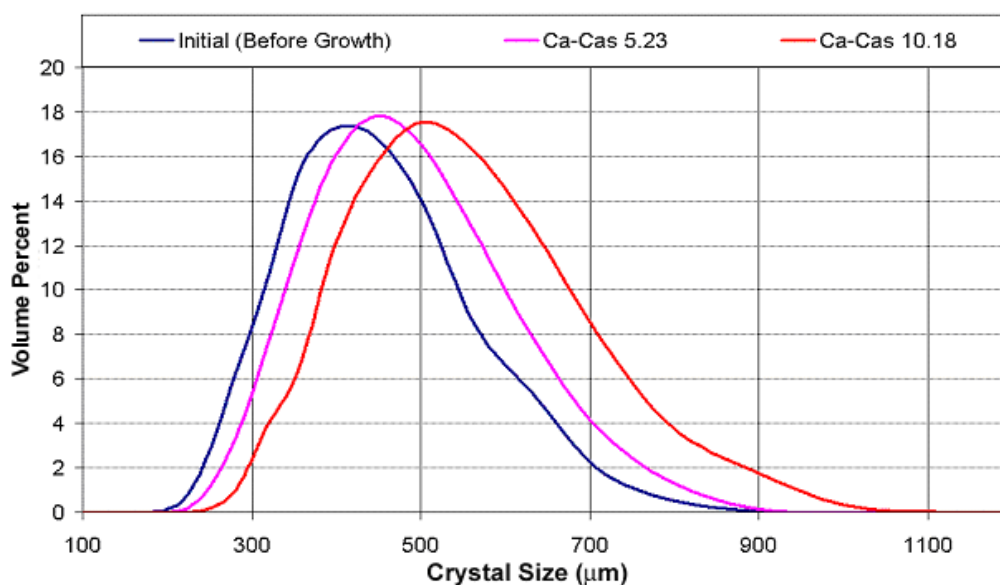
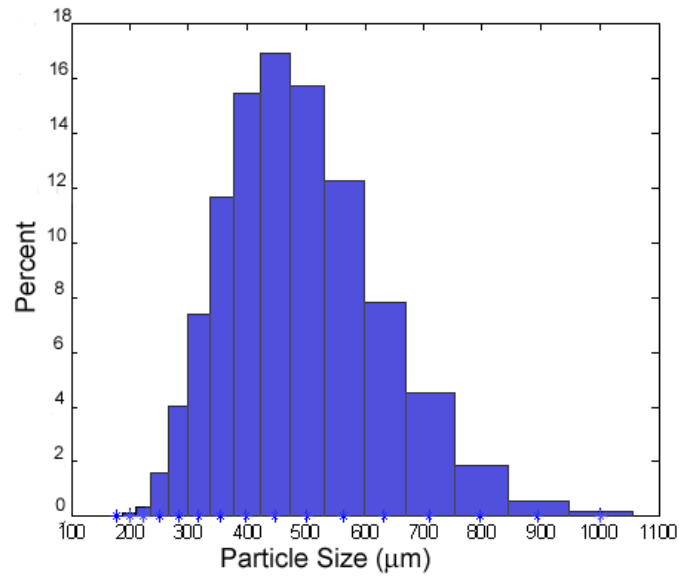


Figure 2-26 Particle size measurements of  $\alpha$ -lactose crystals before growth and after growth of four hours at the supersaturations of 5.23 and 10.18 (g Ca-Ca, g/100g water); expressed on linear scale

In Figure 2-26 it is not clear if growth rate dispersion has occurred. There appears to be a widening of the crystal size distribution, but this may be a consequence of the non-linear grouping of the crystal sizes. When classifying the crystals into their respective size fractions the Malvern MasterSizer 2000 uses a scale that increases at the rate of  $2^{1/6}$ . It can be seen in Figure 2-27, that using this classification, a wider range of crystal diameters is covered at larger size fractions.



**Figure 2-27 The crystal size distribution of  $\alpha$ -lactose monohydrate crystals before growth viewed as a histogram**

To better determine if growth rate dispersion was occurring, the growth of 100,000 crystals with a particle size distribution matching the initial size distribution measured by the Malvern was modelled using different growth conditions. The particle population was developed in MATLAB and a random normal distribution function was used to assign size values to each particle within the range of each bin size. The model was used to examine the scenarios of a constant single growth rate, and distribution of crystal growth rates set around a mean growth rate that was the same as the constant growth rate.

To study the dispersion of growth rates within the crystal population two distribution functions were considered. Firstly a log normal distribution was used; this represents the most commonly considered distribution function and is used by (Mitrovic, Zekic, & Petrusevski, 1999). Secondly a Weibull Distribution was used; this distribution is commonly applied in lifetime analysis, and the reasons for its use here are expanded below.

The Weibull distribution is named after Swedish physicist Waloddi Weibull, who derived it in 1937 and presented it in the paper, *A Statistical Distribution Function of Wide Applicability*. It has found wide use in the area of quality and production control for lifetime analysis (Dodson, 1994). The distribution is described by Equation 2-13. Where  $\beta > 0$  and  $\lambda > 1$  are the shape and scale factors respectively.

$$f(x) = \lambda \beta x^{\beta-1} e^{-\lambda x^\beta}$$

**Equation 2-13 Weibull distribution function**

One advantage of the Weibull distribution is that allows for censoring (Lawless, 2003). Censoring is a situation where part of a population has been removed due to its failure time being outside the range of interest. For example, items that have defects observed immediately after production are not considered as part of the population as they never entered the consumer market. It is easy to relate this to the situation where slow growing crystals are not considered due to their failure to reach the critical mesh size.

The use of the Weibull distribution has had considerable discussion in the field of forest science studying tree growth (Fleming, 2001), (Knowe, Ahrens, & DeBell, 1997) and (Hynynen J., Burkhart, & Lee Allen, 1998). The popularity of the Weibull function is due its shape factor, which manipulates the shape of the distribution as is shown in Figure 2-28.

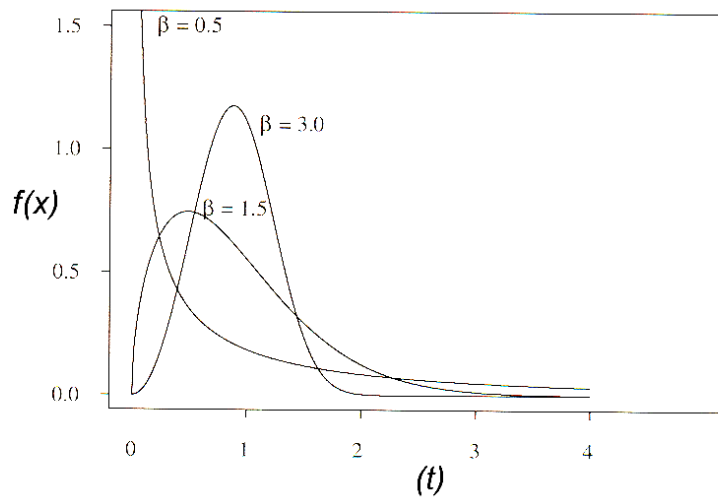


**Figure 2-28 Weibull distribution showing shape factors 0.5, 1.5 and 3.0 (Lawless, 2003)**

Figure 2-29 shows the best-fit predictions for the crystal size distribution after growth had occurred using the growth rate distribution models and a constant growth rate for all crystals. The best growth rate distributions were determined by running a loop in MATLAB to minimise the sum of the differences between the predicted and measured particle size distributions.

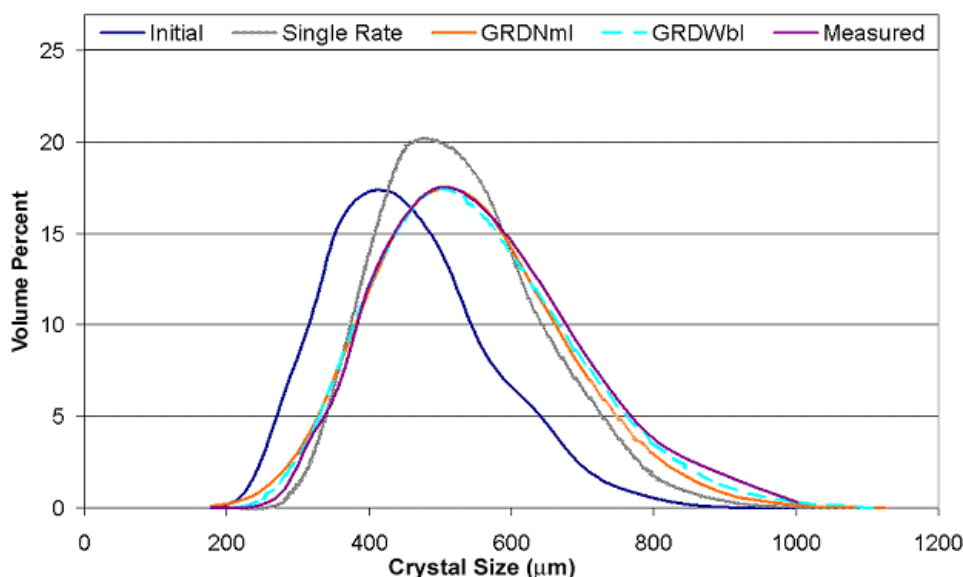


**Figure 2-29 Prediction of crystal size distribution using a single common growth rate and the two growth rate dispersion models**

Table 2-5 shows the best-fit parameters and the sum of their squares for each of the growth rate distributions. For the Normal distribution, the standard deviation was the variable manipulated to obtain the best fit. The best fit for the Weibull distribution was obtained by varying the shape factor. No use of the scale factor was made, as this would have shifted the mean growth rate. The growth rate is reported as a constant value specific to the supersaturation at which the crystals were grown.

Conditions	Growth Rate ( $\mu\text{m}\cdot\text{min}^{-1}$ )	Variable	Sum Diff <sup>2</sup>
Single rate	0.388	None	364.2
Log-Normal	0.388	St.dev - 0.431	7.72
Weibull	0.388	Shape F - 1.17	3.05

**Table 2-5 Parameters used in predicting final crystal size distribution**

It is observed that without growth rate dispersion the CSD prediction is less accurate. This observation shows that growth rate dispersion is a necessary component in a lactose crystallisation model, validating the work of Butler, (1998) and Shi *et al* (1989). The flexible shape of the Weibull model provides a more accurate prediction than the more rigid log normal distribution. This is demonstrated by the sum of differences squared value shown in Table 2-5 being the smallest for the Weibull model.



The Weibull shape factor of 1.17 is also of interest. In Figure 2-28 a shape factor of 1.5 shows a distribution that lacks a fines tail, indicating some censoring has occurred, this compares to a shape factor of three where a normal distribution appears. The shape factor of 1.17 would indicate that some censoring of slow growers has occurred because of the sieving of the crystals. This assumes that the crystal growth rate under standard conditions is log-normally distributed. The work by Butler, (1998) demonstrates this to be the case. The effect censoring of crystals of different sizes has on the shape of the growth rate distribution is an area where further work may be of interest.

## **2.8 Conclusion**

This section of work has provided a review of the literature on lactose crystal growth in a water solution. Carried out in conjunction with the review have been a number of experiments that have sought to validate the results reported by the literature. It has been found that when the work carried in the literature is viewed using common units the results are consistent. The results from this study are in agreement with the literature results.

One difference with that recently reported in the literature is the effect of temperature. In this work and in the majority of historical studies when they were viewed in terms of absolute  $\alpha$ -lactose supersaturation, apart from its affect on solubility, temperature has no significantly observable effect on the rate at which lactose crystals grow. This differs from the most recently reported equation for lactose crystal growth, Butler, (1998), where temperature was included as a variable. A comparison between the equation developed in this work and the equation previously reported found that at low supersaturations there was little difference between the results predicted. However, at higher supersaturations and temperatures, beyond the limits of Butler's equation, the difference becomes significant. The equation developed in this work, Equation 2-11, will be used to model lactose crystal growth in the remainder of this work.

Growth rate dispersion was investigated in this work and it was found to be a necessary factor in predicting the final crystal size distribution of a population of

crystals. In examining the effect of growth rate dispersion two distributions were considered, the first was a log normal distribution and the second a Weibull distribution. The best prediction of the measured final distribution was obtained using the more flexible Weibull distribution. This distribution accounted for the censoring caused by sieving out a particular size fraction of crystals.

The results from this chapter will be used as a basis against which lactose crystal growth in permeate concentrates can be compared. This is the focus of the next chapter.

## **Chapter 3 Industrial crystal growth rates**

### **3.1 Introduction**

Industrially lactose is extracted from concentrated whey permeates. The previous chapter characterised lactose crystal growth in lactose water solutions. Whilst understanding lactose crystal growth in water solutions is a useful place to start, it is important from the industrial perspective to identify any impurity driven change that occurs when crystals are grown in concentrated whey permeates. The effect of impurities on lactose crystal growth is reported in the literature (Visser, 1983), (Modler & Lefkovitch, 1986), (Bhargava & Jelen, 1996), (Nickerson & Moore, 1974), (Smart & Smith, 1991) and (Butler, 1998). Seasonal variations and different process streams make impurity concentrations in whey permeate variable. This means that a clear guide on the expected effect when lactose crystals are grown in permeates is unobtainable from the literature results. To accurately predict and model lactose crystal growth in permeate based on the impurity effect would require an investigation into the effects of all impurities and combinations of impurities encountered. It would require that the impurity levels are measured and monitored prior to and during the crystallisation.

Time pressures in the industrial environment prohibit detailed permeate testing prior to processing. This means that conditions are unable to be individually optimised on a batch-to-batch basis using impurity information. Taking a more realistic approach this study will identify growth variation through the measurement of crystal growth in the complete solution. This growth can be compared to a growth rate already well defined, lactose crystal growth in water. From this, the relative difference will then be used to adjust the predefined growth rate to account for the permeate composition. The adjusted growth rate will be a relative growth rate. This relative growth rate will be used to model the crystallisation in the industrial permeate.

## 3.2 Literature review

The influence of impurities on the crystallisation of lactose can be a factor of any or a combination of the following:

- A shielding effect on the crystal surface preventing incorporation of molecules into the crystal lattice
- Changing the supersaturation through affecting the solubility of the lactose
- Changing the viscosity and effective diffusivity of the solution
- Changing the rate of mutarotation, therefore affecting the availability of the  $\alpha$ -lactose molecule (Roetman, 1972).

Whey permeate contains many different impurities that could produce any of the effects given above. Table 3-1 provides an indication of these impurities and their typical concentration. The values were obtained from an analysis of the remaining liquor after a crystallisation had taken place. In addition to those listed in Table 3-1 impurities in the lactose crystallisation process may be additives to the process. One of these is the chelating agent sodium hexa-meta-phosphate, which some lactose processing plants add to reduce calcium fouling of the evaporators.

Component	Concentration (W%)
Total Solids	32.0-45.0
Total Lactose	12.2-19.7
Total Protein	3.1-5.0
Non Protein Nitrogen	0.4-0.7
Ash	7.5-12.1
Calcium	0.9-2.8
Magnesium	0.2-0.3
Potassium	2.2-2.6
Sodium	0.6-0.9
Chloride	1.5-2.3
Inorganic Phosphate	1.5-3.4
Sulphate	0.9-1.5
Lactate	0-2.9
Lipid	0.2-0.5

**Table 3-1 Components of the remaining liquor after lactose has been removed through crystallisation (Fonterra data, 2005)**

A detailed review of the numerous studies into the affect of impurities on the growth of  $\alpha$ -lactose monohydrate growth is provided in the work of (Butler, 1998). To show

the conflicting nature of the results some these are reported. The information has been divided up into two paragraphs; the first examines the studies into whey permeate systems; the second considers the individual components.

Butler, (1998) studied the growth of lactose crystals in simulated whey permeate (SWP) and found that growth was almost fifty per cent faster than had been measured using the same technique in water. The recipe for simulated whey permeate is given in appendix A1. Observed in this study was a seven-fold increase in the rate of mutarotation, but no change in solubility was observed. Studies in industrial permeate showed results consistent with those in the simulated whey permeate. Haase & Nickerson, (1966b) studied lactose crystallisation in permeate and water solutions and found that crystallisation occurs faster in permeate solutions. The study followed overall crystallisation rates through observing the concentration change. Using this approach it is difficult to distinguish if the faster crystallisation rates were a result of increased nucleation or growth or a combination of both. Bhargava, (1995) found the measured growth rate in three batches of whey permeates and a lactose water system to be the same. Smart, (1988) found that lactose crystallisation in whey and whey permeate was similar to that seen in a lactose water system.

The two main non-lactose components in whey permeate are proteins and salts. The removal of proteins from a whey solution was found by Nickerson & Moore, (1974) to increase the lactose crystal growth rate. Jelen & Coulter S.T., (1973) found that crystals in deproteinated whey grew at about 90 per cent of the rate observed for a pure solution. Kurimoto, Subramony, Gurney, Lovell, Chmielewski, & Kahr, (1999) showed that during growth protein can be incorporated into the  $\alpha$ -lactose monohydrate crystal structure. Impurities can also hinder upstream processing, Modler & Lefkovitch, (1986) found excessive whey protein denaturation increased the viscosity of the mother liquor, decreased the lactose crystal size and made crystal washing difficult. How salts change the lactose crystal growth rate is dependent on the type and concentration of salt. A growth rate three times greater than the control was observed for a ten per cent calcium chloride ( $\text{CaCl}_2$ ) impurity level. The morphology was also changed, with the crystals showing a considerably flatter base. The formation of a calcium and lactose complex was recorded by Herrington, (1934b)

and by Charley & Saltman, (1962). The lactose crystal yield was found by Guu & Zall, (1992) to be affected by the presence of the minerals in sweet whey and skim milk. The two most important minerals were potassium and sodium. The depletion of these monovalent ions by nanofiltration membrane resulted in an increased efficiency of the lactose crystallisation. Mikkonen, Helakorpi, Myllykoski, & Keiski, (2001) compared lactose crystallisation in whey permeates and in nano-filtered whey permeates. They found the yield in the nano-filtered permeate was increased by six percent. The nano-filtered material was concentrated to a higher solids concentration. Because the salts were removed during the filtration step the increase in yield may have resulted from the higher lactose concentration rather than any growth rate changes.

Reactions that occur during the lactose crystallisation process can lead to the creation of impurities initially nonexistent in solution. Maillard Browning is one of these reactions. Maillard Browning provides a simplistic description of a complex series of reactions involving the reaction of free amino groups with carbonyl compounds, particularly reducing sugars (Fayle, 1998). The development of a yellow-brown colour is observed when proteins are heated in the presence of reducing sugars (Fayle & Gerrard, 2002) and (Stockman & Weerakkody, 2000). Whey permeate contains the reducing sugar lactose and a number of proteins. This makes it an ideal substrate for Maillard Browning. The reactions are unlikely to significantly change the concentration of the lactose in the solution. Where Maillard Browning may the effect crystal growth is through any reaction that occurs on the crystals surface. A review of the literature has been unable to find any information on this.

On the industrial scale  $\alpha$ -Lactose monohydrate crystal growth has been modelled by Bulter, (1998) and Werner *et al.*, (2002). Both these studies compared the prediction of their respective models with crystal growth as it occurred in industrial crystallisers. Werner compared a growth rate model against a measured industrial concentration profile. The crystallisation process studied has most of the nucleation occurring during the evaporation stage and consequently the model used did not include a nucleation component. The large number of crystals, and consequently large amount of crystal surface area, entering the crystallisation vessel meant that little individual

crystal growth occurred and the potential for nucleation to have a significant effect (relative to growth) on changing the concentration was minimal. This made it the ideal environment for studying growth as it occurs on the industrial scale.

The study by Werner *et al.*, (2002) reported a difference in the modelled lactose removal rate and what was measured in the industrial crystalliser. The growth rate used in the model was the one reported by Butler, (1998) for a lactose water system. To explain the difference it was hypothesised that growth rate in the whey permeate studied must have been significantly lower. To eliminate the difference the growth reported by Butler reduced by a factor of fifty and it was assumed that in the concentrated permeate the growth rate was fifty times lower. No study examining the growth of crystals in the whey permeates was carried out to validate this hypothesis. This large variation in growth is not reported in the literature growth studies. The two different predictions compared against the measured results are presented in Figure 3-1. Where the growth rate of Butler is used, a rapid drop in the lactose concentration is predicted. This sudden drop was unseen in the measured results and was eliminated by the reduced growth rate.

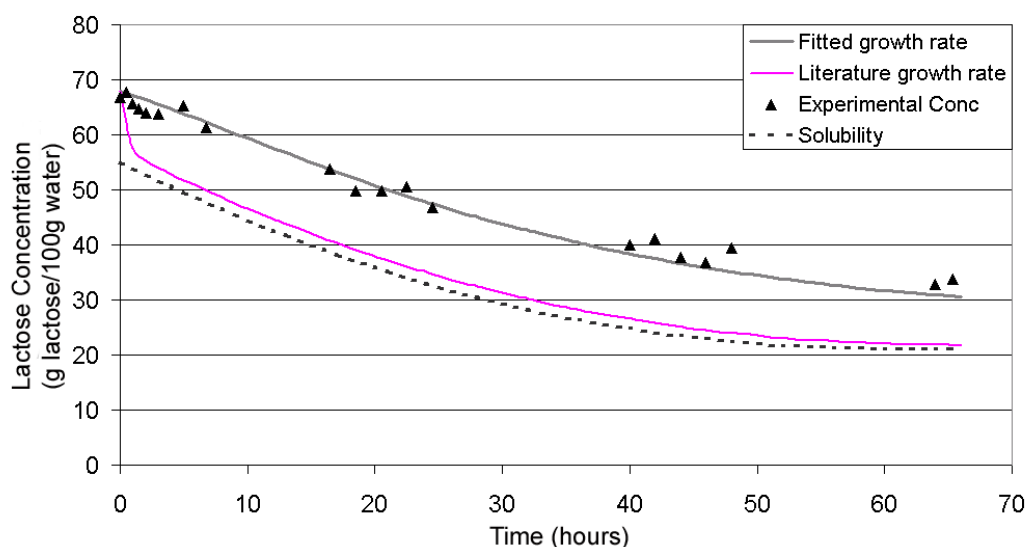


**Figure 3-1 Lactose removal from concentrated permeate solution in an industrial crystalliser as measured and predicted by Werner *et al.*, (2002)**

Butler, (1998) measured three industrial crystallisation concentration profiles, each profile was from a different lactose plant. The approach to nucleation in the plants studied is believed to differ from that used in the plant studied by Werner *et al.*, (2002), with nucleation occurring in the crystallisation vessel during the filling or cooling process. The results from Butler have been scanned from the original work

and are reproduced as Figure 3-2 to Figure 3-4. The exact values for time and concentration were excluded from the original work for confidentially reasons. It was stated that this data was collected over 24 hours. This represents the time required to cool each crystalliser. A much longer time of 68 hours was seen in the results from Werner. This increase in time is a consequence of a different cooling technique and a much larger crystalliser volume. The crystallisers sampled by Butler are reported as 20-35 m<sup>3</sup>, while the crystalliser sampled by Werner was 130 m<sup>3</sup>.

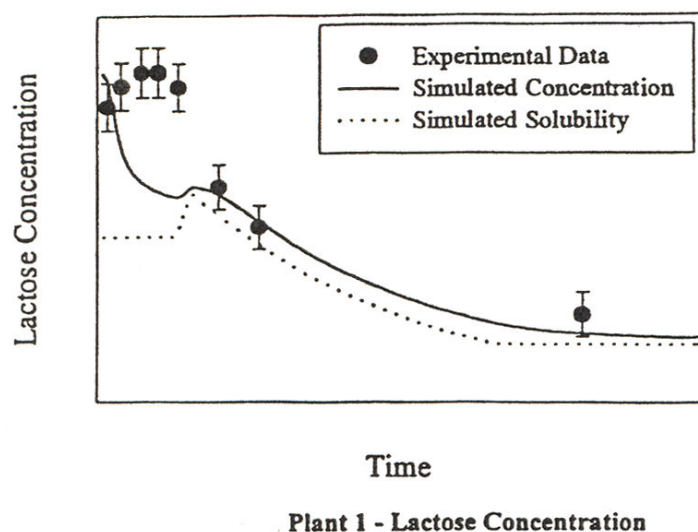


Figure 3-2 Crystallisation profile one, from Butler, (1998) no scale provided

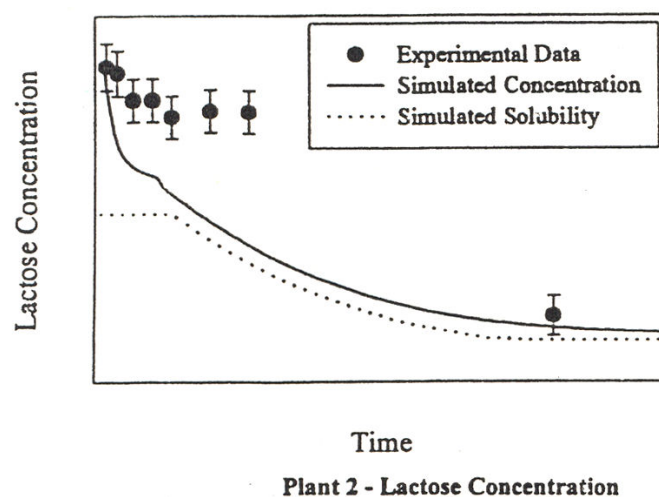
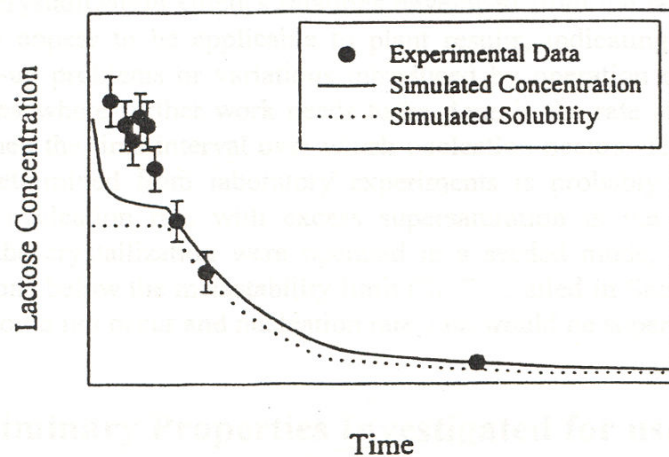


Figure 3-3 Crystallisation profile two, from Butler, (1998) no scale provided





**Plant 3 - Lactose Concentration**

**Figure 3-4 Crystallisation profile three, from Butler, (1998) no scale provided**

In the three profiles presented by Butler, (1998) the measured change in lactose concentration lags behind the predicted concentration at the beginning of the growth process. This trend was also observed by Werner *et al.*, (2002). Unlike the work of Werner the predictions of Butler include a nucleation component in the model. This equation, developed in the same study, was for nucleation of lactose in water. The inclusion of the nucleation equation may be why the initial over prediction occurred. This was unable to be confirmed, as the lack of information prevents a further study of the results using different modelled scenarios.

In the profiles presented by Butler, (1998) eventual agreement occurs between the measured and predicted results. In this regard the results differ from the results seen by Werner *et al.*, (2002) who found a discrepancy between the measured and predicted concentrations throughout the measurements. This discrepancy was accounted for by reducing the growth rate. It is equally well explained by an increase in solubility for lactose in permeates.

As stated in the later stages of the studies done by Butler, (1998) there was good agreement between the predicted and measured values and the model closely follows the concentration profile. This agreement of the predicted and measured data in the results of Butler can be explained by the occurrence of a nucleation event at some point in the process. For plants one and two, the lactose concentration change during the early measurements is small, and then a sudden decrease occurs. This sudden

decrease signifies a nucleation event has occurred. In the case of plant three, lactose removal from solution occurs immediately, indicating that crystals had formed prior to cooling.

The suitability of the growth model at higher supersaturations remains untested in the results of Butler, (1998). In all three cases the model was only tested where the concentration falls close to the solubility line. The governing factor in this case is likely to be temperature change decreasing the solubility and making more lactose available. An over prediction of growth will therefore be concealed as it is constrained by the temperature effect. The same result is seen in the data of Werner *et al.*, (2002) where, using the original growth rate, once the solubility is reached the results follow the measured profile.

When using the model for optimisation, the difference between the measured and predicted results at the beginning of the crystallisation event is a problem. At the start of the crystallisation the lactose concentration is the highest. If growth of the crystals provides insufficient lactose removal, cooling at this point could lead to unwanted nucleation. Of additional concern is the limited information on industrial lactose crystal growth at high supersaturation. Studies up to now have occurred at conditions where an over prediction of the growth rate can be hidden by lactose availability acting as a constraining factor. To address these concerns further studies of lactose crystal growth in the industrial environment are required. The second part of the experimental work in this chapter will address this need.

### **3.3 Measuring lactose crystal growth in permeates**

#### **3.3.1 Lab scale investigation**

This work set out with three intentions; the first was to compare the growth rate of alpha lactose crystals in whey permeate with the growth in water. Chapter 2 presented the growth rates for  $\alpha$ -lactose crystals in supersaturated lactose water solutions. The second was to identify the level of variation between the permeate batches and the third was to use the growth rate measured for a particular batch of permeate as a tool for improving the accuracy the growth model in predicting lactose

removal from whey permeate on the industrial scale. This section describes the methods used to collect this information.

### 3.3.1.1 Growth rate measurement

The experimental method used for measuring the growth rate of lactose in permeates is similar to the one described section 2.6 for measuring growth rates in water. The method was selected, as the lack of visibility and the presence of particulate material that makes the separation of the crystals from the bulk solution were not limiting using this technique.

Measuring growth rates in permeate is made difficult by the fact that the medium already contains an undefined mass of dissolved lactose. This means that unlike water, preparing a permeate solution with a defined lactose concentration is more complicated than weighing out a mass of lactose and dissolving it into the correct mass of solvent. For each series of permeate growth-rate-measurements, two litres of permeate was removed from a crystalliser at the Fonterra Kapuni site. The sample was collected at the end of the cooling process and included a mixture of crystallised lactose and mother liquor. Taking the sample at this point allowed conditions closely resembling those in the crystalliser to be achieved. This was achieved because the reheating process redissolved any other soluble material. After removal from the crystalliser, the sample was placed in a stirred vessel and chilled to 5 °C for a period of at least 48 hours. This removed additional lactose from solution through crystal growth. The removal of lactose from the solution increased the range of concentrations over which growth could be investigated. Chilling was longer where experiments had to be carried out over a series of days. The vessel used was sealed to minimise changes in the solids content of the sample resulting from evaporation and condensation.

Following the chilling period, 200 ml permeate samples were taken and placed in conical flasks sealed with rubber bungs. These samples were then agitated and heated to a preselected temperature for 12 to 16 hours. This process dissolved the lactose crystals in the permeate concentrate up to the solubility point at the selected temperature. The system was found to reach stability within 12 hours. Stability was determined to have occurred when a constant dissolved solids (brix) value was

recorded over a two-hour period. The dissolution temperature was used based upon the solubility temperature for a concentration of a lactose-water system previously investigated.

At the completion of the dissolution period, the sample was removed from the conical flask and added to MSE Basket 300 Centrifuge. The basket centrifuge was used to separate the bulk of the remaining undissolved crystals from the liquor. Any fine material left by the basket centrifuge was removed by centrifuging the liquor collected in a Heraeus Labofuge A centrifuge for 120 seconds at  $3000 \text{ r.min}^{-1}$ . The supernatant from this centrifugation was then carefully syringed off the surface and added to the vessel used for growth, shown in the previous chapter as Figure 2-16. The solution was then cooled to the temperature at which the growth measurement was to be conducted. Once the temperature was achieved the presieved crystals, from the same sample used in chapter two, were added and, as per the method described in section 2.6, left to grow for a period of 240 minutes. The technique used for recovery of the crystals and determination of the growth rate was the same as described in section 2.6.

### 3.3.1.2 Solubility and concentration measurement

Because lactose supersaturation is the dominant factor determining the growth rate, each permeate growth rate measurement was determined from measuring the lactose solubility in permeates at the temperature where growth was conducted and at the temperature used to dissolve the lactose. The lactose concentration in permeate was measured using High Pressure Liquid Chromatography (HPLC). The HPLC used for the analysis was a Waters 590 with a Waters 2410 RI detector and a Phenomenex NH 2-5 column. In preparation for HPLC measurement the permeate liquor samples were centrifuged in Heraeus Biofuge 13 centrifuge at  $13,000 \text{ r.min}^{-1}$  for two minutes. The supernatant was then collected and diluted to bring the concentration within the ideal range of the HPLC, which was 0.4 to 1.2 g per 100 ml solution. To achieve a concentration within this range the solids concentration of the supernatant was measured using an Atago hand held refractometer. Once the dilution ratio had been determined, a mass of the sample was added to a mass of hot distilled water (80 to  $100^\circ\text{C}$ ) up to 100 ml. The hot water was used to redissolve any fine crystals. The final mass was recorded to allow the back calculation of the initial lactose concentration. The diluted sample was left to cool to room temperature, a 3 ml sample

was then taken and recentrifuged to remove any fine solid material remaining. The sample was then placed in a small vial in the HPLC for analysis.

Determination of the lactose concentration as grams lactose per 100 grams water required knowing the total solids of the diluted liquor samples. Total solids were measured by adding 4 to 5 ml of the sample from the Heraeus Biofuge 13 centrifugation to a steel pan. Prior to use, the steel pan was dried in an oven and left to cool to room temperature in a desiccator. The sample and pan were placed in an oven at 102 °C for 120 minutes. After 120 minutes, the pan was removed and cooled to room temperature in a desiccator. The difference between the dry and wet weight was used to determine the total solids of the sample.

### 3.3.1.3 Effect of crystal origin on growth

The majority of work in this section has studied the growth of refined lactose crystals in permeates. To gain a more complete picture it was important that the growth of lactose crystals precipitated in permeate was considered. The need to measure the growth of crystals precipitated in permeate was based on the idea that it is the initial nucleation event that determines the rate at which a crystal grows. This idea is one explanation for growth rate dispersion, as all crystals nucleate under different conditions even if the difference is just their location in the solution. If the initial nucleation event does determine a crystals growth rate then it is equally possible that crystals nucleating in permeate, where a large range of impurities are present, will have different growth rates to crystals which have nucleated in a lactose water solution.

Crystals for the growth rate measurements were collected from the dryer of an edible lactose manufacturing line. These crystals had nucleated in a permeate solution and remained in this unrefined state. The crystals were sieved to create a size fraction of 300-600  $\mu\text{m}$ . This is the same size fraction used for most of the measurements in chapter two. The method used to measure the growth rates of these crystals was the same as the one used in chapter two. All the measurements were made in a lactose water solution. In addition to measuring the growth rate using mass change, crystals were collected from some of the growth measurements and the particle size distribution of these crystals was measured using the Malvern MasterSizer 2000.

### **3.3.2 Industrial scale measurements**

The second objective in this chapter is to compare the results collected on the laboratory scale with lactose growth in the industrial environment. To do this the growth of lactose in an industrial environment needed to be measured. Described in this section are the methods used to collect this growth information.

#### **3.3.2.1 The industrial crystallisers studied**

The crystallisers used for the collection of the growth rate data were the RC crystallisers at the Fonterra Kapuni site. The RC is short for Refined Crystals. After exiting the RC's the lactose crystallised undergoes further processing to produce a refined grade with a higher purity. The RC crystallisers, when full, contain 130,000 litres of concentrated permeate. The crystallisers are sited outside the main processing plant and are therefore exposed fully to the Taranaki weather conditions. The filling process takes six to seven hours. Concentrated whey permeate is pumped from the evaporator at 70 to 73 per cent solids and 60 to 65 °C.

The concentrated permeate is cooled by passing a film of cooling water down the outside of the vessels. This process started after the filling of the crystallisers was complete. The cooling water used to cool the crystalliser is open to atmosphere, surrounded only by a wind jacket that prevents water being blown from the crystalliser wall. Cooling is therefore achieved through a combination of evaporative and conductive cooling. The cooling process takes approximately 72 hours. During the peak of the dairy production season, capacity in the plant is at a premium. As a result, crystallisers are often emptied prior to the completion of the 72-hour period to make room for incoming permeate concentrate. This is reflected in some of the results presented with sample periods finishing before the full 72 hours.

#### **3.3.2.2 Measurements collected**

The study of the industrial crystallisation process looked to compare the industrial results with the predicted results gained from the model of the growth process. The models prediction is only as good as the inputs given to it. The important inputs are the temperature profile, the initial conditions for lactose concentration in solution, the

initial lactose mass crystallised and the initial size distribution of crystallised lactose. The last two measurements are used to determine the surface area for growth.

Temperature was measured using a Brannan mercury bulb thermometer. This measurement was taken immediately following the withdrawal of the sample from the bulk solution in the crystalliser and was found to give the most accurate information with regard to the sample. Temperature was also monitored using the instrumentation installed in the crystalliser. It was assumed that crystallisers are well mixed and therefore the reading was considered representative of the whole crystalliser. Measurements to confirm this assumption were unable to be carried out.

The lactose concentration was measured by the removal of a sample from the top of the crystalliser. A sample cup attached to a chain was dropped approximately one metre below the surface of the permeate concentrate. The exact depth depended on the level to which the crystalliser had been filled. The sample container used to transfer the liquor back to the laboratory was insulated to reduce heat loss and minimise any additional growth or nucleation.

To remove the majority of the crystals from the liquor, the sample taken from the crystalliser was placed in a Heraeus Labofuge A Centrifuge and spun at  $4500 \text{ r.min}^{-1}$  for five minutes. The supernatant was then drawn off the top and re-spun in Heraeus Biofuge 13 centrifuge at  $13,000 \text{ r.min}^{-1}$  for two minutes. This second centrifugation removed any fine lactose crystals remaining in the supernatant after the initial centrifugation. It is believed that these fine crystals may have resulted in an overstating of concentration in the work by Werner *et al.*, (2002). If this were correct it would partially explain the slow growth rate observed, relative to that reported by Butler, (1998), and failure of the system to reach equilibrium.

Four to five grams of supernatant from the second centrifugation was carefully withdrawn from the tube using a syringe and added ten to fifteen grams of distilled water. The dilution allowed the sample to be stored in a fridge at  $4^\circ\text{C}$  without crystals precipitating out. Storage times varied from one to two days depending upon the availability of the HPLC for analysis. The lactose concentration was measured using

the HPLC method described in section 3.3.1.2. A measurement of the total solids was also made. This used the method described in section 3.3.1.2.

To provide a value for the determination of initial crystal surface area a 5 ml sample of the permeate concentrate at the beginning of the crystallisation was added to a Coulter LS1000 with methanol filled hazardous fluid module. This was used to measure the particle size distribution of the crystals. To determine the concentration of crystals in the solution a 75 g sample of the liquor was spun at  $4500 \text{ r.min}^{-1}$  for five minutes in a Heraeus Labofuge A Centrifuge. The supernatant was removed and the separated mass of crystals was placed in an  $80^\circ\text{C}$  oven for three hours. Once dried the sample was reweighed. The value of the dried crystal mass divided by the mass of the initial sample was used to determine the ratio of crystals to solution. This value and the particle size distribution were used to determine the surface area for crystal growth.

## 3.4 Results and discussion for laboratory measurements

### 3.4.1 Solubility

As part of the growth rate testing a measurement of the lactose concentration in the sample used for growth and at the growth temperature was made. This data was used to determine the lactose solubility in permeate at different temperatures. The results are shown in Figure 3-5 alongside the lactose water solubility curve.

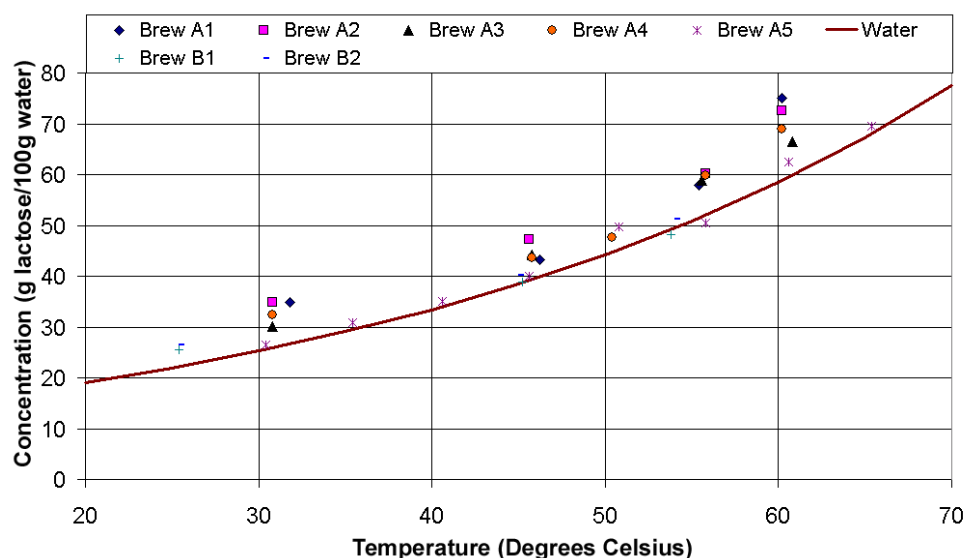


**Figure 3-5 Solubility of lactose in permeate: measured for different batches of permeate (A represents plant A, B represents plant B)**



The solubility of lactose in permeates at plant A was higher than that determined for water, the reason for this increase in solubility is unknown and may warrant further investigation. There was one exception to the permeate concentrate batch five, closely followed the lactose water solubility prediction. Batch five was manufactured at the end of the production season. Owing to a low volumes of permeate entering the plant at this time, more wash water from upstream processing was recycled back into each permeate concentrate batch. It is proposed that this diluted the impurities responsible for the increased solubility seen in the other batches. The same effect is seen at plant B which concentrates permeates to lower total solids than plant A. This means that more water was present in the solution and the impurity concentration is lower. This is supported by the results in Table 3-2 that show lower non-lactose solids in permeate concentrate results in solubility closer to that measured for water. The results are for a temperature of 45 °C as this was a common measurement point.

Batch	Non-lactose solids (g/100 g water)
A1	33.18
A2	43.19
A3	37.54
A4	35.41
A5	28.08
B1	27.34
B2	25.43

**Table 3-2 Measured non lactose solids in different permeates at 45 °C**

This variation in solubility seen in batches one to four, needs to be accounted for when investigating lactose growth rates on both the laboratory and industrial scale. The change in solubility alters the expected yield and the prediction of supersaturation. The change in supersaturation needs to be accounted for when modelling growth, as it is the driving force. The impact of the observed solubility variations on the accuracy of the growth simulation is reported in section 3.6.

### **3.4.2 Effect of temperature on growth rate**

Laboratory scale growth rate measurements were carried out at temperatures between 25 °C and 45 °C, the results are shown in Figure 3-6.

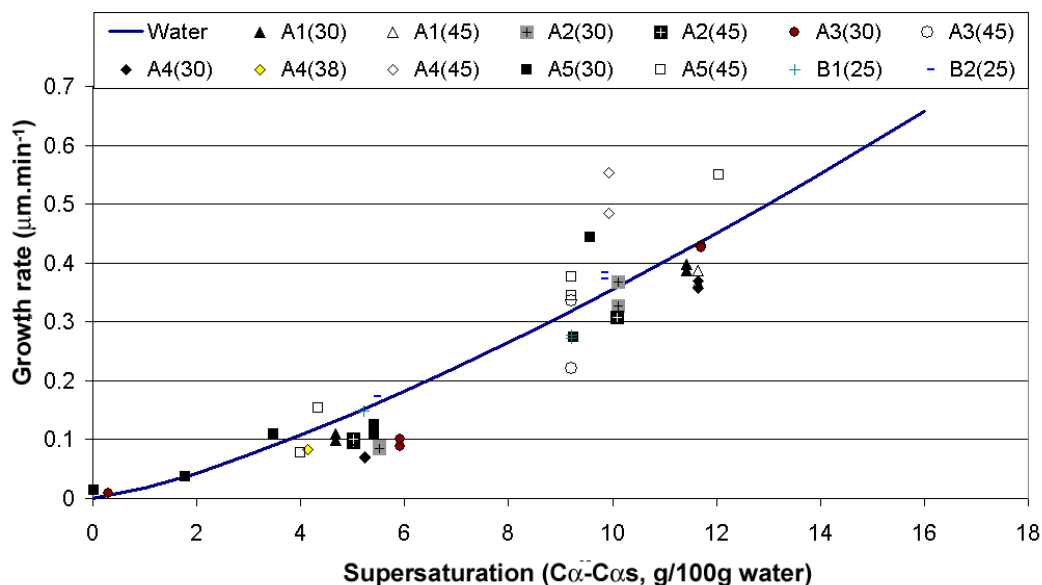


**Figure 3-6 Growth rate of lactose crystals in whey permeate compared against the growth rate observed for a lactose water solution (A represents plant A, B represents plant B)**

The brackets following the permeate concentrate batch identification represent the temperature of the measurement. To determine the significance of temperature on growth in permeates, Student t's test was used to examine if the mean for the normalised results of batch five at both 45 °C and 30 °C were significantly different. The normalisation of the data was achieved by dividing the growth rates at each supersaturation by the supersaturation to the power of 1.31. The exponent 1.31 was determined for the growth rate equation in chapter two. Batch five was selected as this provided the largest two sets of samples from which to draw a comparison. Table 3-3 shows the results.

Temperature	Sample Size	$\mu\text{m}\cdot\text{min}^{-1}/(C\alpha-Cas)^{1.31}$	St.Dev
30 °C	7	0.0177	0.0044
45 °C	6	0.0188	0.0038

**Table 3-3 Comparison of the normalised (as function of supersaturation) growth rates for growth at 30 °C and 45 °C in whey permeate concentrate**

Student t's test was used to determine, to a 95 per cent significance level, if the mean growth rates in Table 3-3 were different. It could not be concluded from this test that the two means were significantly different. The same conclusion is gained from Figure 3-7. The result corresponds with the lactose-water findings and means that when modelling growth of  $\alpha$ -lactose monohydrate in whey permeate concentrate a temperature component in the growth equation is unnecessary.

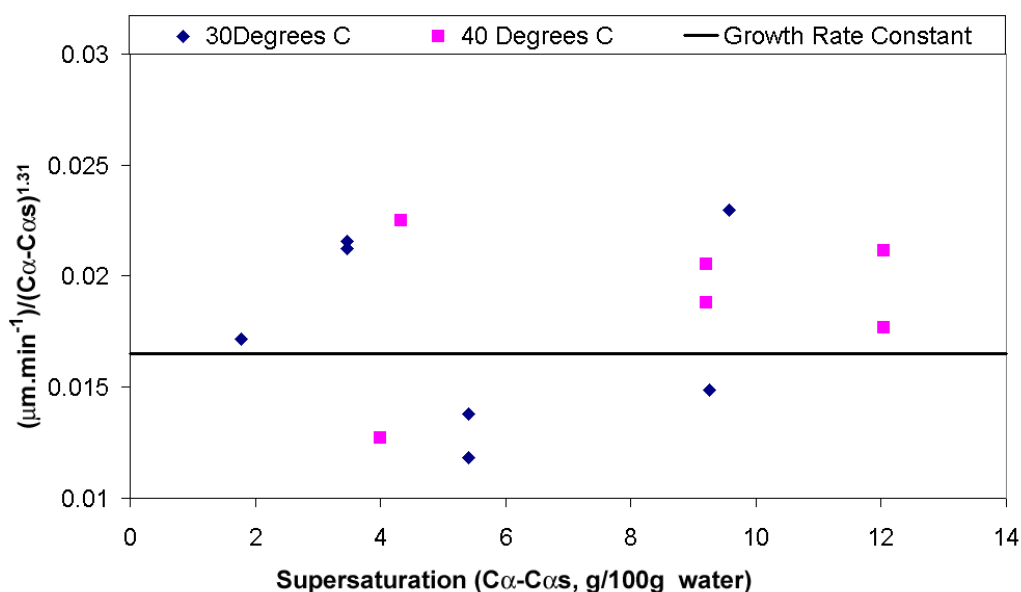
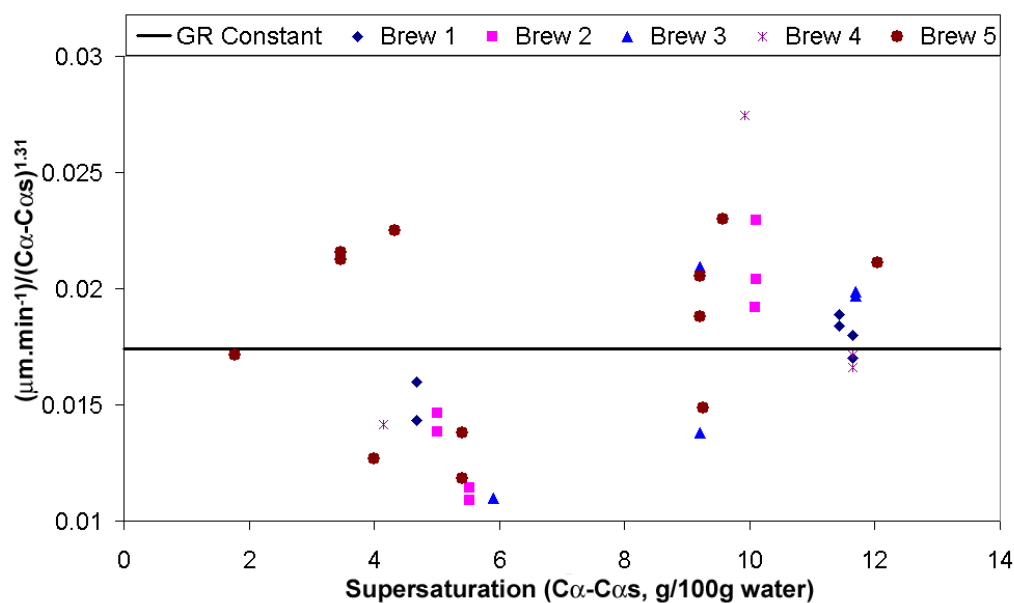


Figure 3-7 Comparison of the normalised (as function of supersaturation) growth rates for growth at 30 °C and 45 °C in whey permeate concentrate

### 3.4.3 Effect of supersaturation on growth rate

The effect of supersaturation on the growth of lactose crystals in whey permeate concentrate was studied in seven different batches sourced from lactose plants A and B. An absolute supersaturation range of 0 to 12  $\alpha$ -lactose per 100 g water was investigated. The absolute  $\alpha$ -lactose concentration was determined using the HPLC technique described in section 3.3.1.2. As the HPLC and total solids measurement gave a value for the total lactose concentration Equation 2-2, Equation 2-6 and Equation 2-7 were used to calculate the  $\alpha$ -lactose concentration.

The lactose crystal growth rates in permeate concentrate in Figure 3-6 are scattered about the growth curve for water. To determine if this scatter concealed significant differences in growth rate, each data set was normalised using the approach given in section 3.4.2. As any temperature effect had been shown in section 3.4.2 to be insignificant, the results for an individual batch of permeate concentrate were considered collectively. The normalised values are shown, in Figure 3-8, alongside the growth rate constant.



**Figure 3-8 Normalised (as function of supersaturation) growth rate results for  $\alpha$ -lactose monohydrate crystals grown in permeate compared against the mean value obtained for crystals grown in lactose water solution**

Using the normalised data the mean and standard deviation were calculated and these were used to determine the student t values for a one-tailed test to 95 per cent significance.

Solution	$\mu\text{m.min}/(\text{C}\alpha\text{-C}\alpha\text{s})^{1.31}$	St.dev	Sample Size	t value
Water	0.0174	0.0039	92	n/a
Batch 1	0.0181	0.0022	6	0.607
Batch 2	0.0161	0.0047	7	0.713
Batch 3	0.0166	0.0057	6	0.381
Batch 4	0.0187	0.0099	7	0.318
Batch 5	0.0191	0.0053	11	0.969

**Table 3-4 Normalised (as function of supersaturation) crystal growth results with and calculated student's t value**

Table 3-4 shows that after the solubility effects have been accounted for at the 95 per cent significance level the growth rates in permeate concentrate and water are insignificantly different. For a significant difference to be claimed at this level the student's t value would need to be 1.661 or greater. Based on the result, the growth rate equation developed in chapter two for a lactose water system will be applied when modelling growth in permeate concentrates.

### 3.4.4 Effect of crystal origin on growth rate

The effect of crystal origin on the growth rate was investigated by comparing crystals that had nucleated in permeate concentrate (impure crystals) and to those obtained from crystals that had nucleated in water (refined crystals). The growth rates of permeate concentrate nucleated crystals are shown in Figure 3-9 alongside Equation 3-8 generated using the refined crystals.

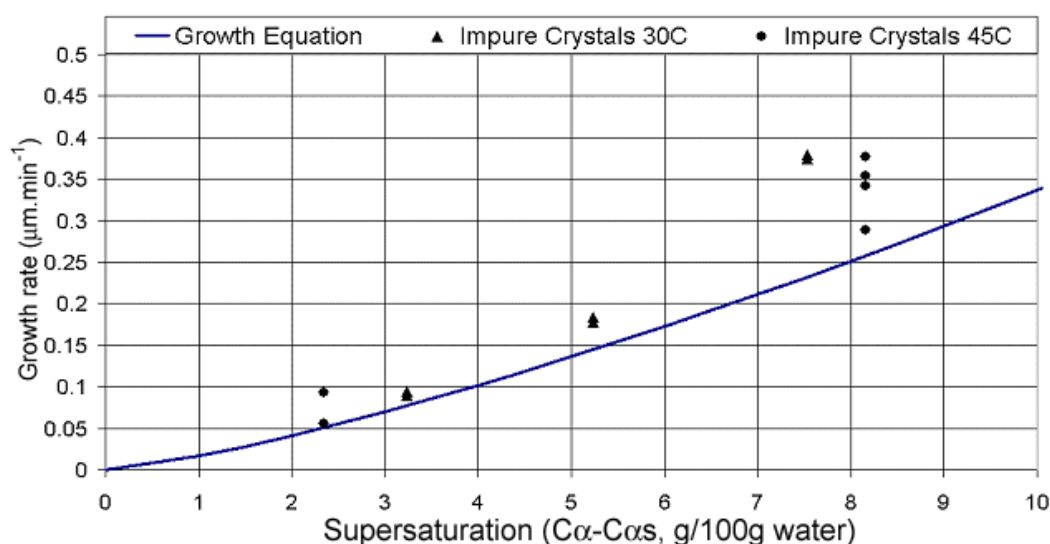


**Figure 3-9 Comparison of impure (crystals that had formed in permeate) crystal growth rates with Equation 3-8 developed using refined (crystals formed in a lactose water solution) crystals**

At low supersaturations, the impure lactose crystals and the refined lactose crystals grow at a similar rate. At the higher supersaturation, the impure crystals show a faster growth rate than the refined lactose curve. There is, however, considerable scatter in the results. To determine if a significant difference existed the mean growth rates for the refined and impure results for growth at 45 °C and a supersaturation of 8.15 were evaluated, using a one tailed student t's test, to determine if they were different at a level of 99 per cent significance. As the conditions were identical for all factors other than crystal source normalisation of the growth rates was unnecessary. The mean growth rates and standard deviations are presented in Table 3-5.

Sample	n	Mean µm/min	St.dev
Refined	8	0.252	0.015
Impure	4	0.340	0.037

**Table 3-5 Comparison of impure (crystals that had formed in permeate) and refined crystal (crystals formed in a lactose water solution) growth rates at 45 °C and an absolute alpha supersaturation of 8.15**

The calculated t value for the comparison of the two means is 4.54. This is above the required 2.764 and shows the two sets of results are significantly different. From this the impure crystals can be considered faster growing than the refined crystals.

The method used for manufacture and preparation of the crystals provides an explanation for the faster growth of the impure crystals. The impure crystals were sourced from a plant where nucleation occurs in the crystalliser with conditions set to achieve a single nucleation event. This compares with the refined crystals that were manufactured using a crystallising evaporator operated semi-continuously. Growth rate dispersion means that sieving of the impure crystals will have selected the faster growing crystals. In the crystallising evaporator multiple nucleation events occur, creating conditions where crystals are exposed to different growth times and therefore slow growing crystals are able to reach a similar size as fast growers. These ideas were investigated using the distribution model discussed in section 2.7.5. A prediction of the final population was made using the conditions of a single common growth rate; growth rate dispersion described using a log normal distribution and growth rate dispersion using a Weibull distribution. The parameters used in the prediction are presented in Table 3-6; the curves generated are presented in Figure 3-10. The parameters were determined by running each scenario until the sum of the differences squared was minimised.

Conditions	Growth Rate ( $\mu\text{m}/\text{min}$ )	Variable	Sum Diff <sup>2</sup>
Single rate	0.177	None	54.734
Normal	0.177	St.dev - 0.115	4.748
Weibull	0.177	Shape F -0.65	0.982

**Table 3-6 Parameters used in predicting crystal size distribution after growth had been allowed to occur**

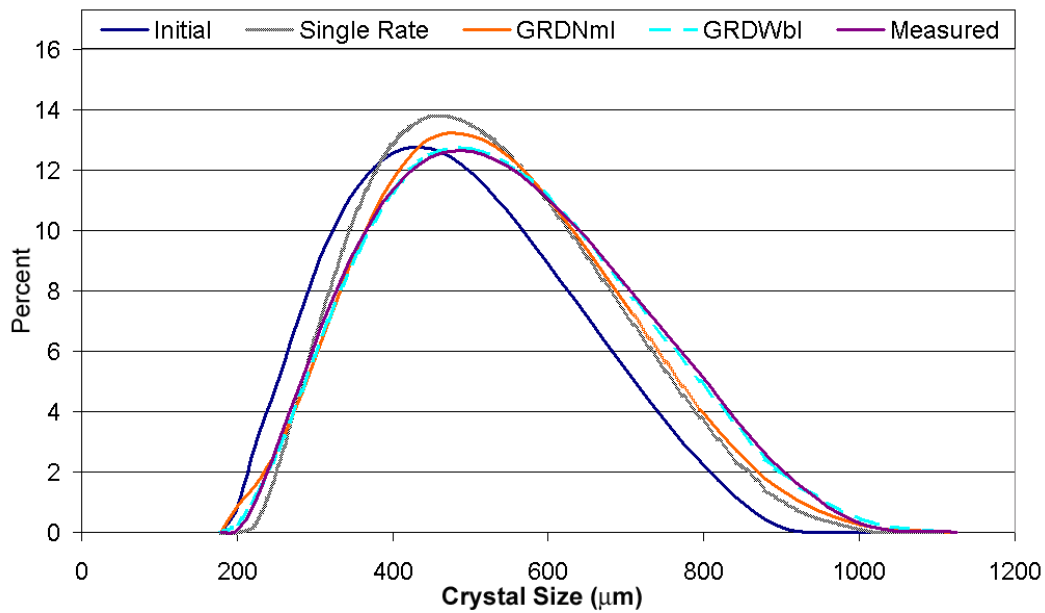


**Figure 3-10 Prediction of crystal size distribution using a single common growth rate and the growth rate dispersion models**

Figure 3-10 shows the best prediction of the crystal size distribution after growth is given when a Weibull Distribution model of the crystal growth rates is applied. The Weibull Distribution shape factor in Table 3-6 varies from the value of 1.17 found to provide the best fit for the refined crystals. The plot of the two Weibull Distributions in Figure 3-11 demonstrates the effect of these changing shape factors. As the two growth studies were carried out at different supersaturations and therefore had different average growth rates a scale is not provided.

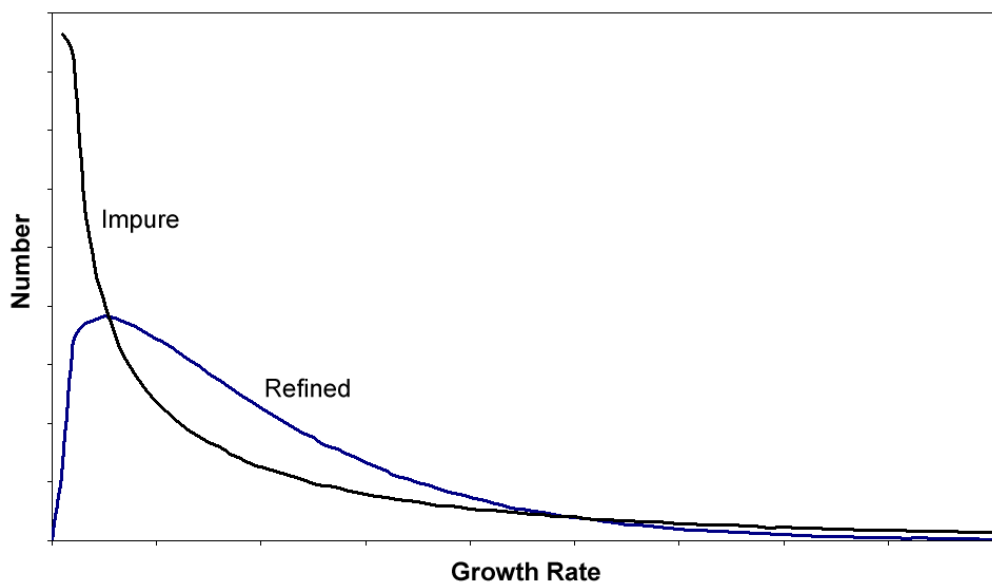


**Figure 3-11 Comparison of the Weibull generated growth rate distributions required to predict the crystal size distribution after growth had occurred**

Figure 3-11 shows the majority of the impure crystals have a growth rate that falls about a single point. This gives them a tighter distribution than the refined crystals. This demonstrates that the sieving of crystals that originate from a single nucleation event show the effect of censoring more clearly than the refined crystals that have been manufactured in a continuous process where slow growing crystals have the potential to grow up to large crystals given enough time.

The selection process used to collect the crystals appears to have influenced the shapes of the distributions as in Figure 3-11 a tail exists on the right hand side of both distributions. This can be explained by the fact that to provide crystals that were easy to separate after the growth experiments sieving focused on the collection of large crystals eliminating the small crystals. As no censoring at the large end of the size-distribution occurred there was no elimination of crystals with growth rates at the upper limits of the growth distribution and consequently the tail seen in Figure 3-11 appears.

### **3.5 Model of $\alpha$ -lactose monohydrate crystal growth**

The growth of lactose on the industrial scale occurs in an environment where concentration, crystal size and temperature all change constantly. The result of this is that the best way to relate laboratory measurements to the industrial process is through a model that can calculate these changing variables simultaneously. The basis of the model used here is the same as that presented in the work by Werner *et al.*, (2002). The model was reformulated into MATLAB Version 7.0, with changes being made to account for the refinements to the equations identified as necessary by the results collected in this study. The data from the literature used to obtain the equations has already been presented in chapter two. The equations are repeated here to present a complete version of the growth model.

#### **3.5.1 Mutarotation**

Mutarotation is responsible for the establishment of a dynamic equilibrium in solution between the two structural isomers of lactose. The growth rate of alpha lactose monohydrate crystals is dependent on the concentration of alpha lactose in solution, the kinetics of the mutarotation process play an important role in determining this



concentration. The equilibrium ratio of  $\beta$ -lactose and  $\alpha$ -lactose is described by the equilibrium constant  $K$ .

$$K = \frac{C_{\beta}}{C_{\alpha}}$$

**Equation 3-1 Equilibrium ratio of lactose in solution**

The equilibrium constant is dependent on temperature. The equation used for  $K$  in the model is shown in Equation 3-2. This was obtained by fitting data from (Roetman & Buma, 1974).

$$K = -0.0024T + 1.6353$$

**Equation 3-2 Temperature effect on the equilibrium constant of lactose solution**

At equilibrium, the rate of transformation from  $\alpha$ -lactose to  $\beta$ -lactose should be equal to the rate of transformation from  $\beta$ -lactose to  $\alpha$ -lactose as shown in Equation 3-3.

$$K = \frac{k_1}{k_2}$$

**Equation 3-3 Description of rate mutarotation equilibrium**

The rate of mutarotation increases with increasing temperature. The expression used in the model for the mutarotation rate is shown in Equation 3-4. This was obtained by fitting data from (Haase & Nickerson, 1966b), (Kendrew & Moelwyn-Hughes, 1940) (van Krevald, 1969) and (Haase & Nickerson, 1966a). Values of  $2.25 \times 10^8 \text{ s}^{-1}$  and  $68.46 \times 10^3 \text{ J}$  were obtained for  $k_o$  and  $E_a$  respectively.

$$k_1 = k_o \exp \frac{-E_a}{RT_K}$$

**Equation 3-4 Temperature effect on the dissolved alpha and beta lactose mutarotation rate**

### 3.5.2 Solubility

The solubility of  $\alpha$ -lactose is determined by the  $\alpha$ -lactose and  $\beta$ -lactose equilibrium and by the equilibrium between the solid and dissolved lactose. In this work the expression in Equation 3-5 for the total lactose solubility (corresponding to full equilibrium between the anomers).

$$C_{Ls} = 10.9109 \exp^{0.02804T}$$

**Equation 3-5 Solubility of lactose in water**

Concentration is expressed in the model as a mass ratio, mass of dissolved (anhydrous) lactose to mass of water. The mass of  $\alpha$ -lactose monohydrate can be converted to anhydrous lactose by multiplying it by 0.95. This fraction is the molar mass of the lactose molecule to the molar mass of the water molecule incorporated in the monohydrate structure. This equation will be adjusted in the model to take into account of the values obtained from measuring the solubility of lactose in permeates concentrates.

The initial solubility of  $\alpha$ -lactose is defined as the  $\alpha$ -lactose solubility, as it would have been if the mutarotation rate were infinitely slow.  $\beta$ -Lactose depresses the  $\alpha$ -lactose solubility, the expression used to account for this is given by Visser, (1982) and shown in Equation 3-6.

$$C_{\alpha s} = \frac{C_{Ls} - FK(C_L - C_{Ls})}{1 + K}$$

**Equation 3-6  $\alpha$ -lactose solubility**

Factor  $F$  is temperature dependent, and it was calculated by using the expression in Equation 3-7, which was obtained by fitting data from (Visser, 1983)

$$F = 0.0187 \exp^{0.0236T}$$

**Equation 3-7 Correction factor to account for solubility depression of  $\alpha$ -lactose caused by the presence of  $\beta$ -lactose in solution**

### **3.5.3 Lactose growth rate**

Butler, (1998) and Shi *et al.*, (1989) provide strong evidence of growth rate dispersion in the lactose crystallisation process. The results of the laboratory scale growth experiments in chapter two and this chapter confirmed the results of Butler, (1998) and Shi *et al.*, (1989). The incorporation of growth rate dispersion into a model means that a distribution of growth rates is required.

Butler, (1998) found that the relative growth rate of lactose crystals remains constant, fast growers remain fast growers and slow growers remain slow growers. This distribution of growth rates for a population that had not been censored was found to

be a lognormal one. To account for growth rate dispersion a crystal population is simulated where each crystal is assigned a growth rate multiplier, used to define the crystals growth rate relative to then mean growth rate defined in Equation 3-8. This multiplier is obtained from a log normal distribution with a standard deviation, which is determined by nucleation or seeding conditions. A log normal function was used in the model as no censoring occurs in the industrial process. The expression used for the growth rate shown in Equation 3-8, is the equation developed in chapter three.

$$G = 0.0165(C_a - C_{as})^{1.31}$$

**Equation 3-8  $\alpha$ -lactose monohydrate crystal growth rate (used to determine the mean growth rate in a crystal population)**

The growth of each crystal is described by the mean growth rate multiplied by the growth rate multiplier as shown in Equation 3-9; This equation determines the change in the size of an individual crystal over time as function of mean growth rate and correction factor that allows growth rate dispersion.

$$\frac{dx_i}{dt} = G\xi_i$$

**Equation 3-9 Growth of individual crystals**

The mass of all crystals is calculated as the sum of the volume of each individual crystal multiplied by the density of alpha lactose monohydrate, as shown in Equation 3-10: This value is subtracted from the total mass of lactose in the system to determine the mass of lactose remaining in solution.

$$X = \rho_x \frac{4\pi}{3} \sum_{i=1}^N x_i^3$$

**Equation 3-10 Mass of all crystals in solution**

Following a common practice the crystal size is described as the radius of an equivalent sphere. As long as the shape of the growing crystal is maintained this does not represent any loss of generality (Mullin, 2001). It is important to note that growth rate in terms of an equivalent radius represents an average over the crystal surface, and real crystals grow at different rates depending on the face.  $\alpha$ -Lactose monohydrate grows mainly at the base of the tomahawk.

The mass of all materials, lactose, non-lactose solids and water in the system remains constant throughout the cooling process. The changes that occur to the system are in the transfer of lactose and water from the solution into the crystal phase. Equation 3-11 shows the mass balance for lactose.  $L_{ini}$  is a constant representing the total mass of lactose in the system, in the model this value is set as an initial condition and is determined by defining the initial mass of crystallised and dissolved lactose. The distribution of this mass changes as crystal growth occurs, reducing the mass of alpha and beta lactose in solution.

$$(C_{\alpha} + C_{\beta})(W_{ini} - 0.05X) + 0.95X = L_{ini}$$

**Equation 3-11 Mass balance for lactose in crystalliser**

Here, the factors 0.05 and 0.95 account for the 5 per cent (by weight) of water in crystallised lactose monohydrate. This incorporation of one water molecule for every one alpha lactose molecule in the crystal structure means that mass of water in the solution is also reduced.

The rate of mutarotation is given by Equation 3-12:

$$\frac{dC_{\beta}}{dt} = k_1 C_{\alpha} - k_2 C_{\beta}$$

**Equation 3-12 Mutarotation rate**

Since  $\beta$ -lactose does not crystallise under the conditions being considered by the model, Equation 3-12 is used to describe the changing  $\beta$ -lactose concentration under crystallisation conditions. As  $\alpha$ -lactose is removed from the system and  $\beta$ -lactose converts to  $\alpha$ -lactose to restore the equilibrium.

The  $\alpha$ -lactose concentration changes because of both mutarotation and the crystallisation process. A separate equation for the  $\alpha$ -lactose concentration is not required in the model. The  $\alpha$ -lactose concentration is given by combining Equation 3-9, Equation 3-10, Equation 3-11 and Equation 3-12. The MATLAB code for this model is presented on the compact disc at the back of the thesis.

### 3.6 Industrial results and discussion

The accuracy of models prediction of changing concentration due to growth needed to be validated against profiles measured in industrial crystallisers. To provide data against which the model could be run the changing concentration profiles of four industrial lactose crystallisations were monitored. Two simulations were carried out on each set of industrial results. The first simulation used the parameters presented by Butler, (1998). The second prediction used the growth rate and solubility parameters determined from measurements made in this investigation. The solubility equation and initial conditions used for each trial are given in a table above the figure of each set of results.

The solubility equation used for the second prediction of each of the crystallisations was determined from an exponential fit to the solubility measurements reported in section 3.4.1. An exponential fit was applied separately to the measurements made for each individual permeate concentrate solution. The use of an exponential fit is inline with the solubility equation reported in the literature for a lactose-water solution. The results measured in this work, seen in Figure 3-5, gave no reason to suggest this trend differed for permeate concentrate solutions.

The equation used for the temperature cooling profile in the model was a third order polynomial fitted to measurements taken throughout the cooling of each crystalliser. A different temperature profile was obtained for each crystallisation and consequently a different polynomial was used in each of the simulations.

The initial particle size distribution used in the model was obtained using the Coulter Counter. A population of 10,000 crystals was created with a size distribution matching the distribution obtained from the Coulter Counter. This population was used to define the initial crystal population in the simulation. The size groupings in the model were obtained from the Coulter Counter, with each size being  $2^{1/6}$  of the previous smaller size. The number of crystals in each group of the simulated particle size distribution was set to match the measured one as closely as possible. The measured particle size distributions are presented in section A2 of the appendix.

Batch one		
Initial conditions	Units	Results
Concentration	g lactose/100 g water	76.45
Temperature	°C	58.45
Crystal mass	g / g water	1.50
Solubility equation	g lactose/100 g water	$C_{Ls}=14.387\exp^{0.0259T}$

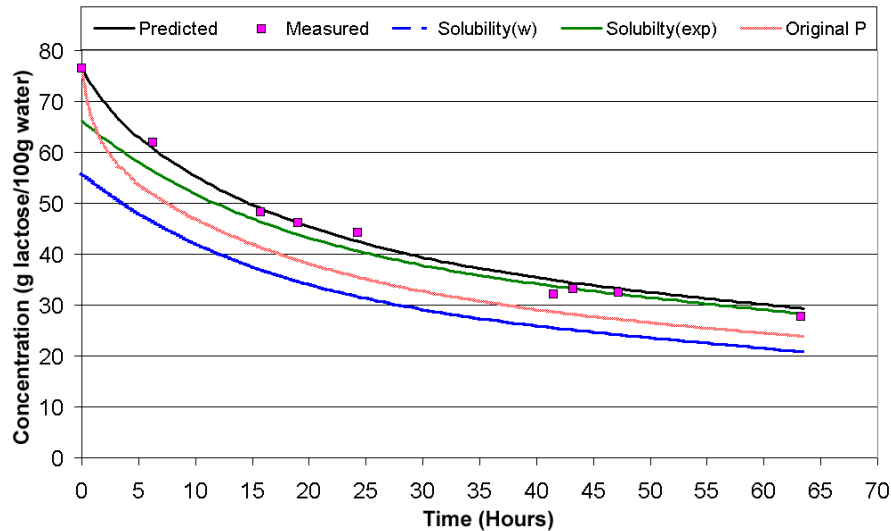


Figure 3-12 Batch one – measured and predicted concentration profiles for the crystallisation. Original P uses Equation 2-8 given by Butler, (1998) Predicted uses Equation 3-8 and the modified solubility equation

Batch two		
Initial conditions	Units	Results
Concentration	g lactose/100 g water	101.94
Temperature	°C	58.744
Crystal mass	g / g water	1.57
Solubility equation	g lactose/100 g water	$C_{Ls}=16.251\exp^{0.0241T}$

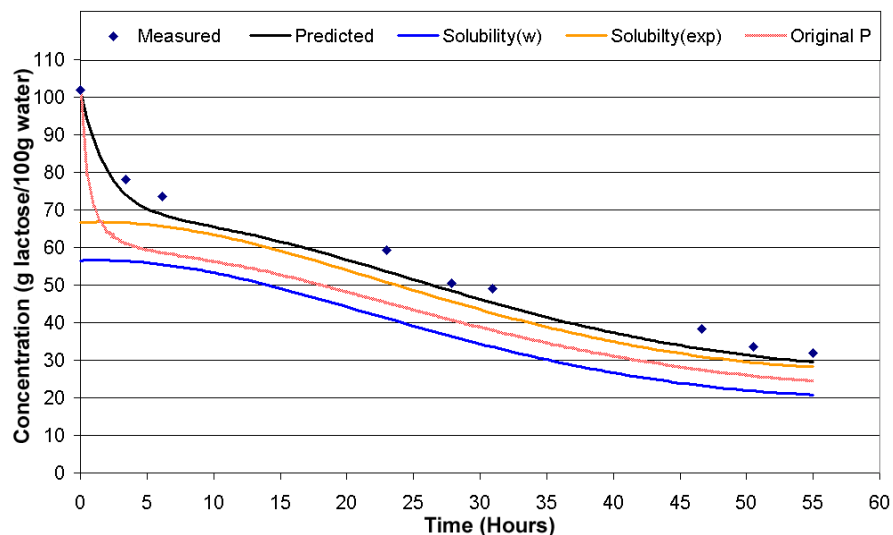


Figure 3-13 Batch two – measured and predicted concentration profiles for the crystallisation. Original P uses Equation 2-8 given by Butler, (1998) Predicted uses Equation 3-8 and the modified solubility equation

Batch three		
Initial Conditions	Units	Results
Concentration	g lactose/100 g water	78.35
Temperature	°C	60.24
Crystal mass	g/g water	1.50
Solubility equation	g lactose/100 g water	$C_{Ls} = 13.229 \exp^{0.02661}$

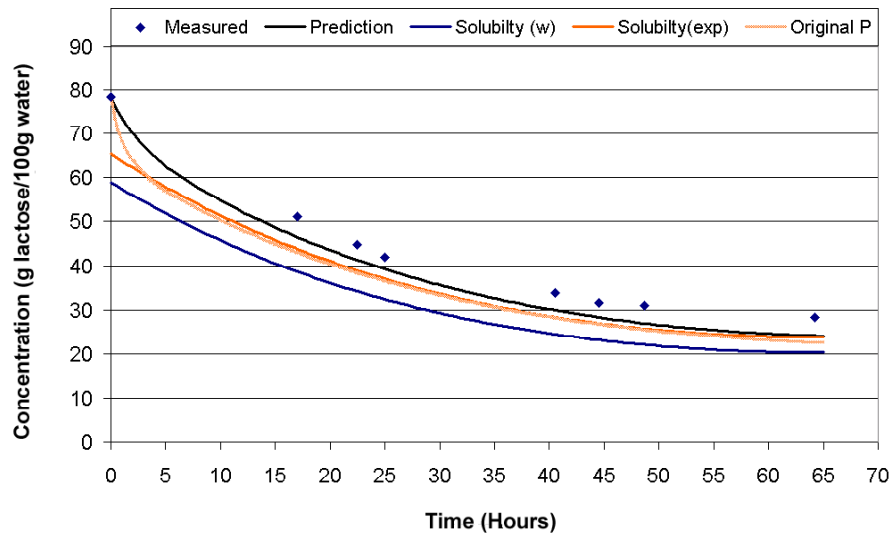


Figure 3-14 Batch three – measured and predicted concentration profiles for the crystallisation. Original P uses Equation 2-8 given by Butler, (1998) Predicted uses Equation 3-8 and the modified solubility equation

Batch four		
Initial conditions B4	Units	Results
Concentration	g lactose/100g water	86.49
Temperature	°C	57.4
Crystal mass	g/g water	1.49
Solubility equation	g lactose/100 g water	$C_{Ls} = 14.24 \exp^{0.02541}$

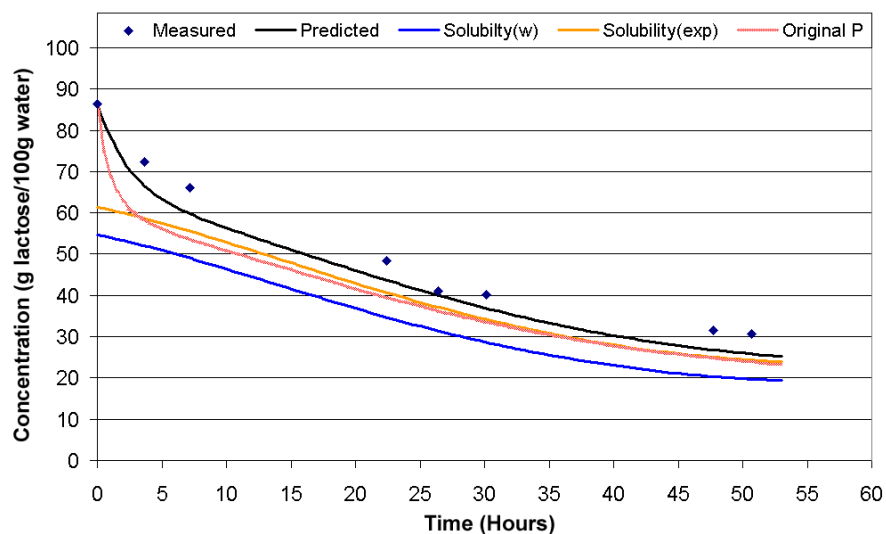


Figure 3-15 Batch four – measured and predicted concentration profiles for the crystallisation. Original P uses Equation 2-8 given by Butler, (1998) Predicted uses Equation 3-8 and the modified solubility equation

Figure 3-12 to Figure 3-15 show the simulated and measured results for the industrial crystallisations. The predictions using experimentally determined equations are labelled “predicted” and the predictions the use the literature based conditions are labelled “original P”. Shown also in Figure 3-12 to Figure 3-15 are the solubility profiles determined using the equation for water (w) and the equation developed from experimental data (exp). The solubility profiles represent the solubility as calculated from the temperature of the solution at a time point.

Figure 3-12 to Figure 3-15 show that when the experimentally determined sets of parameters are incorporated into the model improved predictions result. The prediction using the original set of parameters shows, in all four cases, a rapid initial decrease in concentration. This rapid drop is not seen in the measured data, but was seen in the prediction of Werner *et al.*, (2002), Figure 3-1. Once this decrease has occurred, the prediction is unable to recover, giving a lactose concentration constantly lower than the measured value. Where the experimentally determined values are used, the rapid initial decrease does not occur to the same extent. This enables the simulation to follow the measured result with improved accuracy. The predictions made using the experimentally determined set of parameters also follow the concentration profile at concentrations above the limits defined by the solubility curve. This demonstrates that the growth model is following lactose removal as it occurs through growth limiting factors, not the increased mass of lactose made available though the temperature induced solubility

The experimentally determined solubility equation was critical to the improved prediction of the measured results. In all the permeate concentrate batches against which simulations were run the solubility was higher than reported for a lactose-water system of the same temperature. This increased solubility changes the supersaturation and decreases the driving force for growth. The reduced growth rate decreases the rate of lactose removal from solution. Through accounting for the change in solubility, the model follows the concentration profile with increased accuracy before and after the cooling rate becomes a limiting factor in growth. The importance of solubility in obtaining an accurate prediction of the concentration profile means that it needs to be considered in any future study of lactose crystal growth in industrial media.



### 3.7 Conclusion

Experiments have been conducted investigating the growth of  $\alpha$ -lactose monohydrate crystals in whey permeate concentrate. These experiments were performed on both the laboratory and industrial scale. The hypothesis that initiated this investigation was that “growth in permeate concentrate was considerably slower than was reported in the literature for a lactose water system”. This hypothesis was proposed in the work by Werner *et al.*, (2002), who found that to accurately simulate growth in an industrial crystalliser a substantial reduction in the literature growth rate was required for the prediction to follow the measured results.

Experiments performed in the laboratory found, under the same conditions, the lactose crystal growth rates in permeate concentrate and in lactose water solutions were insignificantly different. Part of the procedure for conducting these growth rate measurements measured the solubility of lactose at different temperatures. The permeate concentrate solubility measurements were found to be different from what was reported for a lactose water system. As supersaturation is the driving force for growth any variation in solubility needs to be accounted for in a model that looks to predict a changing concentration profile as it occurs through growth.

Measurement of changing concentration and temperature profiles in industrial crystallisers was conducted in parallel with the laboratory work. Using the laboratory results to set the parameters, the model was run with the aim of simulating the measured concentration profiles. It was found that when the experimentally determined values were incorporated into the model a good prediction of the measured data was obtained. When the model was run using the literature information the accuracy of the prediction was reduced.

A key parameter modification was the adjustment of the solubility equation to account for experimentally determined values. For future work in this area, determination of the solubility profile should be considered a critical area. Where the impurity concentration was lower the solubility deviation was not observed. A better understanding of why the high impurity levels increased solubility could lead to the

opportunity to eliminate the effect and could lead to an increase in recoverable lactose.

The model presented in this chapter is limited to predicting changing concentration in an industrial crystalliser where no nucleation occurs. This makes it suitable for situations such as the crystallisers studied in this chapter. The real value of a model exists its ability to be able to predict the effect changes will have. This allows it to be used as a tool for identifying potential improvements on the current operating procedures. This requires an understanding of both growth and nucleation. The following sections of this work look to expand on the knowledge of nucleation.

## Chapter 4 Nucleation

### 4.1 Introduction

The process of crystal formation from solution, nucleation, is equally as important to the crystallisation process as crystal growth. Being able to control the rate and timing of crystal formation provides a tool that can be used to maximise solids recovery, produce a product with a desirable particle size distribution and optimise processing time. Controlling nucleation requires an understanding of the key variables and requires knowledge on how changes in these will impact the process. This chapter is an investigation into these key variables as they apply to  $\alpha$ -lactose monohydrate crystallisation.

### 4.2 Nucleation literature

The nucleation process has been continuously studied over the last 150 years. Like a chemical reaction, nucleation is an activated process in which the transition state is associated with an assembly of molecules held together by intermolecular interactions. These may be hydrogen bonds,  $\pi$ - $\pi$  and van der Waals interactions, columbic forces and co-ordinate bonds. Unlike a chemical reaction, the viability of this assembly depends on size. In a supersaturated solution, there will be a steady state distribution of assemblies, and depending on the supersaturation imposed, there will be a critical size, above which the assemblies can grow and below which they are unstable. The higher the supersaturation the smaller the size, the easier nucleation becomes and the more crystals will be formed.

Nuclei can form in a pure supersaturated solution (homogeneous nucleation), on foreign particles (heterogeneous nucleation), on crystals (surface nucleation) or as attrition fragments (attrition induced secondary nucleation). An expanded list of the nucleation mechanisms is given in Figure 4-1. The supersaturation controls the dominant mechanism. At low supersaturation attrition provides the main source of nuclei where as at high supersaturation activated nucleation is dominant (Mersmann,

Braun, & Loffelmann, 2002). The system under consideration defines what constitutes a high or low supersaturation.

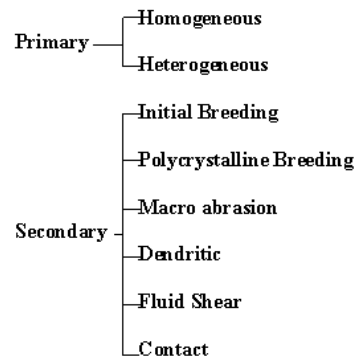


Figure 4-1 The different mechanisms of nucleation (Myerson, 2002)

### 4.2.1 Primary nucleation

Primary nucleation is the formation directly from solution of nuclei that grow into crystals, it can occur homogenously or heterogeneously. The difference between the two mechanisms is demonstrated in Figure 4-2.

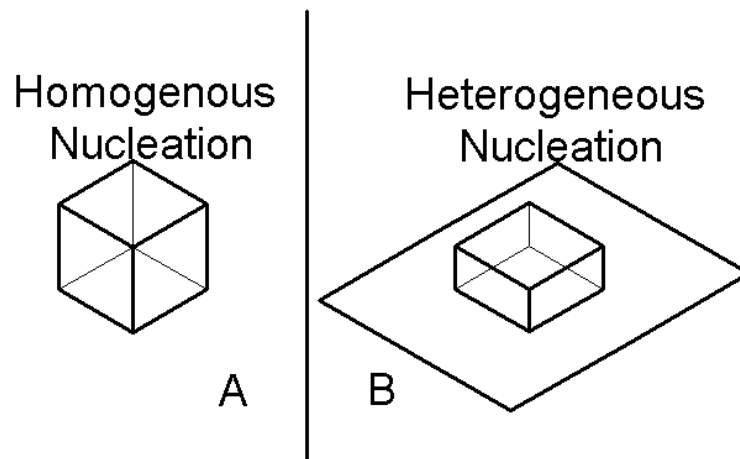


Figure 4-2 Comparison of homogenous and heterogeneous nucleation mechanisms (adapted from Lacmann, Herden, & Mayer, 1999)

The main driving force of primary nucleation is supersaturation. It represents the difference in chemical potential between the solution phase and crystal phase (Equation 4-1).

$$\Delta\mu = \mu - \mu_{eq*}$$

Equation 4-1 Driving force for nucleation

Equation 4-1 can be expressed in the form shown in Equation 4-2.

$$\Delta\mu = kT_K \ln S_R$$

**Equation 4-2 Driving force for nucleation expressed as a function of relative supersaturation (Kashchiev & van Rosmalen, 2003).**

The relative supersaturation is the ratio the solute concentration to the equilibrium solute concentration, shown in Equation 4-3

$$S_R = C / C_{eq}$$

**Equation 4-3 Supersaturation expressed as a relative function of the equilibrium concentration**

When using the expression in Equation 4-2 and Equation 4-3 for lactose nucleation it is important to remember the exponential relationship between temperature and solubility.

Primary nucleation creates a new crystal surface and mass (nuclei), and an energy barrier must be overcome. The free energy for formation of the crystal surface is positive and proportional to the surface area (diameter squared) and interfacial tension of the nuclei. In opposition to this is the negative free energy associated with the volume generation (latent heat generation). This is proportional to the volume (diameter cubed). The net free-energy change during the nucleation process is the sum of these terms; the surface area term dominates at small nuclei sizes and the volume term dominates at larger nuclei sizes (Hartel & Shastry, 1991) (Parsons , Black, & Colling, 2003).

Classical nucleation theory describes the variables that influence the rate of primary nucleation using Equation 4-4 (Kashchiev, 2000). This equation is derived from the Arrhenius reaction velocity equation, commonly used for a thermally activated process (Mullin, 2001).

$$J_{Hom} = A \exp\left(-\frac{16\pi\sigma^3 V_m^2}{3(kT_K)^3 (\ln S_R)^2}\right)$$

**Equation 4-4 Classical nucleation equation for homogeneous nucleation**

As heterogeneous nucleation occurs on a surface, the energy barrier, which must be overcome in the creation of a new solid liquid interface, is reduced. This is accounted for in Equation 4-5, by the introduction of a factor ( $q$ ), which compensates for the reduced interfacial energy barrier. Where heterogeneous nucleation is occurring it is likely that the system will contain multiple surfaces. The interactions between the nucleating substance and the different surfaces will vary creating different reductions in the energy barrier to nucleation. The value of ( $q$ ) used in this work represents an average of these multiple interactions.

$$J_{Hen} = A \exp \left( - \frac{16\pi\sigma^3 V_m^2 (q)}{3(kT_K)^3 (\ln S_R)^2} \right)$$

**Equation 4-5 Classical nucleation equation for heterogeneous nucleation**

It is likely that both forms of nucleation will occur together; although the lower barrier to formation means that heterogeneous nucleation will dominate at lower supersaturations where the energy driving force is lower. The slight difference in the equations and mechanism allows primary nucleation to be considered as the sum of the homogenous nucleation and the heterogeneous nucleation as presented in Equation 4-6. An additional term to account for secondary nucleation can also be added in this equation.

$$J_T = J_{Hom} + J_{Hen}$$

**Equation 4-6 Nucleation as a sum of homogenous and heterogeneous nucleation**

### 4.2.2 Induction time

One approach for studying primary nucleation is the determination of the induction time ( $\tau$ ). This technique uses the concept that following the initiation of supersaturation, a certain time elapses prior to the formation of an appreciable amount of the new phase. Given that this time is experimentally observable, it is a measure of the ability of the system to remain in metastable equilibrium.

The theory defines the induction period as consisting of three distinct periods. These are the relaxation time, the nucleation time and the growth time. The relaxation time

is how long the cluster distribution needs to respond to the imposed supersaturation. The nucleation time is the time required for the production of nuclei that are stable and will not be absorbed back into the solution. The growth time is the time necessary for the nuclei to grow to a detectable size (Mullin, 2001). In this work, a supersaturated system will be created through cooling it in a static solution. The system will then be altered by suddenly starting agitation. These changing conditions make it difficult to assign an induction time value to the system. To overcome this, a variation on the method of induction time was proposed, where after the introduction of agitation the time required to reach a detectable number of nuclei will be determined as  $t_N$ .

Assuming that the number and size of particles per unit volume detected by observation at time  $t_N$  is constant and that steady state nucleation prevails during the detection period, the following relationship can be developed.

$$t_N \propto \frac{N_N}{J_T}$$

**Equation 4-7 Relating induction time to nucleation rate**

Combining Equation 4-4 and Equation 4-7 gives Equation 4-8;

$$t_N = \frac{N_N}{J} = \frac{N_N}{A \exp\left(-\frac{16\pi\sigma^3 V_m^2}{3(kT_K)^3 (\ln S_R)^2}\right)}$$

**Equation 4-8 Incorporation of induction time into classical nucleation equation**

Using this relationship, a plot of  $t_N$  vs.  $(\ln S_R)^{-2}$  enables the interfacial energy to be determined from the slope, given that all the other parameters are known. The molecular volume is calculated as shown in Equation 4-9

$$V_m = M / \rho_x N_A$$

**Equation 4-9 Determination of molecular volume**

An approximation of the interfacial energy can be made using the Stefan-Skapski-Turnbull formula (Kashchiev, 2000). This is given in Equation 4-10.  $\beta_c \approx 0.2$  to  $0.6$  is a numerical factor dependent on the shape of the cluster; depending on the value selected a range for the interfacial energy from  $7.61$  to  $22.81 \text{ mJ}\cdot\text{m}^{-2}$  is obtained for alpha-lactose monohydrate.

$$\sigma = \frac{\beta_c k T_K}{V_m^{2/3}} \ln \left[ \frac{1}{V_m C_{eq}(T_K)} \right]$$

**Equation 4-10 Prediction of interfacial energy**

Using the value for the interfacial energy the size of the critical nucleus can be determined. The critical nucleus represents the minimum number of molecules a cluster must possess, to exist as a stable entity in the solution. Only super-nuclei (clusters of size  $n > n^*$ ) are capable of spontaneous overgrowth, leading to the formation of crystals. Sub-nuclei (clusters of size  $n < n^*$ ) are unable to grow spontaneously and may dissolve back into the solution. The equation for determining the size of the critical nucleus is given in Equation 4-11 (Kashchiev, 2000).

$$n^* = \frac{32\pi V_m^2 \sigma^3}{3(kT_K)^3 \ln^3 S_R}$$

**Equation 4-11 Prediction of critical nucleus size**

### 4.2.3 Secondary nucleation

Secondary nucleation is the formation of new crystals induced by the introduction (seeding) or presence of crystals of the crystallising material. For secondary nucleation to occur lower levels of supersaturation, than needed for primary nucleation, are required. The lower supersaturation reduces the potential for production of a large number of fine crystals from excessive nucleation. The rate of secondary nucleation increases with increasing supersaturation. This is explained using survival theory; where if a distribution of secondary nuclei are formed, those below the critical size re-dissolve (Mandare & Pangarkar, 2003).

Secondary nucleation can occur from the breakage of crystals through surface erosion (attrition) and particle splitting (fragmentation). The crystal fragments produced in an industrial crystalliser typically falls between  $1$  and  $150 \text{ }\mu\text{m}$ . In accordance with survival theory the larger the fragment size, the lower the supersaturation required for



formation of stable nuclei. In a crystalliser the stresses imposed on the crystals that lead to breakage result from turbulence in the fluid and mechanical collisions that occur during crystal-crystal, crystal-wall or crystal-impeller contact (Pratola, Simons, & Jones A.G., 2002). In all of these factors the mechanical design of a crystalliser is important in controlling the contact nucleation rate (Bennett, 1988). The number and physical properties of the crystals such as the Vickers hardness, the shear modulus the fracture resistance and the crystal density also influence the contact nucleation rate (Mersmann *et al.*, 2002).

Initial breeding is a form of secondary nucleation that occurs when a seed crystal is introduced into a supersaturated solution. A crystalline dust may be washed from the surface; the tiny crystallites making up this dust then grow up to macroscopic size. These tiny crystals are thought to originate during the evaporation of the solvent from the crystal surface during drying (Qian & Botsaris, 1998). The number of nuclei has been shown to be a function of the crystal surface area. (Triboulet, Cournil, & Crawley, 1992). It is possible that during the drying process the concentration within the droplets becomes high enough for primary nucleation to occur, this would result in a large number of small crystals being generated.

### **4.3 Studies of lactose nucleation**

The importance of controlling lactose nucleation has long been recognised. Herrington, (1934a) states “In the manufacture of lactose it is desirable to secure a maximum yield of crystals in a minimum time, and to secure crystals which may be readily washed with a minimum of loss.” Little has changed since the writing of that paper, although it may be added that with the increased use of lactose in the pharmaceutical industry, better control of the specific particle size distribution of the crystals produced is desirable.

Despite its importance in crystallisation, lactose nucleation is less studied in the literature than lactose crystal growth. This is perhaps recognition of the difficulties associated with measuring the formation of new crystals.

### 4.3.1 The effect of supersaturation on lactose nucleation

Supersaturation is the key driving force for nucleation, for lactose nucleation it is typically expressed as the difference between the solubility concentration and the actual concentration. The supersaturation also represents the quantity of lactose that can be extracted from the solution at a particular set of conditions.

Leighton and Peter (1924) cited from Herrington, (1934a) found that for nucleation to be initiated from a lactose water solution cooling of 30 °C below the solubility temperature was necessary. The temperature of these experiments is not reported and therefore the absolute alpha supersaturation cannot be determined. Herrington studied crystallisation from solution and found similar results, although it was found that even when super cooled by 53 °C some solutions took over 68 days to nucleate. The results of Herrington for an experiment at 30 °C are reproduced in Table 4-1.

Saturation temperature	Supersaturation glac/100 g water	10 Hours	34 Hours	58 Hours	136 Hours	360 Hours
96 °C	135.7	TMC	TMC	TMC	TMC	TMC
90 °C	110.8	TMC	TMC	TMC	TMC	TMC
86 °C	96.4	TMC	TMC	TMC	TMC	TMC
84 °C	89.7	29-20	TMC	TMC	TMC	TMC
80 °C	77.5	38-3	TMC	TMC	TMC	TMC
75 °C	64.1	22-1	TMC	TMC	TMC	TMC
66 °C	44.1	1	2	30-2	TMC	TMC
61 °C	35.0	1	1	0	0	TMC
54 °C	24.3	0	0	0	0	0
53 °C	22.9	0	0	0	1	0
51 °C	20.3	0	0	0	0	0
46 °C	14.3	0	0	1	0	0
46 °C	14.3	0	0	1	0	0

TMC = too many to count

Double numbers = single crystals first, clusters second

**Table 4-1 The appearance of crystal nuclei at 30 °C, in solutions saturated at temperatures between 46 °C to 96 °C –reproduced from (Herrington, 1934a)**

Table 4-1 shows that even at high supersaturations considerable time was required for nuclei to appear. What defines an acceptable time for nucleation is process specific. A study into lactose crystallisation in ice cream, which may have a storage time of months, would define conditions where nucleation occurs after a week as

unacceptable. This study is concerned with industrial crystallisation where production speed is critical and so nucleation needs to occur in minutes, and then be controlled over the next 24 to 72 hours as growth occurs.

Studying lactose crystallisation in the absence of agitation, Raghavan, Ristic, & Sherwood, (2001), observed that even at supersaturations of 1.3 times the solubility concentration no nucleation occurred after 96 hours, after which point the experiments were stopped. With the introduction of agitation, applied using a Perspex paddle (speed not reported), lactose crystals were observed in the solution after two hours. The results from the agitated experiments are reproduced in Table 4-2

Solubility temp °C	Nucleation temp °C	Supersaturation g lac/100 g w	Induction time (hours)
50	40	10.7	17
50	31	18.1	8
50	20	25.0	2
60	50	14.2	16
60	42	23.0	8
60	31	32.4	3
50	20	25.0	2
50	20	25.0	2
50	20	25.0	2

**Table 4-2 Induction time for  $\alpha$ -lactose monohydrate crystallisation at a range of supersaturations (Raghavan *et al.*, 2001)**

The results of Raghavan *et al.*, (2001) show considerably lower supersaturation than reported by Herrington, (1934a) is required for lactose nucleation. As in the absence of agitation no nucleation was seen, the reduction is likely to be a consequence of the agitation. The effect of agitation in reducing the time required for nuclei formation shows lactose nucleation is system specific.

Walstra & Jenness, (1984) reported that the metastable zone lies at relative supersaturations of approximately 1.6 to 2.1 times the solubility limit, with secondary nucleation occurring at supersaturations above 1.6 times the solubility limit; and primary nucleation occurring at supersaturations above 2.1 times the solubility limit. No details are given about the system where these conditions were determined. Recognition by Walstra and Jennes, that the nucleation rate measured depends upon

the system could be inferred from the statement, “in the intermediate range crystallisation depends on several factors, such as composition and time”.

Lactose nucleation rates were measured by Shi *et al.*, (1990) using a population balance technique. To initiate nucleation a supersaturated solution was seeded with fine lactose crystals. The results can therefore be considered a measure of the secondary nucleation rate. The data from Shi *et al.*, (1990) has been reproduced in Figure 4-3. For comparison with the other literature, the results in Figure 4-3 have been converted to absolute alpha supersaturation.

A population balance technique was also used by Griffiths *et al.*, (1982) for determining the  $\alpha$ -lactose nucleation rate. This data has been plotted in Figure 4-3. Their experiments were carried out in a 2000 ml Plexiglas vessel, diameter 12.70 cm, fitted with a 7.62 cm cylindrical baffle. A double propeller mixer with 5.08 cm blades operating at  $550 \text{ r}\cdot\text{min}^{-1}$  provided agitation in the vessel. For some of the experiments 0.2 g of seeds crystals (100 to 120  $\mu\text{m}$ ) were added to reduce the time required for nucleation to occur.

Butler, (1998) measured the secondary nucleation rate over a range of supersaturations of lactose by adding two large lactose crystals to solutions. The solutions were shaken at  $200 \text{ r}\cdot\text{min}^{-1}$  throughout the experiments. Nucleation was measured using a Malvern MasterSizer/E to provide crystal size and content data. The results from this study are reproduced in Figure 4-3. The work of Butler showed a supersaturation threshold above, which the rate of secondary nucleation only increases very slowly. This contradicts the commonly held view that the rate of nucleation increases faster with increasing supersaturation. A possible explanation for the observation of Butler is that the nucleation observed was controlled by the agitation of the solution. If new crystals were being formed through the removal of fines from the surface of the crystals, it could be expected that the nucleation rate would reach a plateau as observed. The initial increase would reflect the fact that the supersaturation had reached a point where small nuclei broken off the surface could survive. After this, the rate would continue to increase as supersaturation increased, allowing smaller

crystals to survive. At some point, assuming a constant agitation rate, a plateau would be expected as the attrition of the surface reached a maximum.

Kauter, (2003) measured the nucleation rate of lactose using a Malvern MasterSizer/E to determine size distribution and volume concentration of crystals. The experiments were carried out in an agitated vessel with a diameter of 100 mm and a height of 160 mm. 500 ml of solution was used in the experiments, which meant the operating height of the vessel was 65 mm. The agitator used was a 50 mm pitched blade turbine with four blades at a 45° angle. The standard mixing speed used in the experiments was 600 r·min<sup>-1</sup>. All experiments investigated secondary nucleation, using seed to initiate the nucleation. It was found that nucleation increased with increasing supersaturation. The results are reproduced in Figure 4-3.

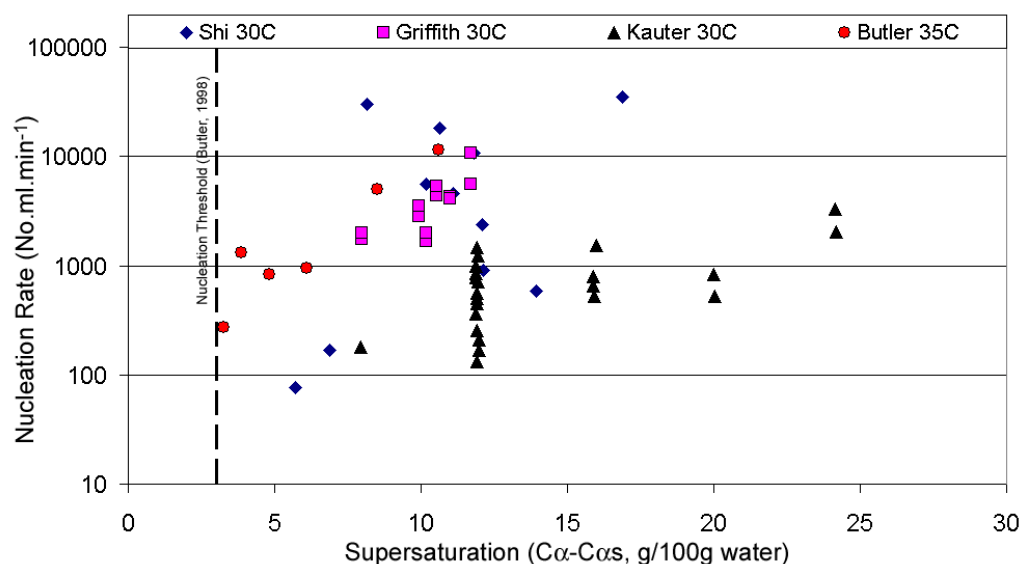


**Figure 4-3 The nucleation rate data of Shi *et al*, (1990), Griffiths *et al*, (1982), Kauter, (2003) and Butler, (1998) expressed in terms of absolute alpha supersaturation**

There is a considerable scatter in the results presented in Figure 4-3. Nucleation rates are orders of magnitude different at similar supersaturations. These differences occur between different studies and in results collected in the same study. The differences between the studies can be explained by variations in the methods and equipment used. The variations in the results of each individual study highlight the difficulties associated with obtaining repeatable results from nucleation experiments. It is possible to observe an overall trend with nucleation rate seeming to increase with increasing supersaturation. All the results presented are from investigations into

secondary nucleation. For a complete understanding of nucleation, this information needs to be combined with primary nucleation results.

### 4.3.2 The effect of temperature on lactose nucleation

The effect of temperature on the secondary nucleation of lactose from a lactose-water solution has been studied in detail by two authors who found opposing results. Shi *et al.*, (1990) reported the nucleation rate increased with temperature. The opposite effect was found in a more recent study by Kauter, Litster, & White, (2003) who reported a decrease in nucleation rate with increasing temperature. The two sets of results have been reproduced in this work so the different findings can be considered.

The work of Shi *et al.*, (1990) was analysed using relative supersaturation and the observed results were a consequence of the units used to express supersaturation. The results from the work are viewed in Figure 4-4 from the position of absolute alpha supersaturation. In the results, there is considerable overlap at the different temperatures, and an effect on the rate of nucleation is not observed.

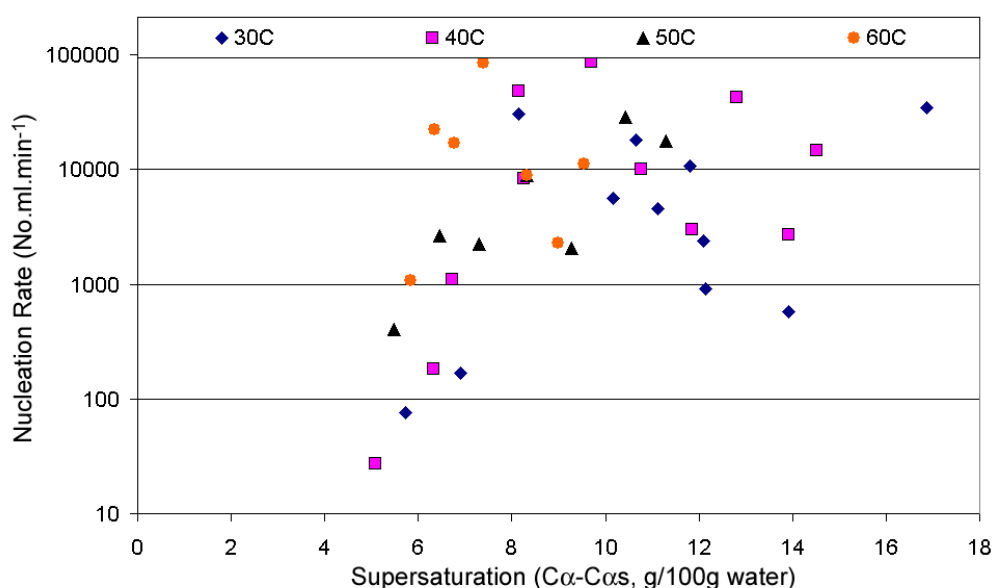


**Figure 4-4 Temperature vs. nucleation rate data from Shi *et al.*, (1990) viewed in terms of absolute alpha supersaturation**

The results from the Kauter, (2003) showing the effect of temperature on the nucleation rate are reproduced in Figure 4-5. All the experiments were carried out at an absolute alpha lactose supersaturation of 11.89 g  $\alpha$ -lactose per 100 g water. The results have been converted for comparison from  $\text{No.}(\text{kg}\cdot\text{slurry}\cdot\text{min})^{-1}$  into

No.(ml.min)<sup>-1</sup>. A trend of decreasing nucleation with increasing temperature is shown. There is considerable scatter in the results. If the results at 53 °C or the highest two results at 23 °C are neglected, it would be difficult to conclude that temperature changes the rate of nucleation. A more detailed investigation that examines this effect over a range of supersaturations is required.

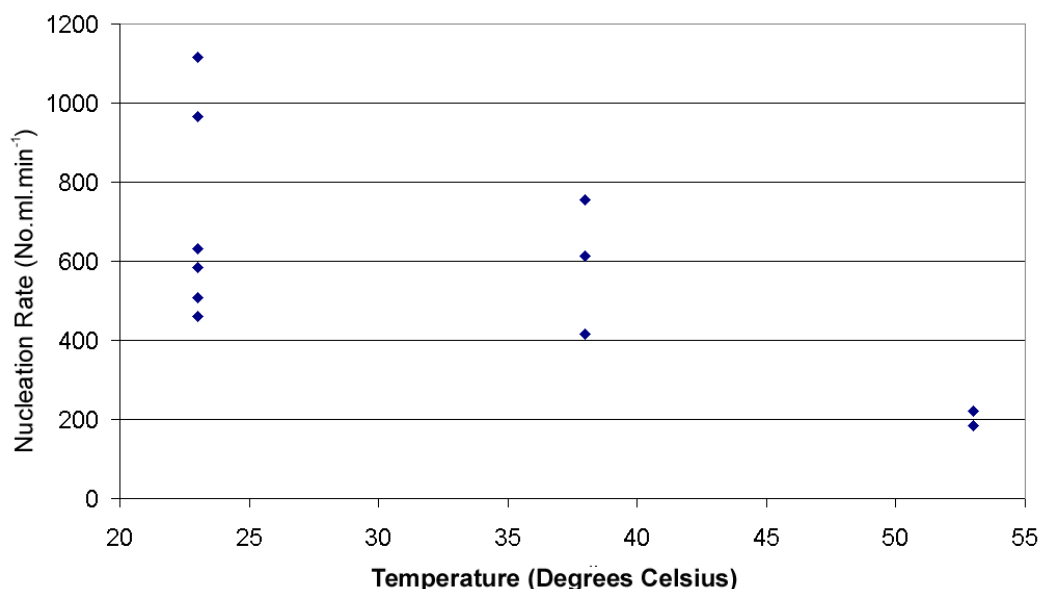


Figure 4-5 Effect of temperature on the lactose nucleation rate as reported by Kauter, (2003)

Primary nucleation of  $\alpha$ -lactose monohydrate as a function of supersaturation and temperature was studied by Arellano, Aguilera, & Bouchon, (2004), in the absence of agitation. The study used digital microscopy to follow nucleation as it occurred in a heated cell. The results were reported as a function of relative supersaturation. Increases in supersaturation and temperature were both reported as leading to an increased nucleation rate. As quantitative nucleation, rates were not reported a comparison of these results with other data could not be conducted.

### 4.3.3 The effect of impurities on lactose nucleation

#### 4.3.3.1 Simulated whey permeate

Simulated whey permeate is a solution made in the laboratory that attempts to match the salts as they occur in industrial whey. It has the advantage over industrial whey in that the impurity concentration is known and it is the same from batch to batch. This permits all the experiments to be conducted with the knowledge that the starting

material is identical. A second advantage is its transparency, unlike whey permeate that contains protein and fine precipitates. When studying nucleation this is an advantage because crystals can be seen when they form.

A study of the secondary nucleation rate in simulated whey permeate was conducted by (Kauter, 2003). The study found secondary nucleation rate in simulated whey permeates occurred faster than that measured at the same supersaturation in water. The results for nucleation in water and simulated whey are presented in Figure 4-6. Included also in Figure 4-6 are the nucleation rate measurements made by Kauter in industrial permeate solutions. In Figure 4-6 the slope of the nucleation curve for impure solution is greater than the pure lactose water system. This demonstrates that impurities amplify the effect of increasing supersaturation on the secondary nucleation rate.

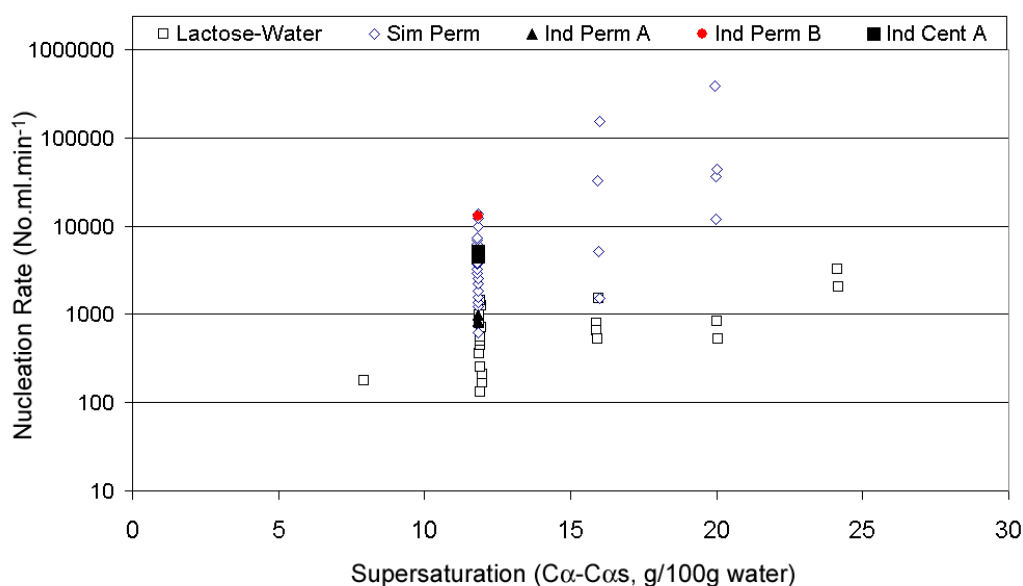


**Figure 4-6 Comparison of secondary nucleation rate in water, in simulated whey permeate and in industrial permeate (Cent A is industrial permeate A that had been centrifuged to remove the undissolved solids) (Results reproduced from Kauter, 2003)**

In the study by Butler, (1998) a secondary nucleation threshold was determined. The secondary nucleation threshold represents the supersaturation below which the solution remains stable with no additional nuclei being formed. This was determined to be 8 g lactose per 100 g water, which corresponds to approximately 3.2 g  $\alpha$ -lactose per 100 g water. The exact  $\alpha$ -lactose concentration depends on the equilibrium ratio of alpha and beta lactose; this is temperature dependent. Kauter, (2003) investigated



the secondary nucleation threshold supersaturation value of 8 g lactose per 100 g water in simulated whey permeates. No change in this value was found.

#### 4.3.3.2 Industrial permeate

Simulated whey solutions do not include the proteins or any precipitated minerals found in industrial whey permeate. For this reason it is necessary to measure nucleation as it occurs from an industrial permeate. Plotted in Figure 4-6 are the results for secondary nucleation in industrial permeate solutions from Kauter, (2003). These experiments occurred at a single concentration of 50 g anhydrous lactose per 100 g water, at temperature of 23 °C. This corresponds to an absolute supersaturation 11.8 g  $\alpha$ -lactose per 100 g water (assuming a similar solubility and equilibrium ratio to that found in water). As water was used to dilute permeates to the desired concentration the above assumption is considered justified. It was found in chapter three that diluted permeate had a solubility resembling water.

In Figure 4-6 the labels Perm A and Perm B identify nucleation data measured in two different industrial permeates. The value for Cent A was obtained from a sample of permeate A which had been centrifuged to remove solid impurities. The amount of scatter in the simulated whey data, and lack of experimental results for permeate means solid conclusions are cannot be drawn. Based on the limited data nucleation in simulated whey and industrial whey appear to be similar. The lack of information in this area means that more investigation into nucleation in whey permeates is required.

#### 4.3.3.3 Summary of the literature

The work in the literature shows clearly that increasing supersaturation increases the  $\alpha$ -lactose monohydrate nucleation rate. It also shows the presence of impurities increase the nucleation rate from what is observed in a pure lactose water solution. The results for the effect of temperature are ambiguous with the interpreted effect being dependent on the method used to express the results. The literature in the area of lactose nucleation is focused on secondary nucleation. The exceptions to this are the studies by (Herrington, 1934a), (Raghavan *et al.*, 2001) and (Arellano *et al.*, 2004). In these studies, the primary nucleation results are not clear and appear to be system specific. It is concluded that the greatest contribution can be made through the

development of knowledge in the area of primary nucleation. The work from here on will focus on understanding the key parameters in the area of lactose nucleation as it occurs directly from solution. Industrially, understanding primary nucleation is essential when looking to improve yield through increasing the solids concentration of permeate exiting the evaporation process. Failure to appreciate the effect of changes can lead to the production of fine crystals that are difficult to recover and process.

## **4.4 Measuring lactose nucleation**

### **4.4.1 A review of techniques for measuring nucleation**

There are several techniques available for measuring the primary nucleation of lactose from solution. A brief review of the different approaches is discussed below.

#### **4.4.1.1 Heat of reaction**

One approach to determining nucleation kinetics is to measure the reaction energy released during transformation from solution phase to solid phase. A differential scanning calorimeter (DSC) can be used to make this measurement. Shi & Rousseau, (2001) used a DSC to measure the metastable limits of  $\text{Na}_2\text{CO}_3$  at a range of concentrations. A 100  $\mu\text{l}$  sample of solution was rapidly heated, in 0.15  $\text{cm}^3$  pan, to a temperature well above the solubility point and then slowly cooled until nucleation was detected. The metastable limit was defined as the point just before a sharp decrease in the heat flow curve was recorded. The results obtained using this technique compared closely with another method that defined the metastable limit as the point where crystals were first observed visually. Myerson & Jang, (1995) used a DSC to investigate how impurities changed the metastable zone width of adipic acid. This work also investigated the solubility and found the results reproducible to within 0.1  $^{\circ}\text{C}$ . Darcy & Wiencek, (1999) used a DSC in conjunction with turbidity measurements to determine the metastable limit for lysozyme nucleation. Varying scan-rates showed different results and it was concluded that the DSC measurement showed a phase separation occurring rather than the originally postulated nucleation event. Visual observation was assessed to be a better method for detecting nucleation.

The DSC technique has the advantage that it can independently determine the metastable limit without needing to physically detect crystals. This makes it useful

when studying an opaque material like whey permeate concentrate. A series of experiments was carried out in this work using this technique to measure  $\alpha$ -lactose nucleation. The study found that despite a high degree of subcooling no heat of reaction could be detected. This made the technique unsuitable for studying lactose nucleation. The inability to detect any heat of reaction was believed to be due to the high stability lactose displays in the absence of any mixing (Raghavan *et al.*, 2002). As the technique does not allow mixing, the industrial applicability of the results would have been limited.

#### 4.4.1.2 Counting-Microscope

The number of crystals resulting from nucleation can be determined by counting them. The size of a newly formed crystal makes a microscope a better tool during the early stages of growth than the human eye. Using a microscope the crystal size and shape can be documented as growth progresses. Microscopy is limited to solutions where the transmission of light can occur through the solution. When using it to study opaque solutions such as whey permeate concentrates, dilution is required to increase the clarity. A second limitation of the technique is that when high crystal concentrations are present it becomes difficult to separate and count crystals. A partial solution to this is the dilution of the crystals though the addition of a slightly supersaturated solution. A similar approach is common in microbiology where high bacterial cell concentrations exist.

Arellano *et al.*, (2004) used polarised light microscopy to measure the primary nucleation of lactose from solution. The polarised light allows the crystals to be distinguished from the black background and identified earlier. In the work by Arellano the microscope induction times were compared against those obtained measured using refractive index to determine concentration change. The microscope allowed nucleation to be detected earlier.

#### 4.4.1.3 Turbidity and absorbance

The presence of solid particles, such as crystals in a liquid changes its optical properties. This change can be measured as a change in turbidity or, where a spectrophotometer is used, as a change in absorbance. This approach can be used to measure nucleation rates if the relationship between the number of crystals in solution

and absorbance is known. It is more commonly used to determine induction times from which an understanding of nucleation is gained (Hu, Hale, Yang, & Wilson, 2001) and (Parsons *et al.*, 2003).

Absorbance provides a way of monitoring changes in solution that are beyond the detectable limits of the human eye. It also allows a large number of samples to be made and measured in a short timeframe. Where the nucleation to be monitored occurs in a highly turbid or opaque solution, the changes in turbidity resulting from nucleation are difficult to detect. This limits the techniques use in whey permeate concentrate.

#### 4.4.1.4 Concentration change

Used in conjunction with a population balance an understanding of the nucleation kinetics can be obtained by measuring the changing concentration as lactose crystallises out of solution. This technique allows a large amount of kinetic data to be obtained over a range of supersaturations. When using the approach to measure primary nucleation it is necessary that a sufficiently high supersaturation be maintained to avoid the secondary nucleation mechanisms becoming dominant (Garside, Mersmann, & Nyvlt, 2002).

#### 4.4.1.5 Light scattering

Laser light scattering is a tool commonly used for measuring particle size distributions. In some devices, such as the Malvern Master Sizer 2000, it is possible to obtain a volume concentration. Using the particle size and the volume concentration of particles at each size the number of nuclei in solution can be calculated. This approach was used by Kauter, (2003) where a more detailed explanation on the method can be found. The use of light scattering as a tool for measuring nucleation in industrial permeate concentrates is made difficult by the presence of fine non-lactose precipitates. There is potential for these non-lactose precipitates to cause large errors in measurement of the number of lactose crystals and the volume of solids present in the solution.

#### 4.4.1.6 Measuring nucleation from the mass crystallised

Separating the crystals from the solution and measuring the mass collected provides a simple method for determining the amount of substance that has nucleated from solution. When used in conjunction with a particle size measurement the number of crystals can be calculated from the mass collected. The approach is limited to situations where the newly formed crystals are easily separated from other solids also present such as seed crystals or foreign matter. This prevents such an approach being used with whey permeate where a large amount of non-lactose solids are present in the solution.

#### 4.4.2 Nucleation in a lactose and water solution

The technique selected for quantifying lactose nucleation in a lactose-water system was absorbance. The method was selected due to its simplicity, the speed at which it enabled measurements to be made and its ability to provide information on changes in the solution prior to them being detectable to the unassisted human eye. The nucleation of  $\alpha$ -lactose monohydrate was investigated through a series of batch experiments, with the time to reach the critical number of nuclei ( $t_N$ ) being determined for each. Supersaturation was achieved by dissolving a predetermined mass of lactose into 500 ml of distilled water. The lactose used in all the experiments was pharmaceutical grade  $\alpha$ -lactose monohydrate of the Wyndale brand, purity 99.8 per cent. The experiments were all carried out in a 750 ml baffled vessel, shown in Figure 4-7.

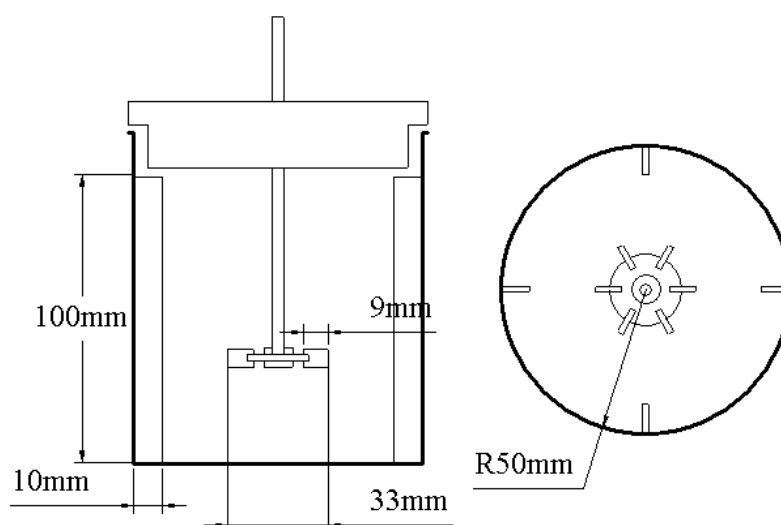
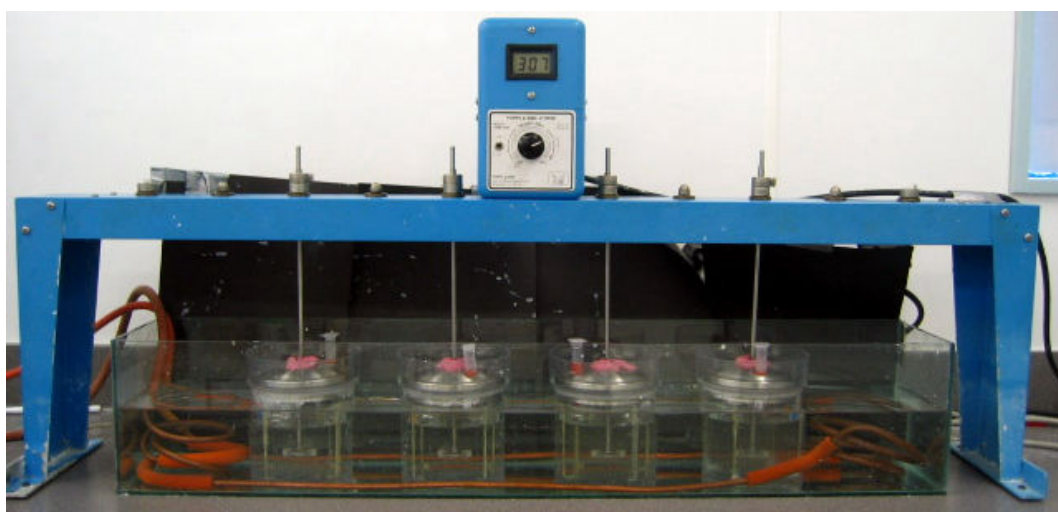


Figure 4-7 Baffled 750 ml vessel and Rushton agitator used for the nucleation experiments

Agitation was used in all the experiments as it has been shown to decrease the time required for crystals to form (Raghavan *et al.*, 2001). Industrially lactose solutions are exposed to a form of agitation, either directly from application of impellor driven mixing, or inadvertently when pumped around the plant.

Agitation was applied using a six-blade Rushton turbine, with a diameter of 33 mm. The agitator used was selected because it is a well-studied mixing impellor. The experimental set up and design used were typical of those used for mixing experiments where a Rushton turbine was studied. The dimensions for the agitator and mixing vessel were scaled according to specifications of Lee & Yianneskis, (1998). The agitators were driven using a Phipps and Bird Model 7790-402 stirrer, as shown in Figure 4-8



**Figure 4-8 Image of the mixing equipment used for the nucleation experiments**

Nucleation was examined using two techniques; the principal method used was monitoring of the absorbance. The absorbance was measured using a Unicam Helios  $\beta$  UV/Visible spectrophotometer. Absorbance at 550 nm was measured relative to distilled water. The nucleation process was also monitored using a web cam, which recorded images of the vessels every 15 minutes. Where experiments required a time greater than twelve hours these images were used to provide a guide as to the point at which nucleation had reached the critical absorbance. This was achieved by comparing these images against images where the absorbance level was known

Supersaturated lactose solutions were created by dissolving a mass of lactose and then cooling the solutions to the desired temperature. An absolute supersaturation range from 37.70 to 9.31 g  $\alpha$ -lactose per 100 g water was used in the experiments. Water at 95 °C was used for all dissolutions; it exceeded the solubility concentration for the range of lactose solutions studied. Complete dissolution was determined by visual examination. To ensure that no “ghost nuclei” remained, the solutions were heated for a further 15 minutes beyond the point where no crystals could be visually observed. Following dissolution, the solutions were poured into the vessels in the water bath, where they were left to cool, without agitation, to the desired temperature. Cooling typically took between 90 to 100 minutes, after which the agitators were added to the vessels and the mixing process initiated. In all experiments a constant agitation rate of 400 r·min<sup>-1</sup> was used, this was used as it maintained any crystals that had nucleated in suspension.

Throughout the experiments, 1.5 ml samples were taken from the solution and the absorbance was measured. To provide a record of the turbidity changes in the system, these samples were taken every five minutes for the first fifteen minutes and then at quarter hour intervals. At low supersaturations where long induction periods were expected the sample period was expanded to reduce the volume of solution removed from the vessels over the course of the experiment.

Time zero was the point at which mixing was initiated. To determine if the cooling time had a significant effect on  $t_N$  a trial was carried out at the absolute supersaturation of 26.03 g  $\alpha$ -lactose per 100 g water. In the trial three, nucleation experiments were left for an additional 100 minutes before mixing, at a rate of 400 r·min<sup>-1</sup>, was initiated. The results were compared against four experiments where mixing was initiated immediately upon reaching the desired temperature.

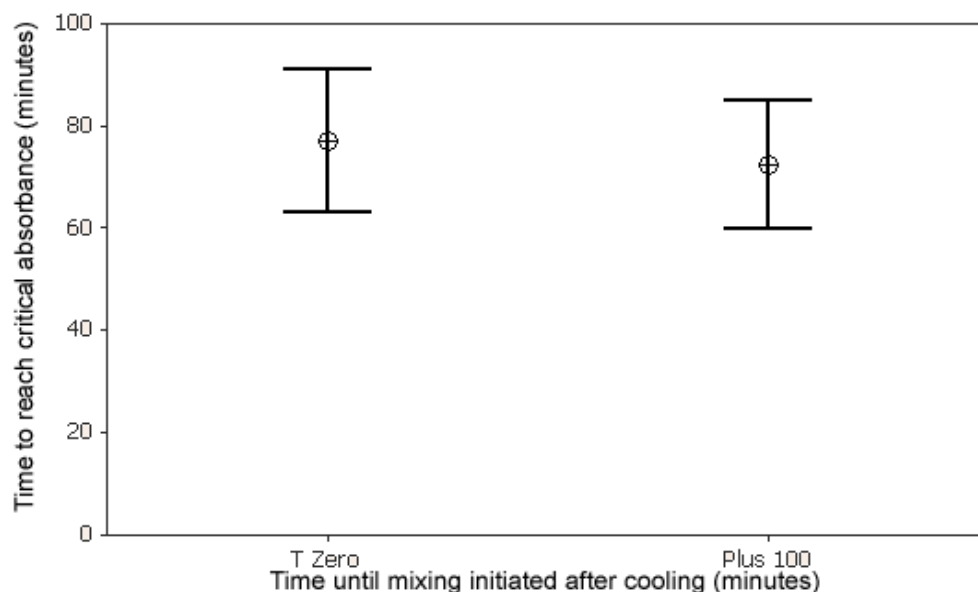


**Figure 4-9 Results from investigation into the effect of pre-mixing cooling time on nucleation results (Results show mean and 95 per cent confidence limits)**

The two data sets in Figure 4-9, show no significant variation in the value of  $t_N$ . The result is in accordance with the long induction time observed for static solutions reported by (Raghavan *et al.*, 2001). This result allows small variations in cooling time to be considered to have an insignificant influence on the nucleation results.

#### **4.4.3 Nucleation in simulated whey permeate**

Simulated whey provides a solution that can be used to study the effect the salts in whey have on the nucleation rate. The formulation used for this study was the same as that used by Kauter, (2003). The formulation is reproduced in section A1 of the appendix. It should be noted that this technique is not purely representative of the industrial situations as it creates a constant non-lactose solids concentration and varying lactose concentration. In the industrial environment, both the lactose concentration and non-lactose increase as water is removed by the evaporation process. As the solution has similar optical properties to water, the absorbance technique used for quantifying nucleation in water was used. All the measurements were carried out at 40 °C. This temperature was selected, as it was high enough above typical room temperature that it was easily maintained. The temperature is at the middle of the temperature range found in industrial lactose crystallisations.



The method used for the measurements was almost identical to that used for lactose water solutions described in section 4.4.2. The one difference was the preparation of the simulated whey solution, which was prepared the day before and left to stand overnight. The next day, to remove any fine undissolved impurities, it was filtered through a 0.45- $\mu\text{m}$  filter after which lactose was added and dissolved to create the desired concentration.

#### **4.4.4 Nucleation in industrial permeate**

The permeate concentrate solutions used in the study were made up from mother liquor collected from the Fonterra Kapuni lactose plant. The total solids and lactose concentration of the mother liquor were determined using the techniques described in section 4.4.1.2. Using this information it was possible to prepare a series of solutions with an absolute supersaturation range of 26.17 to 10.04 g  $\alpha$ -lactose per 100 g water. This was achieved through the addition and then dissolution of further lactose to the solution.

Once the desired mass of lactose had been dissolved at 95 °C, the solutions were poured into the mixing vessels and cooled to 40 °C, after which agitation was initiated. All the experiments were carried out at 40 °C, which allowed for the direct comparison of the results with the measurements made in water and simulated whey.

The opacity of industrial permeates meant that light absorbance, as a technique for monitoring nucleation, was unsuitable. To overcome this nucleation was measured using a polarised microscope. Nucleation was monitored in each of these solutions by taking a 2.5 ml sample of the solution and adding it to 7.5 ml of saturated lactose water solution. The dilution of the sample stopped any further nucleation and increased the clarity of the solution making it easier to observe crystals under the microscope. The solution was shaken lightly to ensure an even dispersion of any crystals. A small sample of the solution was then placed into a Neubauer counting chamber and polarised light was used to illuminate any crystals. To provide polarised light two polarised camera filters were used on a standard light microscope. The first was placed immediately after the light source and the second over the top of the slide. One of the polarised filters is shown alongside the Neubauer counting chamber in Figure 4-10.

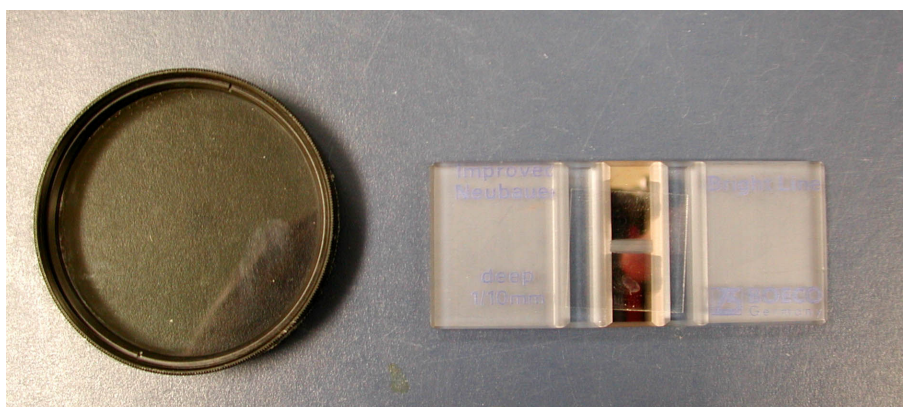


**Figure 4-10 Polarised filter and Neubauer counting chamber used for counting of nuclei**

Samples from the supersaturated solutions were photographed under the polarised microscope. The capturing of any crystals present on digital camera allowed them to be accurately counted later. Samples were taken until the number of crystals observed under the microscope became too dense for individual crystals to be easily distinguished.

#### 4.4.4.1 Relating absorbance measurements to the number of crystals

The relationship between the number of crystals in solution and the absorbance reading given on the spectrophotometer was determined. This facilitated the comparison of the results measured in the industrial solution against the results obtained for lactose-water solutions and simulated whey solution. It also enabled the results from the spectrophotometer to be compared against literature results that were expressed in terms of number of crystals.

The method described in section 4.4.2 was used. In addition to making the absorbance measurements, 1 ml samples of the solution were withdrawn from the crystallisation vessel and added to 5 ml of slightly supersaturated lactose solution at 20 °C. The dilution minimised the occurrence of additional nucleation between sampling and when measurements were made. Each sample was viewed under polarised light in a Neubauer counting chamber, as seen in Figure 4-10 above and the method given in section 4.4.4 was used to determine the number of crystals. The crystal counts were compared against the absorbance reading taken at the corresponding time and a relationship between the number of crystals in solution and absorbance was obtained.

## 4.5 Results and Discussion

### 4.5.1 Relating Absorbance to Number of Crystals

The opacity of industrial permeate required that crystal counting under a microscope was used measure nucleation, instead of the absorbance technique used for water and simulated whey solutions. Relating the two methods required a relationship between the spectrophotometer measured absorbance value and the number of crystals in solution. To determine this four experiments were carried where nucleation was measured using both absorbance and crystal counting. Samples of solution were taken over the course of the experiments and for each sample collected nine separate counts of the crystals in solution were carried out, from which a mean number of crystals was determined. The number of crystals per millilitre of solution and the corresponding absorbance value is shown in Figure 4-11. Each data point is plotted with its 95 per cent confidence interval.

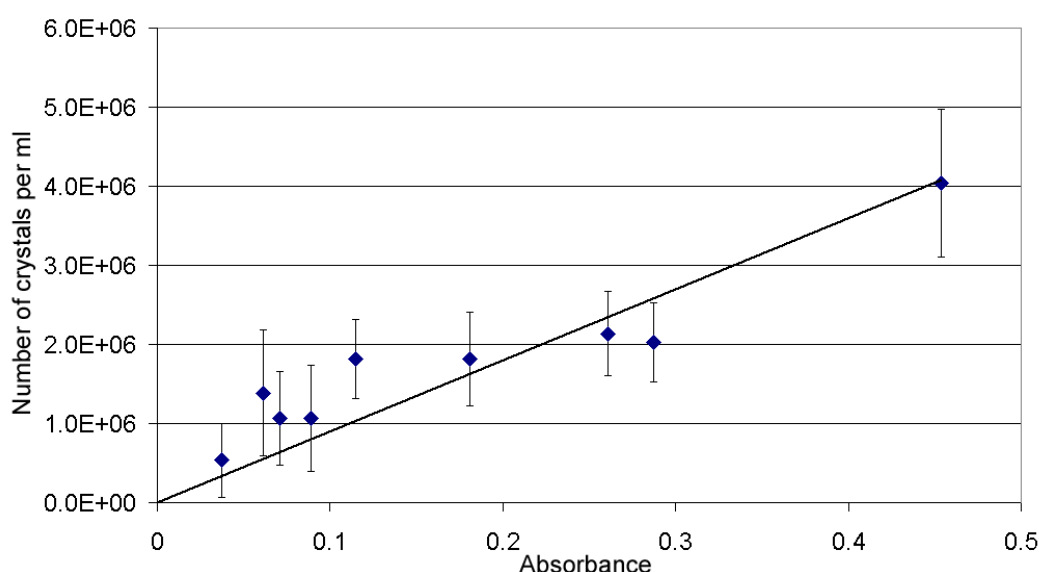


**Figure 4-11** The relationship between the absorbance at 550 nm and the number of crystals per ml solution (determined by sampling solution and counting the crystals under a light microscope)

Using the results collected, Equation 4-12 was fitted to calculate number of crystals required to produce the critical absorbance of 0.1 was calculated; this value was 899699 crystals per millilitre.

$$N_{cry} = 8996990 \times Abs$$

**Equation 4-12** Equation used to convert absorbance reading to number of crystals nucleated in the solution

As the number of crystals in solution increased the potential for error in the measurements became greater. This is seen in the increased scatter and increased confidence interval range at the upper ranges of the prediction. Where the crystal density becomes very large it becomes difficult to gain an accurate count as the potential for crystal overlap increases making it difficult to separate and count individual crystals. This is demonstrated by the images in Figure 4-12.

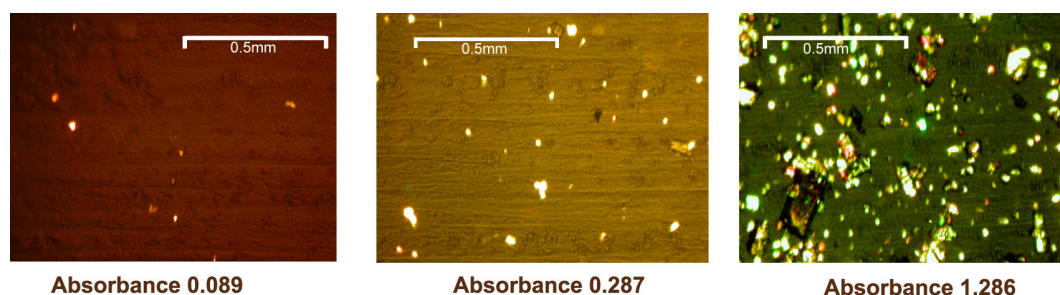


Figure 4-12 Comparison of number of crystals in solution at different absorbencies

#### 4.5.2 Determination of time to reach critical number of nuclei ( $t_N$ )

For the experiments in water and simulated whey, nucleation of lactose in the solution was measured from the absorbance measured by the spectrophotometer. This absorbance reading was monitored throughout each experiment by taking samples from the solution. Figure 4-13 shows a typical set of results for the experiments.

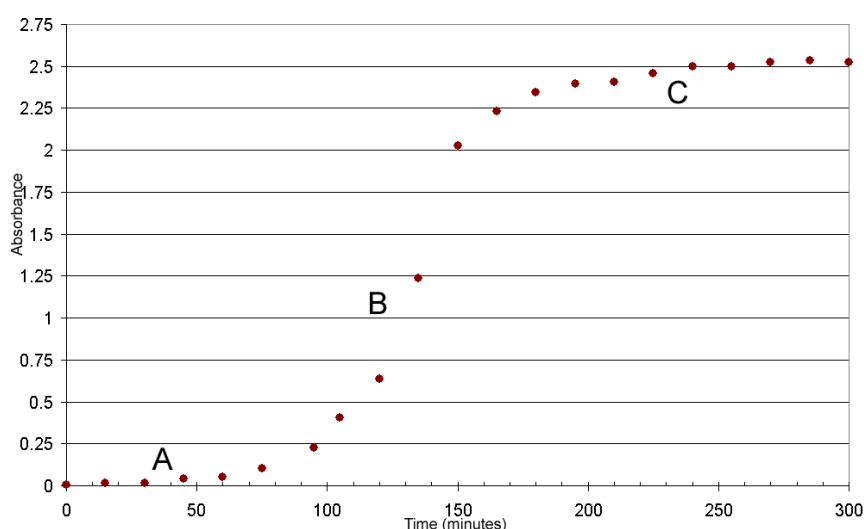


Figure 4-13 Typical absorbance curve for induction time experiments (Relative supersaturation 4.61, mixing speed 400 r·min<sup>-1</sup>, temperature 25 °C)

The absorbance curve, in Figure 4-13, can be divided into three sections; (a) the initial induction period where little change occurs in the absorbance, (b) a rapid rise in

absorbance, and (c) a plateau. In stage (c) the solution had become so turbid that the limits of the spectrophotometer were reached and further increases were not registered. When using data such as that presented in Figure 4-13 to determine the induction time El-Shall, Jeon, Abdel-Aal, Khan, Gower, & Rabinovich, (2004) determined the induction time to correspond to a point at which two asymptotic lines drawn along sections (a) and (b) intercepted. A similar method was used by Bernardo, Calmanovici, & Miranda, (2004) who set the induction time to be the point at which a sudden change in the absorbance profile occurred.

The approach of the induction time assumes that suddenly nucleation occurs. A more realistic view is that at some point crystals in solution become detectable. Taking this view, this study did not use the induction time, but determined the time required for a certain number of nuclei to form. To do this a fixed absorbance value was used instead of the methods described above. A fixed absorbance value is based on the idea that the absorbance corresponded to a number of crystals and that the time to reach this value was dependent on the nucleation rate. The critical time ( $t_N$ ) was set as the point where the absorbance was equal to 0.1, the exact time was determined by fitting an exponential curve to data points either side of the 0.1 value. An exponential curve was selected as this corresponds with the expected trend for nucleation offered in Equation 4-4. Section C in Figure 4-13 was not included in the data used for determining  $t_N$ . A value of 0.1 was selected because it represented a point, which was high enough to account for any scatter in the measurements and at the same time low enough that changes in absorbance would be dominated by nucleation.

To test how the critical absorbance value selected influenced the nucleation results, a range of absorbance values were considered for their affect on the calculated nucleation rate. The values for each absorbance were converted to number per millilitre per minute. This was achieved by dividing the number of crystals determined to apply each absorbance (using Equation 4-12) by the time required to reach this value. The values obtained are plotted, in Figure 4-14, against their respective absolute supersaturations

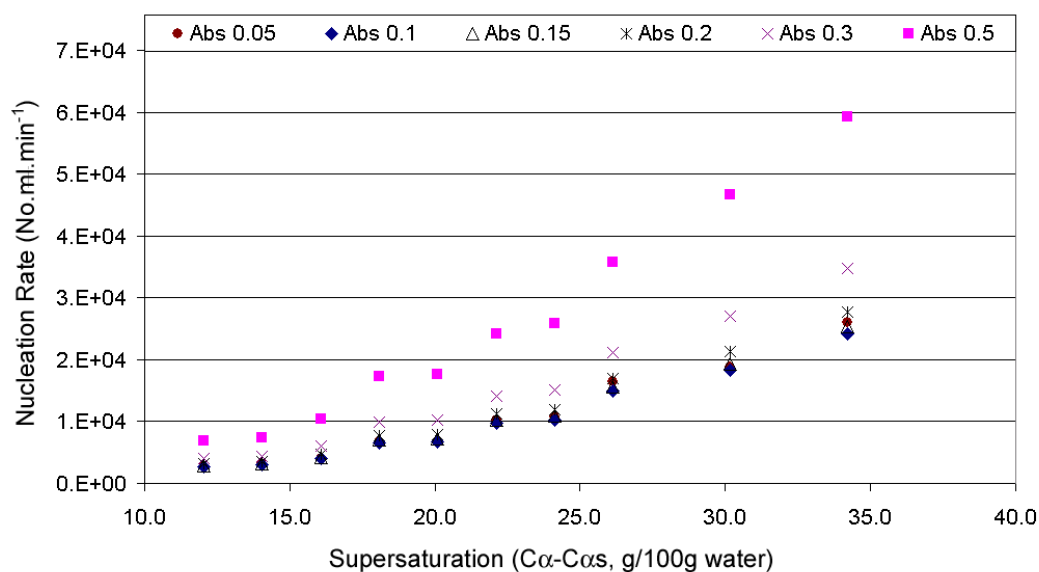


**Figure 4-14 The effect of the selected absorbance value on the calculated the nucleation rate**

Figure 4-14 shows that within the range of 0.05 to 0.2 the selection of the absorbance value has no observable affect on the nucleation rate. Once the value moves up to 0.5 the calculated nucleation rate becomes a factor of two greater, this is likely to a be a consequence of the large amount of crystals in the solution at this point leading to significant secondary nucleation. Given the results in Figure 4-14 and for the reasons given in the above paragraph the selection of 0.1 as a critical absorbance value was considered justified

An additional benefit of selecting 0.1 is that at this point the volume of lactose nucleated is negligible relative to the total volume of lactose in solution. This permits a constant supersaturation to be assumed. To confirm this a crystallisation was stopped early at an absorbance value of 0.137. A 100 ml sample of solution was filtered and the mass of solids per 100 ml determined. This value was found to be 0.117 g per 100 ml. Even at the lowest supersaturation investigated, this represents only 0.53 per cent of the available lactose. Given this result the condition of constant supersaturation is valid. It also demonstrates that at this point the nucleation rate will not be mutarotation limited.

### 4.5.3 Nucleation in a lactose and water Solution

#### 4.5.3.1 The effect of temperature on nucleation

The relationship between temperature and lactose nucleation in a lactose-water solution was investigated at 25 °C, 40 °C, 50 °C and 60 °C. A range of supersaturations was evaluated at each temperature. The results for the time required for the number of crystals in solution to produce the critical absorbance value on the spectrophotometer are plotted against the absolute alpha supersaturation in Figure 4-15. In all cases a minimum of two experiments were carried out to obtain an individual data point.

The results plotted in Figure 4-15 represent the average of these repeat experiments. The average instead of all the data has been plotted to reduce the noise in the graph making the results easier to interpret. To provide an indication of the uncertainty associated the standard errors of each data point has been plotted.

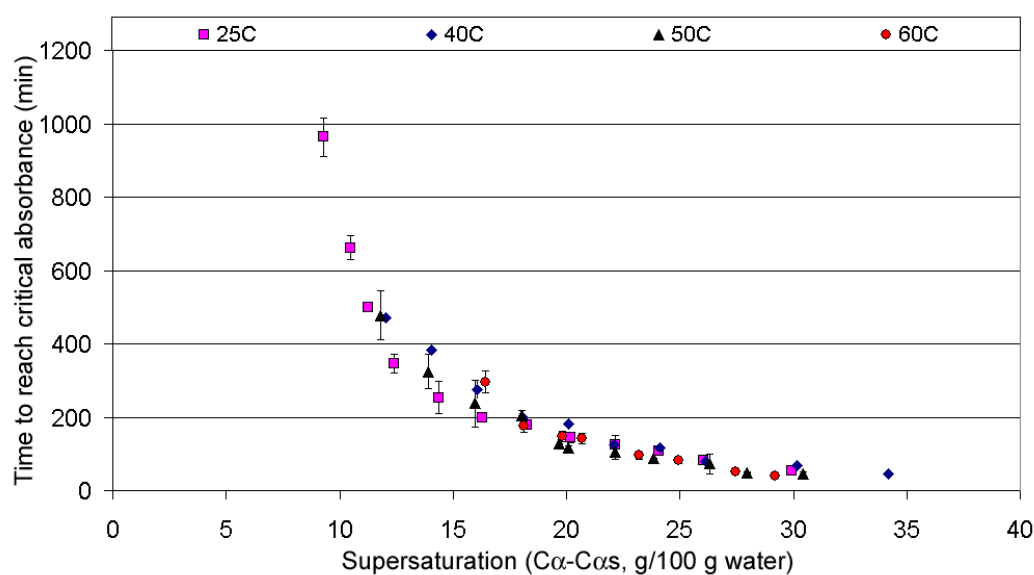


**Figure 4-15 Effect of temperature on the time required to reach the critical absorbance value of 0.1; measured over a range of absolute supersaturations**

The results in Figure 4-15 suggest that, above an absolute alpha supersaturation of 20g per 100 g water the nucleation rate is independent of temperature. Below this supersaturation there is more scatter suggesting a temperature effect. A trend appears that shows an increase in  $t_N$  with an increase in temperature. This is the same trend

reported by Kauter, (2003) who showed a decrease in the rate of nucleation with increasing temperature.

The rate of nucleation according to Equation 4-4 is variable with temperature. The position of temperature in the equation denotes that an increase in temperature should correspond to an increase in the rate of nucleation. The supersaturation in the nucleation theory is a relative, meaning that the effect of temperature on solubility is built into the equation. To understand the results requires that classical nucleation theory be considered at conditions of constant absolute supersaturation. Figure 4-16 shows this as a series of curves that are plotted at constant absolute supersaturations.

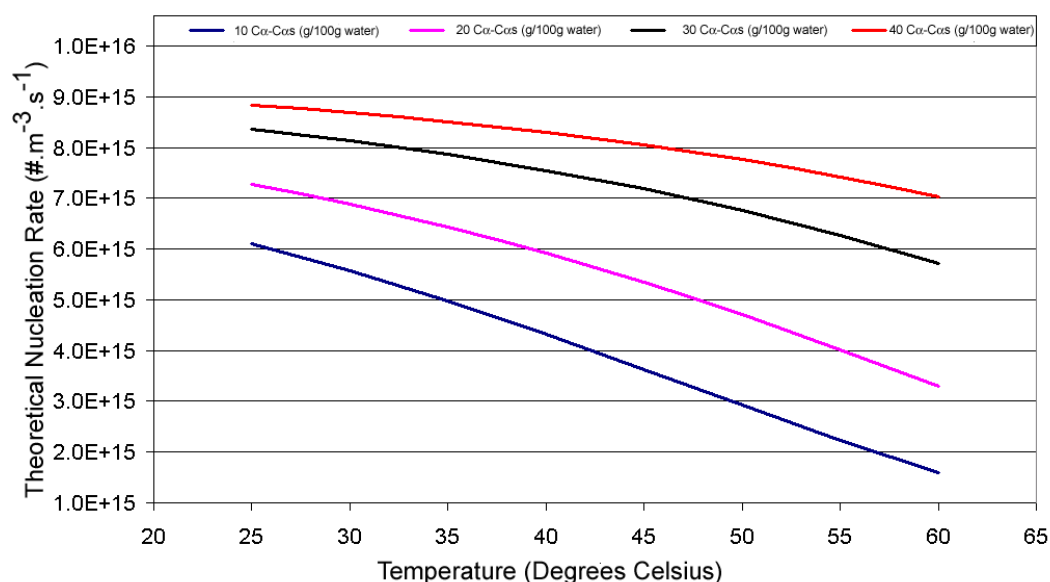


**Figure 4-16 Effect of temperature on the theoretical nucleation rate of lactose; determined at the absolute alpha lactose supersaturations of 10, 20, 30 and 40 (g/100 water)**

The curves in Figure 4-16 predict a decrease in nucleation rate with increasing temperature. Kauter, (2003) observed this at an absolute supersaturation of 11.66 g  $\alpha$ -lactose per 100 g water. There is also some evidence of this in the data collected in this study at lower absolute supersaturations. Figure 4-16 shows why a temperature effect is not seen at supersaturations above 20 g  $\alpha$ -lactose per 100 g water. As the absolute supersaturation is increased, the difference over the range of temperatures considered becomes smaller. At an absolute  $\alpha$ -lactose supersaturation of 10 g per 100 g water, the difference between the rate at 25 °C and at 60 °C is a factor of 3.83. The difference at a supersaturation of 40 g per 100 g water is a factor of 1.26. A factor of



1.26 is beyond the detectable limits of the measurement technique used in this study. Consequently, no effect of temperature is observed.

#### 4.5.3.2 The effect of supersaturation on nucleation

The relationship between supersaturation and the primary nucleation rate will be considered at isothermal conditions. This permits supersaturation to be expressed as a ratio without the need to account for any solubility effect of temperature.

A plot of  $\ln t_N$  vs.  $(\ln S_R)^{-2}$  allows the change in dominant mechanism of either homogenous or heterogeneous nucleation to be observed as a change in slope (Mullin, 2001). Primary nucleation is the sum of homogenous and heterogeneous nucleation, whilst one may be more dominant than the other, both occur to some extent. To account for this a slightly different approach to that given by Mullin, (2001) was taken. Using the relationships given in equations Equation 4-4 and, Equation 4-7 the results were plotted as  $t_N^{-1}$  vs.  $(\ln S_R)^{-2}$ . A curve using the sum of two exponentials seen in Equation 4-13 was then fitted using CurveExpert 1.38. Using this approach nucleation can be viewed as a combination of the two mechanisms. The values for  $B_{Hen}$  and  $B_{Hom}$  were used to determine the interfacial energy values for heterogeneous and homogenous nucleation respectively. A single exponential curve was also applied, however, it was found that this under predicted the results at the higher supersaturations and over predicted at the lower supersaturations. This was expected, as it only accounts for a single mechanism.

$$t_N^{-1} = A_{Hen} \exp^{(-B_{Hen}[\ln S_R]^{-2})} + A_{Hom} \exp^{(-B_{Hom}[\ln S_R]^{-2})}$$

**Equation 4-13 Equation used to fit curve to induction times measured at different supersaturations**

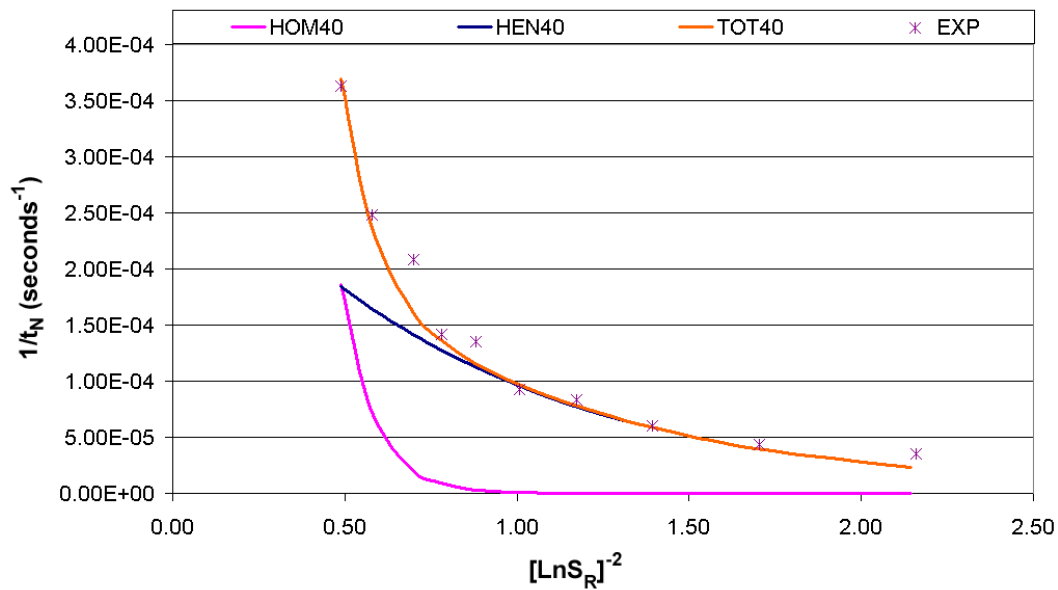


**Figure 4-17 Nucleation results viewed using classical nucleation theory (Temperature 40 °C)**

The point where the change in dominant nucleation mechanism occurs can be easily identified in Figure 4-17. At a  $(\ln S_R)^{-2}$  value of approximately 1.0 homogenous nucleation begins influencing the overall nucleation rate. When this value reaches 0.6, heterogeneous nucleation is the dominant mechanism.

The point at which homogenous nucleation appears as a factor in the overall nucleation process was investigated at the temperatures of 25 °C, 40 °C, 50 °C and 60 °C. Equation 4-13 was applied to the results presented in section 4.5.3.1 and these were then plotted in Figure 4-18 to Figure 4-20. The point where the homogeneous line leaves the  $x$ -axis, determined as the point where  $t_N^{-1}$  became greater than  $1.0 \times 10^{-7}$ , has been recorded in Table 4-3. The value of  $1.0 \times 10^{-7}$  was selected, as within the scale of the experimental results the change at this point is visible.

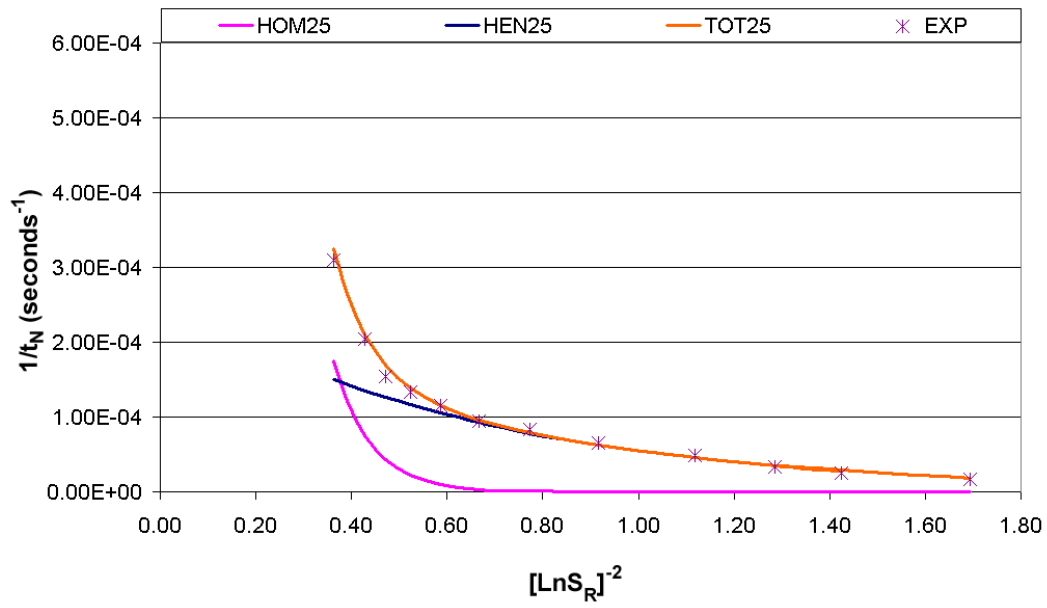


Figure 4-18 Nucleation results viewed using classical nucleation theory (Temperature 25 °C)

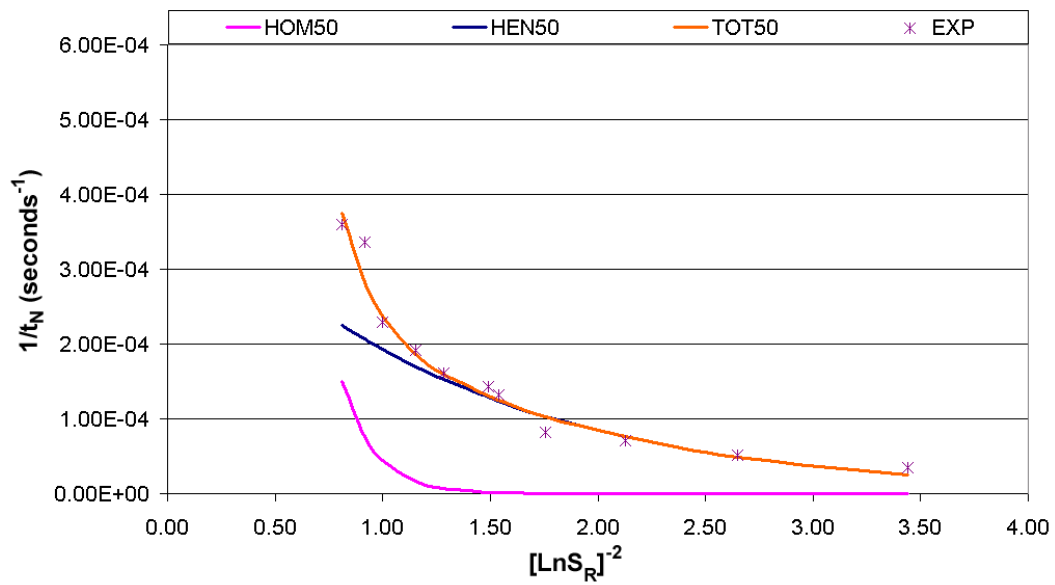
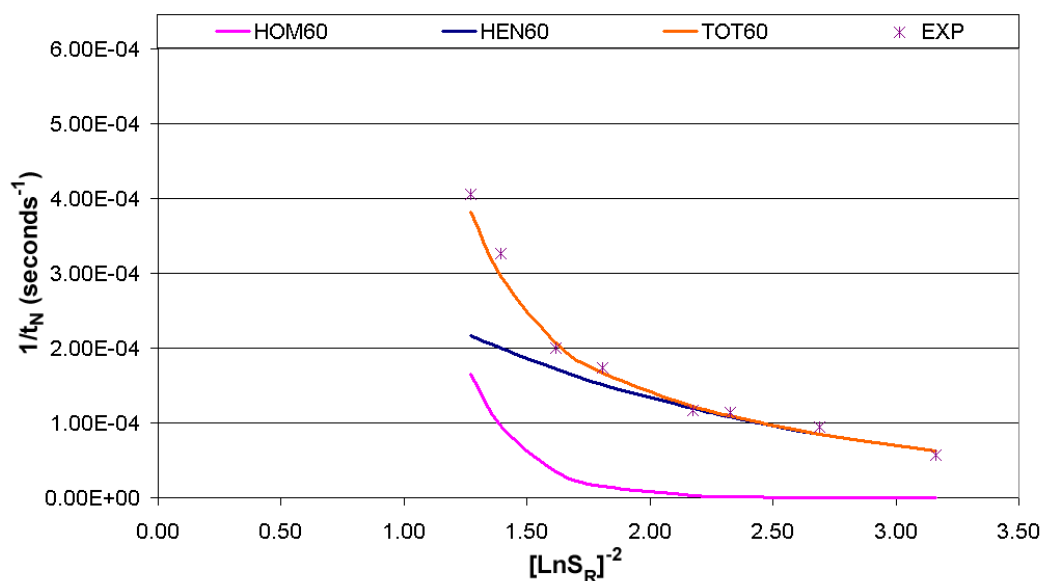


Figure 4-19 Nucleation results viewed using classical nucleation theory (Temperature 50 °C)



**Figure 4-20 Nucleation results viewed using classical nucleation theory (Temperature 60 °C)**

In Table 4-3 the  $(\ln S_R)^{-2}$  values for the initiation of homogenous nucleation have been expressed as relative and absolute supersaturations to enable the effect of temperature on the point at which homogenous nucleation becomes an important factor to be evaluated.

Temperature °C	$(\ln S_R)^{-2}$	Relative Supersaturation ( $C\alpha/Cas$ )	Absolute Supersaturation $C\alpha-Cas$ (g /100 g water)
25	0.59	3.69	20.20
40	1.01	2.71	20.12
50	1.48	2.27	20.10
60	2.17	1.97	20.67

**Table 4-3 Effect of temperature on initial homogeneous nucleation point compared used relative and absolute alpha lactose supersaturations**

When viewed in Table 4-3 as a function of relative supersaturation increasing the temperature results in a lower threshold for the initiation of homogenous primary nucleation. However, when viewed as a function of absolute alpha supersaturation the threshold is almost constant and independent of temperature. The value falls at approximately 20 g  $\alpha$ -lactose per 100 g water. Because the nucleation rate increases rapidly at supersaturations above this value, industrially this value is likely to represent the point above which small changes will have a large impact on the number and size of crystals produced

#### 4.5.4 Nucleation in simulated whey permeate

Nucleation measurements were conducted in simulated whey permeate solutions using the method described for a lactose water solution. A minimum of two experiments was carried out at each supersaturation, from which the average obtained is reported. The results are expressed using the classical nucleation approach in Figure 4-21. Included for comparison are the results collected under the same conditions for water.

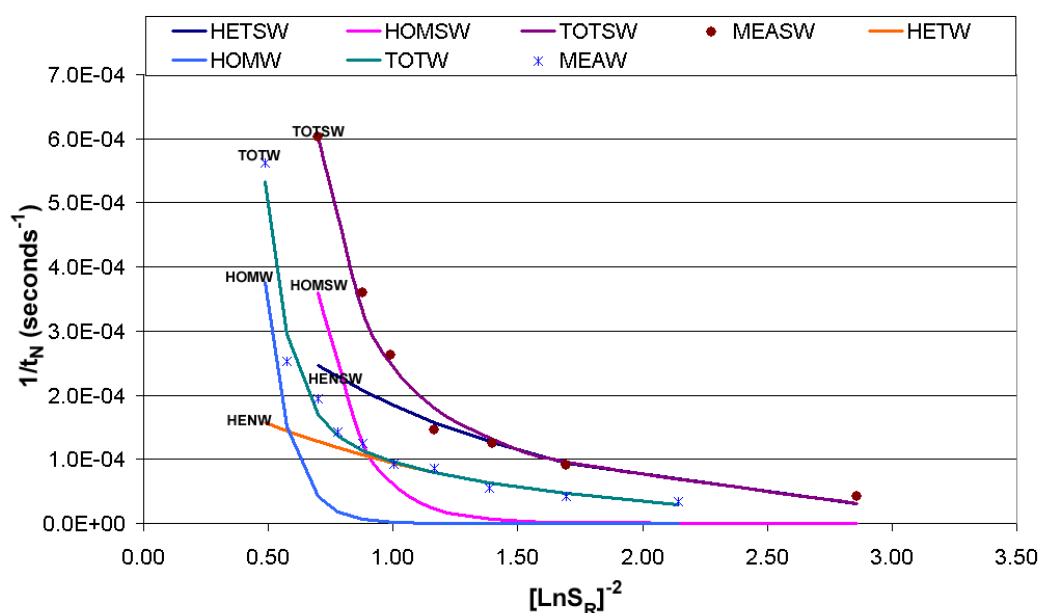
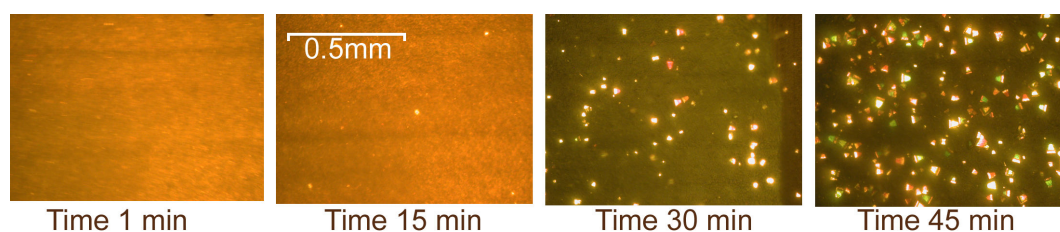


Figure 4-21 Comparison of lactose nucleation in simulated whey permeate (SW) and water (W) (Temperature 40 °C)

In Figure 4-21 it can be seen that in simulated whey permeate the time required to reach the critical number of nuclei at a particular supersaturation is less than is needed in water. This decrease corresponds to an increased nucleation rate. Figure 4-21 also shows that, when compared to water, simulated whey permeate requires a lower supersaturation for homogenous nucleation to influence the nucleation rate. A further discussion of these results follows in the section below where the nucleation rate in permeates is also considered.

### 4.5.5 Nucleation in industrial permeate

Nucleation in permeate was monitored through the process of counting the crystals in solution using a polarised microscope. A sample of the microscope images used in determining  $t_N$  for whey permeate are shown in Figure 4-22.



**Figure 4-22 Permeate nucleation measured using microscope (Absolute  $\alpha$ -lactose supersaturation 20.12 g per 100 g water, relative supersaturation 2.71)**

Figure 4-23 compares the  $t_N$  for industrial permeate, simulated permeate and water. Due to the opacity of industrial permeate the results shown were converted back to absorbance measurements using Equation 4-12. Each data point for permeate represents the average of duplicate experiments carried out under identical conditions.

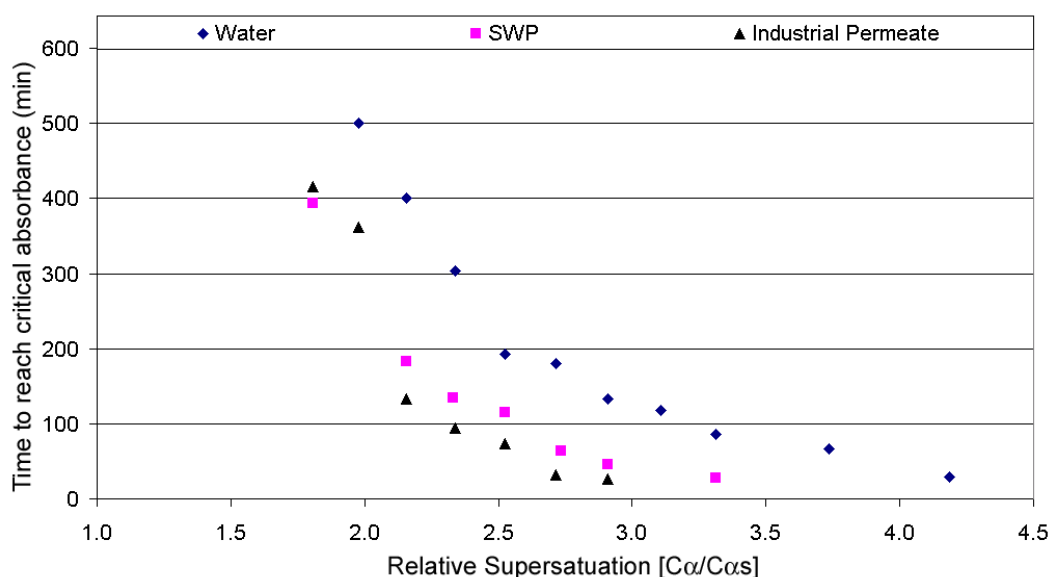


**Figure 4-23 Time to reach critical absorbance value of 0.1 as measured for supersaturated lactose solutions made up of water, simulated whey permeate and industrial permeate (Temperature 40 °C)**

Figure 4-23 shows at high supersaturations  $t_N$  is shorter in industrial permeate than was measured in water and simulated permeate. It was expected that the fine non-

lactose solids present in the whey permeate would provide surfaces upon which nucleation would occur. However, unexpectedly the time required to reach the critical absorbance at the lower supersaturations was almost identical to what was measured for the simulated whey. At lower supersaturation, heterogeneous nucleation is dominant and it would be expected that fine particles in the solution would have resulted in a faster nucleation rate. To further investigate, the results in Figure 4-23 were replotted using the approach to classical nucleation theory described in section 4.5.3.2. The results are presented in Figure 4-24.

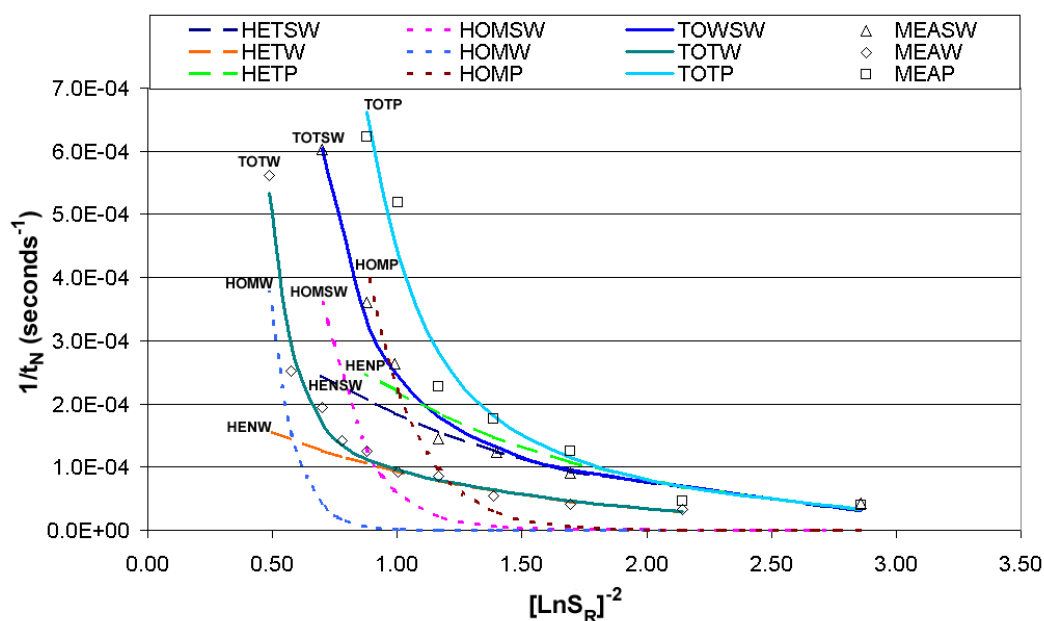


**Figure 4-24 Comparison of lactose nucleation in whey permeate (P), simulated whey permeate (SW) and water (W) (Temperature 40 °C)**

The curves in Figure 4-24 show the heterogeneous nucleation rate in industrial permeate at the lower supersaturations is similar to that seen in simulated permeate. The major change in the nucleation rate appears to be in the region of homogenous nucleation, with a reduction in supersaturation required for homogenous nucleation to appear as a factor in the overall nucleation rate. To allow further analysis, Equation 4-13 was fitted to the results.

Solution	$A_{Hen}$	$B_{Hen}$	$A_{Hom}$	$B_{Hom}$
Water	0.00026	1.01	0.0616	10.44
SWP	0.00048	0.96	0.0216	5.89
Permeate	0.00061	1.01	0.0338	5.02

**Table 4-4 Homogenous and heterogeneous nucleation parameters for water, simulated whey permeate and industrial permeate, determined using classical nucleation theory**

Of particular importance in Table 4-4 are the  $B_{Hom}$  and  $B_{Hen}$  values of the heterogeneous and homogenous nucleation curves. An examination of Equation 4-4 reveals the significance of these values. A change in the value of  $B_{Hom}$  or  $B_{Hen}$  indicates a change in the interfacial tension value or the energy barrier, which must be overcome in creation of a new solid liquid interface. A reduction in this value, as is shown in Equation 4-11, reduces the size of the critical nucleus meaning that fewer molecules are required to come together for a new stable nucleus to be formed.

Figure 4-23 shows that the rate of nucleation in simulated whey and industrial whey is faster than water. However, nucleation in industrial permeates appears to be only slightly faster than is observed in simulated whey permeates. Although the additional solid material in industrial permeates presents a surface on which new nuclei could form, it appears that this is not the dominant influence on increased nucleation rate. The parameters in Table 4-4 indicate that the fine material is a source of nucleation sites only when the supersaturation becomes great enough.

The major factor affecting the nucleation rate is the presence of salts in the solution, which lower the interfacial energy barrier to nucleation. This is shown by the  $B_{Hom}$  value for homogenous nucleation for nucleation in simulated whey and in permeate being approximately half that seen for a lactose water solution. Although the  $B_{Hom}$  values for industrial and simulated permeate are similar, the salt concentrations are different. The industrial permeate was analysed using Inductively Coupled Plasma–Optical Emission Spectroscopy (ICP-OES) to determine the minerals in the solution. The results from this are presented in Table 4-5 alongside the mineral concentrations for the simulated whey permeate.



<b>Mineral</b>	<b>Simulated Permeate (mg·kg<sup>-1</sup>)</b>	<b>Industrial Permeate (mg·kg<sup>-1</sup>)</b>
Calcium	1000	1800
Phosphorus	6000	8800
Sodium	5700	9100
Potassium	13500	35700
Chloride	3810	19700
Magnesium	700	750

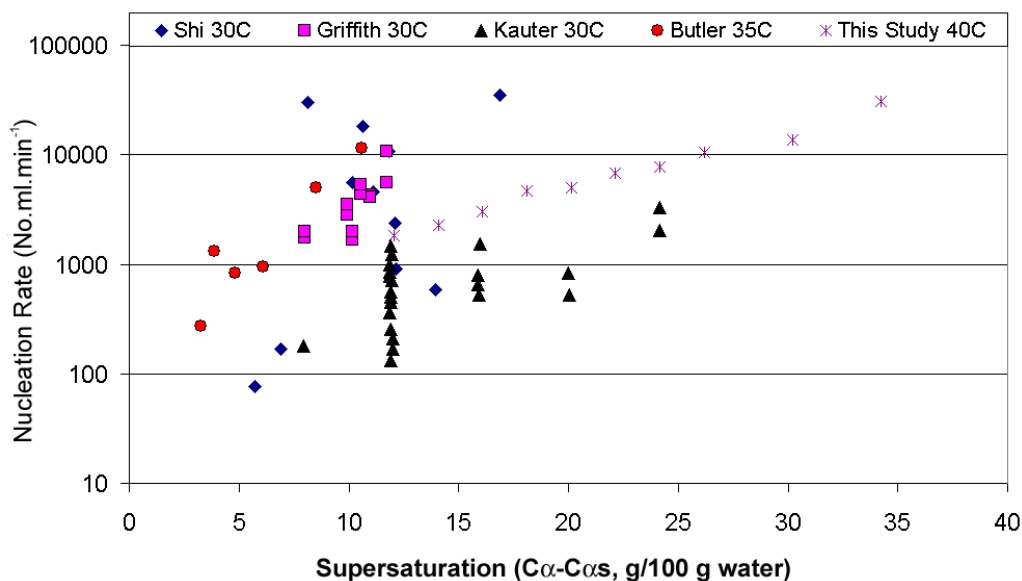
**Table 4-5 Comparison of mineral components measured in simulated whey and whey permeate**

Table 4-5 shows that the salt concentration was higher in the industrial permeate in all cases. It was concluded from this that the decrease in induction time was due to a lowering of the interfacial energy barrier by the salts.

Seasonal and process differences mean that the salt concentrations in industrial permeate are variable. This means that even with a detailed examination into how different salts change the nucleation rate an exact prediction for individual permeates would be difficult to obtain. It is still important to note the large increase in nucleation seen in the simulated whey and industrial permeates when compared against water. In addition, worth noting are the values of supersaturation at which homogenous nucleation appears as a factor in the simulated and industrial whey permeates. These are approximately 16 g  $\alpha$ -lactose per 100 g water and 14 g  $\alpha$ -lactose per 100 g water respectively. This compares with the value of 20 g  $\alpha$ -lactose per 100 g water obtained for a pure lactose water solution.

## **4.6 Comparison with literature**

The results collected in this study were compared against the literature results by converting the values for  $t_N$  to number per ml per minute. This was achieved by dividing the number of crystals determined in section 4.5.1 to represent an absorbance value of 0.1 by the time  $t_N$  at a specific supersaturation. The values obtained were then plotted against the literature nucleation values presented in Figure 4-3. The results are shown in Figure 4-25.



**Figure 4-25 Comparison of nucleation results from this study with literature nucleation rates reported for a lactose water solution**

The results from this work have a trend which are at the upper limit of the results generated in the study carried out by (Kauter, 2003). This may indicate that in some of the experiments carried out by Kauter some primary nucleation occurred resulting in an exaggeration of the secondary nucleation rate.

The results sit at the lower limits of those produced by Shi *et al.*, (1990), Griffiths *et al.*, (1982) and Butler, (1998). The reasons for this are unclear although a likely cause is the different approaches used in initiating and measuring the nucleation. The data from the three above-mentioned authors shows considerable scatter, again suggesting that whilst the experiments were aimed at measuring secondary nucleation, primary nucleation may have also occurred in some cases. The agitation conditions may also explain variation in the results (Raghavan *et al.*, 2001), this is an area where further investigation is required.

## 4.7 Conclusion

The primary nucleation of  $\alpha$ -lactose monohydrate from a lactose-water solution was investigated over a range of supersaturations and temperatures. Temperature was found to be an insignificant factor on the nucleation rate when supersaturation was considered in term of absolute alpha lactose supersaturation. When considering this result using the trend predicted by classical nucleation theory, the effect of

temperature was found to be smaller than could be detected using the experimental approach taken. The effect of temperature on the nucleation rate becomes more significant as the absolute supersaturation decreases. This explains why the study of Kauter, (2003) found a temperature effect as the supersaturation considered in the study was at the low end of the range investigated here. A similar relationship was observed in this study when the results of the experiments in a similar range were investigated.

As expected nucleation increased with increasing supersaturation. Using classical nucleation theory the effect of supersaturation on the homogenous and heterogeneous nucleation mechanisms was examined. A value of 20 g  $\alpha$ -lactose per 100 g water was observed to be the point at which homogenous nucleation significantly contributed to the total nucleation rate in lactose water solutions.

The effect of impurities on the rate of primary nucleation was investigated. Simulated whey permeate made in the laboratory and industrial permeate were used. An increase in overall nucleation rate when compared to water was observed in both solutions. The main factor responsible for this increase was the presence of the salts in the solutions. The salts had the effect of lowering the interfacial energy barrier to nucleation, effectively decreasing the number of molecules required to form a stable nuclei at a particular supersaturation. The fine precipitated solids in permeate had only a small effect on the overall nucleation rate.

The nucleation results obtained for a lactose water system were compared against the literature data. All the literature data used in the comparison was obtained from studies that used seed crystals to initiate nucleation and so are likely to have measured secondary nucleation. The scatter in the literature data made it difficult to make comparisons, but it appears that the results from this study compare favourably with the literature results. The system specific nature of the nucleation rate makes the comparison difficult. The rate of agitation is identified in the literature as being a key cause of the difference in measured nucleation rates. This will be investigated in the next chapter.



## **Chapter 5 Nucleation: The effect of mixing**

### **5.1 Introduction**

To achieve control over the final lactose crystal size distribution an understanding of the relationship between different variables and the nucleation rate is required. Chapter four discussed literature reports that identified mixing as having a significant effect on the observed nucleation of alpha lactose monohydrate (Valle-Vega & Nickerson, 1977), (Shi *et al.*, 1990) and (Raghavan *et al.*, 2001). A comprehensive study which has quantified or developed a relationship to enable this ‘mixing effect’ to be used as a tool through which lactose nucleation can be manipulated has yet to be carried out. This work looks to authenticate the existence, or not, of the so called “mixing effect”. This will be achieved by reviewing the literature as well as by conducting experiments that investigate lactose primary nucleation under different agitation conditions.

### **5.2 Mixing and nucleation**

The addition of an external energy source to stimulate the nucleation of crystals from solution is well documented. Young , (1911) remarked, “In the labile state the crystallisation must spontaneously occur sooner or later. The time required may be very short or very long, and may, in general, be reduced by a variety of causes, especially by agitation.” Young went on to conclude that the idea of a metastable limit was “fallacious and untenable”, with the whole unstable field (concentration above the solubility limit) being able to be crystallised by the production of sufficient mechanical shock.

Studies carried out since that of Young, (1911) have shown that the metastable limit is specific to the conditions under which it is determined. Ultrasound, agitation and shear all appear in the literature as techniques by which nucleation can be coerced. During the processing of fondant, for example, the sugar mass is cooled to the desired temperature and then beaten extensively to promote a massive nucleation event. This

results in the production of many small crystals and produces a smooth fondant (Myerson, 2002). The following section provides a short review of the results observed using these techniques. There are countless more studies than those presented here, the ensuing review only seeking to recapitulate the observed effects.

### 5.2.1 Ultrasound induced nucleation

Ultrasonic energy affects both nucleation and crystal growth. Its application as a means of enhancing crystallisation was first reported in 1927 when it was applied to induce nucleation in a thiosulphate system (Patrick, Blintt, & Janssen, 2004). In lactose crystallisation Butler, (1998) used it to induce a single nucleation event in the preparation of common history seed. Vu, Durham, Hourigan, & Sleight, (2004) used it to enhance nucleation for the creation of fine lactose crystals. In studying how the application of ultrasound changed the activation of a reaction between diethyl malonate and chalcone Ratoarinoro, Contamine, Wilhelm, Berlan, & Delmas, (1995) found ultrasound provided a dramatically better performance than mechanical agitation applied using the same power input. Hagenson & Doraiswamy, (1998) showed that the application of ultrasound both enhances mass transfer and increases the effective diffusivity of a liquid reactant through the interfacial film.

Ultrasonic energy is suggested to increase the rate of nucleation by increasing the number of potential nucleation sites. Nucleation sites are formed by either cavitation or by the creation of surface imperfections that act as heterogeneous nucleation sites. The formation and collapse of cavities occurs when ultrasound of appropriate energy and frequency is applied. A diagram demonstrating this process is presented in Figure 5-1 (Devarakonda, Evans, & Myerson, 2003).

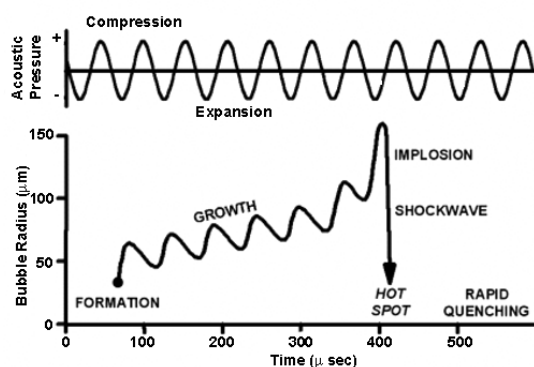
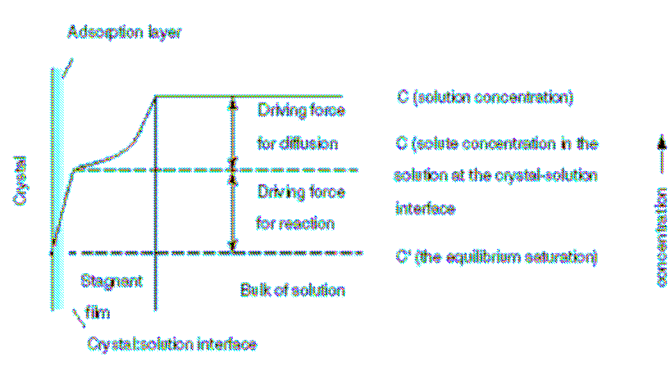


Figure 5-1 The scheme of the growth and destruction of a cavitation bubble (Devarakonda *et al.*, 2003)

Hagenson & Doraiswamy, (1998) assert that cavitation induced by the application of ultrasound to a solution creates shockwaves that propagate to the surrounding solids causing microscopic turbulence and/or the thinning of the solid film. This phenomenon is known as microstreaming and is thought to be responsible for increasing the rate of mass transfer through the solid liquid interface film.

Guo, Jones, & Li, (2006) observed the nucleation of barium sulphate ( $\text{BaSO}_4$ ) from solution, and found ultrasound improved the diffusion process. It increased the mass deposition rate and therefore the number of clusters crossing the size barrier and becoming nuclei. Diffusion is the second step in the model of the mass deposition process given in Mullin, (2001) as shown in Figure 5-2. Solute molecules are transported via a diffusion process from the bulk of the fluid phase through a stagnant film to the solid surface. This process is followed by a first order reaction when the solute molecules arrange themselves into the crystal lattice.



**Figure 5-2 Concentration driving forces in crystallisation from solution (Mullin, 2001)**

Lyczko, Espitalier, Louisnard, & Schwartzentruber, (2002) found ultrasound significantly decreased the induction time of a potassium sulphate solution. They found also that increasing the power input into the system leads to further decreases in induction time. As was discussed in the previous chapter, a decrease in induction time corresponds to an increase in the nucleation rate. Figure 5-3 shows the results from Lyczko *et al.*, (2002). A change in the slope of the graph as a function of supersaturation was reported; this indicates a decrease in the interfacial energy value and a consequent decrease in the critical nucleus. The opposite affect was reported by

Guo *et al.*, (2006) who found no change in slope but a change in intercept, signifying ultrasound alters the diffusion process.

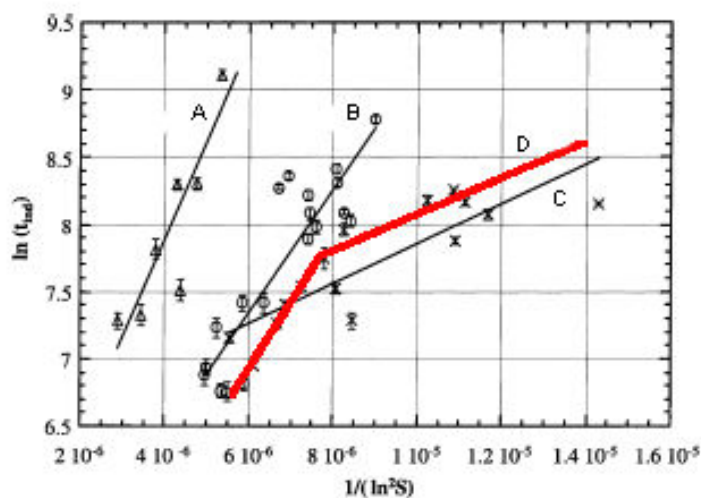


**Figure 5-3 Induction time as a function of supersaturation for potassium sulphate crystallisation (A) without ultrasound, (B)  $P_{\text{Dissipated}} = 0.043 \text{ W} \cdot \text{g}^{-1}$  (C)  $P_{\text{Dissipated}} = 0.114 \text{ W} \cdot \text{g}^{-1}$  (Lyczko *et al.*, 2002) (D) Lines by this work added to demonstrate that at higher supersaturations slope is similar, and that a second mechanism appears below a certain supersaturation**

It is observed in Figure 5-3 that in the data of Lyczko *et al.*, (2002) against which line (C) is plotted, at the higher supersaturations, a similar slope exists to that seen in data sets (A) and (B). Line (D) has been added to demonstrate this. When considered from this position, a similar conclusion to that drawn by Guo *et al.*, (2006) can be reached, that ultrasound acts to change the intercept. Therefore the data also shows that ultrasound alters the position at which the change in dominant nucleation mechanism occurs.

### 5.2.2 Agitation induced nucleation

Agitation and the role it plays in nucleation are discussed in the literature. However, the primary focus is on systems where a reaction between two or more chemicals is required prior to precipitation occurring. This means that agitation is considered for its role in the blending of the different molecules, allowing them to react and form the precipitating substance (Zauner & Jones, 2002), (David, 2001). Lactose nucleation involves the formation of crystals from a single molecular species and therefore the blending of two chemicals is not a concern. Mixing still, as is discussed by Raghavan *et al.*, (2001), influences the rate at which nucleation occurs. Studies of solution precipitation for materials other than lactose have also found mixing to be important



in the number of crystals formed. Chew, Ristic, Dennehy, & De Yoreo, (2004) found that where all other conditions were constant the precipitation of paracetamol is strongly influenced by the hydrodynamic environment.

Using a propeller agitator, Barata & Serrano, (1996) investigated the precipitation of potassium dihydrogen phosphate (KDP) under different agitation intensities. Above  $400 \text{ r}\cdot\text{min}^{-1}$  mixing began to reduce the induction time. They concluded that at this point the Kolmogorov eddies were small enough to reduce the barrier to processes at the molecular level. Examining the results using nucleation theory, the intercept, rather than the slope changed on the plot of  $\ln(\tau)$  versus  $(\ln S_R)^{-2}$ . This demonstrates that the interfacial energy barrier was independent of the agitation intensity and that mixing changed the frequency of molecular interactions.

Investigating nucleation at different agitation conditions Myerson, (2002) found, at constant supersaturation, increasing the intensity decreases the induction time up to a certain point, beyond which it reaches a plateau. Studying the precipitation of potash-alum, Mydlarz & Jones, (1991) observed a decrease in the induction time with increasing agitation rate of a paddle stirrer. Below  $200 \text{ r}\cdot\text{min}^{-1}$  no primary nucleation was observed. As the speed was increased from  $400 \text{ r}\cdot\text{min}^{-1}$  to  $500 \text{ r}\cdot\text{min}^{-1}$  a continued shortening of the induction time was observed. As the rate was increased progressively from  $600 \text{ r}\cdot\text{min}^{-1}$  to  $700 \text{ r}\cdot\text{min}^{-1}$ , the induction time decrease became less with each increase in speed. Mandare & Pangarkar, (2003) found that an increasing agitation rate lead to a decrease in crystal size. The impeller type was also factor, final particle size increased in the following order, flat blade turbine, pitched blade turbine and hydrofoil impellor.

### **5.2.3 The effect of shear flow on nucleation**

The nucleation of crystals under different shear flow conditions has been studied in the field of polymer crystallisation. There are also studies that examine the nucleation of colloidal suspensions. The application of shear to a system is qualitatively different to the effect of pressure, temperature or additives as the latter affect the thermodynamic driving force for crystallisation. In contrast a system under shear ends up in a nonequilibrium steady state (Blaak, Auer, Frenkel, & Lowen, 2004).

The general consensus is that the crystallisation of polymers is enhanced through the application of a shear flow (Vleeshouwers & Meijer, 1996), (Azzurri & Alfonso, 2005) and (Watanabe, Nagatake, Takahashi, Masubuchi, Takimoto, & Koyama, 2003). It is proposed that enhancement of nucleation is due to the creation of “thread-like precursors” resulting from the molecular orientation during flow (Jay, Haudin, & Monasse, 1999). The investigations into relationship between shear and polymer nucleation have been conducted using a variety of rheometer designs (Jay *et al.*, 1999).

The literature on how shear alters nucleation of colloidal suspensions is less conclusive. Palberg, Monch, Schwarz, & Leiderer, (1995) report shear to suppress nucleation. Amos, Rarity, Tapster, & Shepherd, (2000) reported shear to enhance the nucleation rate. Blaak *et al.*, (2004) explains both phenomena: “On the one hand shear may induce layering in the metastable fluid, thus facilitating nucleation. On the other hand, shear can remove matter from small crystallites and therefore work against the birth of new crystals”. For low shear rates Blaak *et al.* found that shear increases the size of critical nuclei effectively suppressing the nucleation rate.

The presence of particles in a solution alters the flow field and creates a hydrodynamic disturbance. This disturbance, first calculated by Einstein cited in (Macosko, 1994), changes the viscosity of the solution. For dilute particle concentrations (less than two per cent), the effective viscosity of the particle fluid mixture is determined using Equation 5-1.

$$\psi_m = \psi_f (1 + \phi_p)$$

**Equation 5-1 Equation for determining the effective viscosity of a particle fluid mixture**

As nucleation leads to the formation of particles in a system it should be possible to detect lactose nucleation as it occurs in a solution through measuring the changes in viscosity. The relationship between shear and the nucleation of lactose from solution has not been studied. Given this, an investigation into this variable is warranted.

## 5.3 Theory of mixing and fluid flow

As this chapter examines the relationship between nucleation and mixing, a basic summary of mixing principles is provided as a foundation from which a discussion into their potential role in the nucleation process can be drawn. This review is not meant to serve as a comprehensive examination of the areas under discussion; there are many well written text books on both subjects, some many hundreds of pages long, written by authors much more well versed in the area. In this study the works by Paul, Atiemo-Obeng, & Kresta, (2004) and Granger, (1995) were particularly useful additions to the large amount of information found in the journals.

### 5.3.1 Mixing levels

The mixing process can be divided into three levels (Paul et al., 2004);

- Macromixing is mixing driven by the largest scales of motion within the fluid; it is characterized by the blend time in a batch system.
- Mesomixing is mixing on a smaller scale than the bulk circulation (or the tank diameter) but larger than the micromixing scales. It is most frequently evident at the feed pipe scale of semi batch reactors.
- Micromixing is mixing on the smallest scales of motion (the Kolmogorov scale) and at the final scale of molecular diffusivity (the Batchelor Scale). Micromixing is the limiting step in the process of fast reactions, because micromixing dramatically accelerates the rate of production of interfacial area available for diffusion. This is the easiest way to speed up contact at the molecular level, since molecular diffusivity is more or less fixed.

For molecules to react or bind together, they must be in contact. Turbulence alone cannot provide this degree of mixing, so molecular diffusion will always play a role. This diffusion process is slow this makes the mixing process dependent on both bulk mixing and turbulent diffusion to reduce the scales over which molecular diffusion must act. To accomplish chemical reactions and nucleation, bulk mixing, efficient turbulence and molecular diffusion are all required for the final molecular contact to occur.

The micromixing kinetic process is a function of the macromixing kinetics. The size of the smallest eddies and thereby the length scales necessary for diffusion to complete molecular mixing are a function of the turbulence intensity and the specific power input (Schwarzer & Peukert, 2001). These small eddies can be defined by scales such as the Kolmogorov scale.

The Kolmogorov scale is a description of the smallest scales of motion. The smallest eddy dimensions are characterised by the Kolmogorov length scale, shown in Equation 5-2.

$$\eta = \left( \frac{\nu^3}{\varepsilon} \right)^{1/4}$$

**Equation 5-2 Kolmogorov length scale**

This represents the scale at which the deforming forces due to turbulence are balanced by the resisting forces due to viscosity. At this point the energy contained in the turbulent eddies is absorbed by viscous dissipation (Kresta, 1998).

At this scale the Kolmogorov time scale ( $t_k$ ) shown in Equation 5-3 applies, which represents the time taken to dissipate the energy contained in the smallest Kolmogorov eddy.

$$t_k = \left( \frac{\nu}{\varepsilon} \right)^{1/2}$$

**Equation 5-3 Kolmogorov time scale**

Relating the Kolmogorov length scale to operating variables requires a measure of the rate of dissipation of turbulent kinetic energy per unit mass. Since the system is batch and therefore the energy put into a tank from mixing can only be dissipated, an approximate measure of the turbulent energy per unit mass can be obtained from the power per unit volume put into the system via the agitation mechanism. This is discussed in section 5.3.4 below.

#### 5.3.1.1 Mixing patterns in an impeller agitated vessel

Although the tank is geometrically simple in an impeller-agitated vessel, the flow structure is complex. Close to the impellers, the flow has a jet structure with high

turbulence intensity and a strong periodic motion introduced by the impeller motion. Further away, in the bulk zone, the flow is dominated by slowly varying large scale structures (Revstedt & Fuchs, 2002).

The mean flow in a Rushton agitated tank can be considered to be made up of three different flow elements: circumferential flow, a jet flow and pair of tip vortices associated with the impeller blades (Yoon, Hill., Balachandar, Adrian, & Ha, 2005). Assirelli, Bujalski, Eaglesham, & Nienow, (2002) observed that the best micromixing in Rushton agitated tank occurred in the trailing vortices which extend off the tips of the impeller blades. It was estimated that the maximum specific local energy dissipation rate was approximately seventy-times the mean specific energy dissipation rate. Due to this uneven distribution of energy, where mixing energy is important to nucleation, the region near the impellers should dominate the process.

### **5.3.2 Cavitation**

Cavitation in a system where ultrasound has been applied was discussed in section 5.2.1. It provides an explanation for why ultrasound enhances the nucleation of crystals from solution. Cavitation can occur in the absence of ultrasound in a system where fluids are flowing. In a flowing system, the liquids are subject to local accelerations and at the points of high velocity, low pressures occur and cavities form. These cavities extend until they reach an area of lower velocity and higher pressure when they collapse (Pearsall, 1972). Kumar, Kumar, & Pandit, (2000) demonstrated that inducing cavitation using hydrodynamic conditions is a more energy efficient technique than the acoustic approach.

The fundamental requirement for the occurrence of cavitation is a sufficient reduction in the static pressure. In order to meet this requirement, the area in the flow passage has to change. This may be induced by a converging-diverging conduit, or a section of pipe which contains a valve or an orifice (Yan & Thorpe, 1990). Once cavitation occurs in a flowing system, the single liquid phase first appears as a two-phase effervescent medium in the cavitation zone. As cavitation increases in severity, both the size and the number of cavities are increased. To describe the severity of cavitation the cavitation number a dimensionless parameter is widely used. The cavitation number is defined in Equation 5-4.

$$Cav = \frac{p_2 - p_v}{0.5 \rho_L U_{th}^2}$$

**Equation 5-4 Determination of the cavitation number**

A cavitation number of one represents the point where the inception of cavitation occurs, with significant cavitation occurring below this value (Gogate & Pandit, 2001). Dissolved gasses or suspended particles in the liquid can act as weak spots providing nuclei for cavitation to occur at values greater than one. (Gogate & Pandit, 2000). Yan & Thorpe, (1990) found the cavitation inception number increased with increasing orifice diameter. The value reached 2.4 at an orifice diameter of 3.0 cm and decreased linearly to a value of 1.6 at an orifice diameter of 1.52 cm.

Under conditions of extreme flow, condition cavitation becomes choked, and following this supercavitation occurs. At the point of supercavitation, the liquid jet becomes visually separated from the vapour and the jet contains no bubbles. The flow downstream of the orifice following supercavitation can be divided into three sections; these are shown in Figure 5-4

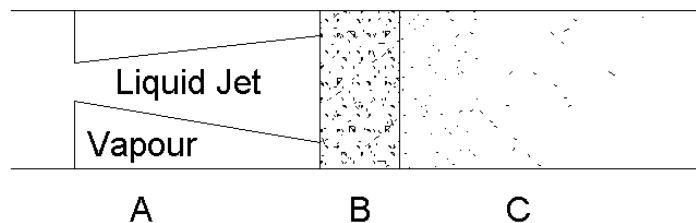


**Figure 5-4 Flow regions at conditions of supercavitation (redrawn from Yan & Thorpe, 1990)**

- Region A - a single cavity with a liquid jet in the middle of the vapour pocket.
- Region B - white clouds where the big cavity breaks into smaller cavities these then collapse.
- Region C – a clear liquid region where the cavities have collapsed. Though this region is termed the clear region, a small number of bubbles formed during cavitation continue to exist for sometime before redissolving (Yan & Thorpe, 1990).

If cavitation increases the nucleation rate, then the most nucleation would be expected to occur in region B. It is this region where the highest numbers of cavities (bubbles) are present.

### 5.3.3 Reynolds number

The Reynolds number is a dimensionless quantity representing the ratio of inertial forces to viscous forces, and is used for characterizing the transition from laminar to turbulent flow. These changes in flow patterns may influence the nucleation process, through the different mixing conditions created. The Reynolds number for flow in a pipe is calculated using Equation 5-5 and for flow in an agitated vessel (from the impeller) is calculated using Equation 5-6.

$$\text{Re}_p = \frac{\rho_L D_p U}{\mu}$$

**Equation 5-5 Reynolds number for flow in a pipe**

$$\text{Re}_{imp} = \frac{\rho D_{imp}^2 N_R}{\mu}$$

**Equation 5-6 Reynolds number for flow in an agitated vessel**

Laminar flow occurs at low Reynolds numbers, where viscous forces are dominant and flow is characterised by smooth, constant fluid motion. Turbulent flows occur at high Reynolds numbers and are dominated by inertial forces, producing disordered flow fluctuations including random eddies and vortices (Granger, 1995). For flow through an open circular pipe, there are three distinct flow regions. These are approximately defined by the following conditions:

- $\text{Re} < 2100$                       Laminar
- $2100 < \text{Re} < 10\,000$           Transitional
- $\text{Re} > 10\,000$                     Fully turbulent

For mechanical mixers, where the Reynolds number is under 10, the process is laminar. Fully turbulent conditions are achieved at Reynolds numbers greater than 10,000. Between these conditions the flow is considered transitional (Paul et al., 2004), (Metzner & Taylor, 1960). The extent of turbulent flow in a stirred vessel varies with Reynolds number and with the location in the vessel. Near the impeller,

the flow can be turbulent and then with increasing distance from the blades become transitional and even laminar. The Reynolds numbers does not guarantee a certain flow pattern will be observed. Metzner & Taylor, (1960) found that, in the same vessel, a change in the type of fluid produced a change in the flow pattern for the same Reynolds number. As crystals form they can change the properties of the fluid and because of this mixing patterns may change during crystallisation.

### 5.3.4 Power input

An energy barrier must be overcome in order for the creation of a new crystal surface to take place. Typically, this energy is provided by a difference in chemical potential. The addition of energy provided by mixing may assist in overcoming this barrier. In an impeller-agitated vessel, the power input is related to the agitation rate, the impeller diameter, and the density of the liquid, and can be determined using Equation 5-7.

$$P_{wr(m)} = \frac{P^{\#} \rho_L N_R^3 D_{imp}^5}{g}$$

**Equation 5-7 Power consumed by a mixer**

It is useful to consider power input per unit mass of the fluid in order to account for differences in scale. A simple measure of this is given in Equation 5-8.

$$\varepsilon_p = \frac{P_{wr(m)}}{\rho_L V_{tank}}$$

**Equation 5-8 Power input per unit mass of fluid**

This equation assumes that homogeneous turbulence occurs in a tank. This can be a poor assumption, with turbulence levels in a tank varying by a factor of 100 from the impeller to the bulk. Where geometric similarity is maintained between vessels, Equation 5-8 provides a method of comparison, as the energy distribution patterns are likely to be similar. Where the objective is to characterise the physics in the problem, the local dissipation should be separated from the effects of other variables. The best available scaling for local dissipation uses the swept volume instead of the total tank volume (Paul et al., 2004).



A fluid flowing through a pipe has a velocity head, defined as seen in Equation 5-9.

$$p_H = \frac{1}{2} \rho_L U^2$$

**Equation 5-9 Velocity head of a fluid**

A pressure must be applied to generate an increase in velocity. Typically, a pump transforms electrical energy into the increase in pressure. Ignoring the pump inefficiency, the power required to increase the pressure in a fluid is defined in Equation 5-10.

$$P_{wr(f)} = \Delta p Q$$

**Equation 5-10 Power stored in a flowing fluid**

### 5.3.5 Vortex formation

The application of a force that produces a fluid flow can create instabilities. The flow instabilities produce large scale eddies which give rise to smaller ones and so on until at the smallest scales viscosity becomes important. The large scales contain the largest component of the turbulent kinetic energy. This is continuously fed to the smallest scales where it is dissipated. If the Reynolds number is large enough the dynamics of the large scales are essentially inviscid and insensitive to the precise value of the Reynolds number. At high Reynolds numbers the mean velocity and root-mean squared fluctuations approach limiting profiles (Mathieu & Scott, 2000). The exact Reynolds number at which instabilities will form in a fluid is dependent on the situation.

It is well reported that flows around bluff bodies at a sufficiently large Reynolds number lead to the periodic shedding of vortices with alternating circulation resulting in the von Karman vortex street (Ahlborn, Seto, & Noack, 2002). Vortex shedding from a bluff body is a commonly observed phenomenon in nature. It is exploited for sound production by the Aeolian harp and is seen in a river where the flow of the water is obstructed by a lodged stick. The frequency of the generated vortices is directly proportional to the flow velocity and is a function of a dimensionless constant known as the Strouhal number, seen in Equation 5-11 (Panknin, 2005).

$$e_f = S_T \frac{U}{D_{obs}}$$

**Equation 5-11 Frequency of vortex generation for flow obstructed by a cylinder**

Figure 5-5 shows the relationship between the Strouhal number and the Reynolds number. The Strouhal number is constant for a range of Reynolds number from 1000 to 150000.

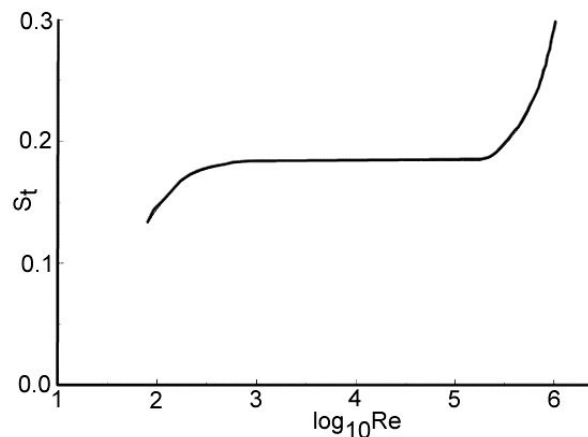


**Figure 5-5 Changes in the Strouhal number versus changes in the Reynolds number (reproduced from (Panknin, 2005))**

#### 5.3.5.1 Agitated tank

In a Rushton agitated tank vortices follow the tips of the impellers as they pass through the solution (Sharp & Adrian, 2001). The vortices that form at the impeller tips break off and, according to the energy cascade model proposed by Kolmogorov, transport their energy to smaller eddies with the energy eventually being dissipated at the smallest scales. Sharp and Adrian observed that in the region of the tip vortices energy dissipation is higher than in the bulk flow demonstrating the importance of them as a major mixing mechanism in stirred tank flow.

Revisiting the analogy of the stick in the river, a logical conclusion would be that just as the velocity of the river determines the frequency of at which vortices form, the frequency at which vortices are shed from the impeller should be determined by the speed of the impeller. In a study, using direct numerical simulation of the trailing edge flow of a turbine blade Yao, Savill, Sandham, & Dawes, (2002) calculated that the flow oscillated in a similar way to the von Karman vortex street produced downstream of bluff body flow. The vortices that form off the tips of the impellers are one of the effects that occur in mixed vessels. When they are viewed collectively, they are

termed in the literature as macro instabilities. The factors which combine to make up the instabilities are the tip vortices, large scale ring vortices generated by the radial jet (Sharp & Adrian, 2001), as shown in Figure 5-6, and vortices forming off the shaft (Galletti, Paglianti, Lee, & Yianneskis, 2004).

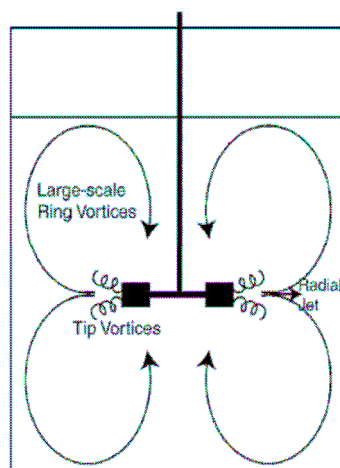


**Figure 5-6 Flow in a Rushton agitator tank, showing radial jet, large scale ring vortices and tip vortices (Reproduced from Sharp & Adrian, 2001)**

The frequency of instabilities in a stirred vessel was demonstrated to be linearly related to the impeller speed (Galletti *et al.*, 2004). The equation used to define the frequency of these instabilities is presented as Equation 5-12. The nondimensional frequency ( $e_f'$ ) was found to vary when considered at low, intermediate and high Reynolds number regions. At low Reynolds numbers the nondimensional frequency was seven times higher than observed for the high Reynolds number region.

$$e_f' = \frac{e_f}{N_R}$$

**Equation 5-12 Frequency of macroinstabilities in an agitated vessel**

The scale of these macro instabilities is greater than the molecular scale at which nucleation occurs. Their formation is still important as they break up into the small eddies examined by the Kolmogorov length scale.

### 5.3.5.2 Through an orifice

Up to the point where the Reynolds number exceeds 2100 the flow of a liquid through a straight pipe is considered laminar. It can be seen in the images reproduced from

Nakayama, (1988) in Figure 5-7 that this is untrue in the case where the diameter of the pipe expands. If the flow conditions are the controlling variable defining the relationship between mixing and nucleation then it is important that expansions in pipes are considered. Industrially constrictions frequently appear in pipelines, they may be flow control valves, flow measurement systems (for example orifice plates) or it may be just the case of the fluid exiting the pipeline and entering the crystalliser.

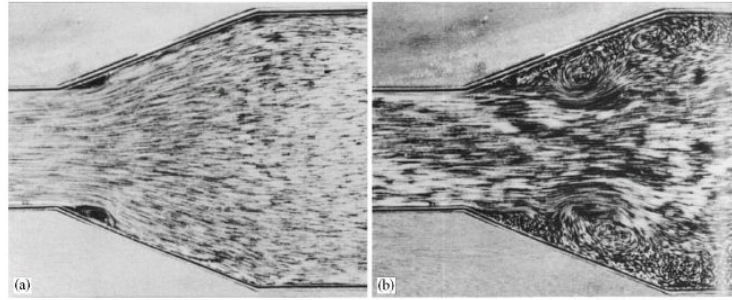


**Figure 5-7 Flow of water through a diverging channel (a) Reynolds number# 70 (b) Reynolds number 350 (Nakayama, 1988)**

Swirling vortices at the walls of the pipe are clearly visible at a Reynolds number of 350. The formation of vortices resulting from the expansion of a fluid into a larger pipe was discussed in the literature as early as 1929 by Johansen, (1929), who likened it to the flow which occurs past a bluff body, except that the flow was symmetrical and three dimensional. In agreement with the observation of Johansen the frequency of vortex shedding is defined using the Strouhal number in Equation 5-13 (Bruns, 1959).

$$e_f = St_o \frac{U}{D_{or}}$$

**Equation 5-13 Vortex shedding frequency for flow through an orifice**

This same equation was presented in Equation 5-11, except that the diameter of concern, in Equation 5-13, is the orifice diameter.

An abnormal narrowing in the cardiovascular system is known as a stenosis. The turbulence that results as blood passes through a stenosis can dramatically influence the pressure drop and wall shear stresses in the post-stenotic region. Both effects can negatively influence the cardiovascular system (Lee, Liao, & Low, 2004). For these

reasons work into the area of vortex shedding as fluid flows from a narrow tube into an expansion has been carried out in the field of hemodynamics. The fluctuations of the blood flow velocity downstream of the stenosis cause the vibration of the vessel walls. This vibration is transmitted to the skin where it is detected as a murmur (Lu, Hui, & Hwang, 1983). Studying flow through a stenosis Bluestein, Gutierrez, Londono, & Schoepfoerster, (1999) observed the onset of vortex shedding at a Reynolds number of 350. The vortices were observed to affect flow near the wall once the Reynolds number reached 1000. In flow through an expanding pipe Iribarne, Frantisak, Hummel, & Smith, (1972) found turbulence began occurring at a Reynolds number of 350. The agreement in the results is not surprising as both studies looked at similar systems, only in different fields.

Young & Tsai, (1973) observed three basic regimes of flow through a constricted tube:

- (a) For very low Reynolds numbers no separation was observed and flow is laminar and unidirectional throughout.
- (b) For larger Reynolds numbers the flow remains laminar but a zone of back flow exists.
- (c) The third regime is one where flow downstream from the separation point is highly turbulent and no localised discrete region of flow is discernible. As the Reynolds number increases, the dimensionless pressure drop becomes essentially independent of Reynolds number indicating that turbulence is the dominant factor.

Specific values of Reynolds number delineating these regions were dependent on the geometry of the constrictions. Solzbach, Wollschlager, Zeiher, & Just, (1987) found that the tube geometry changed the Reynolds number at which flow instability occurred. Increasing the constriction decreased the Reynolds number required for flow instability, while increasing length of the constriction increased the Reynolds number required for flow instability. The distance from the constriction is also important in defining the flow conditions. Deshpande & Giddens, (1980) found that once the Reynolds number increases above 5000 for a stenosis of 75 per cent, the reattachment point remains constant at 4.5 diameters from the neck of the stenosis, at which point the turbulent intensity reaches its maximum.

### 5.3.6 Shear

Section 5.2.3 discussed that the application of shear to a system has been observed to enhance the nucleation rate. Wherever there is relative motion of liquid layers, shearing forces related to the flow velocities will occur (Paul et al., 2004). Therefore, shear forces will be present in all applications where an external force is applied to a fluid to induce mixing. Where the conditions are turbulent, the shear forces will fluctuate with space and time. Berger & Jou, (2000) found that oscillating shear, not constant high or low shear, is responsible for plaque growth in arteries

The application of agitation to the system creates shear between the impeller blades and the fluid. Shear is created at the vortices that form within the fluid and are dispersed through the system. In both Newtonian and non-Newtonian systems the fluid shear rates were observed to be directly proportional to the rotational speed and the type of impellor (Metzner & Taylor, 1960). This is defined in Equation 5-14, the Metzner-Otto relationship. The value of  $\kappa$ , is 13 for a Rushton turbine, this decreases rapidly with distance from the tip of the blade (Paul et al., 2004).

$$\gamma = \kappa N_R$$

**Equation 5-14 Shear in an impeller agitated tank**

## 5.4 Experimental investigation into effect of mixing

Chemical reactions, nucleation and crystal growth are molecular level processes, so only micromixing can directly influence their course (Baldyga & Orciuch, 2001). Mixing at the microscale can be induced using two mechanisms. The first termed active mixing, occurs when energy input from the exterior is used. Methods used include ultrasound, pulsing of the flow, or the addition of an impeller. The second approach, passive mixing, seeks to restructure the flow so that faster mixing results (Hessel, Lowe, & Schonfeld, 2005). Crystallisation processes in the industrial setting frequently employ active mixing through the use on an impeller driven agitation to maintain crystals in suspension and to ensure a system is evenly blended. Often passive mixing in a crystallisation plant occurs inadvertently as solutions flow through valves and changing pipe diameters. This work looks to use both these approaches for

studying the relationship between mixing and nucleation. The methods selected for doing this are outlined below.

#### **5.4.1 Effect of agitation on nucleation**

In order to investigate how agitation influences nucleation a similar method to that described in section 4.4.2 of chapter five was used. A range of supersaturated lactose solutions was made up and the time to reach a critical absorbance was determined. In this section of the work, the rate of agitation was changed. All experiments were carried out under isothermal conditions at 25 °C.

Supersaturated lactose solutions were created by dissolving a mass of lactose and then cooling the solutions to the 25 °C. The water used for all dissolutions was 95 °C. This temperature exceeded the solubility concentration of all the lactose solutions used. Complete dissolution was determined by visual examination. In order to ensure that no “ghost nuclei” remained, the solutions were heated for a further 15 minutes beyond the point where no crystals could be visually observed. Following dissolution, the solutions were added to the vessels in the water bath, where they were cooled, with no agitation. The cooling process typically took between 90 to 100 minutes.

Once cooling was complete, the agitators were added to the vessels and the mixing process initiated. Four different mixing rates were used; 200 r·min<sup>-1</sup>, 300 r·min<sup>-1</sup> 400 r·min<sup>-1</sup> and 500 r·min<sup>-1</sup>. This equates to a power per unit volume range of 0.015 to 0.27 W·m<sup>-3</sup> and tip speed range of 0.37 to 0.92 m·s<sup>-1</sup>. The range used was limited at the high end by the capability of the motor driving the mixers and at the low end by the agitation necessary to maintain the crystals in suspension. Two experiments were carried out under conditions of no agitation to provide a comparison with the agitated results.

#### **5.4.2 Effect of shear on nucleation**

Section 5.2.3 discussed how shear has been observed to initiate nucleation events. This section of work describes a method conceived to study how the nucleation of lactose changes when a shear is applied to a supersaturated solution. A Rheometric Scientific SR4500 rheometer with a cone and plate attachment cone was used to

apply a shear to a supersaturated lactose solution. A diagram showing the set up for a cone and plate rheometer is presented as Figure 5-8.

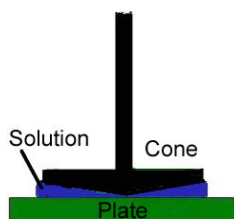


**Figure 5-8 The position of the solution in a cone and plate rheometer**

The angle between the cone and plate ( $1^\circ$ ) means that the shear is constant at all radial positions. In this study, the controlled variable was shear stress, so the rotational speed of the cone was varied to maintain a constant shear stress in each experiment. To test the suitability of the technique, a lactose solution of 60 g hydrous lactose per 100 g water was prepared and dissolved, ensuring no fine crystals remained. Once dissolved, the solution was stored in a water bath at  $60^\circ\text{C}$  to prevent the formation of any crystals. To begin the test approximately one millilitre of solution was drawn up into a syringe and gently applied to the surface of the plate. The cone was lowered on to the plate and adjusted to a gap of 0.05 mm. Once in position, the rheometer was started and left to run. A computer controlled the rheometer and logged the results. The run conditions were preset prior to addition of solution to the plate surface.

All experiments were carried out at  $20^\circ\text{C}$ . This represented the set temperature of the room housing the rheometer. The small sample size meant that only a short time was required to equilibrate the temperature with room conditions. The solution added to the plate was at  $60^\circ\text{C}$ , this done to standardise the time the solution existed below the solubility temperature.

### **5.4.3 Flow through an orifice/Venturi**

A solution flowing through an orifice enables the study of different factors associated with the mixing process. These include cavitation, Reynolds number, vortex formation and power input. The diameter of the orifice, as discussed in section 5.3, has a different effect on all of the phenomena listed. Because of this, these factors can be viewed independently by varying of the fluid flow rate and the orifice size.



The Venturi orifice design was selected for use in the experiments. Devices using this design are commonly used for flow measurement. The design is named after the Italian physicist, Giovanni Battista Venturi. In the Venturi design the flow is streamlined at the entrance and exit of the constriction. The critical dimensions used in the design of the Venturi were obtained from Spink, (1967). This image has been reproduced in Figure 5-9.

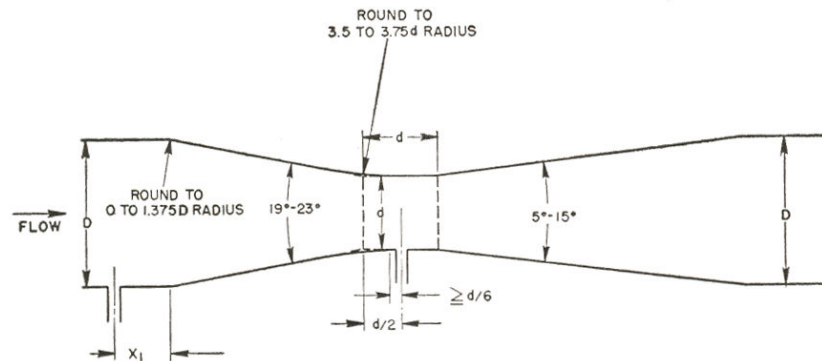


**Figure 5-9 The critical dimensions of the classical Venturi tube (reproduced from Spink, 1967)**

Three Venturi devices were built with orifice diameters of 1.0 mm, 2.0 mm and 3.0 mm. The drawings of the devices and their critical dimensions are shown in Figure 5-10, Figure 5-11 and Figure 5-12 respectively. For all three tubes inlet angles of 20° and an exit angles of 10° were used.

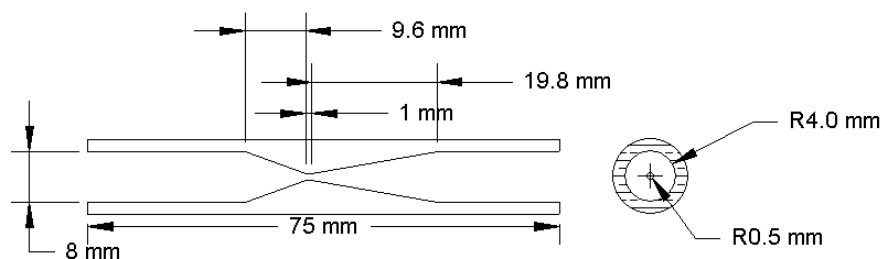


**Figure 5-10 Design of Venturi used this work with 1.0 mm orifice**

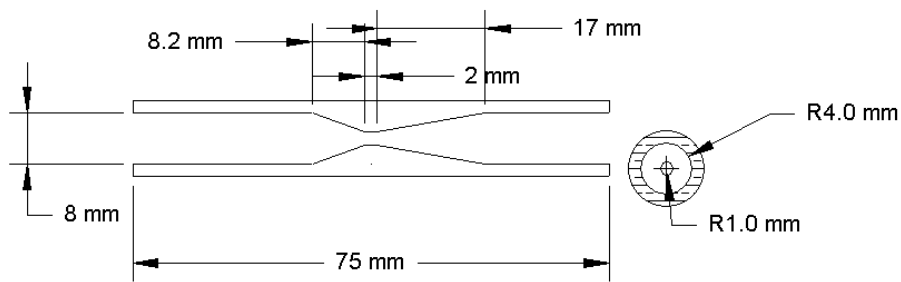


**Figure 5-11 Design of Venturi used this work with 2.0 mm orifice**

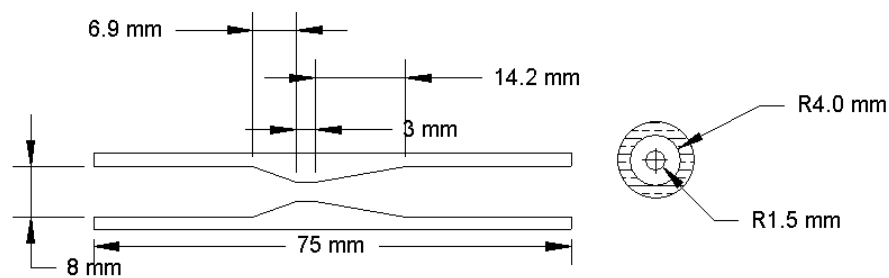


**Figure 5-12 Design of Venturi used this work with 3.0 mm orifice**

Flow through the Venturi was achieved using two hydraulic cylinders, each with a bore diameter of 38.1 mm and a stroke range of 305 mm. The cylinders were the “Compact S” design manufactured by Victor Hydraulics, New Zealand. The drawing showing the specifications of the cylinder can be found in appendix A3. The first cylinder acted as the motor. The second cylinder contained the lactose solution. The first cylinder was powered using a hydraulic gear pump. Hydraulic oil was pumped into the cylinder driving out the ram this forced the ram of the second cylinder inwards. This forced the supersaturated lactose solution out through the Venturi and into the bulk solution. A diagram showing the set up used is presented in Figure 5-13.

Heating tape wrapped around the second cylinder was used to regulate the temperature of the lactose solution. The heating tape was controlled using a CAL 3200 autotune temperature controller; feedback to the controller came from a T type thermocouple connected to the cylinder.

The ram was controlled using four valves. The position of each valve can be seen in Figure 5-13. Valves A and B were used to control the speed of the ram. They were used to manipulate the pressure drop across the valve. Increasing the pressure drop decreased the fluid flow to the cylinder and decreased the ram speed. Valve C was also used to control flow to the cylinder. Rather than increase the pressure drop, this valve acted as a by-pass, diverting flow from the cylinder back to the main fluid chamber. Valve C was an addition to the original design and was included to give a greater flexibility over the range of ram speeds. Valve D was the on/off control used to operate the cylinder. It had three functions forwards, backwards and off.

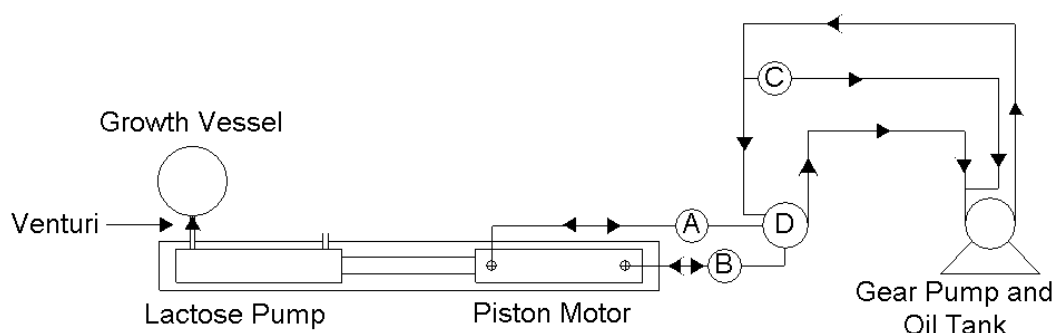


**Figure 5-13 Diagram showing equipment used for conducting the Venturi initiated nucleation experiments**

The pump used to drive the hydraulic ram was a gear pump with a maximum flow rate of  $7.5 \text{ l} \cdot \text{min}^{-1}$ . The pump was powered using a three phase 1.5 kW electric motor. The motor size meant a maximum pressure of approximately 14 MPa could be generated. The hydraulic oil used to supply the hydraulic ram was pumped from a 12-litre tank. Valve D, when in the off position, allowed oil to flow back to the main tank. The pump can be seen in the background of Figure 5-14. Also shown are the two cylinders, the Venturi and the agitated vessel into which the solution exiting the Venturi was pumped.

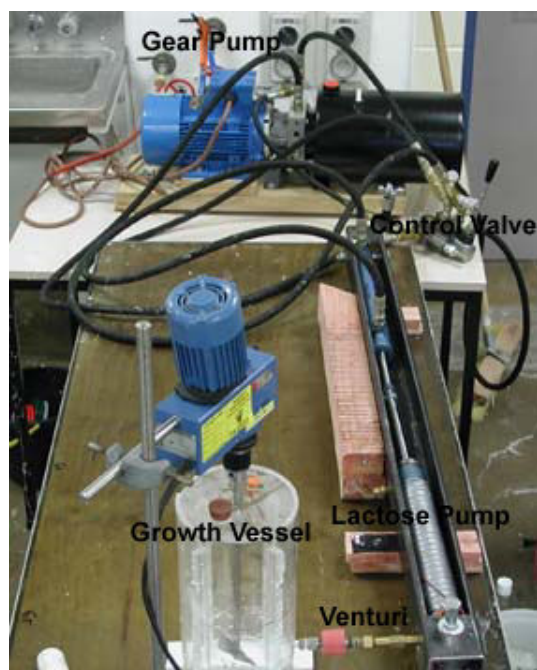


**Figure 5-14 Set-up of system used for Venturi experiments**

The flow rate through the Venturi was determined from measurements of the ram speed as it was pressed into the lactose filled piston. A ruler was placed along side the ram and a web cam placed above it. The web cam recorded the ram's movement at a rate of twenty frames per second. At the end of each experiment, frames were grabbed from the web cam footage at particular time intervals and from the change in position the ram speed was calculated. A series of images showing the ram movement at measured time intervals for one of the experiments is presented in Figure 5-15.

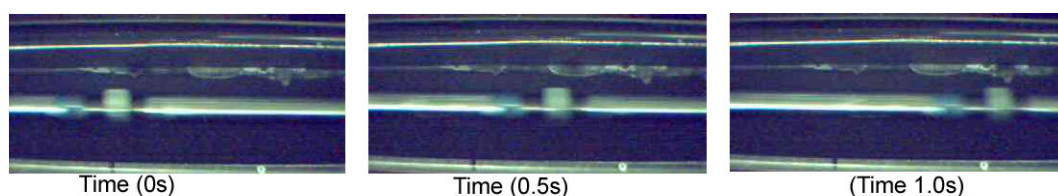


**Figure 5-15 The ram movement on the lactose pump during the plunging phase of the Venturi nucleation experiments (images used to determine the fluid velocity)**

The lactose solution in the cylinder was made up to the desired concentration by adding lactose to distilled water. The masses of lactose and water were calculated to produce 200 ml of solution. The solution was heated to 95 °C to dissolve all the lactose into solution. To remove any insoluble foreign matter the solution was passed through a Whatman No.1 filter and then reheated to 95 °C for 30 minutes to

redissolve any nuclei. The hot solution was then gently poured into the cylinder where it was left to cool to 40 °C. The cooling process took 60 to 70 minutes and was monitored using a T type thermocouple immersed in the solution. Once the solution had cooled, the cylinder was attached to the Venturi and the solution forced through the Venturi at the desired rate.

After the supersaturated solution had passed through the Venturi, it was collected in an agitated vessel containing 2000 ml of lactose solution. The solution in the agitated vessel was made up to a concentration of 45 g lactose per 100 g water, maintained at a temperature of 40 °C and was therefore slightly supersaturated. The agitated solution acted to quench the highly supersaturated Venturi solution. The final concentration supplied sufficient lactose for crystal growth, but minimised additional nucleation. Agitation was used to disperse the Venturi solution into the quenching solution as quickly as possible. The solution was agitated using a two blade pitched turbine operated at 300 r·min<sup>-1</sup>. The impeller was positioned just above the entry point of the solution coming from the Venturi. In preliminary experiments it was found that at high speeds the jet from the Venturi hit the vessels' rear wall and passed up and out over the side. To eliminate this, the vessel used in the actual experiments was much taller than required to hold the solution.

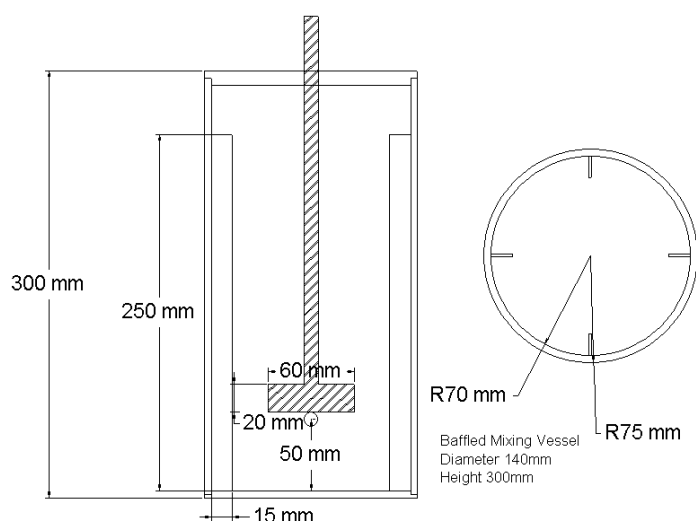


**Figure 5-16 Agitated vessel used to collect supersaturated lactose solution exiting the Venturi tube**

The mixture of the two solutions was agitated for three hours; this allowed any crystals formed to grow up to a size detectable under a microscope. The time required

for growth was obtained from the growth relationship determined in chapter three. After the three-hours, five, 3 ml samples were withdrawn from the bulk solution. A sub-sample of each of these samples was then viewed under a microscope where the number of crystals per unit volume in solution was counted using the method described in section 4.4.4. From the five samples collected, an average number of crystals per millilitre of solution were obtained.

## 5.5 Results and discussion

It is apparent from the above sections that how the mixing process changes the nucleation rate is difficult to isolate due to the number of mixing associated variables and combination thereof that may play a role. To provide further understanding of the relationship between mixing and nucleation the investigations described in section 5.4 were conducted, the results are considered separately in the sections below.

### 5.5.1 Agitated vessel

To allow the results to be analysed using both nucleation and mixing theory, the experiments in the Rushton agitated vessels were conducted over a range of supersaturations. The following sections consider the perspectives individually.

#### 5.5.1.1 Results considered from nucleation theory perspective

In chapter four a plot of  $(\ln S_R)^{-2}$  vs.  $t_N^{-1}$  was used to investigate the primary nucleation process and to ascertain how temperature and impurities changed both the homogenous and heterogeneous mechanisms. The approach has been used here to examine how the agitation rate influences nucleation. A plot showing all the results along with the curve generated using Equation 4-13 (repeated here as Equation 5-15) can be seen in Figure 5-17.

$$t_N^{-1} = A_{Hen} \exp^{(-B_{Hen}[\ln S_R]^{-2})} + A_{Hom} \exp^{(-B_{Hom}[\ln S_R]^{-2})}$$

**Equation 5-15 Equation used to fit curve to induction times measured at different supersaturations**

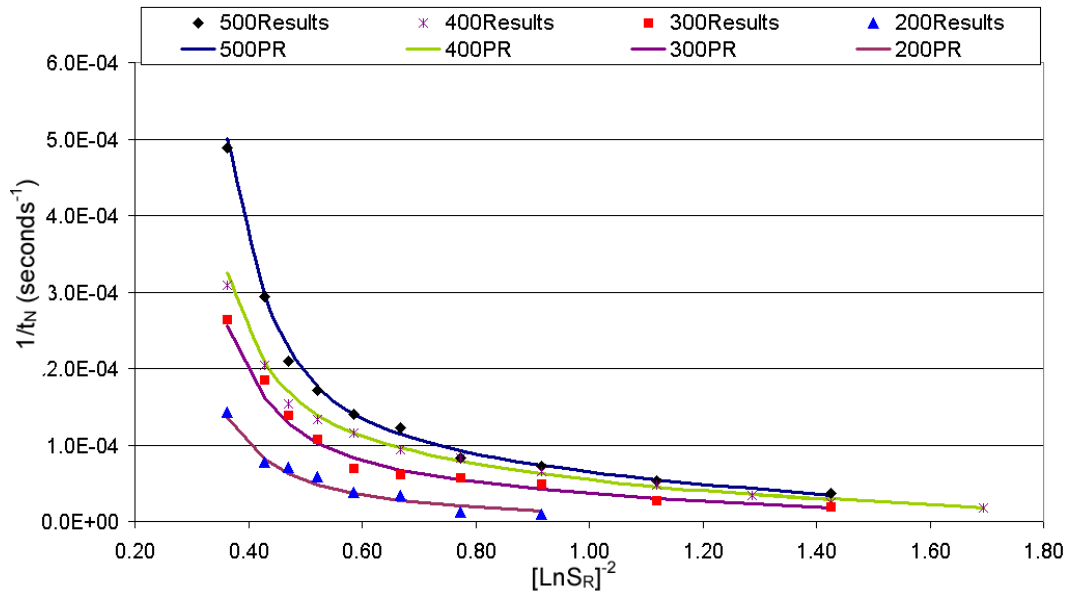


**Figure 5-17** The relationship between the mixing rate of supersaturated lactose solutions in a Rushton agitated vessel and the time required to reach the critical number of nuclei

The experimental results presented in Figure 5-17, show that agitation influences the time required for the number of nuclei to reach the critical value and hence the nucleation rate.

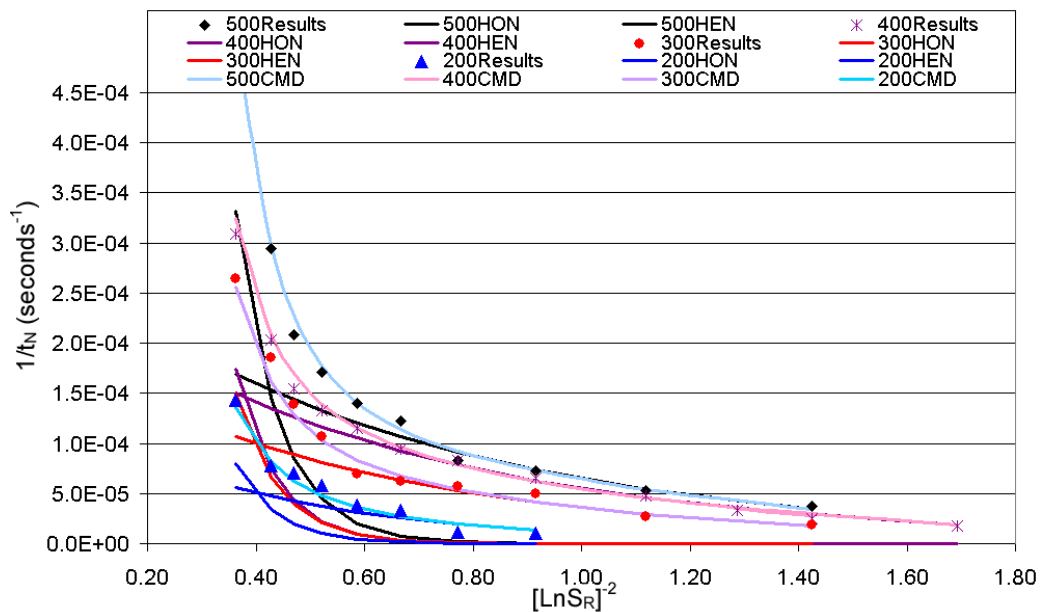


**Figure 5-18** Homogeneous and heterogeneous nucleation curves for supersaturated lactose solutions at different mixing rates in a Rushton agitated vessel.

To examine agitations influence on the nucleation rate, the curves for homogenous nucleation and heterogeneous nucleation are plotted in Figure 5-18. These curves represent the two separate exponential equations from Equation 5-15, which, when

combined, form the single curves seen in Figure 5-17. In Table 5-1 are the fitted constants  $A_{Hen}$ ,  $B_{Hen}$ ,  $A_{Hom}$  and  $B_{Hom}$ . These were obtained by using Curve fit 1.3 (a non-linear curve fitting package) to fit the experimental data in Figure 5-18

Agitation Rate	$A_{Hen}$ Intercept HEN	$B_{Hen}$ Slope HEN	$A_{Hom}$ Intercept HON	$B_{Hom}$ Slope HON
500 r·min <sup>-1</sup>	0.00029	1.52	0.032	12.61
400 r·min <sup>-1</sup>	0.00026	1.58	0.019	12.67
300 r·min <sup>-1</sup>	0.00020	1.70	0.013	12.27
200 r·min <sup>-1</sup>	0.00014	2.60	0.008	12.71

**Table 5-1 Homogenous and heterogeneous nucleation parameters for different mixing rates in a Rushton agitated vessel**

There is little difference in the  $B_{Hom}$  values observed for the different agitation rates. This suggests that for homogeneous nucleation the interfacial energy barrier and consequently the size of the critical nucleus is not affected by agitation. Figure 5-18 shows that the point at which the homogenous nucleation lines begin to leave the  $x$ -axis remains constant despite an increasing agitation rate. It is concluded from this that the homogenous nucleation threshold is independent of the agitation rate.

The results in Figure 5-18 and Table 5-1 show that agitation changes the intercept of the homogeneous nucleation curves. A fourfold reduction in the intercept is seen from 500 r·min<sup>-1</sup> to 200 r·min<sup>-1</sup>. The consequence of this is that the pre-exponential factor  $A_{Hom}$  in Equation 5-15 is changed. A similar result was reported by Barata & Serrano, 1996), when studying potassium dihydrogen phosphate nucleation at different mixing rates. Guo *et al.*, 2006) also reported the same findings in their study into how ultrasound influenced nucleation.

Explaining the result requires an examination of what the pre-exponential factor is. The pre-exponential factor  $A_{Hom}$  (Equation 5-16) is a product of the Zeldovich factor, the frequency of monomer attachment to the nucleus and the concentration of nucleation sites. Smaller values are indicative of the presence of active centres, such as seeds or foreign bodies in the system and/or for a lower frequency of monomer attachment to nuclei (Kashchiev, 2000).

$$A = Zm_f^* C_0$$

**Equation 5-16 Pre exponential factor  $C$**



$$Z = (W^* / 3\pi k T_K n^{*2})^{1/2}$$

**Equation 5-17 Zeldovich factor**

The Zeldovich factor, seen in Equation 5-17, is a function of the maximum energy barrier to nucleation and the size of the critical nucleus. These variables are both functions of the interfacial energy barrier, which is constant throughout the changing mixing conditions.

For the case of homogenous nucleation, the number of available molecules represents the number of active nucleation sites in the solution phase. This is defined in Equation 5-18.

$$C_0 = M / V$$

**Equation 5-18 Number of nucleation sites in system**

The number of available molecules in a solution is a function of the supersaturation and is independent of the mixing rate. If mixing creates sites upon which nuclei could form, therefore increasing the number of active centres, a change in the slope would have been expected due to a change in the energy barrier to formation. This was not observed.

The third term in Equation 5-16 is the monomer attachment frequency. In a solution, monomer-attachment usually occurs by diffusion of solute in the volume of the solution towards the nucleus or by transfer of solute across the nucleus diffusion interface. Where attachment is controlled by volume diffusion, the attachment frequency is a product of the incoming diffusion flux of monomers to the nucleus surface. Where interface transfer controls attachment, the monomer to be attached is in immediate contact with the nucleus and joins it by making the jump over a distance comparable to the molecular diameter (Kashchiev, 2000).

Agitations' affect on mass transfer is limited to diffusion in the liquid film surrounding the solid particle (Paul et al., 2004). This scale limits the role of mixing to volume diffusion, altering the flux of monomers to the nucleus surface.

It can be seen from the results that an increase in agitation increases the rate of homogeneous nucleation by increasing the frequency of activated molecular collisions. This results from an increase in the rate of movement of molecules to the surface of the active centers. The consequence of this increased frequency, when considered in the context of the classical nucleation theory, is a change in the value of pre-exponential factor  $A_{Hom}$ . The interfacial energy barrier to nucleation remained constant throughout the range of agitation intensities studied.

The results for heterogeneous nucleation are similar to those seen for homogeneous nucleation. There is a progressive decrease in the pre-exponential value ( $A_{Hen}$ ), from which it can be concluded that the decreasing agitation rate is lowering the frequency of activated molecular collisions. Seen also in the results for heterogeneous nucleation is a progressive increase in the slope with the decreasing agitation rate. This indicates that the energy barrier to nucleation is being changed by the agitation rate. A possible explanation for this is that at the faster agitation rate, there is greater removal of fine crystals from the surface of existing crystals; this would create more surfaces on which new crystals could grow and have a direct impact on the number of crystals in solution. The overall result is an increased nucleation rate, which is projected as a lowering of energy barrier to nucleation.

#### 5.5.1.2 Results considered from mixing perspective

The above discussion identifies that an increase in agitation increases the nucleation rate. For the primary nucleation of  $\alpha$ -lactose monohydrate from solution, increasing the agitation intensity acts to increase the frequency of activated molecular collisions. This increase is not quantified by classical nucleation theory, which has no factor in it to account for agitation. To develop further the understanding of the role mixing plays in the nucleation process, this part of the discussion will examine the results from the perspective of mixing theory.

Section 5.3.4 discussed that nucleation is a process where by energy barrier must be overcome and that given this, it can be foreseen that mixing may assist in overcoming this barrier through addition of energy. Using this idea, the results from the agitation studies were replotted as energy input to the process to reach the critical number of

nuclei vs. supersaturation. The energy added to the process was determined by multiplying the mixer power input, as determined by Equation 5-7, by the time required to reach the critical number of nuclei.

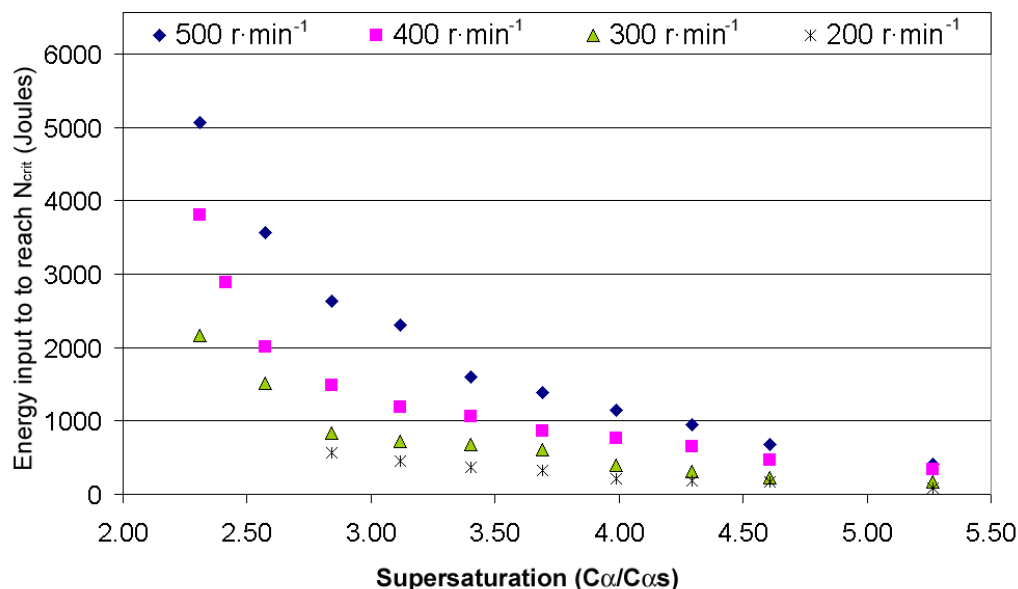


**Figure 5-19 Supersaturation vs. energy input required to reach  $N_{crit}$  for Rushton agitated supersaturated lactose solutions**

Figure 5-19 shows that as the supersaturation is increased the amount of energy input required to generate the critical number of nuclei decreases. This is expected as the chemical driving force increases the nucleation rate increases. The fact that this approach fails to produce a common curve means the statement that a relationship exists between the external energy input and the nucleation rate is unable to be validated. In fact, the results in Figure 5-19 show that at the lower agitation rates less energy input is required for the system to reach the critical number of nuclei. Presupposing that the application of an external energy source does play a role in increasing the nucleation rate, the lower energy requirement at the lower agitation rates suggests that the way in which the energy is applied is important, as is the mechanism through which dispersion occurs.

In an agitated solution, the mechanism through which the energy is dispersed is the small-scale vortex dissipation. Based on this concept and on the simple relationship presented in Equation 5-12, the number of revolutions required to reach the critical number of nuclei was plotted against supersaturation in Figure 5-20.

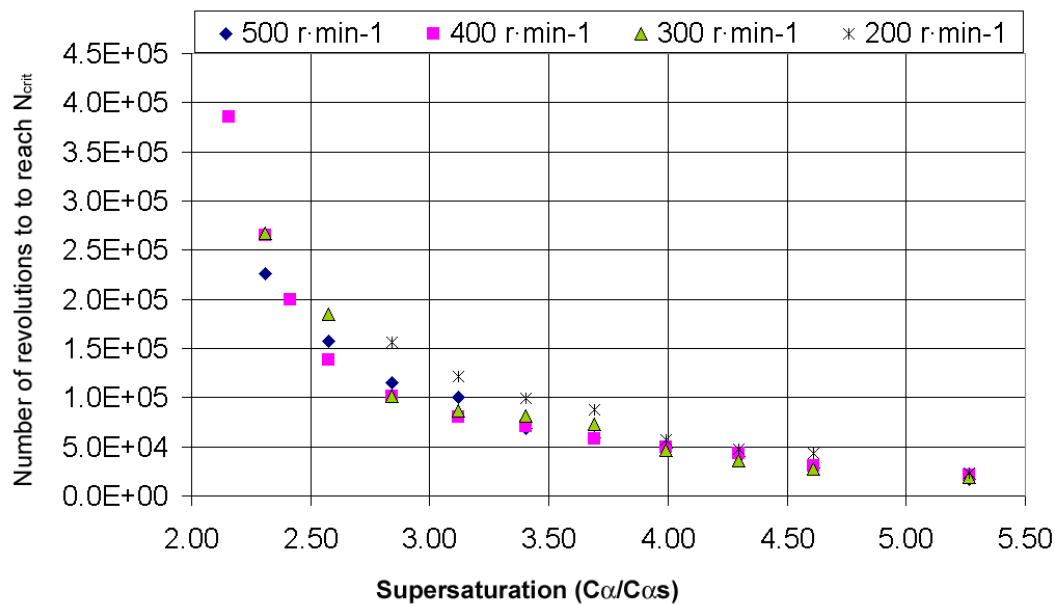


**Figure 5-20 Supersaturation vs. number of impellor revolutions required to reach  $N_{crit}$  for Rushton agitated supersaturated lactose solutions**

Figure 5-20 demonstrates a relationship between the number of impeller revolutions and the number of nuclei formed. Section 5.3.5.1 discussed that the number of number of vortices formed by a Rushton turbine, over a set time, is proportional to the velocity of the tip. Given this and the results seen in Figure 5-20 it appears a relationship between the number of vortices formed and the nucleation rate exists. This strengthens the idea that the mixing energy dispersion process is a defining factor in determining how agitation affects lactose nucleation.

### 5.5.1.3 Discussion

The results from the agitation study showed, as reported in the literature Raghavan *et al.*, 2001), that the agitation of a supersaturated lactose solution increases the nucleation rate. It has been shown that increasing agitation increases the frequency of activated molecular collisions and the critical nucleus size remains constant. It was found that the number of impellor revolutions had a strong relationship with nucleation. In contrast, when total energy input was considered it was found that to reach the critical number of nuclei, less energy was required at the lower agitation rates. Section 5.3 discussed that an increase in the agitation rate changes in multiple

mixing parameters. For this reason the specific mixing variables responsible for increased nucleation are cannot be identified.

### 5.5.2 Shear flow

The results in this section were found to provide little indication into how shear impacted on the nucleation rate. The reasons are identified below. The results are included here as they may be of interest for future work in this area.

Three shear stresses of 6.0 Pa, 5.0 Pa and 4.0 Pa were studied. These approximately correspond to shear rates of  $900 \text{ s}^{-1}$ ,  $800 \text{ s}^{-1}$  and  $650 \text{ s}^{-1}$ . The shear rate needed to apply a constant shear stress changed as the viscosity changed; therefore, the values given are only a rough guide. The results from the work can be seen in Figure 5-21.

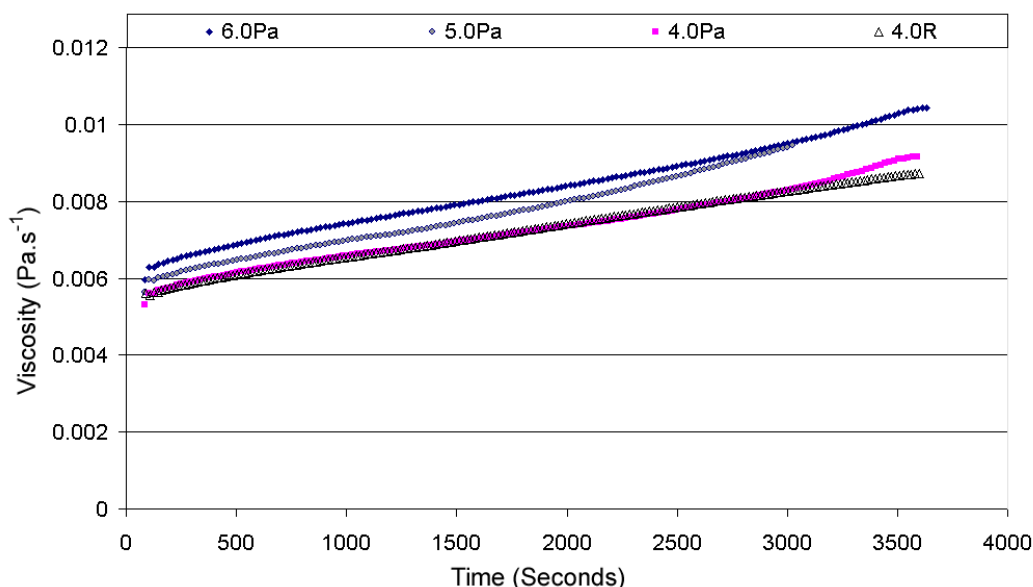


**Figure 5-21 Change in lactose solution viscosity over time at different shear stresses applied using a plate and cone rheometer**

The initial results in Figure 5-21 appeared promising. A change in the solution viscosity overtime was seen suggesting that the properties of the solutions were changing. To obtain a better idea on how increasing shear stress impacted on nucleation, the change in viscosity between each logged measurement ( $t_x$  to  $t_{x+1}$ ) was plotted in Figure 5-22. The results are inconclusive, with overlap occurring between the different shear stresses.

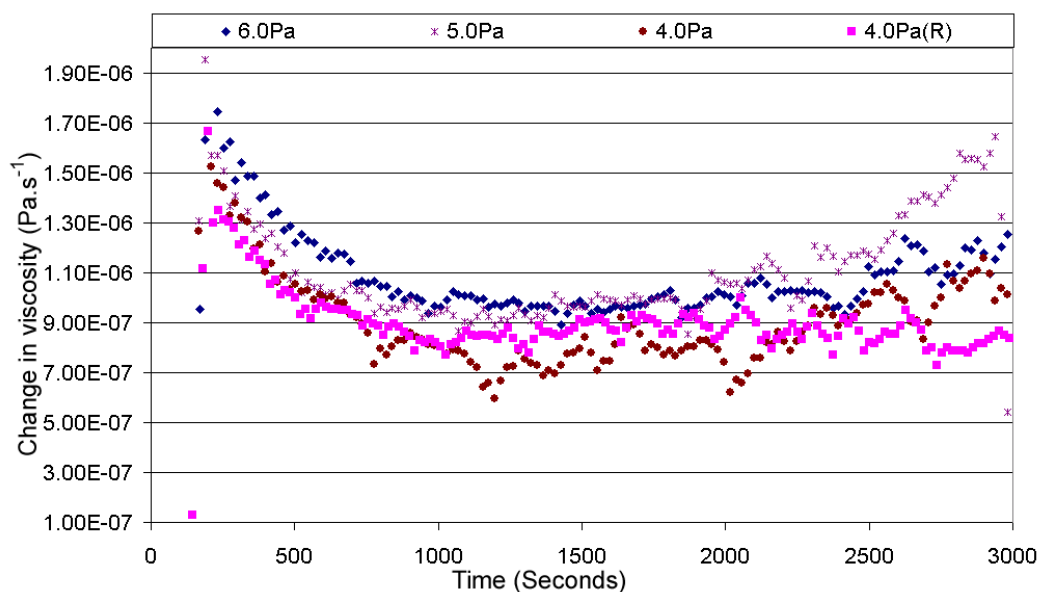


**Figure 5-22 Change in lactose solution viscosity at different shear stresses applied using a plate and cone rheometer**

To determine if the shear was leading to the viscosity change four experiments were conducted, each with a different delay time before the rheometer was started. The delay time was measured from the point where the cone was lowered on to the plate and the gap set. All the experiments were conducted at a shear stress of 4.0 Pa. For comparison, the viscosity of water was measured. To allow for any temperature effect the water added was heated to 60 °C. The results are shown in Figure 5-23, so a comparison can be made the delay time has been added on to the result. In all the data sets the first 90 seconds of the experiment has been excluded from the plot as the scatter during the start up makes it difficult to obtain information from the data that follows. It can be seen that the change in viscosity is independent of the shear applied. A solution, which has been left stationary on the plate for 40 minutes, shows the same viscosity as a solution to which a shear stress of 4.0 Pa has been applied for the same period. Two explanations exist for this observation either shear has no effect on the nucleation rate at these conditions, or the change is not detectable using this method

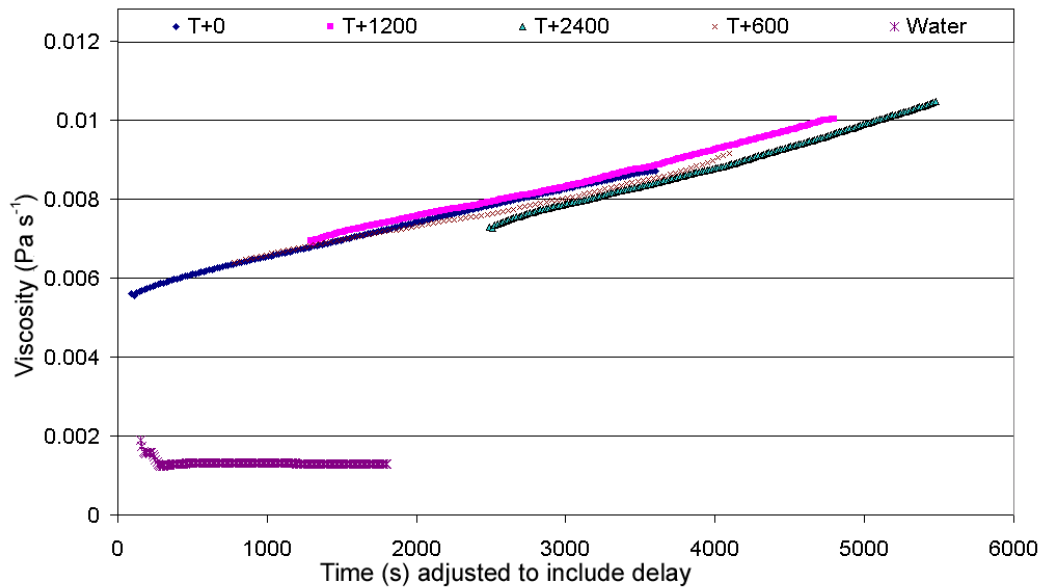


**Figure 5-23 Viscosity of lactose solution over time with a delay (Shear Stress 4.0 Pa). Measured using a plate and cone rheometer**

Inspections by eye at 600 and 1200 seconds found that no crystals in the solution could be observed. In some of the latter experiments, a “crust” formed around the edges of the cone. Because of this, it is believed that the increased in viscosity observed resulted from evaporation occurring during the experiment. Given the low thermal mass of the sample relative to the rheometer it is unlikely that temperature change played a role. The fact that the water measurements are stable after 180 seconds supports the belief that temperature was not a factor.

The results from this section of work are inconclusive, with evaporation likely to be the cause of the change in viscosity. An improved experimental set up may find that viscosity can be used as a tool to measure nucleation and from this, how shear changes the process can be studied in detail. This was not done in this work as it was considered that the Venturi technique, which is discussed in the next section, would be more beneficial for this project.

### 5.5.3 Venturi

This section investigates the relationship between passive mixing and the nucleation rate. It has been carried out to supplement and expand on the ideas gained in section 5.5.1 where nucleation was examined under changing active mixing conditions. A

Venturi styled pipe constriction was selected as the apparatus where the passive mixing will be initiated. The reasons for this and the design of the device are discussed in section 5.4.3. In the passive mixing experiments three parameters were varied, these were the supersaturation, the fluid flow rate and the diameter of the orifice. Through changing these parameters, both the nucleation and fluid flow conditions can be varied.

#### 5.5.3.1 Venturi orifice diameter

To examine how different flow conditions impact on the nucleation rate, experiments were conducted over a range of fluid flow rates. To expand the flow conditions and information collected, three separate Venturi devices with varying orifice diameters were used. The orifice diameter comparison experiments used the single absolute alpha lactose supersaturation of 26.17 g per 100 g water.

The results were considered with regard to the power per unit volume supplied to accelerate the solution through the orifice. The power input was determined using Equation 5-10. Pressure drops other than those required to generate the velocity of the fluid through the orifice were assumed negligible. The volume component of the power per unit volume value (Figure 5-24) refers to the 200 ml of lactose solution, which passed through the Venturi. The results are reported as number of crystals in the bulk solution. The bulk solution is the combination of the quenching solution and the solution that passed through the Venturi. This applies to all the results reported in this section.



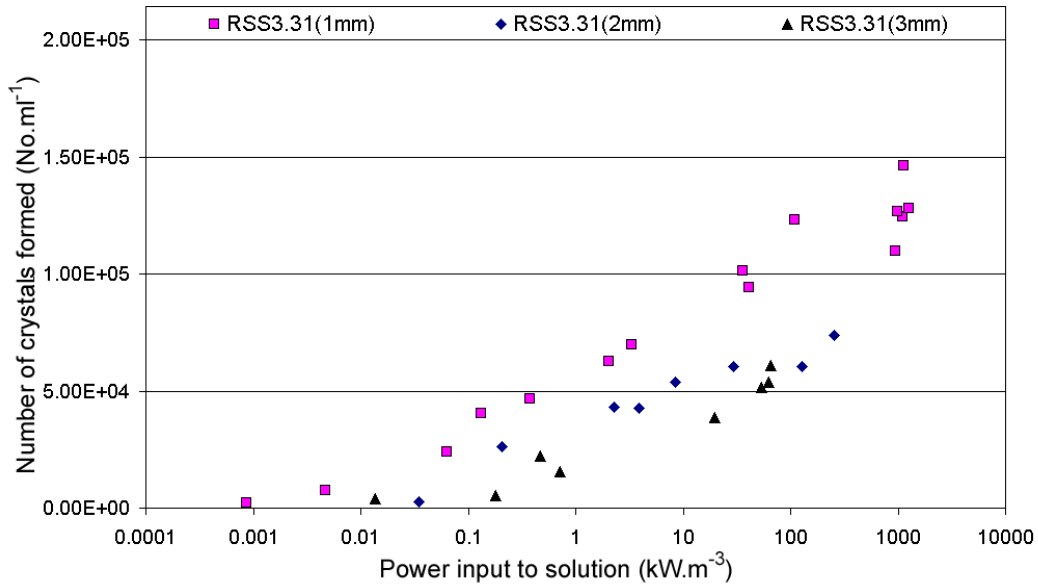


**Figure 5-24 Comparison of Venturi orifice diameter on the number of crystals produced per ml of at different power inputs. Experiments used 200 ml of solution with an absolute alpha lactose supersaturation of 26.17 g per 100 g water**

Figure 5-24 shows that an increase in the orifice diameter reduces the number of crystals formed at a specific power input. This agrees with the results seen for the agitated vessel. This reinforces that the key element of the relationship between nucleation and mixing is not how much energy is put into the system but the way in which the mixing energy is distributed. The fact that the smaller diameter orifice leads to greater crystal production at a particular power input may result from the smaller diameter orifice causing greater flow instability, as was reported by Solzbach *et al.*, (1987).

At the suggestion of Abrahamson, (2007), the power input per unit volume was recalculated as a function of the volume of the throat; the volume of the throat being the throat cross sectional area multiplied by the length of the throat. The results are presented in Figure 5-25.

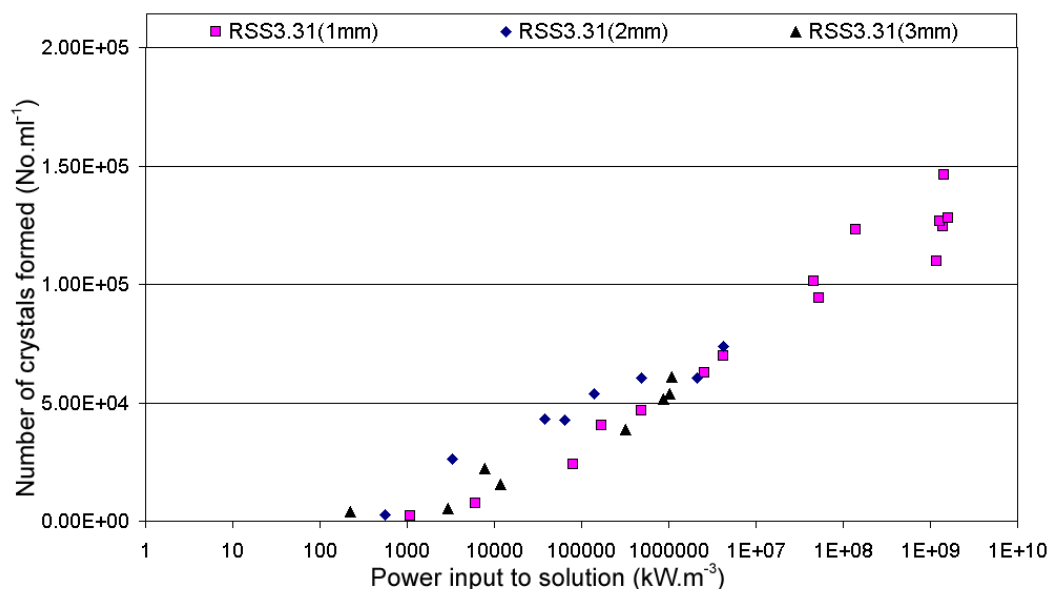


**Figure 5-25 Power per unit volume where the volume under consideration is that of the throat of the Venturi tube**

The use of the Venturi throat volume as the defining volume results in the curves for all three-orifice diameters collapsing onto a single line. The exact reasons for this are not clear. It is expected that the point of expansion is where the majority of the energy dissipation would have occurred; for this reason the collapsing of the curves is not believed to be result of the large amount of energy being released from the fluid as the majority of the energy dissipated in a Venturi occurs in the expansion zone. The throat does however, represent the point where fluid had the greatest amount of kinetic energy and so it is possible that this kinetic energy was also transferred to the lactose molecules in the solution, increasing the frequency and energy of the collisions.

The results here and those presented in section 5.5.1, indicate that flow instability plays a key role in determining how mixing changes the nucleation rate. A well-used gauge of the flow patterns in a fluid is the Reynolds number. To examine this Figure 5-26 was drawn showing the relationship between the Reynolds number and the number of crystals formed. The Reynolds number reported was that determined, using Equation 5-5, at the orifice of the Venturi.

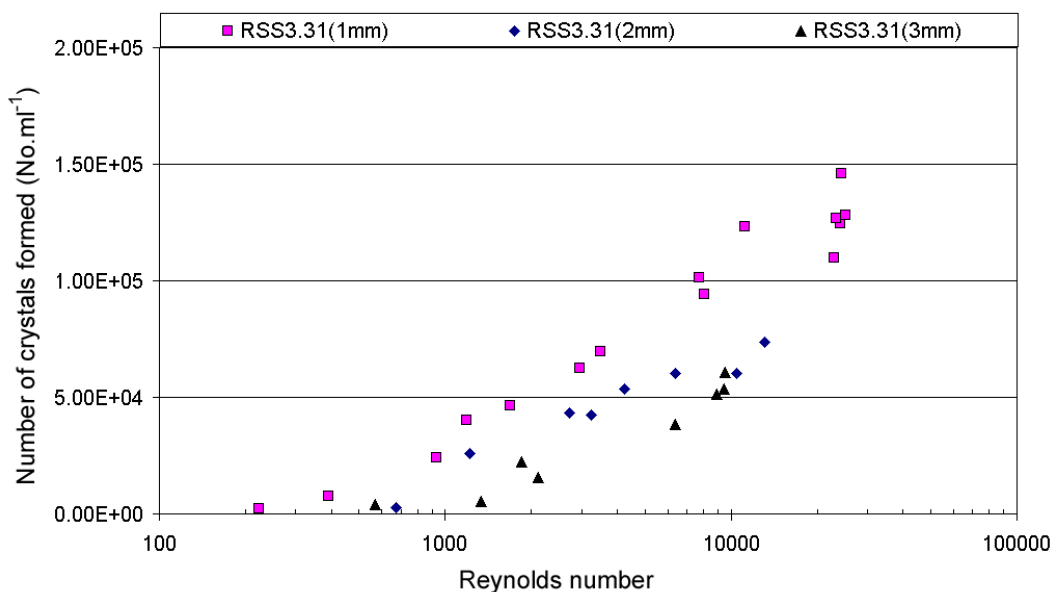


**Figure 5-26 Comparison of the Venturi orifice diameter on the number of crystals per ml at different Reynolds numbers (log scale) Experiments used 200 ml of solution with an absolute alpha lactose supersaturation of 26.17 g per 100 g water**

The results in Figure 5-26 show a similar pattern to those seen when examining the power input as a variable. This is expected, as the only variable that has been changed in both situations is the fluid velocity. Once again, the smaller orifice diameter shows increased nucleation when a single Reynolds number is considered. In section 5.3.5.2 the orifice diameter was identified as the variable to change the Reynolds number where flow-instability occurs. A narrowing of the flow constriction decreases the Reynolds number required for flow instability and increasing the length of the constriction increased the Reynolds number required for flow instability (Solzbach *et al.*, 1987). This pattern is seen in Figure 5-26. If flow instability is required for mixing to begin to influence the nucleation process, the intercept of the plots with the *x-axis* should provide an indication of the flow rate where the flow exiting the Venturi ceases to be laminar. Based on the observations of Solzbach flow instability should begin at progressively decreasing Reynolds numbers as the diameter of the orifice is decreased. This is seen in the results in Figure 5-26.

A log scale was used in Figure 5-26. When viewed using this scale it is easy to visualise a straight line running through each of the data sets. This demonstrates a log relationship that when viewed on a linear scale (Figure 5-27) flattens out at higher Reynolds number with only small gains to be made by additional input.

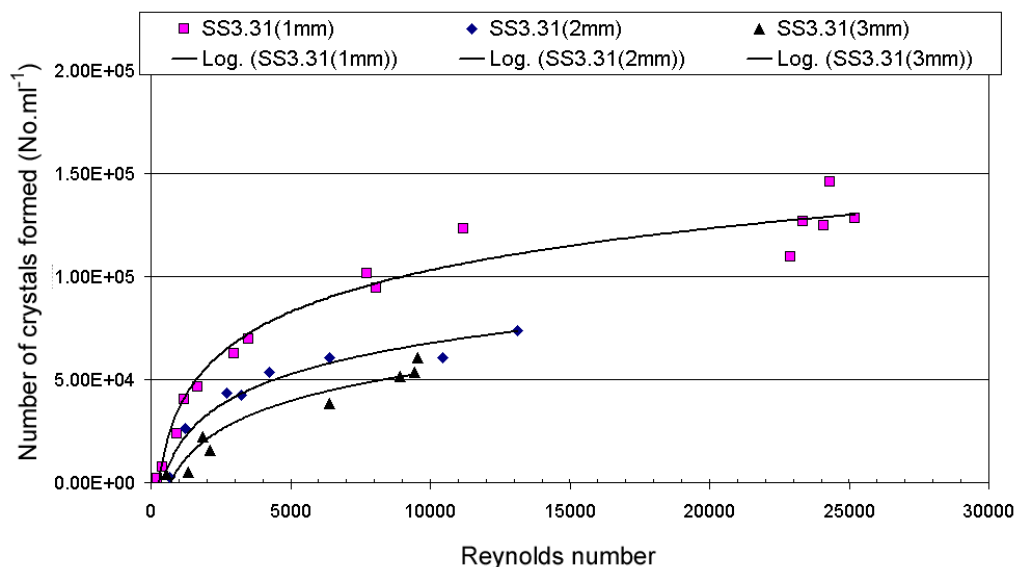


**Figure 5-27 Comparison of the Venturi orifice diameter on the number of crystals per ml at different Reynolds numbers (linear scale) Experiments used 200 ml of solution with an absolute alpha lactose supersaturation of 26.17 g per 100 g water**

Young & Tsai, (1973) observed that once the Reynolds number reached a certain position, the turbulence intensity became independent of the Reynolds number. A similar observation was made by Deshpande & Giddens, (1980) who found that in the stenosis studied, once the Reynolds number reached 5000 turbulence intensity reached a maximum. This provides an explanation for the results presented in Figure 5-27. Once a critical Reynolds number is reached, the turbulence intensity reaches what can be considered a maximum. Once this maximum is achieved, any additional input generates little gain in nucleation rate. This is consistent with the observation of Myerson, (2002), who found when increasing the stirring intensity at constant supersaturation the induction time decreased up to a certain stirring speed beyond which it remains constant. It is also consistent with the results of Mydlarz & Jones, (1991) who found that increasing the agitation rate gave diminishing returns in lowering the induction time.

It was proposed, that because the different agitation rates in section 5.5.1 collapsed on to a single curve when considered with respect to the number of revolutions, the vortices created in the solution were responsible for how mixing influences the nucleation process. The results from the Venturi experiments, when considered from

a Reynolds number perspective, failed to come together to fit a single curve. They did show trends that agree with the idea that turbulence is a key factor defining how mixing influences nucleation.

Section 5.3.5 discussed that fluid flow through an expansion leads to vortex formation. The vortex shedding frequency was defined as the Strouhal number multiplied by the fluid velocity over the diameter. There are varying reports in the literature on the Strouhal number for a constriction in a pipe and the value appears to be system specific.

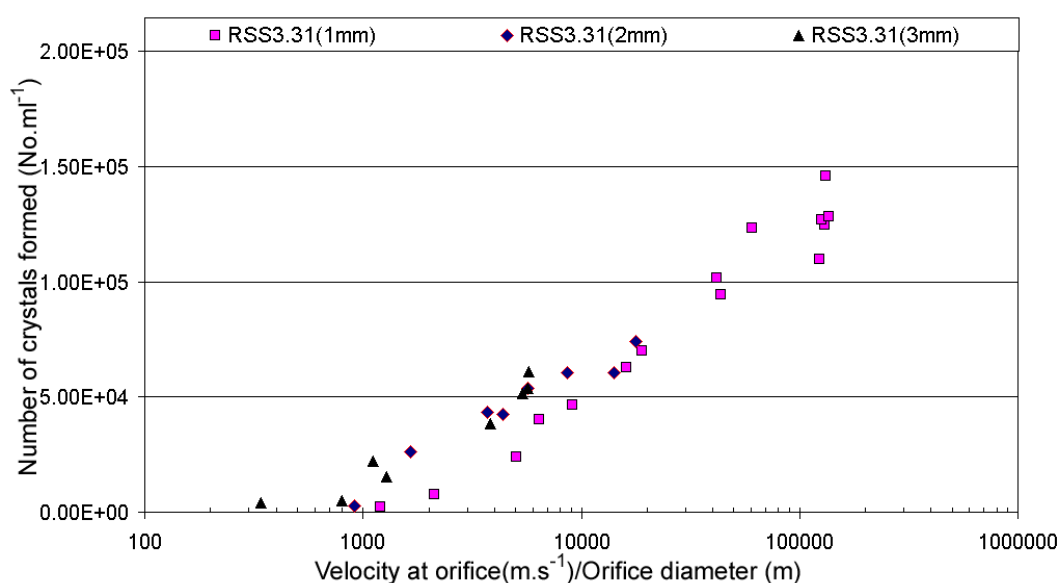


**Figure 5-28 Comparison of the Venturi orifice diameter on the number of crystals per ml based on the relationship given for Strouhal number. Experiments used 200 ml of solution with an absolute alpha lactose supersaturation of 26.17 g per 100 g water**

To examine how vortex formation influences crystal formation in the Venturies, the number of crystals per ml versus the fluid velocity over the orifice diameter was plotted as Figure 5-28. The *x-axis* is the basis of the relationship given for Strouhal number. It can be seen that the Strouhal relationship collapses all three data sets into a single curve. The exception to this is at the lower end of the scale where the values for the 1 mm orifice drop below the trended results. It is suspected that this is a consequence of the Strouhal number changing as the Reynolds number enters a low region. Figure 5-5 showed that for vortex formation past a bluff body once the Reynolds number drops below 1000 then the Strouhal number moves from being a constant and decreases. This leads to a decrease in the vortex shedding frequency. At

the same point on Figure 5-28, the Reynolds number for the 2 mm and 3 mm orifice is larger and consequently the Strouhal number is still in the higher constant region. This means that the vortex shedding frequency is greater and with this, more nucleation is observed.

The results seen in Figure 5-28 are consistent with the results seen in section 5.5.1.2. From this it is concluded that vortex formation plays a significant role in determining how mixing changes the nucleation rate. It is the microscale fluid mechanics that influence the mass transfer rates, the turbulent collisions and the micromixing of reactants (Rielly & Marquis, 2001). The small eddies responsible for the mixing at the microscale are created from the break up of larger eddies. The more small scale eddies that are formed in the solution, the more lactose molecules that will be drawn together to form nuclei.

If great enough fluid velocities can be generated when studying the mixing process using flow through an orifice, cavitation can be considered as a variable. The system in this study easily created conditions where the cavitation number was reduced below the value of one. The value of one approximately represents the point below which cavitation will occur.

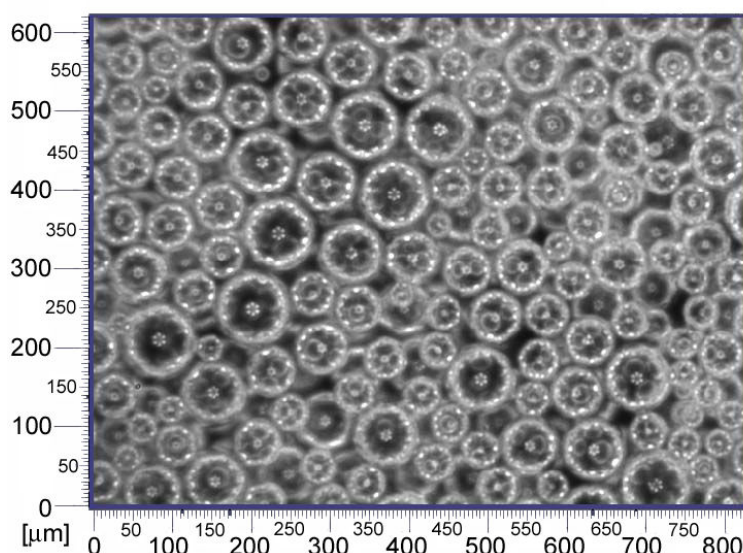


**Figure 5-29 Bubbles in bulk solution after the lactose solution had been passed through the 1.0mm Venturi at a flow rate of  $1.02 \times 10^{-4} \text{ (m}^3 \cdot \text{s}^{-1})$  (Cav number. 0.009). Images taken using a Lasentec PVM.**

As an aside to the main study, a Lasentec PVM (Particle Vision Measurement) camera was used to examine the cavitation bubbles exiting the Venturi and into the bulk solution. The probe was available only as a demonstration for one measurement and so was not able to be used to study a range of flow rates and orifice diameters. The image in Figure 5-29 shows the bubbles in the bulk solution formed from the cavitation that occurred as the fluid exited the 1 mm Venturi constriction at  $140 \text{ m}\cdot\text{s}^{-1}$ . At these conditions the fluid has a cavitation number of 0.008 and as was expected a significant amount of cavitation occurred. Continuing with the study of cavitation, a plot (Figure 5-30) was drawn, using Equation 5-4, to compare the number of nuclei formed against the cavitation number.

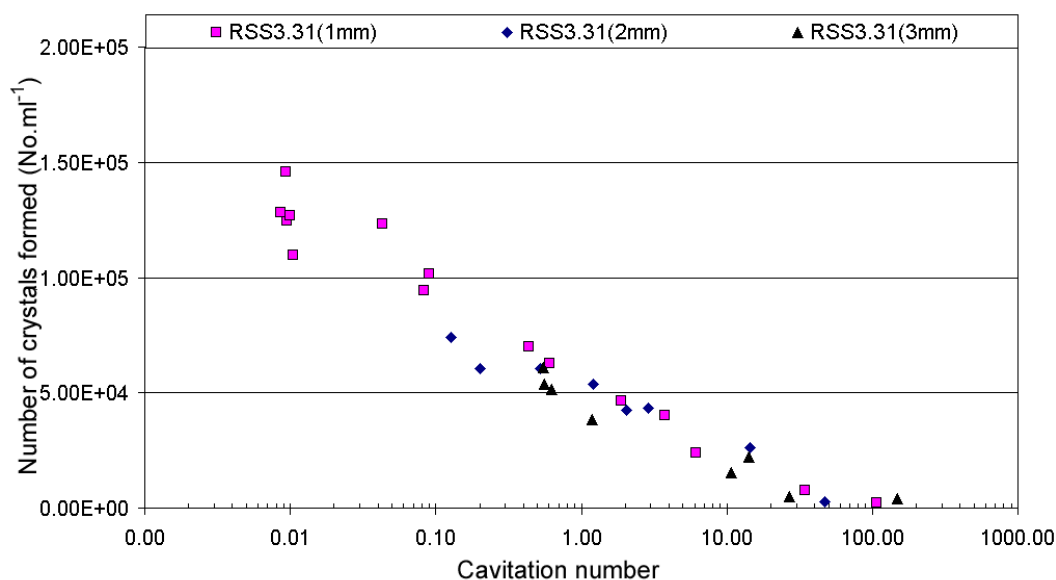


**Figure 5-30 Comparison of how the Venturi orifice diameter changed on the number of lactose crystals formed per ml of solution at different cavitation numbers. Experiments used 200 ml of solution with an absolute alpha lactose supersaturation of 26.17 g per 100 g water**

Figure 5-30 shows that the cavitation number collapses the results collected at the different orifice diameters on to one curve. Crystals were still being formed at a cavitation number of ten, well above the point where cavitation would be expected to have stopped. Additionally the trend seen is constant even after the cavitation number drops below one. It is proposed, because of this affect, that the fact that the curves all fall on to the single line is more a matter of coincidence rather than cavitation having any significant role in the nucleation process.

Figure 5-29 shows that even after the solution has been blended into the bulk solution, a large number of bubbles remain. It is during the collapse phase of the bubbles in ultrasound that nucleation is believed to be induced (Hagenson & Doraiswamy, 1998). The length of the tube following the Venturi section was only 35 mm, this short length means that the bubbles had only a short distance to form and then collapse before they entered the bulk solution. The solution was then quenched to a supersaturation level where nucleation was unlikely. It is therefore possible that if the bulk of the bubbles had been able to collapse in the highly supersaturated solution then a change in the nucleation trend may have been observed once the flow conditions fell below the critical cavitation number. More work would need to be carried out to confirm this.

#### 5.5.3.2 Supersaturation

Experiments were conducted to examine the relationship between supersaturation and nucleation in the Venturi system. The 1 mm Venturi was used because it provided the greatest range of flow conditions.

Four alpha lactose supersaturations were studied at 40 °C. These were 18.11 (2.52), 22.14 (2.91), 26.17 (3.31) and 34.24 (4.18). The numbers outside the brackets are the absolute supersaturations (g  $\alpha$  lactose per 100 g water) and the numbers inside the brackets are the relative alpha supersaturations. At the relative supersaturation of 2.52 no crystals were observed in the solution, even when the device was run at the maximum flow rate, and consequently no further experiments were carried out at this concentration.

The previous sections found the Strouhal relationship provided an effective explanation for the link between changing mixing conditions and the nucleation rate. For this reason the different supersaturation in Figure 5-31 are examined using the Strouhal relationship.



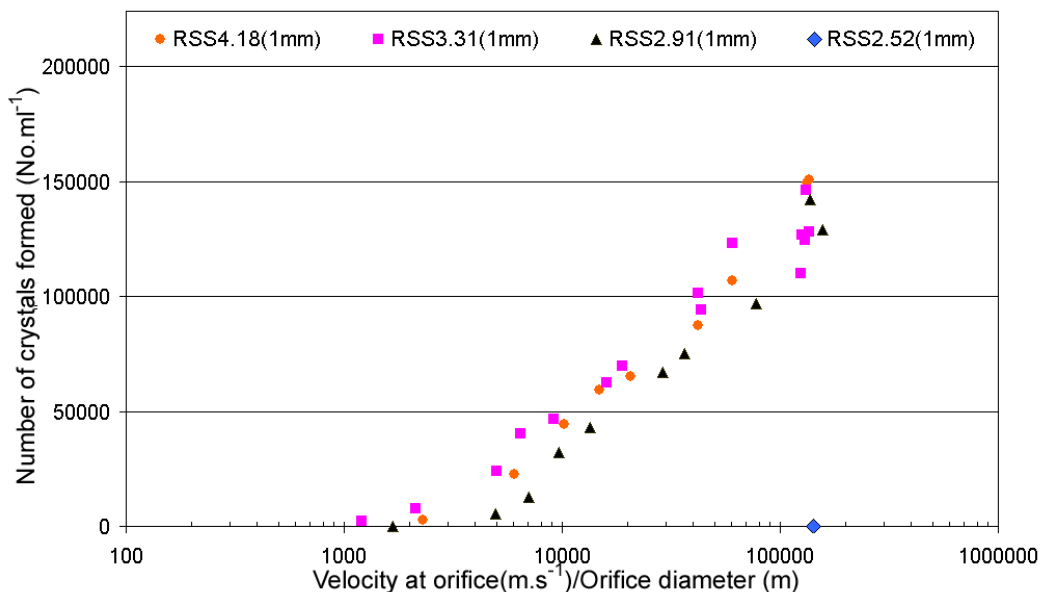


**Figure 5-31 Nucleation of differently supersaturated solutions passed through a Venturi with a 1.0 mm orifice. Results compared using Strouhal relationship**

In Figure 5-31 two factors are observable, firstly no nucleation occurred at the supersaturation of 2.52 and secondly at relative supersaturations above 2.52, the number of crystals formed is not changed by increasing the supersaturation. This is different to previous work carried out in this study and in the literature that demonstrated that supersaturation plays a major role in the lactose nucleation process. That no nucleation occurred at the relative supersaturation of 2.52 reinforces the importance of supersaturation. These two points are discussed separately in the following paragraphs.

The lack of nucleation at supersaturation of 2.52 requires that results from previous sections of this work be considered. In chapter four, primary nucleation was divided into two mechanisms, homogeneous nucleation and heterogeneous nucleation. These two mechanisms were expressed as single curves extracted from Equation 4-13. The curves for the 40 °C results are reproduced in Figure 5-32.

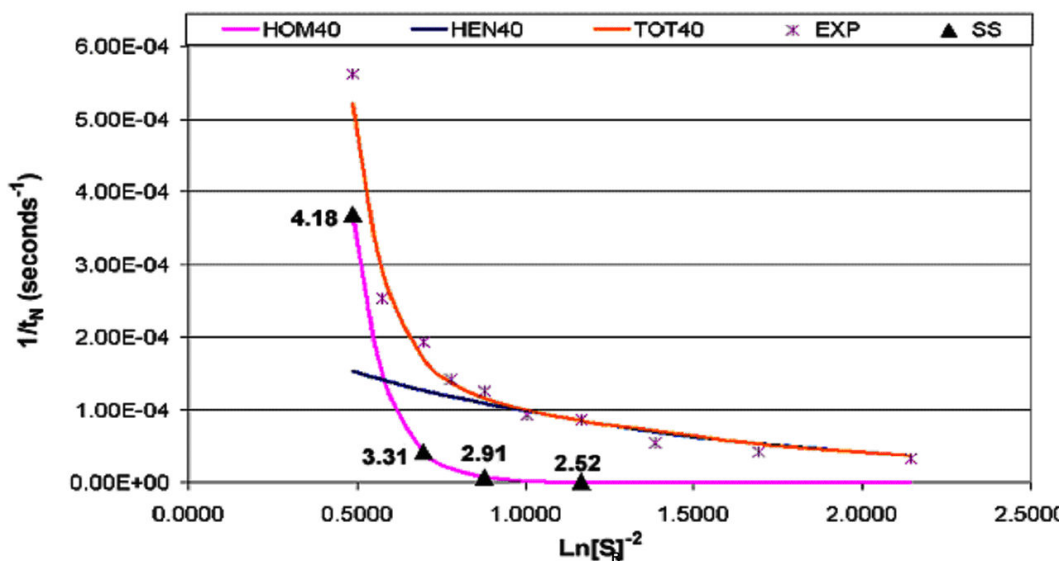


Figure 5-32 Lactose nucleation in supersaturated lactose-water solutions agitated by a Rushton Turbine (Temperature 40 °C). Included also are the four supersaturations studies using the Venturi these are marked by the black triangles

Figure 5-32 shows that of the four supersaturations studied only the supersaturation of 2.52 represents a point on the supersaturation curve where homogeneous nucleation is still a negligible mechanism in the overall nucleation rate. It is proposed that at this point the chemical potential driving force in the system was too small for the creation of a new crystal to occur directly from solution and that the creation of a new surface required a foreign body to reduce the energy barrier for nucleation. At the relative supersaturation of 2.91 the curve begins to enter the region where homogeneous nucleation had begun to appear as an identifiable factor and therefore new crystals are able to form directly from the solution. Further increases in supersaturation move the system more into the homogeneous nucleation region and the rate of homogenous nucleation consequently increases.

In section 5.5.1, the point at which homogenous nucleation becomes a factor in the overall nucleation kinetics was shown to be independent of mixing. This explains why even under conditions of extreme flow-instability, no nucleation was observed at the supersaturation of 2.52 as any nucleation seen at this point was due to heterogeneous nucleation.

The second point in the results was the absence of a supersaturation affect on the nucleation rate once the critical threshold had been passed. Mixing appears in this

case to be the variable controlling the number of crystals formed. Figure 5-31 shows a potential difference for nucleation observed at the supersaturation of 2.91 when compared to the two higher supersaturations. To determine if a significant difference occurred the data was analysed using MINITAB 14. A regression equation was fitted to the natural log of the velocity/diameter versus the number of crystals for both the 2.91 and 3.31 supersaturation data sets. Additionally as part of the process, MINITAB was used to determine the 95 per cent confidence limits about the regression equation.

In fitting the regression equation to the data, values where the observed nucleation was zero or close to zero were excluded. The justification for this is that these points provide a false reflection of the relationship, which only demonstrates a log relationship once a critical flowrate, has been achieved. Because these data points were near or below the critical fluid flow there was a potential for them to skew the regression equation. Figure 5-33 shows the regression equation of both data sets and the upper and lower confidence limits for each equation.

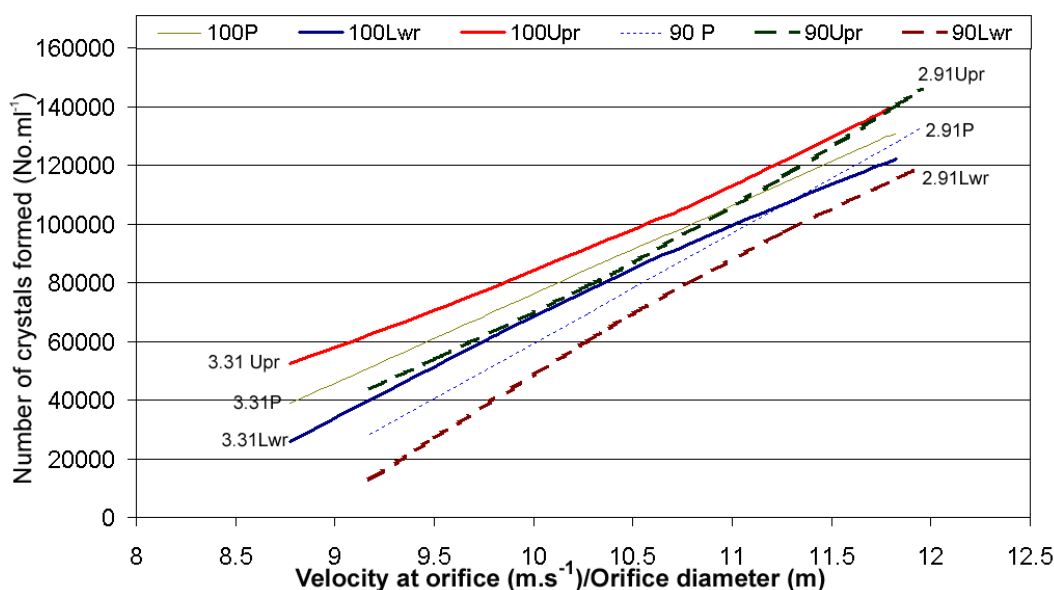


**Figure 5-33 Regression equation fitted to 90 g lactose monohydrate per 100 g water (2.91) and 100 g lactose monohydrate per 100 g water (3.31) results from 1mm Venturi experiments; 95 per cent confidence limits included**

An overlap occurs between the confidence limits of the two data sets meaning a significant difference cannot be said to occur. Lactose has been shown in this work and other work Raghavan *et al.*, (2001) to exist stably in solution for long periods of time where it is left to sit in a relatively stationary manner. The addition of agitation

results in the solution nucleating quickly. The rate is dependent on the amount of agitation added. In this system the mixing structure appears to be defined by the fluid velocity and it exists in the confines of what can be considered a relatively small environment. The fact the flow occurs through a circular pipe also means the flow pattern observed at any point along the pipe length should be constant when examined along the same circumference. Additionally the time the solution was exposed to the conditions of mixing and high supersaturation was short. The combination of these factors means that the chance of random fluctuations in the mixing pattern should be minimal. If, as has been asserted already in this work, the nucleation of lactose crystals from solution is dependent on the number of vortices formed in the solution then an explanation for the similar amount of nucleation observed appears. As the number of vortices formed in the solution is much more a function of the fluid flow than the supersaturation, the mixing in this system has the potential to be the dominant factor driving nucleation.

In a larger system, such as a stirred tank, the conditions studied are less homogeneous and nucleation occurs over a longer period. Where this is the case, supersaturation, as seen in section 5.5.1, becomes a major factor. At higher supersaturation, more lactose can be removed from the system before concentration drops below the critical supersaturation where the nucleation mechanism changes. Additionally, with the longer time frame and inhomogeneous conditions in the agitated tank, higher supersaturations increases the chance that lactose molecules will be in the correct location to be incorporated into a vortex and combine to form stable nuclei.

### 5.5.3.3 Discussion

The results from the Venturi study have provided an insight into the important elements determining the role of mixing on the nucleation process. Areas where further work is required have also been identified. As was found in the study of the impeller-agitated vessel, there is a strong relationship between the number of vortices created in the system and the rate of nucleation. The exact mechanism by which the creation of vortices leads to the enhancement of nucleation is unclear and more work is required to understand this area. It is speculated that the vortices act to decrease the distance for diffusion of the molecules in the solution, increasing the rate at which

they can come together to form stable nuclei. This is in line with conclusions drawn when the results from impeller-agitated vessel were examined using nucleation theory

When investigating nucleation in the Venturi system at different supersaturations, the amount of nucleation was found to remain constant once a critical supersaturation was achieved. It is believed this resulted from a number of factors in the experimental set up which, when combined, lead to mixing being expressed as the dominant variable. The fact that this study has shown that situations can occur when mixing controls the nucleation kinetics, highlights further the need to consider mixing in crystallisation process design.

## **5.6 Conclusion**

The results in this chapter confirm the observations of previous studies in the area of lactose nucleation. Increasing agitation increases the lactose nucleation rate. Advancing the ideas from earlier work, this work has studied mixing and nucleation in detail with the intention of identifying what the relationship is and the extent to which different levels of agitation impact on the nucleation process.

The first section of the study investigated nucleation in a solution agitated by a Rushton turbine. The critical nucleus size remained constant over the different levels of agitation intensity studied. Increasing the agitation rate increased the frequency of activated molecular collisions. It was also found that the supersaturation at which homogenous nucleation became observable was not affected by mixing. When interpreting the results from the perspective of mixing a strong correlation was found between the nucleation rate and the number of revolutions. An explanation for this was given using the Strouhal relationship, which relates the frequency of vortex shedding to the fluid velocity, or in the case of this work the impeller velocity.

Passive mixing was used to investigate the relationship between mixing and the lactose nucleation rate. A supersaturated lactose solution was passed through a Venturi. Through varying the diameter of the orifice, it was possible to examine different mixing parameters in a manner that detached them from the other parameters. The Strouhal relationship again provided an effective mechanism for

describing the results. Once a critical supersaturation was achieved, the nucleation rate in the Venturi system became independent of the supersaturation. It is believed that this is a result of a number of factors in the experimental set up, which when combined, led to mixing becoming the dominant variable. This result highlights the need to consider mixing in crystallisation process design. Further study is required to fully explain and understand the process.

Considered industrially the results identify mixing as an issue that requires consideration in the design of a crystallisation process. The design of a new plant may use mixing as a tool for compartmentalising the nucleation to a particular point in the process. In an existing plant, it needs to be acknowledged that a change in the feed point or agitation rate of the crystalliser may change the nucleation in the crystallisation process. An increase can result in a smaller size distribution as more crystals place a higher demand on available lactose. A decrease can mean that if the plant continues to operate at the same cooling rate, the lower rate of lactose removal, due to less crystal surface area, may result in additional nucleation events occurring.

## **Chapter 6 Use of the model in industry**

### **6.1 Introduction**

The previous chapters have specifically focused on a single aspect of lactose crystallisation. For the results to be useful industrially, it is important to bring together the findings in nucleation and growth into a model of the lactose crystallisation process. The integration of many of the ideas in the growth area was performed in chapter three. This model was then compared and validated against industrial data. In this chapter, the model will be used to examine the industrial situation and determine if the current practice can be improved.

### **6.2 Optimisation with regard to growth**

The  $\alpha$ -lactose monohydrate crystallisation process is a combination of an evaporation process and a cooling process. The capital cost associated with building a crystalliser means that there is a desire to cool the solution as fast as possible, minimising the time a batch must spend in the crystalliser before it is pumped out for processing, which minimises the number of crystallisers necessary. This desire to cool quickly needs to be balanced with the risk that cooling too fast will result in additional nucleation occurring.

A batch cooling process was used in all the lactose crystallisation plants investigated during this study. In all cases the production aim was that nucleation occurred during the early stages of the crystallisation. The type of production process established the definition of “early stages”. Some processes operated with nucleation during the evaporation process and others managed the process so that nucleation occurred during the crystalliser filling or during the very early stages of the cooling cycle. Under this method of operation, there is a potential for the growth only model to be used to determine the optimum cooling profile for a crystalliser.

Additional nucleation after the initial event is avoided, as it leads to the production of fine crystals. Secondary nuclei that form after the initial event are limited by lactose

availability and time available for growth. In the downstream processing unit operations the fine crystals are difficult to remove from solution, and even if separated from solution their increased surface area places an extra load to the driers.

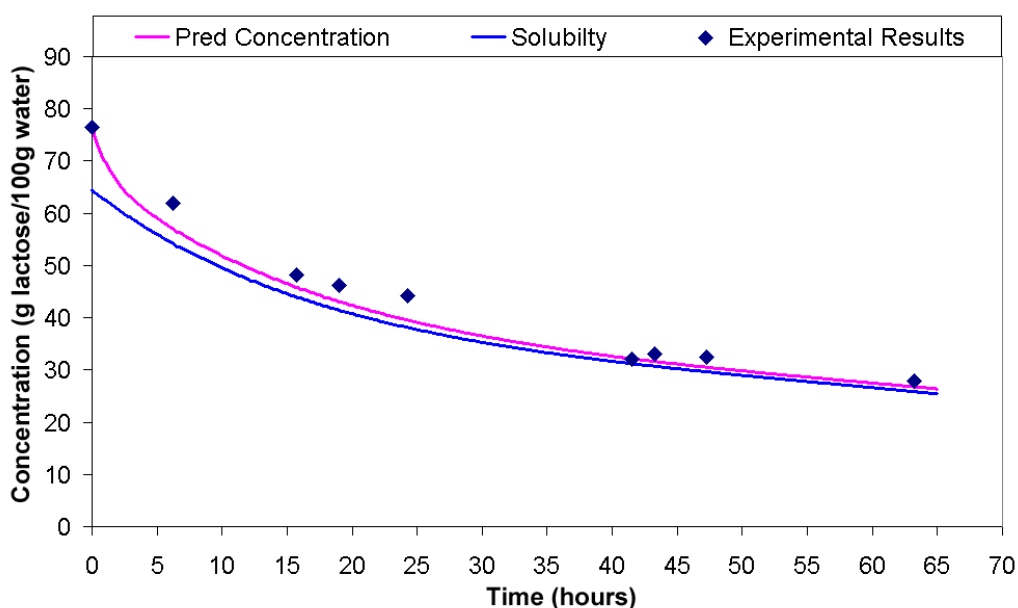
Supersaturation has been shown, in this work and in previous studies, to be the dominant factor controlling growth and nucleation. To obtain the best turn around on crystallisers the cooling process should operate at the maximum supersaturation allowable before nucleation becomes a factor. One such parameter that might be used is the secondary nucleation threshold defined in Butler, (1998). In the absence of nucleation, the growth rate that determines how fast lactose is removed from the solution. Where the process is operated under these conditions the parameter limiting the rate at which a crystallisation can be cooled is the growth rate. This situation assumes heat transfer is unlimited and represents the absolute limits at which cooling may occur. The reality is that heat removal is constrained; this is looked at later in the chapter.

To investigate the absolute cooling limits of a crystalliser, an addition to the model described in chapter three was made. Previously the model was run with an industrially obtained cooling curve set as a function of time. To determine the growth limiting cooling profile the model was set up so a concentration threshold limited the cooling rate. A maximum concentration driving force of 10 g anhydrous lactose per 100 g water (approximate absolute  $\alpha$ -lactose supersaturation 4.25 g per 100 g water) in the bulk solution was set. This is slightly higher than the eight grams given by Butler, (1998); however, given the time frame required for nucleation to occur at this supersaturation it was considered acceptable. The crystalliser was assumed perfectly mixed with no heat transfer limitations, equivalent to an infinite heat transfer surface. Therefore, heat could be removed from the crystalliser as fast as the supersaturation limitation allowed.



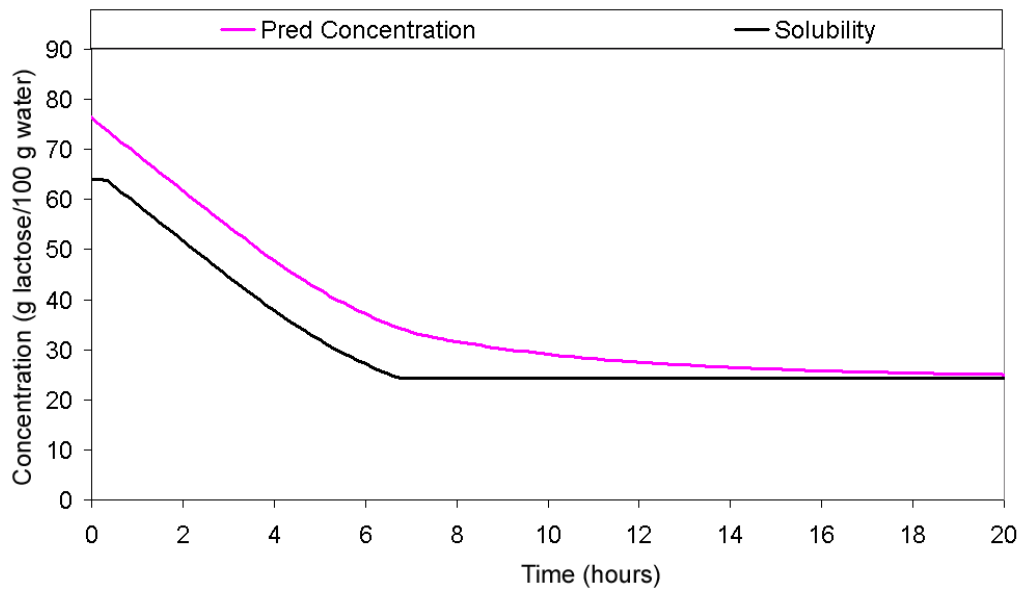
The parameters used as inputs to the model were those measured industrially. They were as follows:

*Initial temperature:* 59 °C  
*Final temperature:* 21 °C  
*Initial dissolved lactose concentration:* 76.75 g lactose/100 g water  
*Initial mass of crystallised lactose:* 1.513 g crystals/g solution  
*Particle size distribution:* as shown for A1 in the appendix



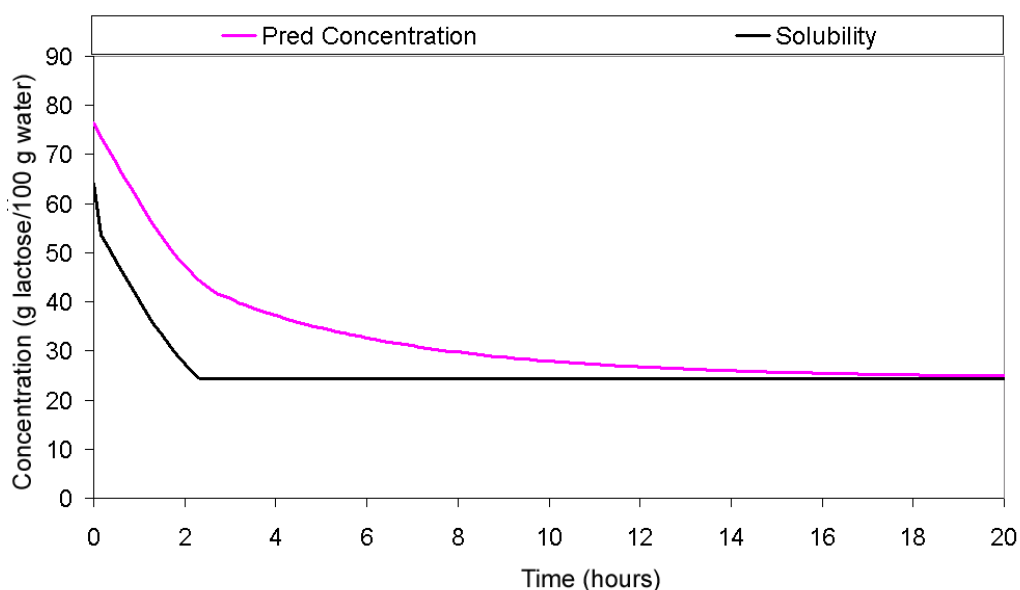
**Figure 6-1 Dissolved lactose concentration profile of crystalliser cooled as per industrial conditions**

Figure 6-1, repeated from chapter three, shows the predicted and measured results for the crystalliser cooled under the conditions used at the studied industrial plant. Standard operating practice dictates that cooling is stopped when the crystalliser reaches approximately 20 °C. In the case of the crystalliser studied and presented here the final temperature was 21 °C. Figure 6-1 shows that sixty-five hours was required for the crystalliser to reach the point where it can be emptied. It can also be seen that the concentration profile in this crystalliser closely follows the solubility line after approximately ten hours. This is a result of the slow cooling profile and the high crystal mass generated in the crystallising evaporator. The high crystal mass in the feed means a significant capacity for lactose removal by growth exists. This should allow the crystalliser to be cooled at a faster rate than is current practice.



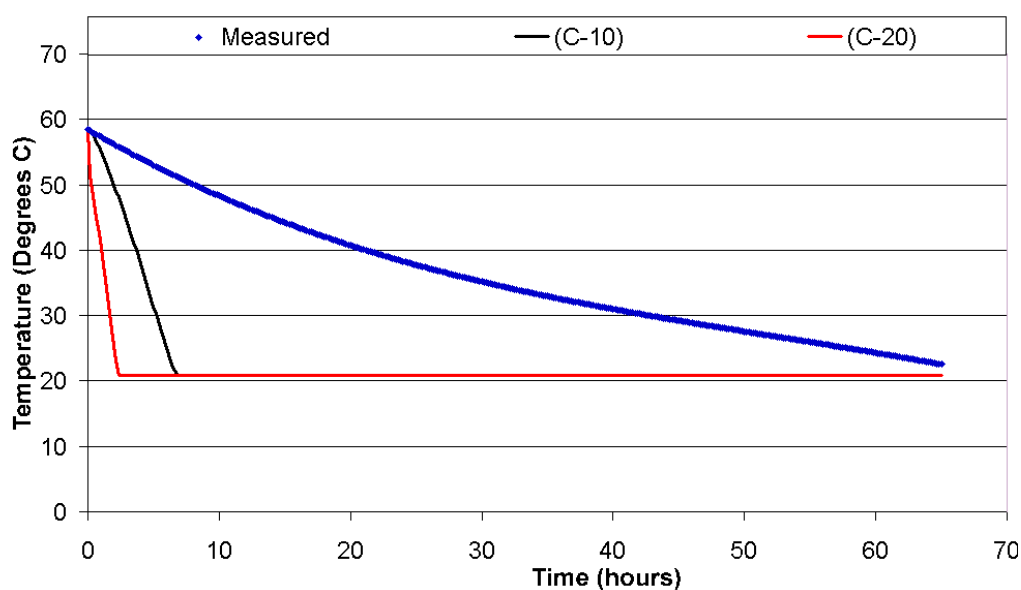
**Figure 6-2 Dissolved lactose concentration of crystalliser cooled based on achieving concentration difference of 10 g lactose/100 g water**

Figure 6-2 shows that using the concentration based model for cooling there is significant potential for reducing the time taken to cool a crystalliser with only 19 hours required to cool the crystalliser. Butler, (1998) suggested an acceptable limit for driving the cooling profile was a supersaturation of 20 g total lactose per 100 g water (approximate absolute  $\alpha$ -lactose supersaturation 8.2 g per 100 g water). This is two and a half times greater than the secondary nucleation threshold defined in the same work. It was proposed to be an acceptable limit because at this supersaturation the secondary nucleation induction time was greater than one hour. The model was rerun using the supersaturation of 20 g lactose per 100 g water to investigate how much faster cooling occurred using a larger driving force.



**Figure 6-3 Dissolved lactose concentration profile of crystalliser using supersaturation of 20g total lactose/100 g water**

Figure 6-3 shows the time to reach the equilibrium concentration using a supersaturation of 20 g lactose per 100 g water is approximately sixteen hours. This is a saving of three hours over the results obtained using the supersaturation of 10 g lactose per 100 g water. It should be remembered that when using the higher supersaturation for the cooling function there is a greater chance for additional nucleation to occur. Industrially this time saving would need to be balanced against the potential for product lost as fine crystals. To demonstrate the difference in cooling profiles the temperature versus time for each of the simulations was also plotted in Figure 6-4.



**Figure 6-4 Temperature profiles for crystalliser using different cooling rates**

Figure 6-4 shows the time for the crystalliser to reach the final temperature, in both of the supersaturation driven simulations, is less than the time required for the system to reach equilibrium. Using a supersaturation of 20 g lactose per 100 g water, cooling took only two and a half hours, compared with the sixteen hours needed to reach equilibrium. For 10 g lactose per 100 g water, only seven hours was need for cooling compared with nineteen hours needed to reach equilibrium. This illustrates that even with a large initial mass of crystals, once the supersaturation becomes low enough the diminishing growth rate becomes a controlling factor in defining the time required to reach equilibrium.

A consequence of growth becoming a limiting factor at low supersaturations is that driving a crystallisation hard from a cooling perspective may only achieve minimal gains in terms of reducing the overall time needed in the crystalliser. Only three hours were gained by doubling the supersaturation driving force, yet the risk of nucleation was substantially increased. There are other benefits in fast cooling of a crystalliser such as the reduced operating time of the pumps and cooling systems. As the total cooling load will be the same, this will be countered by the fact that cooling water flow rates need to be increased and more heat transfer surface will be required to remove the heat. Investigation of these factors requires an incorporation of a heat transfer component into the model. This is looked at in the following section.

### 6.3 Heat transfer from a crystalliser

In the industrial situation the rate at which can heat be removed from a crystalliser is limited. The outcome of this is that cooling, as well as being controlled by the desire to minimise nucleation, is also restricted by the rate at which heat can be removed from the crystalliser. Heat removal from a crystalliser is dependent on the design of the crystalliser, with factors such as the cooling surface area to volume ratio and cooling water flow rate playing an important role. The overall rate of heat transfer from a crystalliser is described by Equation 6-1.

$$H_Q = U_H SA \Delta T$$

**Equation 6-1 Heat flow from crystalliser**

Where the crystalliser is the bottleneck in the process it is desirable to cool the crystalliser as fast as possible. If the only consideration were the cooling then, assuming surface area is fixed fast cooling would be best achieved through the maximisation of the temperature difference between the crystalliser and the cooling fluid. As has been previously discussed, cooling is only one of the limitations, with minimising further nucleation of lactose also being a limiting factor.

In chapter three the crystallisers from which the concentration profiles were obtained are located outside and are cooled using evaporative cooling with a film of water passing down the outside of the crystalliser. There is limited potential, if the existing design of these crystallisers is maintained, to improve cooling. It was found that the temperature of the cooling water quickly comes to equilibrium meaning the effect of the initial cooling water temperature is minimal. The air conditions such as flow rate and temperature are also determined by the environmental conditions at the time. The number of unknown and changing variables meant that an evaporative cooling component was left out of the model. Models for this process have been developed for similar but more controlled systems and can be found in work by (Stabat & Marchio D., 2004) and (Zalewski & Gryglaszewski, 1997) should they be required.

The crystalliser design for most lactose crystallisation plants includes a jacket through which cooling water is pumped. A diagram showing a typical set-up is presented in Figure 6-5.

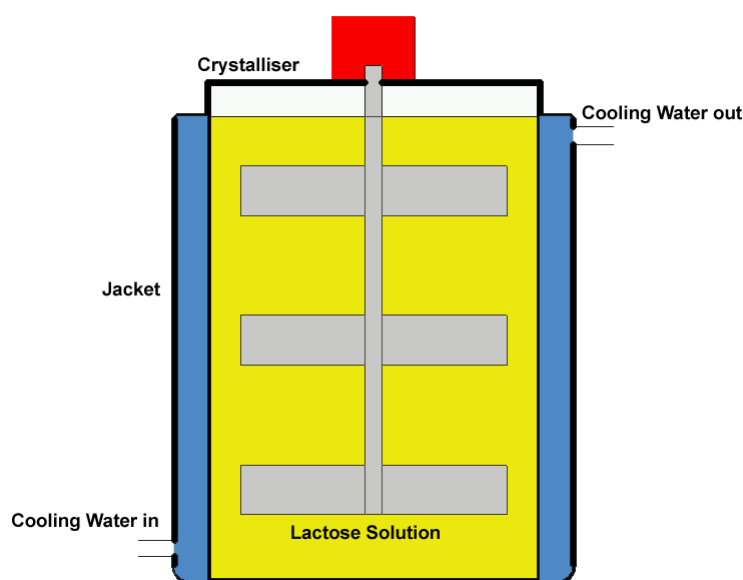
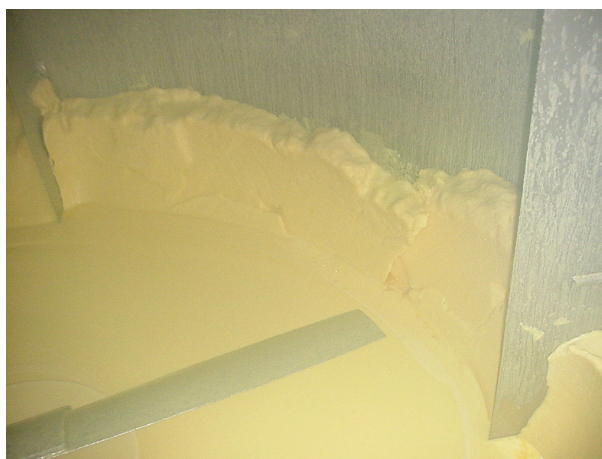


Figure 6-5 Jacket cooled crystalliser

For the crystalliser design presented in Figure 6-5 the key factor from a nucleation perspective is the temperature difference between the solution at the wall and the inlet cooling water. It is here that the greatest supersaturation will exist as the heat is transferred from the permeate concentrate layer at the vessel wall to the cooling water. In the situation where the cooling water creates a large drop in the solution temperature, there is the potential, where a large enough supersaturation is generated, for nucleation to occur. Conditions such as this are undesirable as they can lead to the build-up of a lactose layer at the wall of the crystalliser. An example of a situation such as this occurring can be seen in Figure 6-6.



**Figure 6-6 Lactose nucleation at walls in an industrial crystalliser where the cooling driving force lowers the solubility faster than can be absorbed by crystal growth**

A heat transfer component was built into the model to investigate different cooling profiles for a jacket-cooled crystalliser. Three factors were taken into account; these were the surface area available for cooling, the overall heat transfer coefficient and the temperature driving force. Each of these is considered separately below.

### **6.3.1 Surface area**

The surface area available for cooling was determined by assuming the crystalliser was a cylinder; using this, the surface area was determined using Equation 6-2.

$$SA = \pi D_T H_T$$

**Equation 6-2 Surface area available for heat transfer**

It was also assumed that the jacket height was the same as the height of the lactose solution in the crystalliser. Heat losses from the top and bottom of the crystalliser were assumed negligible. At the top of the crystalliser, the solution is separated from the wall by a 300 mm gap of air; this will have an insulating effect making the assumption of heat losses an acceptable one. The base of the crystalliser sits on a concrete pad. Concrete has a heat transfer coefficient of  $1.2 \text{ W}\cdot\text{m}^{-2}\cdot\text{K}^{-1}$  (Borgnakke & Sonntag, 1997) This is, as will be seen in the following section, over 200 times less than the heat transfer coefficient of the jacket, making the assumption acceptable.

### 6.3.2 Overall heat transfer coefficient

The accompanying limitation to surface area dictating how fast heat can be removed from a crystalliser is the overall heat transfer coefficient. There are a number of approaches for determining a heat transfer coefficient. The simplest one is to obtain an overall heat transfer coefficient for an jacketed agitated vessel from an engineering handbook such as the one by Ulrich, (1984). Using this approach a range of  $250 \text{ W}\cdot\text{m}^{-2}\cdot\text{K}^{-1}$  to  $400 \text{ W}\cdot\text{m}^{-2}\cdot\text{K}^{-1}$  is obtained. This approach assumes that the heat transfer coefficient remains constant during the crystallisation. In actuality the heat transfer coefficient will change as cooling occurs. As more lactose crystallises and the solution temperature decreases the viscosity of the permeate concentrate will change. Viscosity, as will be seen in Equation 6-4 is an important parameter in determining the heat transfer coefficient.

To incorporate the changing physical properties of the permeate concentrate; a second approach can be used. This approach uses empirical relationships to determine the heat transfer coefficient. Equation 6-3 expresses the overall heat transfer coefficient as a function of the product and cooling side heat transfer coefficients, the resistance of the vessel wall and any fouling that may occur.

$$\frac{1}{U_H} = \frac{1}{h_j} + \frac{x_w}{\lambda_w} + Rf + \frac{1}{h_p}$$

**Equation 6-3 Determination of overall heat transfer coefficient using empirical relationships**

For the product side of an agitated vessel, the general form of the empirical equation for determining the Nusselt number is shown as Equation 6-4. This equation considers the physical properties of the system, the geometry of the tank, the impeller type and

the impellor speed (Engeskaug, Thorbjornsem, & Sven, 2005), (Mohan, Boateng, & Myerson, 2000). Values of 0.66 for the Reynolds number exponent  $a$ , 0.33 for the Prandtl number exponent  $b$ , and 0.14 for the viscosity ratio exponent  $c$  are recommended. The value of  $k_L$  varies between 0.3 and 1.5 depending on the impellor type and heat transfer surface (Mohan, Emery, & Al-Hassan, 1992).

$$Nu = k_L \times Re^a Pr^b Vi^c$$

**Equation 6-4 Empirical equation for determining Nusselt number for product side**

To convert the value obtained in Equation 6-4 into the product side heat transfer coefficient Equation 6-5 is used.

$$h_p = \frac{Nu \times K_p}{D_T}$$

**Equation 6-5 Determination of the heat transfer coefficient on product side**

For the cooling side Equation 6-6 can be used to determine the heat transfer coefficient. This equation is for a simple jacket and was obtained from Mohan *et al.*, 1992). Other correlations are available for different jackets, their use being specific to the jacket type.

$$h_j = \frac{.8k_{LJ} Pr^{0.33} [\rho_L^2 g \beta (\Delta T) / u^2]^{0.33}}{K_T}$$

**Equation 6-6 Heat transfer coefficient for jacket side**

An example calculation using the equations given here gave an overall heat transfer coefficient of  $268 \text{ W} \cdot \text{m}^{-2} \cdot \text{K}^{-1}$ . The resistance of the vessel wall and resistance due to fouling were assumed negligible. The calculations used to obtain this value can be found in appendix A4. The resulting value is within the range give by Ulrich, 1984) but requires considerably more information and time to obtain.

The approach used to determine the overall the heat transfer coefficient for the model is the first approach given, with the value of  $300 \text{ W} \cdot \text{m}^{-2} \cdot \text{K}^{-1}$  from Ulrich, (1984) being incorporated into the model. This approach is simple, limits the need for heat transfer



information and reflects the variation in crystalliser design. Where an improved value is sought, it should be obtained for the crystalliser being investigated.

### 6.3.3 Temperature driving force

The driving force for cooling is the temperature difference between the cooling fluid and the lactose solution in the crystalliser. In modelling the optimum cooling profile, the temperature of the inlet cooling water was used as the defining parameter for control of the system.

As the cooling water passes through the jacket, it absorbs heat from the lactose solution and increases in temperature. Consequently, with the exception of where the cooling water flowrate is very large, the temperature difference between the inlet cooling water and the lactose solution is an inaccurate representation of the temperature driving force. To provide a better prediction of the overall temperature difference between the cooling water and the lactose solution the log mean temperature difference (LMTD) was used. Plug flow of the cooling water was assumed and the lactose solution inside the crystalliser was assumed well mixed. The LMTD equation for constant temperature receiver was used (Bejan & Kraus, 2003).

$$LMTD = \frac{T_{cw(in)} - T_{cw(out)}}{\ln \left[ \frac{(T_{cw(in)} - T_b)}{(T_{cw(out)} - T_b)} \right]}$$

**Equation 6-7 LMTD for crystalliser cooling water**

Equation 6-7 requires both the inlet and outlet temperatures of the cooling water. To eliminate the outlet temperature as a required variable the heat balance was rearranged to find the outlet temperature and this was then substituted back into the equation. The working and final equation for the heat balance is shown as Equation 6-8.

$$\begin{aligned}
H_Q &= m_{cw} C p_{cw} (T_{cw(in)} - T_{cw(out)}) = U_H SA \frac{(T_{cw(in)} - T_{cw(out)})}{\ln \left( \frac{T_{cw(in)} - T_b}{T_{cw(out)} - T_b} \right)} \\
\ln \left( \frac{T_{cw(in)} - T_b}{T_{cw(out)} - T_b} \right) &= \frac{U_H SA (T_{cw(in)} - T_{cw(out)})}{m_{cw} C p_{cw} (T_{cw(in)} - T_{cw(out)})} = \frac{U_H SA}{m_{cw} C p_{cw}} \\
\left( \frac{T_{cw(in)} - T_b}{T_{cw(out)} - T_b} \right) &= \exp \left( \frac{U_H SA}{m_{cw} C p_{cw}} \right) \\
(T_{cw(in)} - T_b) \exp \left( -\frac{U_H SA}{m_{cw} C p_{cw}} \right) &= (T_{cw(out)} - T_b) \\
T_{cw(out)} &= T_b - (T_{cw(in)} - T_b) \exp \left( -\frac{U_H SA}{m_{cw} C p_{cw}} \right) \\
H_Q &= m_{cw} C p_{cw} (T_{cw(in)} - T_{cw(out)}) = m_{cw} C p_{cw} \left[ T_{cw(in)} - T_b - (T_{cw(in)} - T_b) \exp \left( -\frac{U_H SA}{m_{cw} C p_{cw}} \right) \right] \\
H_Q &= m_{cw} C p_{cw} \left[ (T_{cw(in)} - T_b) - (T_{cw(in)} - T_b) \exp \left( -\frac{U_H SA}{m_{cw} C p_{cw}} \right) \right] \\
H_Q &= m_{cw} C p_{cw} (T_{cw(in)} - T_b) \left[ 1 - \exp \left( -\frac{U_H SA}{m_{cw} C p_{cw}} \right) \right]
\end{aligned}$$

**Equation 6-8 Heat flow from crystalliser to cooling water (working included)**

### 6.3.4 Application of the heat transfer model

Online temperature measurement is easier and cheaper than measuring the lactose concentration in solution. A consequence of this is that the lactose industry commonly to cool a crystalliser using a temperature difference. The approach sets a maximum temperature difference between the cooling water and the permeate concentrate inside the crystalliser. The aim is maximise cooling whilst reducing the potential for nucleation to occur.

The solubility equation for lactose presented in chapter two and the nucleation and growth results presented in subsequent chapters demonstrate the drawback of this approach. Growth and nucleation have been shown in this work to be a function of supersaturation when they are considered from an absolute perspective. With lactose solubility in water displaying an exponential relationship with temperature, it can be seen that the absolute supersaturations represented by two equal temperature

differences at different points on the solubility curve are potentially largely different. Because of this, what corresponds to a good temperature difference at one point may be a poor representation of the best temperature difference at another. The result is that either cooling occurs below the optimum rate or the supersaturation crosses the threshold where by nucleation becomes a likely event.

To investigate the application of different cooling profiles, the heat transfer version of the model was applied to the crystalliser using two different approaches. In the first approach, a temperature difference of 10 °C between the cooling inlet water and the permeate concentrate was used to control the cooling. In the second approach, the cooling water temperature was set such that a maximum supersaturation was achieved. Maximum supersaturation was defined as the lactose concentration of the permeate concentrate minus the solubility of lactose at the temperature of the cooling water inlet. The supersaturation used for growth in the crystallisation was defined as the concentration of the bulk solution minus the solubility of lactose at the bulk temperature. In the second approach, two maximum supersaturations were investigated, 10 g lactose per 100 g water and 20 g lactose per 100 g water. The initial conditions and cooling related parameters used in the model were as follows.

<i>Initial temperature:</i>	<i>59 °C</i>
<i>Final temperature:</i>	<i>21 °C</i>
<i>Initial dissolved lactose concentration:</i>	<i>76.75 g lactose/100 g water</i>
<i>Initial mass of crystallised lactose:</i>	<i>1.513 g crystals/ g solution</i>
<i>Particle size distribution: as shown for A1 in the appendix</i>	
<i>Cooling water flow rate</i>	<i>18000 litres/ hour</i>
<i>Crystalliser height</i>	<i>5.0 metres</i>
<i>Crystalliser diameter</i>	<i>3.0 metres</i>
<i>Crystalliser volume</i>	<i>30 000 litres</i>

These parameters were based on typical values found in the industrial setting.

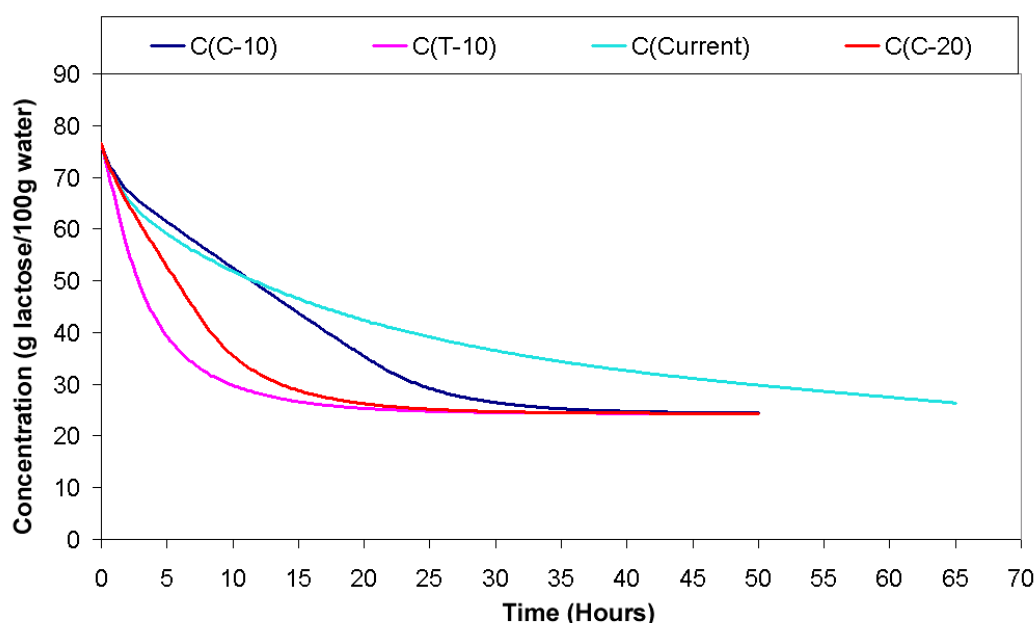


**Figure 6-7 Dissolved lactose concentration profiles of crystalliser cooled using different cooling models**

Figure 6-7 shows that to achieve cooling and concentration equilibrium in the fastest time the best approach uses the temperature difference of 10°C, this is closely followed by the model that sets the inlet cooling water temperature so that a maximum supersaturation of 20 g lactose per 100 g water is achieved. Comparing these results with those predicted in Figure 6-2 and Figure 6-3 it can be seen that heat transfer limitations are important in defining how fast a crystalliser can be cooled. In the model with no heat transfer limitations the times to reach equilibrium for the supersaturations of 10 g lactose per 100 g water and 20 g lactose per 100 g water were nineteen and sixteen hours respectively. With the introduction of heat transfer limitations, typical of those seen in an industrial crystalliser, these times have increased to 35 and 22 hours.

To control nucleation when cooling a crystalliser, the important aspect is the supersaturation generated. To examine this, the supersaturation was calculated in each of the situations modelled. This has been studied from two perspectives. The first, shown as Figure 6-8, examines the supersaturation generated in the bulk solution. The second, shown in Figure 6-9, looks at the maximum supersaturation; this is generated at the cooling water inlet.

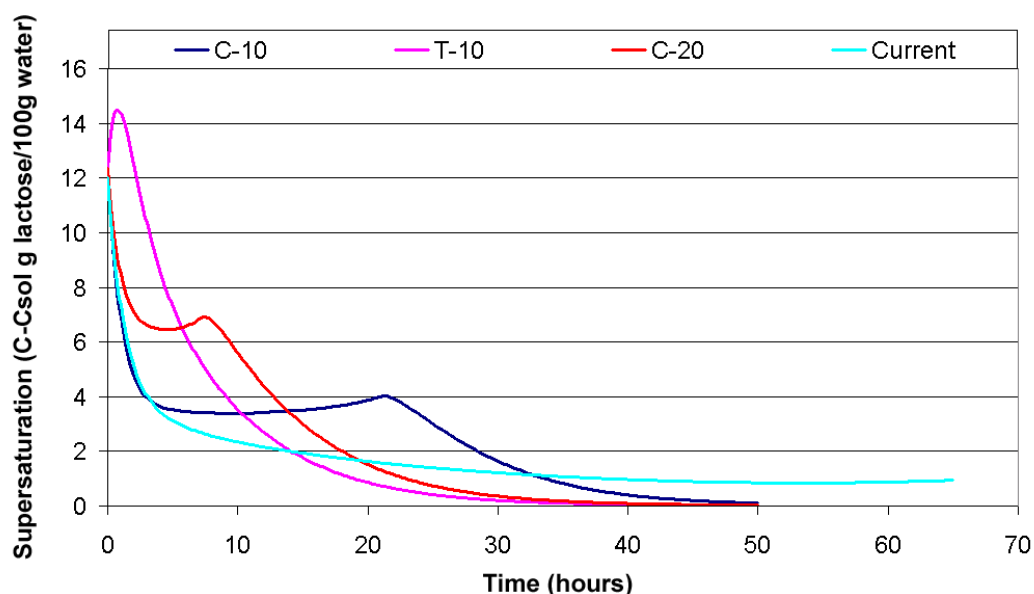


**Figure 6-8 Total anhydrous lactose supersaturation for different cooling profiles (based on temperature bulk solution)**

Figure 6-8 shows that during the initial stages of the cooling process the supersaturation is high. The effect of this is most dramatic for the temperature controlled cooling profile, with the large drop in temperature leading to a spike in the supersaturation. If the secondary nucleation threshold is, as determined by Butler, (1998), 8 g anhydrous lactose per 100 g water, the model is predicting that fines production may occur for five hours using the temperature difference cooling profile. This compares to less than one hour for the two predictions controlled by the maximum supersaturation conditions.

Once the supersaturation is low enough, then the rate of lactose removal through growth and the rate at which lactose becomes available through the lowering of temperature and the subsequent decreasing solubility reach pseudo-equilibrium. This is demonstrated by the flattening out of the supersaturation profile in Figure 6-8. This pseudo-equilibrium point is determined by the maximum supersaturation used to define the cooling water temperature as shown in Figure 6-9. As would be expected the flattening out occurs at a higher value for the higher supersaturation. The flattening out occurs at a different value than the defined supersaturation, demonstrating further the limitations heat transfer place on determining how fast the system can be brought to the desired equilibrium.

Once the solution has reached, the desired temperature there is another changing supersaturation profile as the system moves towards equilibrium. The rate of decrease is not linear and diminishes with lower supersaturation, a reflection of the decreasing growth rate.

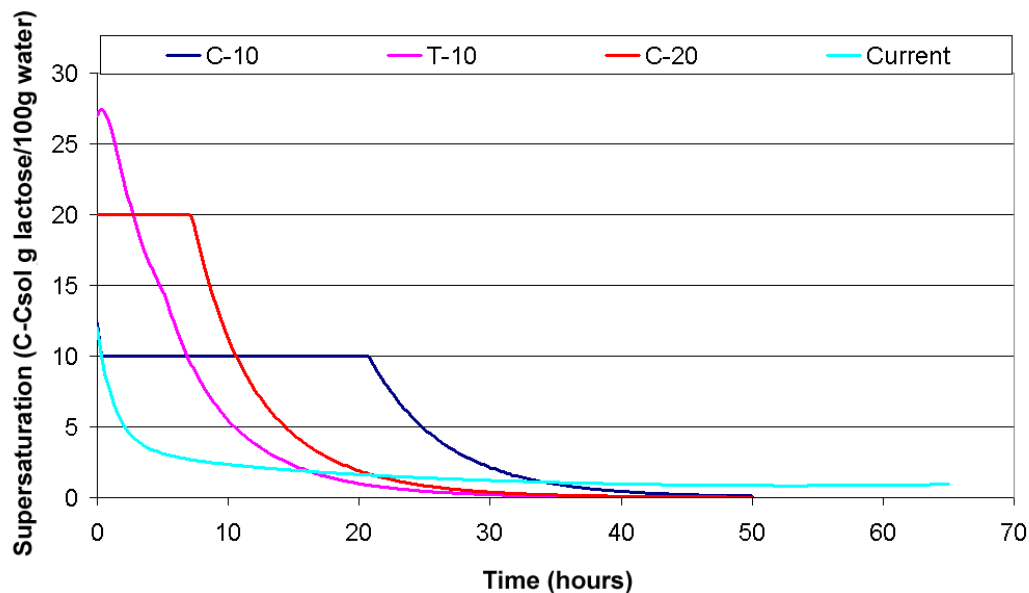


**Figure 6-9 Total anhydrous lactose supersaturation for different cooling profiles (based on temperature of cooling water)**

Figure 6-9 shows the maximum supersaturations at the cooling water inlet is considerably higher than the supersaturation in the bulk solution. It can also be seen that the supersaturation is maintained as constant for the supersaturation controlled cooling. For the temperature driven cooling the supersaturation changes constantly, a result of the fact that solubility is exponential a function of temperature and therefore a constant temperature difference will not achieve a constant supersaturation difference.

Seen again in the result is that once the cooling water reaches the desired final temperature, supersaturation progressively decreases until it reaches equilibrium. With growth being supersaturation dependent there is the potential to reduce the processing time. This would involve using cooling water at a temperature lower than the temperature that equates to the solubility of the final desired concentration. This will create a faster growth, as a higher supersaturation is maintained for a increased

percentage of the cooling process. The additional costs associated with chilling the water needs to be balanced against the potential increased capacity and yield. Where this approach is used, it may be desirable to define a crystallisation as being complete when it reaches a set concentration.

The approach suggested from this modelling work is a non-standard approach to lactose crystalliser operation and control. In the crystalliser modelled in Figure 6-7 the crystalliser contains a large mass of lactose crystals that have been formed in the evaporation stage of the process. This large mass of lactose crystals means that from the start of cooling there is a large surface area available for growth and consequently any supersaturation is removed from solution quickly. In many lactose plants instead of using a crystallising evaporator, nucleation occurs during the crystalliser filling stage of the process. This means that cooling does not begin with a large mass of well-formed lactose crystals. The consequence of this is that surface area available for growth is less substantial than in the situation modelled above.

## **6.4 Nucleation optimisation**

Chapters four and five clearly showed the system specific nature of lactose nucleation. This system specificity makes the task of generating a model of the nucleation process which can be used in industry a difficult one. One of the difficulties is obtaining results from the industrial crystallisation that allow a detailed study of the nucleation process to be undertaken. The costs associated and limited scope for making changes in the operating conditions make it difficult to obtain results from which a substantial amount of information can be gained.

A situation arose during the course of this investigation where an upgrade of a whey permeate evaporator had occurred. This was done with the intention of increasing the solids concentration of the stream exiting the evaporators and being pumped to the crystallisers. The fine-tuning of this upgrade provided a short opportunity to collect information on how changing the feed supersaturation altered the size of the crystals produced in the final product. The information collected was limited but does provide an indication of how supersaturation affects the nucleation of crystals in an industrial crystalliser.

### 6.4.1 Results from industrial study

Three crystallisations were examined during the course of the industrial investigation. These crystallisations varied in both supersaturation and temperature. The fill conditions were as follows:

<i>Crystallisation one</i>	–	<i>59 per cent solids, temperature 72 °C</i>
<i>Crystallisation two</i>	–	<i>62 per cent solids, temperature 72 °C</i>
<i>Crystallisation three</i>	–	<i>62 per cent solids, temperature 78 °C</i>

To investigate the effect of supersaturation on the nucleation process, samples were taken at the end of the crystallisation when the permeate concentrate had reached equilibrium temperature and concentration. This sample was placed in a Heraeus bench top centrifuge and spun at  $5000 \text{ r}\cdot\text{min}^{-1}$  to separate the crystals from the mother liquor. The separated crystals were then placed in methanol for storage, as no particle size measurement was available at the site where sampling took place. An attempt was made to follow the concentration profile during the crystallisations but due to difficulties encountered in coordinating sampling, no useful data was obtained. Time and operational limitations meant that this study was unable to be repeated.

To examine the effect of supersaturation on the nucleation process, the particle size of the crystals collected from the crystallisations was measured. The size of crystals was determined using a Coulter LS1000 with a methanol filled hazardous fluid module. The Coulter LS1000 was used instead of the Malvern MasterSizer 2000, used in earlier chapters, because the methanol filled hazardous fluid module permitted only limited pre-treatment of the crystals. The results of the particle size measurements made for the three supersaturations can be seen in Figure 6-10.



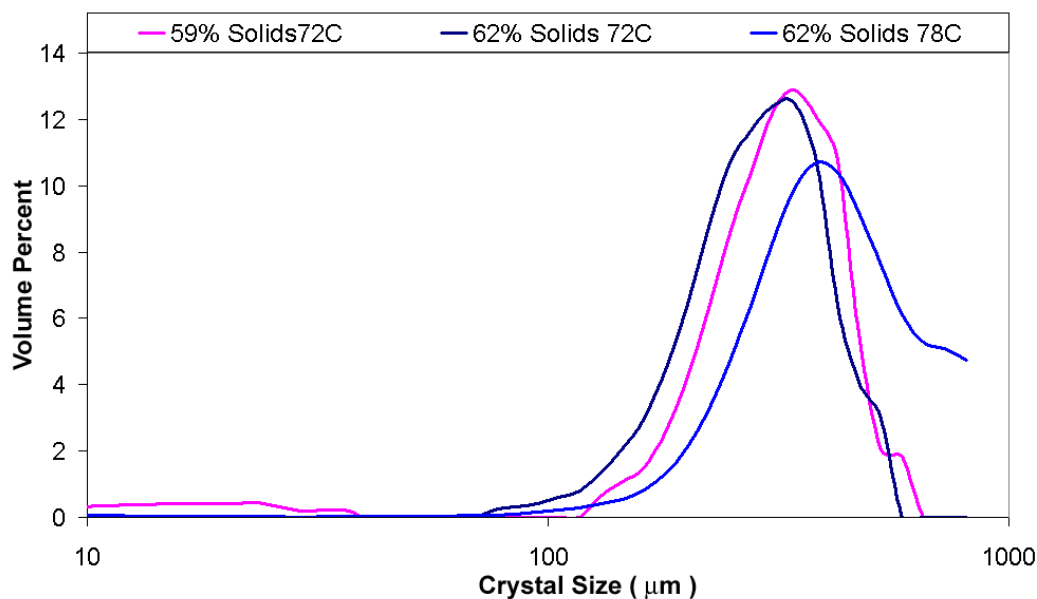


**Figure 6-10 Crystal particle size distributions of lactose crystallised at different supersaturations**

Figure 6-10 shows a definite change in the resulting particle size with changing conditions. Examining the size distributions collected for crystallisations two and three, as they represent the same lactose concentration, it can be seen that the permeate concentrate that entered at the higher temperature had a larger final crystal size. This is concluded to be a result of the lower supersaturation at nucleation, which resulted in less nucleation occurring. The reduced number of crystals allowed for more growth of individual crystals. To provide further detail on the difference in final crystal size, photos of the crystals were also taken under a microscope. These images are presented as Figure 6-11 to Figure 6-13 below.

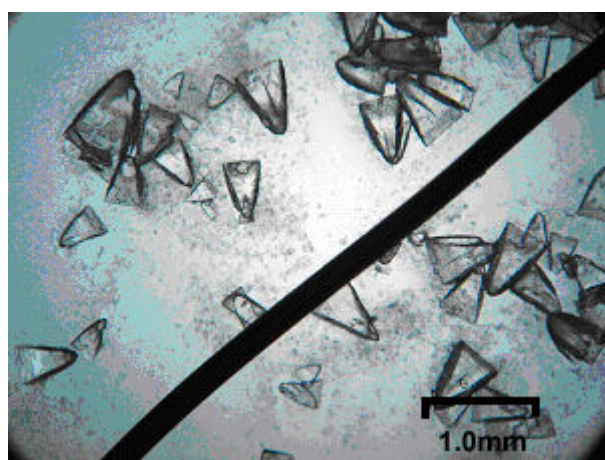


**Figure 6-11 Final crystals produced where initial conditions were 59 per cent solids and 72 °C**

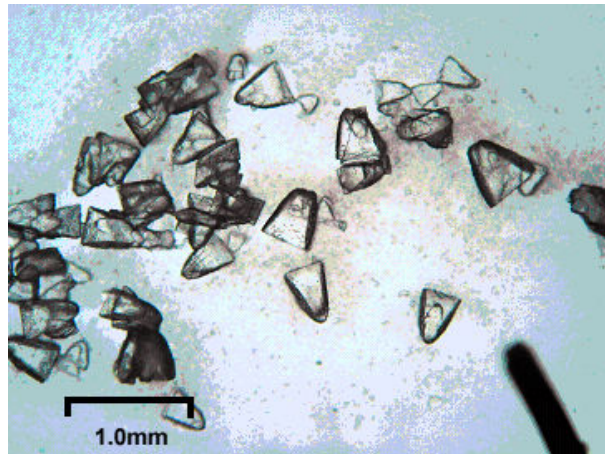


**Figure 6-12** Final crystals produced where initial conditions were 62 per cent solids and 72 °C

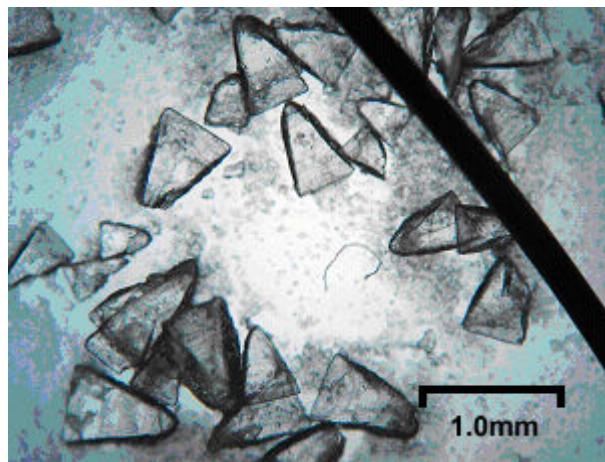


**Figure 6-13** Final crystals produced where initial conditions were 62 per cent solids and 78 °C

As was seen in the particle size distributions, the photos for the two crystallisations that were initiated at 62 per cent solids show a difference in crystal size. With crystallisation started at the higher temperature and corresponding decreased initial supersaturation producing larger crystals. To further examine this, the results were viewed with regard to the laboratory results; this is discussed in the following section.

#### **6.4.2 Relating industrial results to theory**

The feed concentrations of the industrial crystallisations were compared alongside the results collected in the laboratory experiments. It was shown in chapter four that when nucleation is viewed from the perspective of absolute  $\alpha$ -lactose supersaturation temperature has little effect on the nucleation rate. To compare the industrial results against the laboratory results the values for the industrial feed conditions were converted into absolute alpha lactose supersaturation. This calculation assumed that

lactose represents eighty per cent of the dissolved solids in the solution. In measurements made in earlier chapters, this was observed to be typical. The absolute alpha lactose supersaturation values were then converted into their equivalent relative supersaturations at 40 °C. To show where on the nucleation curve the industrial supersaturations studied sit, the equivalent relative supersaturations are plotted over the top of the laboratory-generated curves in Figure 6-14.

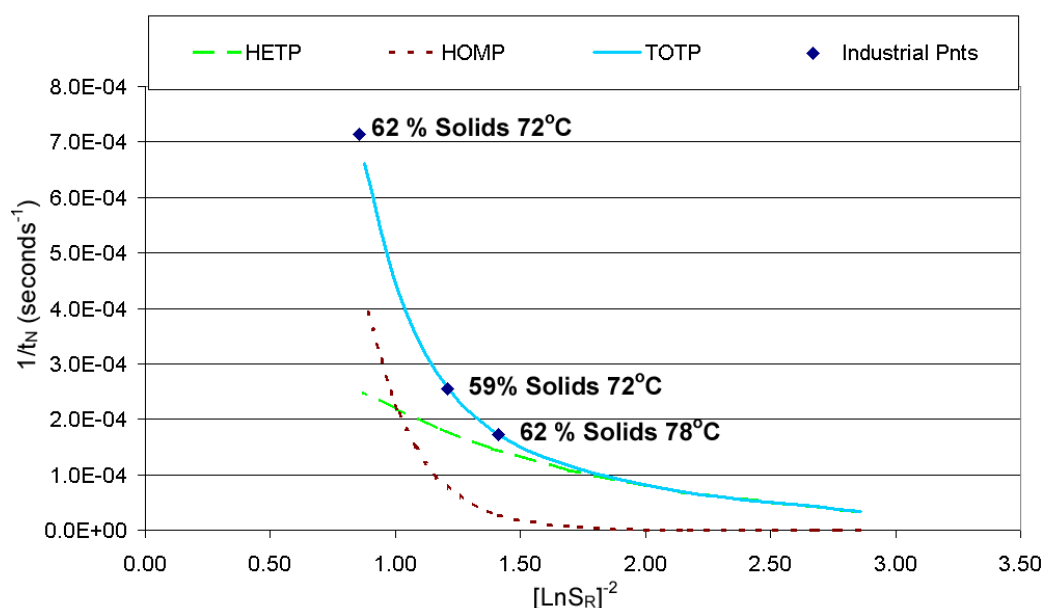


**Figure 6-14 Position of industrial feed in relation to nucleation curves generated using laboratory results for industrial permeate (Points based on prediction of  $t_N^{-1}$  using an equivalent relative supersaturation determined from absolute supersaturation)**

Figure 6-14 shows that in all cases the concentration of the feed solution is such that homogeneous nucleation appears as a significant nucleation mechanism. The position of the points on the nucleation curve reflect the results gained in the particle size measurements, with the largest crystals being generated with smallest feed supersaturation and the smallest crystals being generated by the largest feed supersaturation.

#### 6.4.2.1 Use of nucleation equation to predict final crystal size

The applicability of the nucleation equation to the industrial situation was determined by using it to predict the number of crystals per cubic metre of solution produced during the crystallisation. To do this a number of simplifications were made to the model. The first simplification was to consider nucleation to be a function of only one mechanism. This eliminated the need to find the parameters for both the homogeneous

and heterogeneous equations. This simplified form of the nucleation equation is shown as Equation 6-9. The fully expanded version along with the theory is presented in chapter four. The second assumption was that nucleation occurred a single event. Using this assumption nucleation was defined as the total number of crystals formed, instead of as a rate.

$$NJ_T = A \exp \frac{B}{[\ln S_R]^2}$$

**Equation 6-9 Simplified nucleation equation used for examining industrial results**

In Equation 6-9 there are two unknown variables  $A$  and  $B$ . The work done in chapter four found that the value of  $A$  is dependent on the mechanical properties of the system, such as mixing. The value of  $B$  was shown to be dependent on the impurities in the solution and was largely independent of the mechanical properties. Given these observations it was deemed appropriate that the value of  $B$  should be defined from the laboratory results in permeate concentrate and the value of  $A$  could be determined for the system. In doing this, it was assumed that chemical make up of the permeate concentrates were similar to those used for the laboratory work.

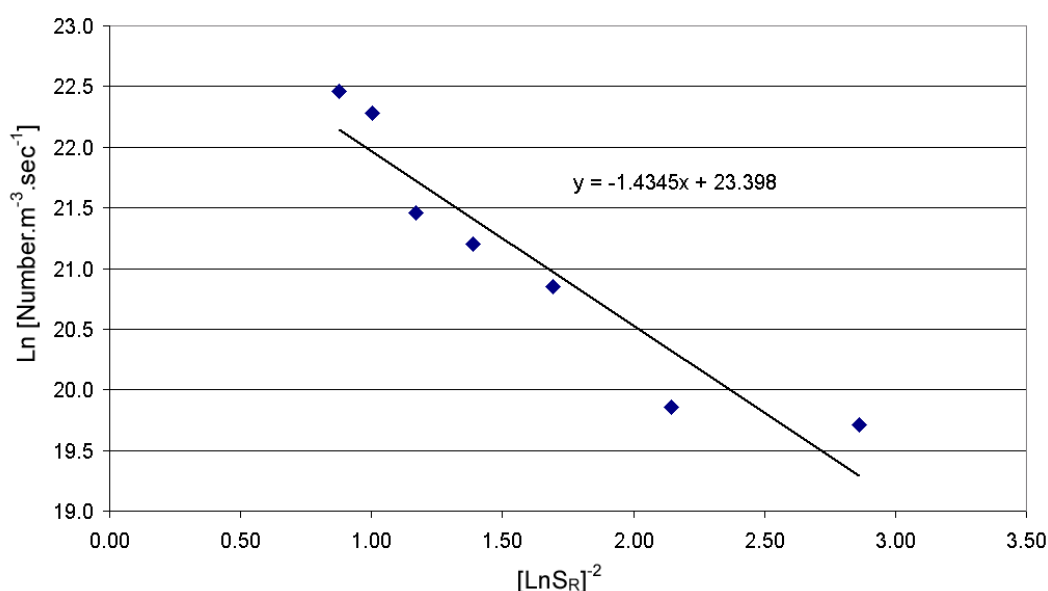


**Figure 6-15 The laboratory permeate nucleation from results Figure 4-23 viewed as single nucleation mechanism**

To determine  $B$  a plot of the laboratory results was drawn using the natural log of the nucleation rate (defined as number of crystals per cubic metre per second) versus the

natural log of the relative supersaturation to the power of negative two was drawn, shown as Figure 6-15. The value of  $B$  found from slope of this graph was determined to be  $-1.4325$ .

As the value of  $A$  was dependent on the system in which nucleation was occurring it was determined for the industrial system. To do this the information available for the crystallisation at 62 per cent solids and 72 °C was used to define the value for  $A$ . The total mass of lactose crystallised at the end of the crystallisation was converted to a volume. The particle size distributions in Figure 6-10 were used to define the percentage of the total volume that each size fraction made up. The number of crystals was then determined by dividing the volume attributable to each size fraction by the volume of a single lactose crystal at the particular crystal. The sum of all the crystals was then calculated and set as the total number of nuclei formed ( $NJ_T$ ). Once the value of  $NJ_T$  had been determined the only unknown variable was  $A$ , and thus  $A$  was calculated by rearranging Equation 6-9. The natural log of  $A$  was found to be 26.077.

Using the  $A$  value calculated for the system the total number of nuclei formed under the crystallisation conditions of 59 per cent solids 72 °C and 62 per cent solids 78 °C were calculated. The calculations used to determine these values are found in appendix A5. Included in Table 6-1 are the values of  $A$  for each crystallisation calculated using the method described for crystallisation of 62 per cent solids 72 °C.

Crystallisation	Measured nucleation event (#.m <sup>3</sup> )	Calculated nucleation event (#.m <sup>3</sup> )	Calculated value of ln A
62 % Solids 72 °C	$6.199 \times 10^{10}$	n/a	26.08
59 % Solids 72 °C	$2.988 \times 10^{10}$	$3.007 \times 10^{10}$	26.26
62 % Solids 78 °C	$2.408 \times 10^{10}$	$2.741 \times 10^{10}$	25.95

**Table 6-1 Measured and calculated results for industrial crystallisations**

The results in Table 6-1 show Equation 6-9 can be used to provide a reasonable determination of the effect changing the supersaturation will have on the nucleation. This demonstrates that the theoretical equation fits with the industrial results. This

determination is based on a number of assumptions and a more detailed study of the industrial nucleation process is required to improve on the understanding developed in the laboratory.

### **6.4.3 The effect of surface area**

The surface area available for crystal growth is important when determining the cooling rate that can be used without creating conditions whereby additional nucleation events will occur. To investigate this, the model was used to examine how the size of the initial nucleation event impacted on the concentration profile. For comparison with an industrial crystallisation, eight measurements of concentration were made during the cooling of an industrial crystalliser. The nucleation event in the crystalliser monitored was targeted to occur during the filling and initial cooling stages. The temperature profile of this crystalliser was collected and was used as the cooling profile on which all simulations in this section were based. The initial conditions of this crystalliser were measured to be 62 per cent solids and 75.2 °C. This equates to an absolute  $\alpha$ -lactose supersaturation of 17.06 g per 100 g water.

In the simulation of the process, the nucleation event was set to have occurred during the filling stage and from this a mass and number of crystals was generated. This filling process occurs over a period of 150 minutes. To simulate the nucleation in the industrial environment Equation 6-9 was used to predict the size of the nucleation event. The value of  $A$  used was the average of the calculated values in Table 6-1, the  $B$  value was that determined from Figure 6-15. As filling occurs over 150 minutes, the size of nuclei at the start of cooling will vary, depending on the time during the filling process they were formed. To simulate the initial particle size distribution the nucleation event was divided up into ten sub events, where nuclei formed and then grew for the time remaining in the filling process. The rate of nucleation was assumed be constant throughout the filling process.

The size of the initial nuclei was determined using the equation given by Kashchiev, (2000) presented here as Equation 6-10. The value determined from Equation 6-10 is the number of lactose molecules required to form a stable nucleus at a defined supersaturation. To convert this into a nucleus volume the dimensions for a lactose

molecule given in section 2.2.1 ( $a = 0.7982$  nm,  $b = 2.1562$  nm and  $c = 0.4824$  nm) were used.

$$n^* = \frac{32\pi V_m^2 \sigma^3}{3(kT_K)^3 \ln^3 S_R}$$

**Equation 6-10 Equation for the number of lactose molecules required to form a stable nuclei**

To investigate the effect of the size of the nucleation event on the concentration profile, simulations were run at the fill temperatures of 75.2 °C (the measured value), 65.2 °C and 85.2 °C ( $\pm 10^\circ\text{C}$  from the measured conditions). The values used and final median crystal size predicted can be seen in Table 6-2. The final particle size distribution produced from the industrial crystallisation was measured and using the method discussed in section 6.4.2 was used to calculate the total number of crystals produced; this is also shown in Table 6-2.

Temperature	Absolute $\alpha$ -lactose supersaturation	SS <sub>R</sub> @ 40 °C	Total nuclei	Total initial mass crystals	Final median size
(°C)	(g/ 100 g water)	Ca/Cas	(#·m <sup>-3</sup> )	(kg/kg water)	(µm)
75.2	17.06	2.61	4.286×10 <sup>10</sup> (3.652×10 <sup>10</sup> )	0.0868	223.9 (276.7)
65.2	25.79	3.36	7.654×10 <sup>10</sup>	0. 6727	145.4
85.2	7.83	1.66	7.833×10 <sup>8</sup>	6.001×10 <sup>-5</sup>	586.1

**Table 6-2 Conditions used to generate concentration profiles and the mean final particle size  
(Brackets are experimentally determined values)**

Using the input values in Table 6-2, the model was run using the preset cooling profile and the concentration profiles for the varying sized nucleation events. The results from the different simulations are presented in Figure 6-16.

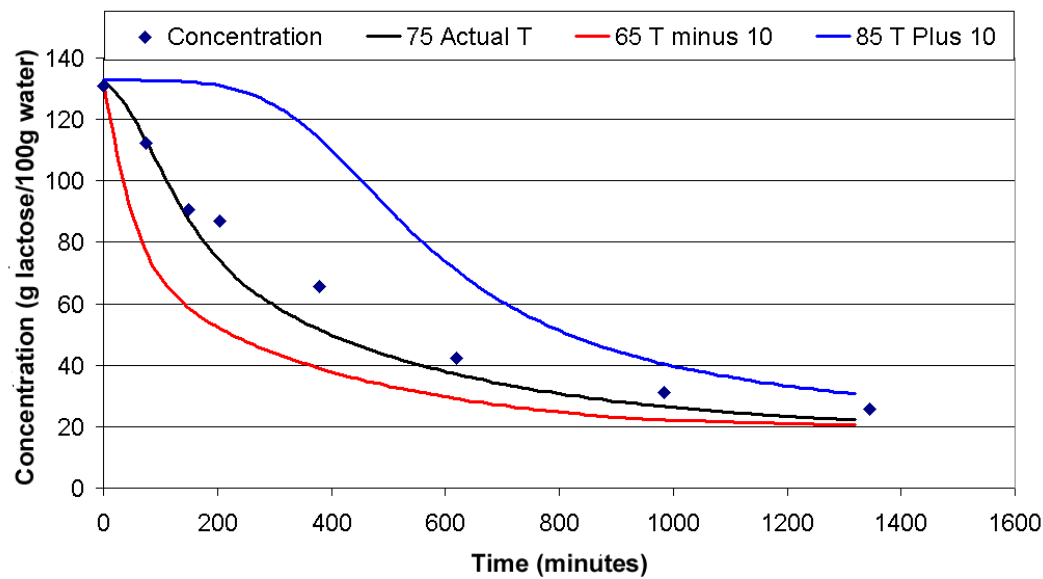


**Figure 6-16 Dissolved lactose concentration profile for different initial nucleation events**

The simulated crystallisation profile at the actual conditions corresponds well to the measured results. This suggests that the assumption of the majority of nucleation occurring during filling is a reasonable one. It also shows that where this is the case Equation 6-9 gives a good estimate of the nucleation that can be expected. The results in Figure 6-16 also demonstrate the importance the number of crystals in the solution has in determining the rate of lactose removal from the solution. With an increase in the size of the nucleation event, lactose removal through growth is enhanced; the opposite is also true. Where the desire is to achieve equilibrium quickly, it is evident from Figure 6-16 that the best approach is to maximise the number of crystals in the solution. In doing this the desired final product must also be considered as the size of the nucleation event also has an impact on the final particle size, as is shown in Figure 6-17.



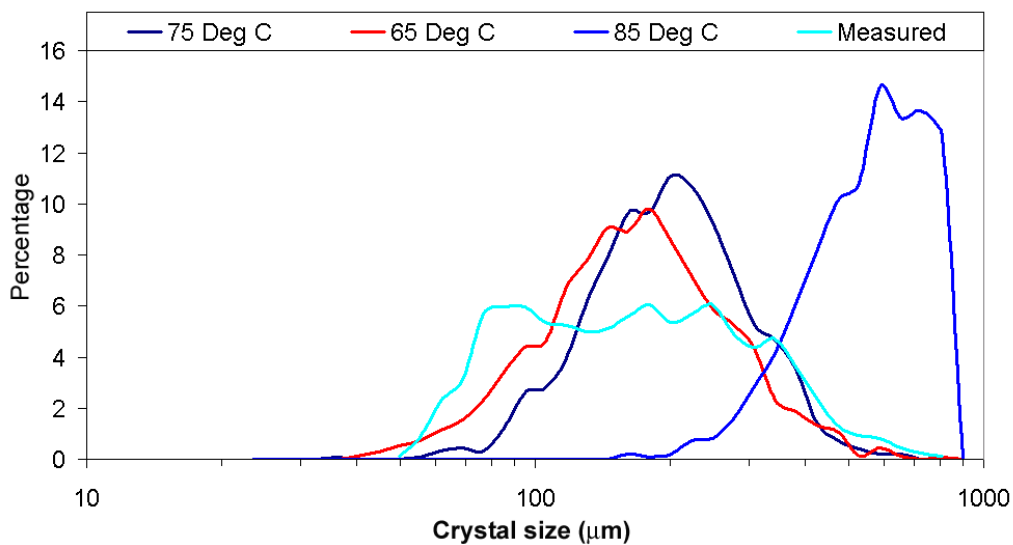


**Figure 6-17 Particle size distributions for simulated nucleation events**

The results in Table 6-2 and Figure 6-17 show that by changing the temperature of the feed solution, whilst maintaining a constant feed concentration, the number of crystals formed can be significantly altered. The number of crystals formed has a big effect on the final particle size. This is to be expected, as the mass of lactose available becomes distributed amongst different numbers of crystals. Also of interest is how the number of crystals impacts the supersaturation profile when the cooling rate is fixed. To look at this the total absolute supersaturation of the bulk solution in each of the simulations has been plotted in Figure 6-18.

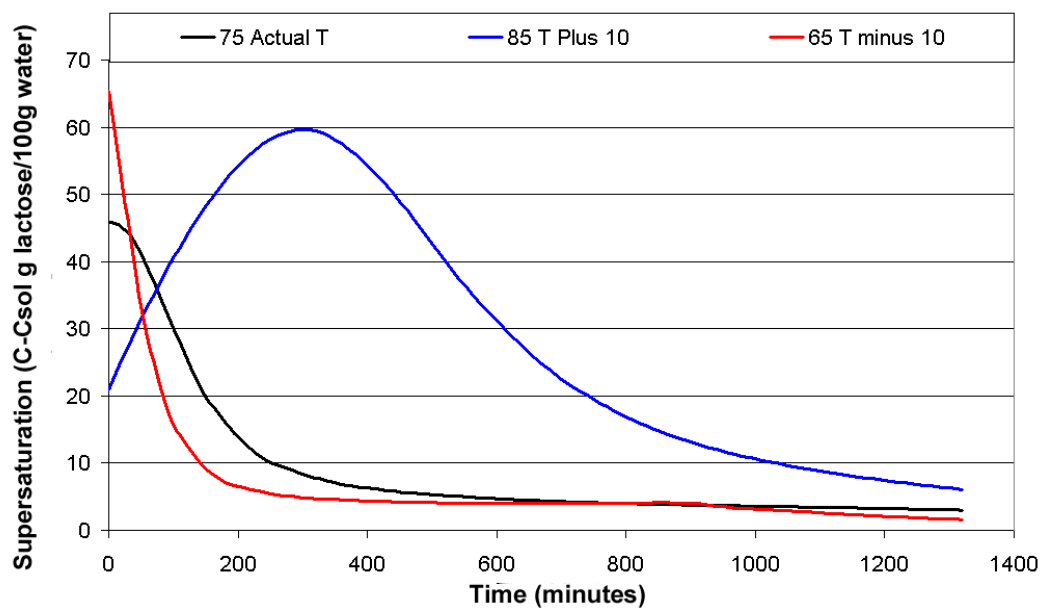


**Figure 6-18 Total anhydrous lactose supersaturation profiles of the bulk solution for different initial nucleation events**

The results in Figure 6-18 demonstrate again that more crystals lead to faster removal of lactose from solution. The consequences of this on supersaturation, where a fixed temperature profile is used to cool the crystalliser, are evident with insufficient surface area leading to an increase in supersaturation. The large increase in supersaturation seen for the profile obtained where the fill temperature was 85 °C moves the system into the range where an additional nucleation event would be expected. Where this occurs the particle size distribution shown for 85 °C in Figure 6-17 will change as more crystals are formed, because these crystals form later in the process the time and lactose available for them to grow is limited. A detailed study of the nucleation process in the industrial environment is required to characterise the conditions and rate at which this subsequent nucleation event will occur.

## 6.5 Conclusion

This chapter has looked at optimising the design of industrial crystallisers. Using an approach equivalent to an infinite amount of heat transfer surface area available it was shown that it was possible to reduce the cooling time of an industrial crystalliser from 65 hours to 19 hours without the possibility of inducing a secondary nucleation event. Because infinite heat transfer is impractical, a heat transfer component was built into the model. Using the same set of initial conditions and applying the heat transfer model to a 30,000-litre crystalliser, three different cooling scenarios were looked at. In these scenarios, the difference between using a temperature based driving force was compared with a concentration based driving force. It was shown that, due to the exponential relationship between lactose solubility and temperature, there is the risk, when temperature difference between the cooling water and the bulk solution is used to control cooling, for the system to become excessively supersaturated.

How the size of the initial nucleation event impacts the supersaturation profile during cooling was investigated. A fixed temperature profile similar to that used in industry was applied to the model and three different nucleation events were considered. It was shown that a larger initial nucleation event provides more surface area for growth and therefore allows lactose to be removed from solution at a faster rate. This limits the potential for the system to move to conditions where excessive supersaturation will lead to further nucleation occurring. The downside of having a larger number of

crystals formed in the initial stages is that the individual growth of each crystal becomes limited. This was also shown in the results obtained from the simulation.

The way in which most of the current industrial crystallisers are operated means that the nucleation rate must be modelled to fully optimise the process. Preliminary studies have confirmed that the laboratory work carried out in chapters five and six are related to what occurs in industry. The nucleation process has however, been shown to be system specific. To improve the understanding of the nucleation process in the industrial environment more work is required and future work should be concentrated in this area.



## Chapter 7 Project Overview

### 7.1 Introduction

This work has studied lactose crystal growth and nucleation. An attempt has been made to study processes as they occur at the laboratory and the industrial scale. Through doing this, an improved understanding has been gained that has application to real world situations.

### 7.2 Conclusions

Under the heading of lactose crystal growth, the work carried out in this investigation, re-examined the results collected in previous studies. Firstly, the growth rate of alpha lactose monohydrate crystals in pure lactose water solutions was studied. The results obtained fitted well with the previously measured values. Obtaining this fit required the results to be expressed as a function of absolute alpha lactose supersaturation.

One difference with that recently reported in the literature was the effect of temperature. In this work and in the majority of historical studies when they were viewed in terms of absolute  $\alpha$ -lactose supersaturation, apart from its affect on solubility, temperature has no significantly observable effect on the rate at which lactose crystals grow. This differs from the most recently reported equation for lactose crystal growth where temperature was included as a variable. A comparison between the equation developed in this work and the equation previously reported found that at low supersaturations there was little difference between the results predicted. However, at higher supersaturations and temperatures, beyond those for which the literature equation was developed, the difference becomes significant.

Experiments have been conducted investigating the growth of  $\alpha$ -lactose monohydrate crystals in whey permeate concentrate. These experiments were performed on both the laboratory and industrial scale. The hypothesis that initiated this investigation was that “growth in permeate concentrate was considerably slower than was reported in the literature for a lactose water system”. This hypothesis was proposed in the work

by (Werner *et al.*, 2002), who found that to accurately simulate growth in an industrial crystalliser a substantial reduction in the literature growth rate was required for the prediction to follow the measured results. Experiments performed in the laboratory found, under the same conditions, the lactose crystal growth rates in permeate concentrates and in lactose-water solutions were insignificantly different. Part of the procedure for conducting these growth rate measurements tested the solubility of lactose at different temperatures. The permeate concentrate solubility measurements were found to be higher than the lactose water system.

Measurement of changing concentration and temperature profiles in industrial crystallisers was conducted in parallel with the laboratory work. Using the laboratory results to set the parameters, the model was run with the aim of simulating the measured concentration profiles. It was found that when the experimentally determined values were incorporated into the model a good prediction of the measured data was obtained. A key parameter modification was the adjustments of the solubility equation to include the experimentally determined values for whey permeate concentrates.

The primary nucleation of  $\alpha$ -lactose monohydrate from a lactose-water solution was investigated over a range of supersaturations and temperatures. Primary nucleation was shown to increase with increasing supersaturation. Using classical nucleation theory the effect of supersaturation on the homogenous and heterogeneous nucleation mechanisms was examined. A value of 20 g  $\alpha$ -lactose per 100 g water was observed to be the point at which homogenous nucleation significantly contributed to the total nucleation rate. Temperature was found to be an insignificant factor on the nucleation rate when supersaturation was considered in terms of absolute alpha lactose supersaturation. When considering this result using classical nucleation theory, the effect of temperature was found to be smaller than was detectable using the experimental method. Temperature's affect on the nucleation rate becomes more significant as the absolute supersaturation decreases. This means that under conditions where secondary nucleation is typically studied a temperature effect would be expected.

Simulated whey permeates (made in the laboratory) and industrial permeate concentrates were used to investigate the effect of impurities on the  $\alpha$ -lactose primary nucleation rate. The results showed an overall increase in overall nucleation rate when compared to water. The main factor responsible for this increase was the presence of the salts in the solutions. The salts had the effect of lowering the interfacial energy barrier to nucleation, effectively decreasing the number of molecules required to form a stable nucleus at a particular supersaturation.

When investigating nucleation in a solution agitated at different rates by a Rushton turbine, the critical nucleus size remained constant. Increasing the agitation rate increased the frequency of activated molecular collisions. It was also found that the supersaturation at which homogenous nucleation became observable was independent of the mixing rate. A strong correlation was found between the nucleation rate and the number of revolutions. This was explained using the Strouhal relationship, which relates the frequency of vortex shedding to the fluid velocity, or in the case of this work, the impellor velocity.

Passive mixing was also used to investigate the relationship between mixing and the lactose nucleation rate. A supersaturated lactose solution was passed through a Venturi. Through varying the diameter of the orifice, it was possible to examine different mixing parameters in a manner that detached them from the other parameters. The Strouhal relationship again provided an effective mechanism for describing the results. Once a critical supersaturation was achieved, the nucleation rate in the Venturi system became independent of the supersaturation. It is believed that this is a result of a number of factors in the experimental set up, which when combined, led to mixing becoming the dominant variable.

The final section of this work examined the design of industrial crystallisers. Using an approach equivalent to having an infinite amount of heat transfer surface area available it was shown that it was possible to reduce the cooling time of an industrial crystalliser from 65 hours to 19 hours without the possibility of inducing a secondary nucleation event. A heat transfer component was built into the model and three

different cooling scenarios were examined. In these scenarios, the difference between using a temperature based driving force was compared with a concentration based driving force. It was shown that, due to the exponential relationship between lactose solubility and temperature, there is a risk, when temperature difference between the cooling water and the bulk solution is used to control cooling, for the system become excessively supersaturated with a strong likelihood of a spontaneous nucleation event occurring.

### **7.3 Suggestions for future work**

For future work in this area, determination of the solubility profile should be considered a critical area. A better understanding of why the high impurity levels increased the solubility could lead to the opportunity to eliminate the effect and may lead to an increase in recoverable lactose.

The area of nucleation as it occurs in the industrial environment needs a detailed study. This work should examine nucleation as it occurs in an evaporator and in an agitated crystallisation tank. The results from this thesis have shown nucleation to be system specific. To develop the understanding to a point where by detailed control over an industrial crystallisation can be achieved a comprehensive understanding of nucleation, as it occurs in the industrial environment, is required.



## Chapter 8 References

- Abrahamson, J (2007). Personal Communication
- Achilles, W. (1997). In vitro crystallisation systems for the study of urinary stone formation. World Journal of Urology, (244-251).
- Ahlborn, B., Seto, M. L., & Noack, B. R. (2002). On drag, Strouhal number and vortex-street structure. Fluid Dynamics Research, 30, 379-399.
- Amos, R. M., Rarity, J. G., Tapster, P. R., & Shepherd, T. J. (2000). Fabrication of large-area face-centered-cubic hard-sphere colloidal crystals by shear alignment. Physical Review E, 61(3), 2929-2935.
- Arellano, M. P. , Aguilera, J. M., & Bouchon, P. (2004). Development of a digital video-microscopy technique to study lactose crystallisation kinetics in situ. Carbohydrate Research, 339, 2721-2730.
- Armenante, P. M., & Nagamine, E. U. (1998). Effect of low off-bottom impeller clearance on the minimum agitation speed for complete suspension of solids in stirred tanks. Chemical Engineering Science, 53(9), 1757-1775.
- Asano, Y., Aoki, Y., & Yamazaki, N. (Inventors). (1978). Meiji Milk Products Company (Assignee). Method of Producing Beta-Lactose. (United States 4,083,733).
- Assirelli, M., Bujalski, W., Eaglesham, A., & Nienow, A. W. (2002). Study of micromixing in a stirred tank using a Rushton turbine. Trans IChemE , 80(A), 855-863.
- Azzurri, F., & Alfonso, G. C. (2005). Lifetime of Shear-Induced Crystal Nucleation Precursors. Macromolecules, 38, 723-1728.
- Baldyga, J., & Orciuch, W. (2001). Some Hydrodynamic Aspects of Precipitation. Powder Technology, 121, 9-19.
- Barata, P. A., & Serrano, M. A. (1996). Salting-out precipitation of potassium dihydrogen sulphate (KDP) II. Influence of agitation intensity. Journal of Crystal Growth, 163, 426-433.
- Beevers, C. A., & Hansen, H. N. (1971). The Structure of  $\alpha$ -Lactose Monohydrate. Acta Crystallographica, B27, 1323-1325.
- Bejan, A., & Kraus, A. D. (2003). Heat Transfer Handbook. U.S.A: John Wiley and Sons.
- Bennett, R. C. (1988). Matching the Crystallizer to Material. Chemical Engineering, 95(8).
- Berger, S. A., & Jou, L. D. (2000). Flows in Stenotic Vessels. Annual Review of Fluid Mechanics, 32, 347-382.

Bernardo, A., Calmanovici, C. E., & Miranda, E. A. (2004). Induction Time as an Instrument to Enhance Comprehension of Protein Crystallization. 4(4), 799-805.

Bhargava, A. (1995). Effect of Impurities on the Growth of Lactose Crystals in Model and Whey Ultrafiltration Permeate Systems. Masters Thesis, University of Alberta, Alberta.

Bhargava, A., & Jelen, P. (1996). Lactose Solubility and Crystal Growth as Affected by Mineral Impurities. Journal of Food Science, 61(1), 180-184.

Blaak, R., Auer, S., Frenkel, D., & Lowen, H. (2004). Crystal Nucleation of Colloidal Suspensions under Shear. Physical Review Letters, 93(6), 1-4.

Bluestein, D., Gutierrez, C., Londono, M., & Schoephoerster, R. T. (1999). Vortex Shedding in Steady Flow through a Model of an Arterial Stenosis and Its Relevance to Mural Platelet Deposition. Annals of Biomedical Engineering, 27(6), 763-773.

Borgnakke, C., & Sonntag, R. E. (1997). Thermodynamics and Transport Properties. U.S.A: John Wiley and Sons.

Bruns, D. L. (1959). A General theory of the Causes of Murmurs in the Cardiovascular System. American Journal of Medicine, 27, 360-374.

Butler, B. E. (1998). Modelling Industrial Lactose Crystallisation. Doctoral dissertation, Queensland University.

Charley, P., & Saltman, P. (1962). Chelation of Calcium by Lactose: Its role in Transport Mechanisms. Science, 139(3560), 1205-1206.

Chew, C. M., Ristic, R. J., Dennehy, R. D., & De Yoreo, J. J. (2004). Crystallization of Paracetamol under Oscillatory Flow Mixing Conditions. Crystal Growth and Design, 4(5), 1045-1052.

Darcy, P., & Buckton, G. (1998). Crystallization of bulk samples of partially amorphous spray-dried lactose. Pharmaceutical Development and Technology, 3(4), 503-507.

Darcy, P. A., & Wiencek, J. M. (1998). Estimating Lysozyme Crystallization Growth Rates and Solubility from Isothermal Microcalorimetry. Acta Crystallographica, D54, 1387-1394.

Darcy, P. A., & Wiencek, J. M. (1999). Identifying nucleation temperatures for lysozyme via differential scanning calorimetry. Journal of Crystal Growth, 196, 243-249.

David, R. (2001). General rules for prediction of the intensity of micromixing effects on precipitations. Powder Technology, 121, 2-8.

Deshpande, M. D., & Giddens, D. P. (1980). Turbulence Measurements in a Constricted Tube. Journal of Fluid Mechanics, 97(MAR), 65-89.

- Devarakonda, S., Evans, J. M. B., & Myerson, A. S. (2003). Impact of Ultrasound Energy on the Crystallization of Dextrose Monohydrate. Crystal Growth and Design, 3(5), 741-746.
- Dincer, T. D., Parkinson, G. M., Rohl, A. L., & Ogden, M. I. (1999). Crystallisation of  $\alpha$ -lactose monohydrate from dimethyl sulfoxide (DMSO) solutions: influence of  $\beta$ -lactose. Journal of Crystal Growth, 205, 368-374.
- Dodson, B. (1994). Weibull Analysis. Milwaukee, Wisconsin: AQSC Quality Press.
- El-Shall, H., Jeon, J., Abdel-Aal, A., Khan, S., Gower, L., & Rabinovich, Y. (2004). A study of primary nucleation of calcium oxalate monohydrate; I-Effect of supersaturation. Crystal Research Technology, 39(3), 214-221.
- Engeskaug, R., Thorbjornsem, E., & Sven, H. F. (2005). Wall Heat Transfer in Stirred Reactors. Industrial Engineering Chemical Research, 44, 4949-4958.
- Farhadi, F., & Babaheidary, M. B. (2002). Mechanism and estimation of  $\text{Al}(\text{OH})_3$  crystal growth. Journal of Crystal Growth, 234, 721-730.
- Fayle, S. E. (1998). Protein crosslinking. Doctoral dissertation, Canterbury University, New Zealand.
- Fayle, S. E., & Gerrard, J. A. (2002). The Maillard Reaction (RSC Food Analysis Monographs). Cambridge: The Royal Society of Chemistry.
- Fleming, R. A. (2001). The Weibull model and an ecological application: describing the dynamics of foliage biomass on Scots pine. Ecological Modelling, 138, 301-319.
- Fox, P. F. (1997). Advanced Dairy Chemistry Volume Three; Lactose, Water, Salts, and Vitamins (Second ed.). London: Chapman and Hall.
- Galletti, C., Paglianti, A., Lee, K. C., & Yianneskis, M. (2004). Reynolds Number and Impeller Diameter Effects on Instabilities in Stirred Vessels. AIChE Journal, 50(9), 2050-2063.
- Garnier, S., Petit, S., & Coquerel, G. (2002). Influence of supersaturation and structurally related additives on the crystal growth of alpha-lactose monohydrate. Journal of Crystal Growth, 234, 207-219.
- Garside, J. (1983). Industrial crystallisation a confluence of science and technology. Chemistry and Industry, July, 509-515.
- Garside, J., Mersmann, A., & Nyvlt, J. (2002). Measurement of Crystal Growth and Nucleation Rates (Second ed.). Rugby: IChemE.
- Girolami, M. W., & Rousseau, R. W. (1985). Size-Dependent Crystal Growth - A Manifestation of Growth Rate Dispersion in the Potassium Alum-Water System. AIChE Journal, 31(11), 1821-1828.
- Gogate, P. R., & Pandit, A. B. (2000). Engineering Design Methods for Cavitation Reactors II: Hydrodynamic Cavitation. AIChE Journal, 46(8), 1641-1649.

Gogate, P. R., & Pandit, A. B. (2001). Hydrodynamic Cavitation Reactors: a State of the Art Review. Reviews in Chemical Engineering, 17(1), 1-85.

Granger, R. A. (1995). Fluid Mechanics (Dover ed.). U.S.A: Dover Publications.

Griffiths, R. C., Paramo, G., & Merson, R. L. (1982). Preliminary investigation of lactose crystallisation using the population balance technique. AIChE Symposium, Ser. 218(18), 118.

Guo, Z., Jones, A. G., & Li, N. (2006). The effect of ultrasound on the homogeneous nucleation of BaSO<sub>4</sub> during reactive crystallization. Chemical Engineering Science, 61, 1617-1626.

Guu, Y. K., & Zall, R. R. (1992). Nanofiltration Concentration Effect on the Efficiency of Lactose Crystallization. Journal of Food Science, 57(3), 735-739.

Guzman, L. A., Kubota, N., Yokota, M., & Ando, K. (2001). Growth Hysteresis of a Potassium Sulphate Crystal in the presence of Chromium(III) Impurity. Crystal Growth and Design, 1(3), 225-229.

Haase, G., & Nickerson, T. A. (1966a). Kinetic Reactions of Alpha and Beta Lactose. I. Mutarotation. Journal of Dairy Science, 49(2), 757-61.

Haase, G., & Nickerson, T. A. (1966b). Kinetic Reactions of Alpha and Beta Lactose. II. Crystallization. Journal of Dairy Science, 49(7), 757-61.

Hagenson, L. C., & Doraiswamy, L. K. (1998). Comparison of the effect of ultrasound and mechanical agitation on a reacting solid-liquid system. Chemical Engineering Science, 53(1), 131-148.

Harper, W. J. (1992). Lactose and Lactose Derivatives. J. G. Zadow (Editor), Whey and Lactose Processing (pp. 317-360). Essex: Elsevier Science Publishers.

Hartel, R. W., & Shastry, A. V. (1991). Sugar Crystallization in Food Products. Critical Reviews in Food Science and Nutrition, 1(1), 49-112.

Haysmith, W., Landsford, J., & McKenzie, B. (2002). Pride of the Lion Waipu: The People and the Place 1939-2000. Wellington : Bookprint International.

Herrington, B. L. (1934a). Some Physio-Chemical Properties of Lactose I. The spontaneous crystallisation of supersaturated solutions of lactose. Journal of Dairy Science, 17, 501-518.

Herrington, B. L. (1934b). Some Physio Chemical Properties of Lactose VI. The solubility of lactose in salt solutions; the isolation of a compound of a compound of lactose and calcium chloride. Journal of Dairy Science, 17, 805-813.

Herrington, B. L. (1936). Some Physio-Chemical Properties of Cheese: IV. The Influence of Salts and Acids Upon the Mutarotation Velocity of Lactose. Journal of Dairy Science, 17(659-669).

- Hessel, V., Lowe, H., & Schonfeld, F. (2005). Micromixers-a review on passive and active mixing principles. Chemical Engineering Science, 60, 2479-2501.
- Hodges, G. E., Lowe, E. K., & Paterson, A. H. J. (1993). A mathematical model for lactose dissolution. The Chemical Engineering Journal, 53, B25-B33.
- Hu, H., Hale, T., Yang, X., & Wilson, L. J. (2001). A spectrophotometer-based method for crystallisation induction time period measurement. Journal of Crystal Growth, 232, 86-92.
- Hynynen J., Burkhart, H. E., & Lee Allen, H. (1998). Modeling tree growth in fertilized midrotation loblolly pine plantations. Forest Ecology and Management , 1007, 213-229.
- Iribarne, A., Frantisak, F., Hummel, R. L., & Smith, J. W. (1972). An Experimental Study of Instabilities and Other Flow Properties of a Laminar Pipe Jet. AIChE Journal, 18(4), 689-698.
- Itoh, T., Katoh, M., & Adachi, S. (1978). An improved method for the preparation of crystalline  $\beta$ -lactose and observations on the melting point. Journal of Dairy Research, 45, 363-371.
- Jay, F., Haudin, J. M., & Monasse, B. (1999). Shear-induced crystallization of polypropylenes: effect of molecular weight. Journal Materials Science, 34, 2089-2102.
- Jelen, P., & Coulter, S. T. (1973). Effect of Supersaturation and Temperature on the Growth of Lactose Crystals. Journal of Food Science, 38, 1182-1185.
- Jelen, P., & Coulter S.T. (1973). Effects of Certain Salts and Other Whey Substances on the Growth of Lactose Crystals. The Journal of Food Science, 38, 1186-1189.
- Johansen, F. C. (1929). Flow through Pipe Orifices at Low Reynolds Numbers. Proceeding of the Royal Society of London. A, 126(801), 231-245.
- Kashchiev, D. (2000). Nucleation Basic Theory with Applications. Great Britain: Butterworth Heinemann.
- Kashchiev, D., & van Rosmalen, G. M. (2003). Review: Nucleation in Solutions Revisited. Crystal Research Technology, 38(7-8), 555-574.
- Kauter, M. D. (2003). The Effects of Impurities on Lactose Crystallization. Doctoral dissertation, The University of Queensland.
- Kauter, M. D., Lister, J. D., & White, E. T. (2003). Secondary nucleation kinetics of alpha lactose monohydrate using laser light scattering. AIChE Conference 2003 .
- Kendrew, J. C. , & Moelwyn-Hughes, E. A. (1940). The Kinetics of Mutarotation in Solution. Proceeding of the Royal Society of London. Series A, 176(966), 352-367.

- Kim, S., & Myerson, A. S. (1996). Metastable Solution Thermodynamic Properties and Crystal Growth Kinetics. Industrial Engineering Chemical Research, 35, 1078-1084.
- Knowe, S. A., Ahrens, G. R., & DeBell, D. S. (1997). Comparison of diameter-distribution,-prediction, stand-table-projection, and individual-tree-growth modeling approaches for young red alder plantations. Forest Ecology and Management, 98, 46-60.
- Kresta, S. (1998). Turbulence in Stirred Tanks: Anisotropic, Approximate, and Applied. The Canadian Journal of Chemical Engineering, 76, 563-576.
- Kubota, N., Yokota, M., Doki, N., Sasaki, S., & Mullin, J. W. (2002). Theoretical Considerations on Growth Rate Hysteresis of Crystals in the Presence of Impurities. International Symposium of Industrial Crystallization .
- Kumar, P. S., Kumar, M. S., & Pandit, A. B. (2000). Experimental Quantification of Chemical Effects of Hydrodynamic Cavitation. Chemical Engineering Science, 55(9), 1633-1639.
- Kurimoto, M., Subramony, P., Gurney, R. W., Lovell, S., Chmielewski, J., & Kahr, B. (1999). Kinetic Stabilization of Biopolymers in Single-Crystal Hosts: Green Fluorescent Protein in  $\alpha$ -Lactose Monohydrate. Journal of the American Chemical Society, 121, 6952-6953.
- Lacmann, R., Herden, A., & Mayer, C. (1999). Kinetics of Nucleation and Crystal Growth. Chemical Engineering Technology, 22(4), 279-289.
- Lawless, J. F. (2003). Statistical Models and Methods for Lifetime Data (Second Edition ed.). U.S.A: Wiley-Interscience.
- Lee, K. C., & Yianneskis, M. (1998). Turbulence Properties of the Impellor Stream of a Rushton Turbine. AIChE Journal, 44(1), 13-24.
- Lee, T. S., Liao, W., & Low, H. T. (2004). Numerical study of physiological turbulent flows through series arterial stenoses. International Journal for Numerical Studies in Fluids, 46, 315-344.
- Loffelmann, M., & Mersmann, A. (2002). How to measure supersaturation? Chemical Engineering Science, 57, 4301-4310.
- Lowe, E. K., & Paterson, A. H. J. (1998). A mathematical model for lactose dissolution, part II. Dissolution below the Alpha Lactose Solubility Limit. Journal of Food Engineering, 38, 15-25.
- Lu, P. C., Hui, C. N., & Hwang, N. H. C. (1983). A Model Investigation of the Velocity and Pressure Spectra in Vascular Murmurs. Journal of Biomechanics, 16(11), 923-931.
- Lyczko, N., Espitalier, F., Louisnard, O., & Schwartzentruber, J. (2002). Effect of Ultrasound on the induction time and the metastable zone widths of potassium sulphate. Chemical Engineering Journal, 86, 233-241.

- Ma, D. L., Tafti, D. K., & Braatz, R. D. (2002). Optimal control and simulation of multidimensional crystallization process. Computers and Chemical Engineering, *26*, 1103-1116.
- Macosko, C. W. (1994). Rheology Principles, Measurements, and Applications. U.S.A: VCH Publishers.
- Majd, F., & Nickerson, T. A. (1976). Effect of Alcohols on Lactose Solubility. Journal of Dairy Science, *59*(6), 1025-1032.
- Mandare, P. N., & Pangarkar, V. G. (2003). Semi-Batch reactive crystallization of sodium perborate tetrahydrate: effect of mixing parameters on crystal size. Chemical Engineering Science, *58*, 1125-1133.
- Mathieu, J., & Scott, J. (2000). An Introduction to Turbulent Flow. U.S.A: Cambridge University Press.
- McLauchlan, G. (1996). The Northland Co-operative Dairy Industry - A History. Auckland: Four Star Books.
- Mersmann, A., Braun, B., & Löffelmann, M. (2002). Prediction of crystallisation coefficients of the population balance. Chemical Engineering Science, *57*, 4267-4275.
- Metzner, A. B., & Taylor, J. S. (1960). Flow patterns in Agitated Vessels. AIChE Journal, *6*(1), 109-114.
- Mikkonen, H., Helakorpi, P., Myllykoski, L., & Keiski, R. L. (2001). Effect of Nanofiltration on lactose crystallisation. Milchwissenschaft, *56*(6), 307-310.
- Miracco, J. L., Alzamora, S. M., Chirife, J., & Ferro Fontan, C. (1981). On the Water Activity of Lactose Solutions. Journal of Food Science, *46*, 1612-1613.
- Mitrovic, M. M., Zekic, A. A., & Petrusevski, Lj. S. (1999). Growth rate dispersion of small crystals. Journal of Crystal Growth, *198/199*, 687-691.
- Modler, H. W., & Lefkovitch, L. P. (1986). Influence of pH, Casein, and Whey Protein on the Composition, Crystal Size, and Yield of Lactose from Condensed Whey. Journal of Dairy Science, *69*, 684-697.
- Mohameed, H. A., Abu-Jdayil, B., & Al Kateeb, M. (2002). Crystallization Kinetics of KCl at Different Cooling Rates. International Symposium of Industrial Crystallization.
- Mohan, P., Emery, A. N., & Al-Hassan, T. (1992). Review: Heat Transfer to Newtonian Fluids in Mechanically Agitated Vessels. Experimental Fluid and Thermal Science, *5*, 961-883.
- Mohan, R., Boateng, K. A., & Myerson, A. S. (2000). Estimation of crystal growth kinetics using differential scanning calorimetry. Journal of Crystal Growth, *212*, 489-499.

- Mohan, R., & Myerson, A. S. (2002). Growth kinetics: a thermodynamic approach. Chemical Engineering Science, *57*, 4277-4285.
- Muhr, H., Leclerc, J.-P., & Plasari, E. (1997). A Rapid Method for the Determination of Growth Rate Kinetic Constants: Application to the Precipitation of Aluminum Trihydroxide. Industrial Engineering Chemical Research, *36*, 675-681.
- Mullin, J. W. (2001). Crystallization (4th ed.). Great Britain: Butterworth Heinemann.
- Mydlarz, J., & Jones, A. G. (1991). Crystallization and agglomeration kinetics during the batch drowning-out precipitation of potash alum with aqueous acetone. Powder Technology, *65*, 187-194.
- Myerson, A. S. (2002). Handbook of Industrial Crystallisation (Second ed.). United States of America: Butterworth Heinemann.
- Myerson, A. S., & Jang, S. M. (1995). A comparison of binding energy and metastable zone width for adipic acid. Journal of Crystal Growth, *156*, 459-466.
- Nakayama, Y. (1988). Visualized Flow: Fluid motion in basic and engineering situations revealed by flow visualization. Oxford: Pergamon Press.
- Nickerson, T. A., & Moore, E. E. (1974). Factors Influencing Lactose Crystallization. Journal of Dairy Science, *57*(11), 1315-1319.
- Olano, A. (1979). Solubility of Lactose and Lactulose in Alcohols. Journal of Food Science and Technology, *16*, 260-261.
- Olano, A., Corzo, N., & Martinez-Castro, I. (1983). Studies on  $\beta$ -Lactose Crystallization. Milchwissenschaft, *38*(8), 471-474.
- Palberg, T., Monch, W., Schwarz, J., & Leiderer, P. (1995). Grain size control in polycrystalline colloidal solids. Journal of Chemical Physics, *102*(12), 5082-5087.
- Pankanin, G. L. (2005). The Vortex Flowmeter: Various Methods of Investigating Phenomena. Measurement Science and Technology, *16*(3), R1-R16.
- Parsons, A. R., Black, S. N., & Colling, R. (2003). Automated Measurement of Metastable Zones for Pharmaceutical Measurement. Trans IChemE, *81A*(July), 700-704.
- Patel, K. N., & Nickerson, T. A. (1970). Influence of Sucrose on the Mutarotation Velocity of Lactose. Journal of Dairy Science, *53*(12), 1654-1658.
- Patrick, M., Blintt, R., & Janssen, J. (2004). The effect of ultrasonic intensity on the crystal structure of palm oil. Ultrasonics Sonochemistry, *11*, 251-255.
- Paul, E. L., Atiemo-Obeng, V. A., & Kresta, S. M. (2004). Handbook of Industrial Mixing. USA: John Wiley & Sons.
- Pearsall, I. S. (1972). Cavitation. London: Mills & Boon.



Pratola, E., Simons, S. J. R., & Jones A.G. (2002). A Novel Experimental Device of Measurement of Agglomerative Crystallization Forces. Trans IChemE, 80(Part A), 441-448.

Qian, R.-Y., & Botsaris, G. D. (1998). Nuclei breeding from a chiral crystal seed of  $\text{NaClO}_3$ . Chemical Engineering Science, 553(9), 1745-1756.

Raghavan, S. L., Ristic, R. I., Sheen, D. B., & Sherwood, J. N. (2002). Dissolution Kinetics of Single Crystals of  $\alpha$ -Lactose Monohydrate. Journal of Pharmaceutical Sciences, 91(10), 2166-2174.

Raghavan, S. L., Ristic, R. I., & Sherwood, J. N. (2001). The Bulk Crystallization of  $\alpha$ -Lactose Monohydrate from Aqueous Solution. Journal of Pharmaceutical Sciences, 90(7), 823-832.

Raghavan, S. L., Ristic, R. L., Sheen, D. B., Sherwood, J. N., Trowbridge, L., & York, P. (2000). Morphology of  $\alpha$ -lactose hydrate grown from aqueous solution. Journal of Physical Chemistry B, 104, 12256-12262.

Ratoarinoro, N., Contamine, F., Wilhelm, A. M., Berlan, J., & Delmas, H. (1995). Activation of a solid-liquid chemical reaction by ultrasound. Chemical Engineering Science, 50(3), 554-558.

Revstedt, J., & Fuchs, L. (2002). Large Eddy Simulation of Flow in Stirred Vessels. Chemical Engineering & Technology, 25(4), 443-446.

Rielly, C. D., & Marquis, A. J. (2001). A particles eye view of crystalliser fluid mechanics. Chemical Engineering Science, 56(7), 2475-2493.

Roelfsema, W. A., Kuster, B. F. M., Heslinga, M. C., Pluim, H., & Verhage, M. (2002). Lactose and derivatives - Lactose. Ullmann's Encyclopedia of Industrial Chemistry (6th ed., ). Weinheim, Germany : John Wiley & Sons.

Roetman, K. (1972). Crystallisation of Lactose. Voedings Middelen Technologie, 3(43), 230-239.

Roetman, K., & Buma, T. J. (1974). Temperature dependence of the equilibrium  $\beta/\alpha$  ratio of lactose in aqueous solution. Netherlands Milk and Dairy Journal, 28, 155-165.

Salvatori, F., Muhr, H., Plasari, E., & Bossoutrot, J. M. (2002). Determination of nucleation and crystal growth kinetics of barium carbonate. Powder Technology, 128(114-123).

Schwarzer, H. C., & Peukert, W. (2001). Tailoring Particle Size Through Nanoparticle Precipitation. Chemical Engineering Communication, 191, 580-606.

Sharp, K. V., & Adrian, R. J. (2001). PIV Study of Small Scale-Flow Structure around a Rushton Turbine. AIChE Journal, 47(4), 766-778.

- Shi, B., & Rousseau, R. W. (2001). Crystal Properties and Nucleation Kinetic from Aqueous Solutions of Na<sub>2</sub>CO<sub>3</sub> and Na<sub>2</sub>SO<sub>4</sub>. Industrial Engineering Chemical Research, 40(6), 1541-1547.
- Shi, Y., Hartel, R. W., & Liang, B. (1989). Formation and Growth Phenomena of Lactose Nuclei Under Contact Nuclei Conditions. Journal of Dairy Science, 72, 2906-2915.
- Shi, Y., Liang, B., & Hartel, R. W. (1990). Crystallization Kinetics of Alpha-Lactose Monohydrate in a Continuous Cooling Crystallizer. Journal of Food Science, 55(3), 817-820.
- Simeone, M., Palomba, M., & Volpicelli, G. (2002). Size Dependent Growth Rate of Gypsum Crystals by Video-Enhanced Optical Microscopy. International Symposium of Industrial Crystallization .
- Smart, J. B. (1988). Effect of Whey Components on the Rate of Crystallization and Solubility of  $\alpha$ -Lactose Monohydrate. New Zealand Journal of Dairy Science and Technology, 23, 275-289.
- Smart, J. B., & Smith, J. M. (1991). Effect of Selected Compounds of the Rate of  $\alpha$ -Lactose Monohydrate Crystallization, Crystal Yield and Quality. International Dairy Journal, 1, 41-53.
- Solzbach, U., Wollschlager, H., Zeiher, A., & Just, H. (1987). Effect of stenotic geometry on flow behaviour across stenotic models. Medical and Biological Engineering and Computing, 25, 543-550.
- Spink, L. K. (1967). Principles and Practice of Flow Meter Engineering (Ninth ed.). U.S.A: Plimpton Press.
- Stabat, P., & Marchio D. (2004). Simplified model for indirect-contact evaporative cooling-tower behaviour. Applied Energy, 78, 433-451.
- Stockman, R., & Weerakkody, R. K. (2000). Formation of Maillard reaction products involving whey proteins and lactose. Australian Journal of Dairy Technology, 55(2), 108 .
- Suplee, G. C. , & Flanigan, G. E. (Inventors). (1934). Process of Producing Beta Lactose. (United States 1,954,602).
- Thurlby, J. A. (1976). Crystallization Kinetics of Alpha Lactose. Journal of Food Science, 41, 38-42.
- Triboulet, P. , Cournil, M., & Crawley, G. (1992). Secondary nucleation of potassium dihydrogen phosphate, interest of a turbidimetric study. Powder Technology, 73, 195-202.
- Troy, H. C., & Sharp, P. F. (1930).  $\alpha$  and  $\beta$  Lactose in Some Milk Products. Journal of Dairy Science, 13, 140-157.

- Twieg, W. C., & Nickerson, T. A. (1968). Kinetics of Lactose Crystallization. Journal of Dairy Science, 51(11), 1720-1724.
- Ulrich, G. D. (1984). A Guide to Chemical Engineering Process Design and Economics. U.S.A: John Wiley and Sons.
- Valle-Vega, P., & Nickerson, T. A. (1977). Measurement of Lactose Crystal Growth by Image Analyzer. Journal of Food Science, 42(4), 1069-1072.
- van Krevald, A. (1969). Growth Rates of Lactose Crystals in Solutions of Stable Anhydrous  $\alpha$ -Lactose. Netherlands Milk and Dairy Journal, 23, 258-274.
- van Krevald, A., & Michaels, A. S. (1965). Measurement of Crystal Growth of  $\alpha$ -Lactose. Journal of Dairy Science, 48, 259-265.
- Visser, R. A. (1982). Supersaturation of  $\alpha$ -lactose in aqueous solutions in mutarotation equilibrium. Netherlands Milk and Dairy Journal, 36, 89-101.
- Visser, R. A. (1983). Crystal Growth Kinetics of Alpha-Lactose Hydrate. Doctoral dissertation, Rijks Universiteit, Groningen.
- Vleeshouwers, S., & Meijer, H. E. H. (1996). A rheological study of shear induced crystallization. Rheologica Acta, 35, 391-399.
- Vu, T. T. L., Durham, R. J., Hourigan, J. A., & Sleigh, R. W. (2004). The Uses of Ultrasonic Power and Solvents in Lactose Cooling Crystallisation. CHEMECA 2004 (p. 67). Sydney.
- Walker Read, A. (1999). The New International Webster's Comprehensive Dictionary of the English Language. Chicago: J.G Ferguson Publishing Company.
- Walstra, P., & Jenness, R. (1984). Chapter 3. Carbohydrates. Dairy Chemistry and Physics (pp. 27-41). New York: Wiley.
- Watanabe, K., Nagatake, W., Takahashi, T., Masubuchi, Y., Takimoto, J., & Koyama, K. (2003). Direction observation of polymer crystallization process under shear by a shear flow observation system. Polymer Testing, 22, 101-108.
- Werner, S. R. L., Tretiakov, A., Paterson, T., & Mcleod, J. S. (2002). Modelling Lactose Crystallisation - Final Report. Massey University: Palmerston North.
- White, E. T., & Kishi, S. (1995). Growth Dispersion Effects during Sugar Crystallization. CHEMECA 95 Australia: CHEMECA.
- Yan, Y., & Thorpe, R. B. (1990). Flow Regime Transitions Due to Cavitation in the Flow Through an Orifice. International Journal of Multiphase Flow, 16(6), 1023-1045.
- Yao, Y. F., Savill, A. M., Sandham, N. D., & Dawes, W. N. (2002). Simulation and Modelling of Turbulent Trailing-Edge Flow. Flow Turbulence and Combustion, 68(4), 313-333.

Yoon, H. S., Hill, D. F., Balachandar, S., Adrian, R. J., & Ha, M. Y. (2005). Reynolds number scaling of flow in a Rushton turbine stirred tank. Part 1 Mean Flow, circular jet and tip vortex scaling. Chemical Engineering Science, 60, 3169-3183.

Young, D. F., & Tsai, F. Y. (1973). Flow Characteristics in Models of Arterial Stenoses-.Steady Flow. Journal of Biomechanics, 6, 395-410.

Young, S. W. (1911). Mechanical stimulus to crystallization in supercooled liquids. Journal of the American Chemical Society, 33(2), 148-162.

Zalewski, W., & Gryglaszewski, P. A. (1997). Mathematical model of heat and mass transfer process in evaporative fluid coolers. Chemical Engineering and Processing, 36, 271-280.

Zauner, R., & Jones, A. G. (2002). On the influence of mixing on crystal precipitation processes-application of the segregated feed model. Chemical Engineering Science, 57, 821-831.

Zumstein, R. C., & Rousseau, R. W. (1987). Growth Rate Dispersion in Batch Crystallization with Transient Conditions. AIChE Journal, 33(11), 1921-1925.

## Chapter 9 Nomenclature

Symbol	Definition	Units
$A$	Pre-exponential factor	$\# \cdot \text{m}^{-3} \cdot \text{s}^{-1}$
$Abs$	Absorbance	-
$A_{Hen}$	Heterogeneous pre-exponential factor	$\# \cdot \text{m}^{-3} \cdot \text{s}^{-1}$
$A_{Hom}$	Homogeneous pre-exponential factor	$\# \cdot \text{m}^{-3} \cdot \text{s}^{-1}$
$a_w$	Water activity	-
$B$	Nucleation equation numerator	-
$B_{Hen}$	Heterogeneous nucleation equation numerator	-
$B_{Hom}$	Homogeneous nucleation equation numerator	-
$C$	Concentration of crystals in solution	$\# \cdot \text{m}^{-3}$
$Cav$	Cavitation number	-
$C_{eq}$	Equilibrium concentration	$\# \cdot \text{m}^{-3}$
$C_L$	Total lactose concentration	$\text{g} \cdot 100 \text{ g water}^{-1}$
$C_{Ls}$	Total lactose solubility	$\text{g} \cdot 100 \text{ g water}^{-1}$
$C_o$	Concentration of nucleation sites	$\# \cdot \text{m}^3$
$C_p$	Specific heat capacity	$\text{J} \cdot \text{kg} \cdot \text{K}^{-1}$
$C_{p_{cw}}$	Specific heat capacity water	$\text{J} \cdot \text{kg} \cdot \text{K}^{-1}$
$C_s$	Total lactose solubility concentration	$\text{g} \cdot 100 \text{ g water}^{-1}$
$C_\alpha$	$\alpha$ -Lactose concentration	$\text{g} \cdot 100 \text{ g water}^{-1}$
$C_{as}$	$\alpha$ -Lactose solubility concentration	$\text{g} \cdot 100 \text{ g water}^{-1}$
$C_\beta$	$\beta$ -Lactose concentration	$\text{g} \cdot 100 \text{ g water}^{-1}$
$D_{imp}$	Diameter if impellor	m
$D_{obs}$	Diameter of obstruction	m
$D_{or}$	Orifice diameter	m
$d_p$	Particle size	m
$D_p$	Diameter of pipe	m
$D_T$	Diameter of tank	m
$E_a$	Activation energy	J
$e_f$	Frequency of eddy formation	$\# \cdot \text{s}^{-1}$
$e_f^*$	Non dimensional frequency of eddies	#
$F$	Factor accounting for $\alpha$ -lactose suppression by $\beta$ -lactose	-
$G$	Growth rate of $\alpha$ -lactose monohydrate crystals	$\mu\text{m} \cdot \text{min}^{-1}$
$g$	Gravitational constant	$9.81 \text{ m} \cdot \text{s}^{-2}$
$h_j$	Jacket side heat transfer coefficient	$\text{W} \cdot \text{m}^{-2} \cdot \text{K}^{-1}$
$h_p$	Product side heat transfer coefficient	$\text{W} \cdot \text{m}^{-2} \cdot \text{K}^{-1}$
$H_Q$	Heat flow	W
$H_T$	Height of tank	m
$I_c$	Impeller clearance from bottom of tank	m
$J_{Hen}$	Heterogeneous nucleation Rate	$\# \cdot \text{m}^{-3} \cdot \text{s}^{-1}$
$J_{Hom}$	Homogeneous nucleation Rate	$\# \cdot \text{m}^{-3} \cdot \text{s}^{-1}$
$J_T$	Total nucleation rate	$\# \cdot \text{m}^{-3} \cdot \text{s}^{-1}$
$K$	Ratio of $\alpha$ -lactose to $\beta$ -lactose	-
$k$	Boltzmann constant	$\text{J} \cdot \text{K}^{-1}$
$k_0$	Pre exponential factor in Arrhenius equation	$\text{s}^{-1}$

$k_1$	Mutarotation rate constant for $\beta \rightarrow \alpha$ transformation	$\text{min}^{-1}$
$k_2$	Mutarotation rate constant for $\alpha \rightarrow \beta$ transformation	$\text{min}^{-1}$
$k_g$	Crystal growth temperature coefficient	$\mu\text{m}\cdot\text{min}^{-1}$
$k_L$	Constant for heat transfer equation	-
$k_{LJ}$	Constant for heat transfer equation (Jacket side)	-
$K_p$	Thermal conductivity of product	$\text{W}\cdot\text{m}^{-1}\text{K}^{-1}$
$K_T$	Thermal conductivity	$\text{W}\cdot\text{m}^{-1}\text{K}^{-1}$
$L_{ini}$	Initial mass of lactose in the solution	kg
$LMTD$	Log mean temperature difference	K
$M$	Molar Mass	$\text{g}\cdot\text{mol}^{-1}$
$M$	Molecules of lactose in solution phase	#
$m_{cw}$	Mass flow of cooling water	$\text{kg}\cdot\text{s}^{-1}$
$m_f^*$	Monomer attachment frequency	$\text{s}^{-1}$
$M_{Grate}$	Measured growth rate	$\mu\text{m}\cdot\text{min}^{-1}$
$N$	Total number of crystals	$\text{m}^{-3}$
$n$	Number of molecules in nucleus	#
$n^*$	Number of molecules in critical nucleus	#
$N_A$	Avogadro's Constant	-
$N_{cry}$	Number of crystals at an absorbance	#
$N_{Grate}$	Normalised growth rate	$\mu\text{m}\cdot\text{min}^{-1}/(C_a - C_{as})$
$N_{js}$	Minimum agitation speed for suspension	$\text{r}\cdot\text{min}^{-1}$
$N_N$	Number of particles per unit volume	$\text{m}^{-3}$
$N_R$	Agitation rate	$\text{r}\cdot\text{s}^{-1}$
$Nu$	Nusselt number	-
$P^\#$	Impeller power number	-
$p_2$	Pressure of fluid	$\text{kg}\cdot\text{m}^{-2}$
$p_h$	Pressure head of fluid	$\text{kg}\cdot\text{m}^{-3}$
$\Delta p$	Pressure drop	$\text{kg}\cdot\text{m}^{-3}$
$Pr$	Prandtl number	-
$p_v$	Vapour pressure of fluid	$\text{kg}\cdot\text{m}^{-2}$
$P_{wr(f)}$	Power to increase flow	W
$P_{diss}$	Power Dissipated into solution	$\text{W}\cdot\text{g}^{-1}$
$P_{wr(m)}$	Power input from mixer	$\text{J}\cdot\text{s}^{-1}$
$q$	Factor to account for interfacial energy reduction	
$Q$	Flow rate	$\text{m}^3\cdot\text{s}$
$R$	Universal gas constant	$\text{J}\cdot\text{mol}^{-1}\cdot\text{K}^{-1}$
$Re_{imp}$	Reynolds number in an agitated tank	-
$Re_p$	Reynolds number in a pipe	-
$R_f$	Fouling factor	$\text{W}\cdot\text{K}^{-1}$
$S_{abs}$	Absolute supersaturation	$C - C_{eq}$
$SA$	Surface area	$\text{m}^2$
$S_R$	Supersaturation ratio	$C/C_{eq}$
$St$	Strouhal number	-
$St_o$	Strouhal number of orifice	-
$T$	Temperature	$^{\circ}\text{C}$
$\Delta T$	Temperature difference	$^{\circ}\text{C}$
$t$	Time	s
$T_b$	Temperature of bulk solution	K
$T_{cw(in)}$	Temperature of cooling water in	K
$T_{cw(out)}$	Temperature of cooling water out	K

$T_K$	Absolute temperature	K
$t_k$	Kolmogorov time scale	s
$t_N$	Time to reach critical number of nuclei	s
$u$	Viscosity of Solution	Pa·s
$U$	Velocity	m·s <sup>-1</sup>
$U_H$	Heat transfer coefficient	W·m <sup>-2</sup> ·K <sup>-1</sup>
$U_{th}$	Velocity at throat	m·s <sup>-1</sup>
$\nu$	Kinematic viscosity	m <sup>2</sup> ·s <sup>-1</sup>
$V$	Volume	m <sup>3</sup>
$Vi$	Viscosity number	$\psi_B/\psi_W$
$V_m$	Molecular volume	m <sup>3</sup>
$V_{tank}$	Volume of tank	m <sup>3</sup>
$W^*$	Work required for nucleus formation	J
$W_{ini}$	Initial mass of water in the solution	kg
$W_P$	Weight percent of solids	-
$x$	Growth rate factor	-
$X$	Mass of crystallised lactose	g
$X_1$	Molar fraction of water	-
$X_2$	Molar fraction of solute	-
$x_i$	Radius of crystal	μm
$x_w$	Wall thickness	m
$Y$	Constant for determining water activity	-
$Z$	Zeldovich factor	-

### Greek Symbols

$\beta$	Weibull shape constant	-
$\beta_c$	Cluster shape factor	-
$\gamma$	Average shear rate	s <sup>-1</sup>
$\lambda$	Weibull scale constant	-
$\pi$	Pi	
$\Delta\mu$	Gain in free energy from phase transition	J
$\mu_c^*$	Chemical potential of molecule in crystal	J
$\xi_i$	Growth rate multiplier	-
$\mu_s$	Chemical potential of molecule in solution	J
$\mu$	Chemical potential of supersaturated solution	J
$\mu_{eq}^*$	Chemical potential of saturated solution	J
$\rho_x$	Density of lactose crystal	kg·m <sup>-3</sup>
$\Delta\rho_s$	Solid-liquid density difference	kg·m <sup>-3</sup>
$\rho_L$	Density of liquid	kg·m <sup>-3</sup>
$\varepsilon$	Rate of dissipation of kinetic energy per unit mass	m <sup>2</sup> ·s <sup>-3</sup>
$\varepsilon_P$	Rate of energy dissipation per unit volume	W·m <sup>3</sup>
$\eta$	Kolmogorov length scale	m
$\kappa$	Constant depending on impeller	-
$\lambda_w$	Thermal resistance of wall	W·m <sup>-1</sup> K <sup>-1</sup>
$\sigma$	Interfacial energy	mJ·m <sup>-2</sup>
$\tau$	Induction time	s

$\varphi$	Volume fraction of particles	-
$\psi_B$	Viscosity in bulk solution	Pa·s
$\Psi_f$	Viscosity of fluid	Pa·s
$\Psi_m$	Viscosity of mixture	Pa·s
$\psi_W$	Viscosity at wall	Pa·s